DAMAGE LOCATION IN STRUCTURES BY MONITORING VIBRATION CHARACTERISTICS

by

ADNAN NAJI JAMEL AL-TAMIMI, B.Sc., M.Sc.

A thesis submitted for the degree of

Doctor of Philosophy

Department of Mechanical and Production Engineering
The University of Aston in Birmingham

February 1985

THE UNIVERSITY OF ASTON IN BIRMINGHAM

DAMAGE LOCATION IN STRUCTURES BY MONITORING VIBRATION CHARACTERISTICS

by

ADNAN NAJI JAMEL AL-TAMIMI

A thesis submitted for the degree
of Doctor of Philosophy 1985

SUMMARY

The aim of this work was to investigate the feasibility of detecting and locating damage in large frame structures where visual inspection would be difficult or impossible. This method is based on a vibration technique for non-destructively assessing the integrity of structures by using measurements of changes in the natural frequencies. Such measurements can be made at a single point in the structure.

The method requires that initially a comprehensive theoretical vibration analysis of the structure is undertaken and from it predictions are made of changes in dynamic characteristics that will occur if each member of the structure is damaged in turn. The natural frequencies of the undamaged structure are measured, and then routinely remeasured at intervals. If a change in the natural frequencies is detected a statistical method is used to make the best match between the measured changes in frequency and the family of theoretical predictions. This predicts the most likely damage site.

The theoretical analysis was based on the finite element method. Many structures were extensively studied and a computer model was used to simulate the effect of the extent and location of the damage on natural frequencies. Only one such analysis is required for each structure to be investigated.

The experimental study was conducted on small structures in the laboretory. Frequency changes were found from inertance measurements on various plane and space frames.

The computational requirements of the location analysis are small and a desk-top micro computer was used. Results of this work showed that the method was successful in detecting and locating damage in the test structures.

KEY WORDS

Non-destructive tests, Defect location, F.E.M.,
Natural frequency, Inertance.

TO MY PARENTS

ACKNOWLEDGEMENTS

The author wishes to express his sincere appreciation to all who have given help and support throughout this thesis. He is particularly indebted to the following:

To his supervisor Dr. J.E.T Penny for his advice, patient and personal guidance and many productive discussions throughout this work.

To Dr. D.A.L. Wilson of the Aston Statistics Group, for his assistance in developing the new method of damage location.

To Mr W.L. Flint and Mr T.H. Richards for their help and useful discussions.

To W.P. Howson, of UWIST, Cardiff, for his assistance and offering one of the computer programs.

To the Technicians in the Department of Mechanical Engineering , particularly Brian and Barry.

To Gill Evans for her help, encouragement and patience.

To Mr G. Seet for his help and useful discussions.

Finally, special thanks to all members of my family for their encouragement and support.

LIST OF CONTENTS

LIST OF TABLES

LIST OF FIGURES

CHAPTER ONE

INTRODUCTION

1.1 General Introduction.

1.2 Structure of the Thesis.

1.1 GENERAL INTRODUCTION.

In recent years, there has been considerable demand for more accurate Non-Destructive Testing (NDT) techniques to detect and locate structural damage. The need for this type of technique is particulary apparent when dealing with large structures such as oil rigs and tall buildings due to the structures being constantly acted on by wave and wind motion respectively. As a result, these forces can introduce vibration at the resonant frequency which may lead to structural failure.

In many applications of this technique it is advantageous to be able to monitor structural integrity. If a non-destructive testing method is reliable it can be used to locate defects before they are severe enough to propagate failure, so long as the structures are subject to periodical in-service inspections. This philosophy is applied in the design of most modern aircraft. The design criterion is that a component remains serviceable for at least one interval between inspection. Bearing in mind the high cost of maintaining a structure in its working environment, a cheap and reliable method of damage detection and location is an obvious advantage.

Various non-destructive methods exist (e.g. X-ray and ultrasonic methods) which are able to detect damage in structures. In large, complicated structures these methods tend to be impractical due either to health hazards or to

operational problems. This necessitates structural overhaul for the purpose of inspection which may result in significant production and associated economic losses.

The primary object of this study is to develop an NDT technique which could be applied to a whole structure to yield information concerning the detection, location and approximate indication of the severity of any damage present.

Testing techniques applied to the structures need not be restricted to visual and ultrasonic tests, but which can also include dynamic tests. Since the dynamic characteristics of a structure are governed by its stiffness and mass properties, then changes in these properties will be accompanied by a change in these characteristics. Therefore, the natural frequencies of any structure are a function of its material constants and dimensions. Hence, damage to the structure might reasonably be expected to change the geometry and stiffness of the structure. Thus, it is apparent that natural frequency is a parameter which might satisfy the requirements of monitoring structural integrity. Because the stress distribution through a vibrating structure is non-uniform and is different for each mode, any localized damage would affect each mode differently depending on the particular location of damage.

The location of a damage site would require the computation of the changes in natural frequencies of several modes. This would be done by modelling the damage as a local decrease in

the stiffness at different sites within the structure and carrying out a corresponding dynamic analysis. The experimentally measured changes would then be compared with the pattern of changes predicted theoretically for damage at different sites and an appropriate statistical method could then be used to correlate these results and predict the location of the damage.

A series of experiments have been performed to test the suitability of a method when applied to structures fabricated from mild steel. Results are presented from tests on plane and space frames of various shapes. Different types of damage including cracks, saw cuts and damage produced by a spark erosion machine have been employed. Frequency measurements were performed using steady-state and periodic random excitation. It was found that changes in natural frequency are easier to measure than changes in damping and for that reason measurement of structural damping has not been undertaken in this work. However, it has been proved (1,2,3) that damping increases with damage.

Analytical and experimental methods for determining the vibration characteristics of structures are also discussed. For the purpose of defect location a comprehensive technique was developed to study the effect of damage severity and position on the dynamic characteristics of structures. To achieve this objective, the work undertaken can be subdivided into the following stages:

1- A computer model was developed to study the effect of damage to structural members on the natural frequencies of a structure using the finite element method. This technique is highly accurate, and can be used for analysing any structure with any type of structural vibration, e.g. torsional, axial, flexural or a combination of these.

2- A mathematical damage model was developed in order to reduce the stiffness of a local area.

3- Test rigs were designed to study the vibrational behaviour of the model structures before and after damage. The majority of tests undertaken in this investigation measured the inertance (acceleration response / force) of the structure. Also, evaluation of the flexible joints used in the vibration analysis of the model structure was made by using the static loading procedure.

4- A statistical model was developed to make the best match between the measured changes in frequency and the family of theoretical predictions. This model in turn will then locate the most likely damage site.

5- A comparison was made between the experimental and theoretical results.

6- Effects of varying parameters on the frequencies and mode shapes was studied, e.g. size, model and position of damage, and also boundary conditions.

1.2 STRUCTURE OF THE THESIS.

This thesis is divided into ten chapters. The present chapter serves to introduce the theme and outline the overall research programme. Various topics are discussed briefly and qualitatively, while details are omitted, to be elaborated on in a later chapter.

A survey of the literature on the existing techniques for detecting and locating structural damage is given in chapter two, together with an indication of their deficiencies in relation to the present problem. In chapter three the theory relating to the detection and location method, which is the subject of this thesis, is developed.

Chapters four and five present the theory relating to dynamic analysis methods using the finite element technique. In chapter four, a mathematical formulation is presented using an assumed polynomial displacement function which leads to frequency-independent mass and stiffness matrices, and thus to a linear EigenValue Problem (EVP). In contrast, in chapter five, a mathematical formulation using the exact displacement solutions of the governing differential equation of motion for the element is discussed. A frequency-dependent dynamic stiffness matrix is obtained and the resulting non-linear eigenvalue problem solved by using a determinant based method, namely, the sign count algorithm.

Chapter six describes the instrumentation and the development of the experimental technique in order to obtain experimental data of an extremely high quality using a desk-top computer as a controller in the experiments.

Chapters seven and eight present the theoretical and experimental results. In chapter seven, a study of theoretical changes in natural frequencies due to the influence of varying parameters was discussed. Chapter eight is devoted to a study of experimental changes in frequencies due to damage. Also, a comparison was made between the theoretical and the measured changes in frequencies, to establish a fair correlation.

Chapter nine gives the results of the damage location for plane and space frame structures. The damage location charts with various damage models are shown by using two statistical approaches. Finally, the last chapter presents a general discussion, conclusions and also suggestions for further work in this area.

CHAPTER TWO

REVIEW OF THE EXISTING TECHNIQUES FOR DETECTING STRUCTURAL DAMAGE

2.1 Introduction.

2.2 The Need for Integrity Monitoring of Structures.

2.3 Review of Existing Non-Destructive Testing Techniques.

2.4 The Use of Vibration Characteristics as an NDT Tool.

2.1 INTRODUCTION.

When a structure operates in a hostile environment and when the results of a failure would be catastrophic, it is important that the structure is inspected regularly.

In recent years a variety of methods of Non-Destructive Testing (NDT) and inspection techniques have been developed. Clarkson (4), has shown how various methods of NDT have proved to be of tremendous value and have become an accepted facility in the field of engineering. Whilst such existing methods can usually be relied upon to locate damage before it is sufficiently severe to be disastrous, all of these techniques have some disadvantages and limitations and no one method is universally applicable. One very common disadvantage is that the component under inspection must be investigated in a piece-wise manner. In some methods, such as Ultrasonic Scan, it is possible to automate this process, but this does not usually decrease the time required for inspection.

Thus, any method which would enable a NDT technique of a structure to be made by simple measurements at one point on that structure would be of value. Such a method would require a parameter to be found which would vary with the damage in a structure but which would be independent of the point on the structure at which the parameter was measured.

2.2 THE NEED FOR INTEGRITY MONITORING OF STRUCTURES.

This work describes such a method for overall assessment of structural integrity. For integrity monitoring to be a reliable tool, it is necessary to establish a recognizable baseline behaviour of the structure such that changes in the behaviour can be interpreted. Such a method of total monitoring should be fast, cheap, safe and permit frequent inspection.

A type of structure for which structural integrity monitoring is both essential and yet difficult to achieve is the offshore platform; examples of which are being erected in progressively deeper water. There is also the problem of on-site inspection of subsurface structural members which is increasingly difficult and expensive. Due to poor visibility, poor lighting and hazardous conditions, the divers task is made very difficult. These obstacles worsen rapidly with increase in depth. Not only does the cost rise steeply with depth, but the danger to human life, though all precautions are taken, must inevitably rise. Hence, the need for structural integrity monitoring.

A more definitive survey of offshore structures is needed since each year the offshore oil industry suffers unacceptable losses in drilling rigs. Present loss rates are unacceptable from the stand point of personnel casualties,

rig down time and outright rig loss. As indicated by Tiedemann (5), drilling rigs cost from $4 million to $25 million to build. Oil rig losses from 1955 to 1971 have totalled more than $131 million for development, inspection and insurance. Also during these 17 years there have been 23 casualties.

In 1976, Loland and Dodds (6) reported there were approximately 80 offshore fixed steel structures installed in the coastal waters off the United Kingdom and they had predicted that by 1980 there would be around 150 steel structures in water depths varying from 30m to 300m. The preceding arguments lead to the conclusion that more frequent and comprehensive inspection is required.

In this survey we shall first of all review some of the well established techniques of testing and inspection, then examine an approach which has the potential to offer a method of non-destructive testing using a single measurement.

2.3 REVIEW OF EXISTING NON-DESTRUCTIVE TESTING TECHNIQUES.

Wherever significant damage to a structure is suspected then inspection is required. Over the past years many types of NDT have been introduced, but unfortunately none of these have been applicable to all types of damage and environment. SILK et al (7) considered a very large range of potential techniques which could be used in inspection. The more

promising include:

I- The Witness System

The witness system of inspection may take a variety of forms. By pressurising a hollow member, any crack developed in this member will be shown up by the rate of loss of the pressure. If it is not possible to pressurise the member, a special pressurised member can be welded to the inside of the member which is to be inspected; these pressurised welded members are designed so as to fracture when a crack develops in the main structure. The accuracy with which the crack is located will depend on the size of these pressurised detectors. This method is consequently not suitable for monitoring complicated structures.

II- Ultrasonic Methods.

Ultrasonic methods fall into three cateogories, high frequency ultrasonic, low frequency ultrasonic used for concrete testing and ultrasonic Lamb wave system. The Lamb wave system is the ultrasonic equivalent to electromagnetic radiation and is sensitive to cracks and areas of corrosion. These methods can be used to locate a wide variety of defects, by studying the extent of transmission between two areas. It may be possible to obtain an approximate estimatation of the defect location, by studying the reflected signals. These methods have the disadvantage that

the component under inspection must be investigated in a piece-wise manner. A further disadvantage is that the structure should be clean, as surface roughness can affect test results: also considerable operator skill is required. A further disadvantage of the ultrasonic method is the need to employ a large number of transmitters and detectors to give adequate coverage. Silk et al (8) reported that defect sizing could be achieved by interpreting ultrasonic time delays.

III- X-Radiography.

This method has been used in many industries, the advantage being that an overall inspection can quickly be made with the structure in situ. Particular areas of interest may then be examined in detail by using X-ray microscopy. There are limitations in the use of radiography for detecting cracks e.g. because of potential health hazards expensive safety precautions are necessary and testing can also take a considerable time. Halmshow et al (9) found that it is necessary to measure two parameters of the crack; the crack opening (the separation distance between the faces) and angle of the crack to the radiation beam.

IV- Dye Penetrants.

This method involves the use of a dye penetrant on the required structure to provide a visual indication of the actual damage site. A disadvantage of this method is the need

to examine the structure in a piece-wise manner. This is time consuming and is limited to detecting damage that is open to the surface which must be smooth and uncontaminated. As a result, this method is not suitable for complicated structures.

V- Television Viewing.

As close inspection of the structure is necessary, the use of a T.V. system installed underwater, with improved cameras and photographic techniques can greatly reduce the divers task. Close inspection must be carried out in a piece-wise manner and is limited to surface defects only. This technique is not really suitable for routine monitoring of structural integrity.

VI- Acoustic Emission.

This technique can be applied in steel structure monitoring systems. When a material cracks, acoustic pulses will be generated from the area, and these pulses are generally at an ultrasonic frequency. The emitted pulses can be detected by an array of ultrasonic detectors, and, by using the time relationship between the detection of impulses by the various detectors, an estimate of the crack location can be made. At present, in offshore technology, the use of such a method still require divers to locate the actual damage site. A moderately large number of detectors would be required,

whatever the type of structure study.

All the above mentioned techniques require that the structure be inspected in a piece-wise manner. None of the methods so far described deals with the structure as a whole and several of them involve serious health hazards. However, even with the successful application of these techniques, what reliability is achieved and at what cost? In addition to these factors, the limitations described increase the cost level of undersea repairs. Quite obviously, such repairs will be greatly assisted and cheapened if structural damage can be detected at an early stage before the primary damage can induce structural failure.

The present research is concerned with the development of a system of integrity monitoring which neither requires piece-wise testing nor poses a health hazard.

2.4 THE USE OF VIBRATION CHARACTERISTICS AS AN NDT TOOL.

A property of a vibrating system is that the resonant frequencies are functions of the physical and geometrical properties: furthermore, they can be excited by forces applied to any point in the structure unless this point is a node for a particular mode of vibration. Thus any changes that occur in the natural frequency of the structure could indicate a change in the physical or geometrical properties

of it. Since cracks and other types of damage represent a change in the physical properties, a change in natural frequency could be used to detect any onset of cracks. So, the measurement of the natural frequencies of a structure at any two consecutively taken measurements of its life might well lead to the possibility of detecting damage in the structure.

The idea of using vibrational monitoring to assess the structural integrity of structures has been the subject of considerable interest in recent years, as reported in references (10,11,12). The concept is based on the assumption that each load carrying member contributes to the overall modes of vibration. The position of the member in the structural topology governs which of the overall modes is most affected if there is damage. The more serious the damage suffered by a member, the bigger the change in vibration characteristics for monitoring purposes.

The literature survey revealed some references dealing with detection of structural damage by using vibration characteristics. Nezu et al (13), suggested a method which could be used to detect damage in structures by using mechanical impedance measurements. A comparison was made between mechanical impedance measurements of a sound structure before use and during service. Whenever a significant difference occurred, then damage was suspected. Three characteristic changes in mechanical impedance of the structure were used by Nezu and are as follows:

1- Difference in the shape of the plot of mechanical impedance over the whole range of exciting frequencies.

2- Difference in the amplitude at a resonant frequency.

3- Difference in a resonant frequency.

Whilst damage can be detected, its location cannot be determined by this method.

Several years ago, H.M.Tiedemann & Co. suggested the use of vibration characteristics of structures to indicate damage in offshore structures (5). The aim was the eventual replacement of the long, expensive and depth limited system of divers while vibration calculations and measurements would predict the damage to the structure at a fraction of the cost of existing techniques.

Recently, further attempts have been reported using vibration characteristics for integrity monitoring. Adams et al (2) found that damage in specimens fabricated from composite materials could be detected by a reduction in stiffness and an increase in damping, with a corresponding decrease in the natural frequencies of the specimen. Similar findings are also reported in (14,15,16,17). Also, DiBenedetto et al (3) investigated the vibration response of glass reinforced epoxy and polyester laminates by measuring the complex modulus and damping capacity as fatigue crack damage accumulated.

Loland et al (18,19,20) investigated the possibility of using vibration analysis to monitor the integrity of offshore

structures by using wave excitation. Their analysis did not attempt to locate the position of damage within the structure but, by measuring changes in the natural frequencies, they detected the existence of structural damage. Similar work is also reported in (21,22).

Recently, Turner and Pretlove (23), investigated the detection of damaged bridges by the measurement of traffic-induced vibration.

Thus, it can be seen that measurements of the vibration characteristics, that is, the natural frequencies and damping of a structure, constitute an alternative form of NDT since these properties can be measured at a single point of the structure and are independent of the position chosen. A test based on these measurements would therefore not require access to the whole of the structure and would not involve time-consuming scanning of the whole surface. A further advantage of such a test would be that the labour involved does not increase with increasing the size of the structure. The testing technique is simple, quantifiable and offers the possibility of automation.

Savings made between installation and operating costs of the monitoring system and current inspection methods must be competitive with other monitoring techniques such as those outlined in section 2.3.

CHAPTER THREE

DETECTION AND LOCATION OF STRUCTURAL DAMAGE USING VIBRATION CHARACTERISTIC

3.1 INTRODUCTION.

The primary objective of this chapter is to develop a method for detecting and locating damage in frame structures which will overcome the difficulties of the existing techniques mentioned in chapter two. As previously stated, the method which makes use of the vibration characteristics of the structure, is based on the fact that in a structure, regardless of type, the natural modes of vibration are dependent on the characteristics of the structure and not on the excitation, so that model characteristics do not change unless the structural stiffness or inertia changes. If the structure is damaged, there is a change in structural stiffness which should be detectable by a change in the vibration characteristics of the structure.

One of the techniques adopted here is a development of that published by Cawley and Adams who used it to detect damage in composite material. They discovered that when specimens made from fibre-reinforced plastics were damaged, the stiffness and consequently the natural frequencies of vibration decreased and an increase in damping was noted. Their initial work on one-dimensional structures was analysed as described in (17). A similar finding was reported in (3). More recently (15,16,24), this principle was extended to two-dimensional structures. Results were presented from these tests on an aluminium and a cross-ply fibre-reinforced plastic plate.

In the present work, the method introduced by Cawley and Adams (15) has been developed further and improved and applied to the task of detecting and locating damage in frame structures.

3.2- DETECTION OF STRUCTURAL DAMAGE USING VIBRATION.

The previously mentioned methods used for the detection of damage have some practical restrictions, due to their high complexity and cost, which effectively inhibit their use for damage detection in complex structures. Thus, the emphasis in this work was on the development of an inspection technique which would provide a measure of the general integrity of the structure without resorting to successive inspections of individual members.

This method is based on comparisons of the frequencies of an original structure before use, with those on the same structure in use. If the comparisons show a significant shift in natural frequencies, then a change in the mass or stiffness of the structure would be indicated. This reduction in stiffness would suggest damage in the structural member.

The essential steps of detecting and locating damage are thus as follows:

I- A theoretical analysis of the structure is undertaken to determine, typically, its lower natural frequencies.

II- Hypothetical damage is introduced at some point in the structure and the natural frequencies of the structure are recomputed. Thus, the theoretical changes in the natural frequencies caused by the hypothetical damage can be obtained. This procedure is then repeated for each and every part of the structure where damage might occur.

III- The natural frequencies are measured on the actual, undamaged structure. These frequencies should be close to, but not necessarily identical to those predicted in (I).

IV- The natural frequencies of the actual structure are remeasured, routinely, until a change is detected. This would imply that damage had occurred. In other words, if one set of frequencies is measured before the structure is put into service, subsequent frequency measurements can be used to test whether the structure is still sound.

V- If and when changes in the natural frequencies are detected, then these changes are compared with the sets of predicted frequency changes caused by hypothetical damage at various points. The location of hypothetical damage which predicts a set of frequency changes giving the best comparison with the measured frequency changes shows the most likely location of the damage. This comparison process is carried out statistically.

In order to test the proposed procedure, laboratory models

have been used. At this stage in the development, tests could not be done in a working environment due to the difficulty of introducing damage in real structures and the fact that testing would take significantly more time. Thus, experimental verification of the model structures was obtained from laboratory measurements on steel plane frames and from a series of tests on space frame structures. In both cases, a variety of types of damage were employed, and the consequent changes in natural frequencies measured.

3.3 METHOD OF DAMAGE LOCATION USING NATURAL FREQUENCIES.

Following Cawley and Adams (15), it is assumed that, in theory, localised damage in a structure at some location specified by a position vector p will cause the natural frequency of mode r to change by an amount that will be denoted by δ_r (p), which is a function not only of p but also of the reduction in stiffness caused by the damage, say Δ K, so that

$$\delta_r(p) = f(\Delta K, p) \qquad (3.1)$$

A formal expansion about the undamaged state ($\Delta K = 0$) using Maclaurin's theorem, ignoring second and higher order terms, then gives

$$\delta_r(p) = f(0,p) + \Delta K \, \partial f(0,p) / \partial(\Delta K) \qquad (3.2)$$

Assuming that there is no frequency change without damage, it follows that $f(0,p)$ is zero for all p and so, writing the partial derivative as $g_r(p)$, (3.2) then simplifies to

$$\delta_r(p) = \Delta K \, g_r(p) \qquad (3.3)$$

Similarly, for any other mode, say s,

$$\delta_s(p) = \Delta K \, g_s(p) \qquad (3.4)$$

If it is assumed further that ΔK is independent of frequency, it follows that the ratio of frequency changes is dependent only upon the damage location as specified by p:

$$\delta_r(p) \; / \; \delta_s(p) = g_r(p) \; / \; g_s(p) = h_{rs}(p), \text{ say.} \qquad (3.5)$$

If these various assumptions are correct and there are no random effects present, actual comparison of natural frequencies in a structure before and after damage should give observed changes for modes r and s, say d_r and d_s respectively, that form a ratio d_r / d_s which exactly equals $h_{rs}(p)$ for some p, thus enabling the position of the damage to be identified, provided there is a suitable method available for calculating values of $h_{rs}(p)$ for all relevant values of p.

If there is damage in the structure, then a position where the changes in the theoretically determined ratio are equal to the changes of experimental ratio for at least two modes

would be required to indicate possible damage sites.

3.4 MODELLING OF THE DAMAGE IN A STRUCTURAL MEMBER.

From equation (3.5), it is now necessary to compute the changes in natural frequencies of the structure due to modelling the damage at a given site.

A computer model of the damage was formulated to predict the changes in natural frequencies of the structures. The purpose of this model was to conduct a parametric study of the effect of simulated structural damage on natural frequency.

The dynamic analysis of a structure with localised damage requires that the damage be modelled. Since many different types of damage could be investigated, a separate model for the study of each type would lead to a cumbersome solution. It was therefore considered that a model with an overall applicability should be used. All forms of damage result in a decrease of the stiffness of the structure and this suggests that it might be possible to represent damage by a local decrease in stiffness. The problem arises of how to represent a local reduction in stiffness, that is to say, how does one model a crack using a relatively simple approach?

Five attempts were made to overcome this problem and are discussed below.

(I) Spring Model.

After splitting the structure into many nodes and elements (for the finite element method), it was decided initially to model damage by the insertion of a massless torsional spring. The spring was positioned at any desired node, a method which defines the damage in terms of spring stiffness alone. This model proved not to be accurate enough to represent a complete failure, but it was good enough to represent the partial damage. Therefore, it was decided to add both axial and transverse flexibility along with the torsional spring to allow for the freedom of movement in all directions.

To obtain values for the equivalent spring stiffness of the model, a series of experiments was performed and details of these will be discussed in chapter (6). When the element (of the member) is undamaged, the spring stiffness would tend to infinity and would decrease as the amount of damage increased.

(II) Two-Cantilever Model.

This particular model was used to represent the damage as complete failure. In the finite element analysis, structural failure was modelled by placing two nodes in the same position, thus allowing complete freedom in each direction. Thus the damaged member is represented as two-cantilevers. In order to calculate theoretical changes in natural frequencies for each and every part of the structure where damage might

occur, the frequencies of the undamaged structure were first calculated. Then, damage was introduced at a desired point on the structure and the frequencies of the structure were re-calculated. The above procedure can be repeated as many times as there are elements in the structure.

(III) Local Reduction in Cross-Sectional Area Model.

The possibility of representing damage to a structural element by reducing the cross-sectional area of a short element was also investigated. This model required two parameters to define the damage, i.e. the length and the cross section of that element. This model proved to be fairly accurate in representing the partial damage.

The changes in natural frequencies were found by analysing the undamaged structure and repeating the analysis as many times as there were elements in the structure, and modelling the damage as a reduction in the cross-sectional area of the desired element.

(IV) Member removal model.

The possibility of simulating damage of a structure by removing a member was also investigated. This model will affect both the stiffness and mass of the structure. The frequency changes were found by analysis of the undamaged structure and then by repeating the analysis as many times as there were members in the structure.

(V) Reduction in Rigidity of Whole Element Model.

Here, the damage is modelled by a reduction in rigidity of the whole element in which the damage is situated. This model required only one parameter to define the damage, i.e. a percentage reduction in rigidity.

This method proved to be accurate enough to represent the damage as either partial or complete failure. Therefore, this model is used to calculate the changes in natural frequencies of the structure due to a reduction in rigidity of each element in turn, in the same manner as explained in the previous models. The primary advantage of this model is that the computational time can be reduced to a single dynamic analysis plus a small amount of time for calculating changes in the frequency caused by changes in the stiffness matrix due to a reduction in rigidity. A more comprehensive description of the application of this model will be shown later in section (4.4). An advantage of this is that there is no need to solve the eigenvalue problem for each case, while this was necessary in methods I to IV above.

3.5 STATISTICAL IDENTIFICATION OF DAMAGE SITES.

Even when the theoretical frequency changes have been calculated by some appropriate method, slight departures from

the theoretical assumptions together with random errors in measuring the actual frequency changes make the practical identification of the actual damage position with some theoretical position p rather more complicated than simply matching d_r / d_s with $\delta_r(p)$ / $\delta_s(p)$ as suggested in section 3.3 above.

Cawley and Adams allowed for d_r / d_s to deviate in some random manner from $\delta_r(p)$ / $\delta_s(p)$ for the correct position vector p but they were not explicit about the form which this deviation took. It would seem, however, that they implicitly assumed that the expected value of d_r / d_s was equal to $\delta_r(p)$ / $\delta_s(p)$ for the correct p.

In practice, the correct position vector p is not known in advance and a method of finding p is required. Cawley and Adams approached this problem by defining an 'error', which is denoted by $e_{rs}(p)$, that is

$$e_{rs}(p) = \left\{ \begin{array}{ll} D_{rs}(p) - 1 & \text{if } D_{rs}(p) \geq 1, \\ [1 / D_{rs}(p)] - 1 & \text{if } D_{rs}(p) < 1, \end{array} \right\} \qquad (3.6)$$

where

$$D_{rs}(p) = \frac{\delta_r(p) / \delta_s(p)}{d_r / d_s} .$$

For each mode pair, according to equations (3.6), the value of the error function, $e_{rs}(p)$, could be computed. The 'total

error' in assuming the position of the damage to be p was defined as the sum of the errors in all the mode pairs:

$$e(p) = \sum_{\substack{\text{all pairs} \\ (r,s)}} e_{rs}(p) \ , \qquad (3.7)$$

from which could be found the minimum,

$$e_{min} = \min_{p} \{ e(p) \} \ . \qquad (3.8)$$

The most probable damage site was taken by Cawley and Adams to be the one at which the value of e(p) in equation (3.7) is a minimum. Let this minimum value be called e_{min}. It might be thought that e_{min} would be zero at the damage site. However, due to errors in the experimental measurements, the use of a simplified model of damage in the determination of the theoretical changes in natural frequencies and the fact that only a finite number of possible positions, p, were considered, this is unlikely to be the case. If more than the minimum requirement of two pairs for the determination of the damage site are used, some averaging of the results is obtained and the position at which e(p) is a minimum can be assumed to lie close to the damage site.

Cawley and Adams used e_{min} to normalise each total error, which was expressed as the "Normalised Percentage Error" for failure at theoretical position p, NPE(p), defined as

$$NPE(p) = 100 * e_{min} / e(p) \qquad (3.9)$$

By this definition, NPE(p) will always be 100 for the position p which gives the smallest e(p), regardless of the size of e(p), so that it does not provide an absolute scale for assessing the adequacy of various theoretical models of failure. Also, as will be shown later, taking all pairs (r,s) produces a large number of ratios from a limited number of frequency measurements but only a few of these ratios are independent.

Despite these defects, the Cawley-Adams method does produce reasonably good results in a variety of practical situations, so in developing a new method the basic approach has been kept fairly close to theirs while, at the same time, attempting to provide a firmer theoretical basis for selecting the best explanation for an observed failure.

3.6 NEW PROPOSED METHOD FOR IDENTIFYING DAMAGE SITE.

To develop the new method, some further notation is required. In considering typical modes r and s an index i is introduced to denote the ordered pair (r,s). As in section 3.5, observed frequency changes will be denoted at these modes by d_r and d_s, the corresponding theoretical changes for failure at a position described by p being $\delta_r(p)$ and $\delta_s(p)$, which will be abbreviated to δ_r and δ_s when there is no ambiguity about which p is being considered.

It will be assumed that in the absence of any random effects,

the relationship between the observed and theoretical frequency changes would be of the form

$$(d_r / d_s) = \alpha (\delta_r / \delta_s)^{\beta} \qquad (3.10)$$

Taking logarithms of (3.10) and introducing an additional random component, a simple linear model is obtained, which is

$$y_i = \beta_0 + \beta_1 x_i + \varpi_i \qquad (3.11)$$

where

$$y_i = \ln (d_r / d_s) \quad , \quad x_i = \ln (\delta_r / \delta_s) \quad ,$$

$$\beta_0 = \ln \alpha \quad , \qquad \beta_1 = \beta \quad ,$$

and ϖ_i denotes a random error, whose properties will be considered in more detail later. First, however, it is noted that (3.11) is in the form of the generalised least squares (GLS) regression model, which is discussed in detail in Appendix 1.

Consider the value that index i may take. Suppose the frequency changes for m modes have been observed and the corresponding theoretical changes for various p are calculated. Following Cawley and Adams, all possible pairs (r,s), might be considered, giving 1 to m(m-1)/2 as the range for i. The objection to this is that only m-1 of the corresponding pairs of frequency changes will be independent, e.g. if observations were made at 4 modes (m=4), then:

$$y_1 = \ln d_1 - \ln d_2 \quad ,$$

$$y_2 = \ln d_1 - \ln d_3 ,$$

$$y_3 = \ln d_1 - \ln d_4 ,$$

$$y_4 = \ln d_2 - \ln d_3 = y_2 - y_1 ,$$

$$y_5 = \ln d_2 - \ln d_4 = y_3 - y_1 ,$$

$$y_6 = \ln d_3 - \ln d_4 = y_3 - y_2 .$$

It is clear that there are only m-1=3 independent values of y_i. These three may be chosen arbitrarily and the remaining values can all be expressed in terms of them. In order to consider independent values only, all those involving the first mode (d_1 or δ_1) will be considered, so that

$$y_i = \ln d_1 - \ln d_{i+1} , \qquad (3.12)$$

$$x_i = \ln\delta_1 - \ln \delta_{i+1} \qquad \text{for } i = 1 \text{ to } n,$$

where $n = m-1$.

To incorporate randomness in a sensible way, suppose that the observed log frequency changes ($\ln d_r$ etc.) are independent random variables with unequal variances, so that
$\text{Var}(\ln d_r) = v_r$, $\text{Var}(\ln d_s) = v_s$ and $v_r \neq v_s$ for $r \neq s$.

Then, by the usual laws of expectation,

$$\text{Var}(y_i) = \text{Var}(\ln d_r - \ln d_s) = v_r + v_s$$

and there will be a non-zero covariance between any y_i and y_j which both depend upon a shared $\ln d_r$ term. Thus, for example, if $y_1 = \ln d_1 - \ln d_2$ and $y_2 = \ln d_1 - \ln d_3$, it is found that $\text{Cov}(y_1, y_2) = v_1$.

These considerations allow the random error ϖ_i to be defined

in more detail. It is assumed that the ϖ_i terms form a column vector ϖ such that $E(\varpi) = 0$ and $E(\varpi \varpi^t) = \sigma^2 \Omega$, where

$$\Omega = \begin{bmatrix} v_1+v_2 & v_1 & . & . & v_1 \\ v_1 & v_1+v_3 & . & . & v_1 \\ . & . & . & . & . \\ . & . & . & . & . \\ v_1 & v_1 & . & . & v_1+v_n \end{bmatrix} \qquad (3.13)$$

Estimation of the v_r terms poses considerable difficulties, but a reasonable assumption is that, to a first approximation,

$$v_r = r \qquad \text{for } r=1 \text{ to } m, \qquad (3.14)$$

so that the uncertainty about the frequency change at any particular mode is directly proportional to the number of the mode. In other words, changes at lower modes are observed more accurately than those at higher modes.

$$\Omega = \begin{bmatrix} 3 & 1 & . & . & . & 1 \\ 1 & 4 & . & . & . & 1 \\ . & . & . & . & . & . \\ . & . & . & . & . & . \\ . & . & . & . & . & . \\ 1 & 1 & . & . & . & n+2 \end{bmatrix} \qquad (3.15)$$

The logarithmic transformation of the ratios of frequency changes introduces a slight problem in that, in a few cases, small negative changes may be encountered, and these have

complex logarithms. When a negative change occurs, it has been treated as a positive change equal to one-thousandth of the smallest actual positive change.

Now is the time to apply the GLS theory from Appendix 1. Using the assumed form of Ω , y_i and x_i are transformed to η_i and ξ_i , then $100R^2$ is calculated for each theoretical failure position p. The p which corresponds to the highest $100R^2$ is then the most likely position for the actual failure. Using the sampling theory of R^2, one can assess the significance of the result, because the values of $100R^2$ which occur with known probalities are known for various values of n (=m-1). The criterion for a best choice of failure position is thus on a known absolute scale, rather than the somewhat imprecise relative scale of the Cawley-Adams normalised percentage error.

3.7 INDICATION OF THE SEVERITY OF THE DAMAGE.

The size of the frequency changes due to damage can be related to the severity of the damage. Comparisons were made between the measured frequency changes in a given mode and those given by the theoretical frequency changes for a certain reduction in stiffness at the predicted damage site. An indication of the severity of the damage was given in terms of the size of a reduction in stiffness which was equivalent to the damage.

Using this method, an outline of the severity of the damage is illustrated. For example, if the model of damage used in the tests on the structure was a spring, a local decrease in stiffness of the structure would be produced. Hence, the theoretical changes in frequencies due to a change in the stiffness of the spring model are calculated. Then a comparison between these theoretical frequency changes and the experimental frequency changes are made. If these changes are equal, then this may give an indication of the damage size related to that spring stiffness. If any other damage model were to be considered, as explained in section (3.4), then the same procedure may be applied.

This method gave a useful indication of the severity of the damage. It can be verified from the results obtained that the predicted severity always increases as the amount of damage is increased.

3.8 IMPLEMENTATION OF THE DEFECT LOCATION PROGRAM.

3.8.1 Introduction.

The defect location programs were based in the analysis given in sections 3.5 and 3.6 respectively. The work implemented in the defect location program required the statistical method to be used in order to locate the damage. Theoretical changes in natural frequencies, together with the experimental measurements were then used as inputs to the program which

computed the relative errors and produced a defect location chart.

Extensive computational effort was required in performing the dynamic analysis of the structure, but this only needed to be performed once for a given type of structure.

The programs were written to run on the Hewlett-Packard HP9845B desk-top computer. The machine has a read/write memory (RAM) of 187 Kbytes available for program and data use, with mass storage provided by two cartridges of .2 Mbyte each and a single flexible disc unit of .5 Mbyte storage capacity. The graphics capabilities allowed outputs to a visual display unit, a Benson 1301 incremental plotter and a HP9872A plotter. This computer was equipped with a BASIC language processor, and therefore the programs required were written in this language. All calculations were performed with 12-digit precision.

The following sections will discuss the rules which must be followed in order to produce the defect location chart. The first section concerns the input data and the last section provides the details of the individual programs and their algorithms, with a view to emphasising the program structure.

For a complete documentation, the listings of the programs are provided in Appendix 2.

3.8.2 Presentation of Input Data.

The input data to the program is divided under three headings:

(I) Theoretical Data.

For the modes of interest it is necessary to calculate the changes in natural frequencies arising from damage to the structure. This data was generated and stored on the disc by the dynamic analysis program, which will be described in detail in the following chapters. This data was in the matrix form and was dependent on the number of elements and the number of modes considered. The file name of the above data must be borne in mind when the defect location program is to be used.

(II) Experimental Data.

Here, for the mode which is of interest, the concern is with the observed changes in natural frequencies due to damage at an unknown position. The number of changes must be at least two for the Cawley-Adams method or four for the present new method, and not greater than the number of frequencies which are calculated in (I). The user must provide this input data via the key board, as requested by the computer.

It is not necessary for the experimental changes in frequencies to be obtained for all the corresponding

theoretical changes, but at least two or four modes of experimental changes in the natural frequencies must be found. So that we have $n \geq 3$ in applying the GLS regression theory. If n=2, the regression line is bound to be a perfect fit, giving R^2 =1 for every p, so it would not be possible to discriminate between possible failure positions.

(III) Plotting Data.

The defect location chart consisted of a plot of the undeflected structure on which the elements were labelled with their normalised percentage error (NPE) or their $100R^2$, for the new method. In either case, the higher numbers indicated most likely damage positions. The plotting data consisted of the geometry of the structure and the topology, including the element connections in which the two nodal numbers associated with each element were given.

This data was already stored by the dynamic analysis program under the same filename which has been mentioned in (I). In both the plane and space frame structures, all the data was implemented from the plane and space frame programs respectively, and will be dealt with later in this thesis.

3.8.3 Description of Programs.

Referring to Fig. 3.1, the computer programs "PFDELO", "SFDELO" and "SPGLS", acronyms for "Plane Frame Defect Location", "Space Frame Defect Location" and "Space and Plane

Generalised Least Square method" respectively, were developed to determine the defect location chart.

The program "START2" shown in Fig. 3.1 begins with an identification of the solution type, method 1 or method 2. Method 1 is based on the Cawley-Adams method as described in sections 3.3 and 3.5. Method 2 represents the new proposed method described in section 3.6. On identification of the solution of method 1, execution proceeds to identify the structure type: plane or space frame. For a plane frame, program "PFDELO" is loaded, and for the space frame program "SFDELO". A similar branching occurs on identification of the solution of method 2: for plane or space frame, program "SPGLS" is loaded.

These programs require the necessary data for the drawing of the defect location chart, including, as it does, a line diagram of the undeflected structure. In order to use this data the programs must have access to a file stored on the disc, in which the calculated predicted changes in frequencies are stored.

The number of changes in frequencies could be chosen according to the requirements of the defect location analysis. In this case, it is not true that all calculated frequency changes should be used, and that it depends on the number of measured changes in natural frequency. If the structure is symmetrical, two or more sites will be predicted, the number depending on the degree of geometric

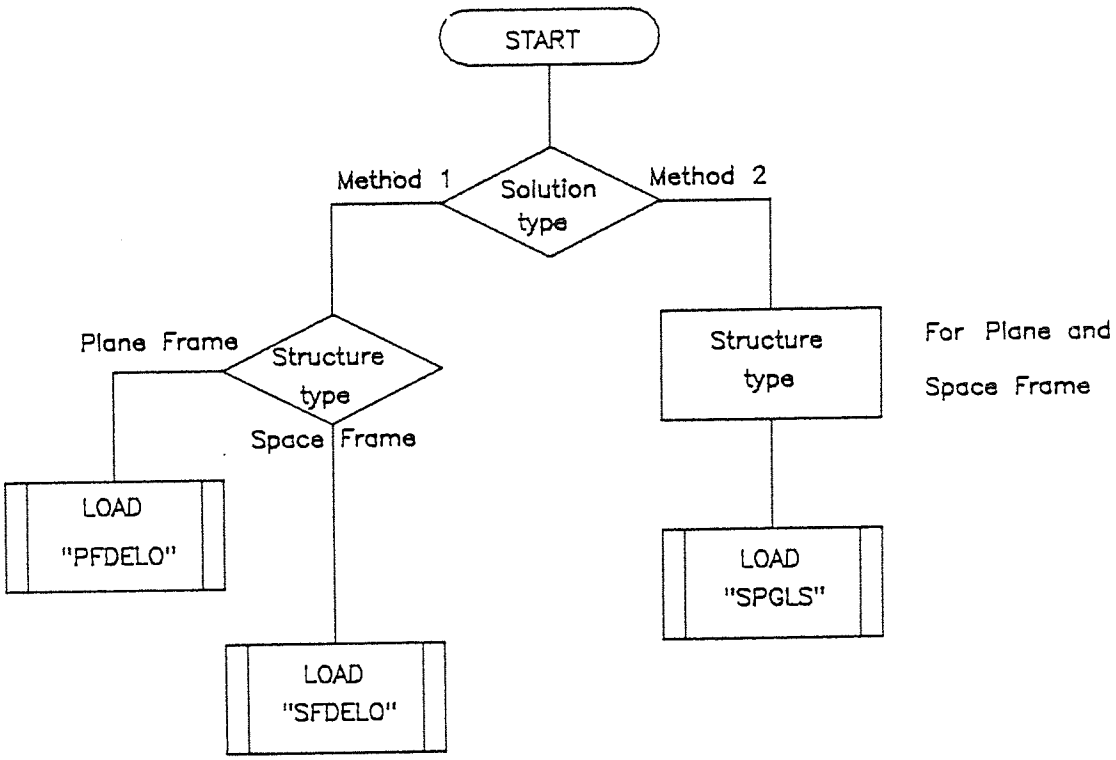

Method 1 The Cawley – Adams Method (see Section 3.5)

Method 2 The New Proposed Method (see Section 3.6)

FIG. (3.1) FLOW CHART OF PROGRAM "START2"

symmetry.

The computer programs are able automatically to check all modes by computing the results firstly with all the modes and then with each mode neglected in turn. The technique uses the fact that if one mode was causing errors in the final results while the other modes gave correct results, removing this mode would tend to make the damage site more clearly defined on the location chart.

Possible errors which could have arisen were:

(I) If the model of damage was not good enough to predict the frequency change accurately.

(II) If the experimental results were interpreted incorrectly. For example, if a pair of very close resonances were not noticed, then every mode of vibration above the pair of close resonances would be incorrectly identified, as shown in Fig. 3.2. With care, this error should not be made, particularly as a theoretical analysis of the structure will have already been made, helping to identify the likely location of the modes of vibration.

With reference to the flow charts, as illustrated in Figures (3.3) and (3.4), the main steps in the program are listed below:

(1) Dimension of arrays and variables and the input of the title of the problem are required.

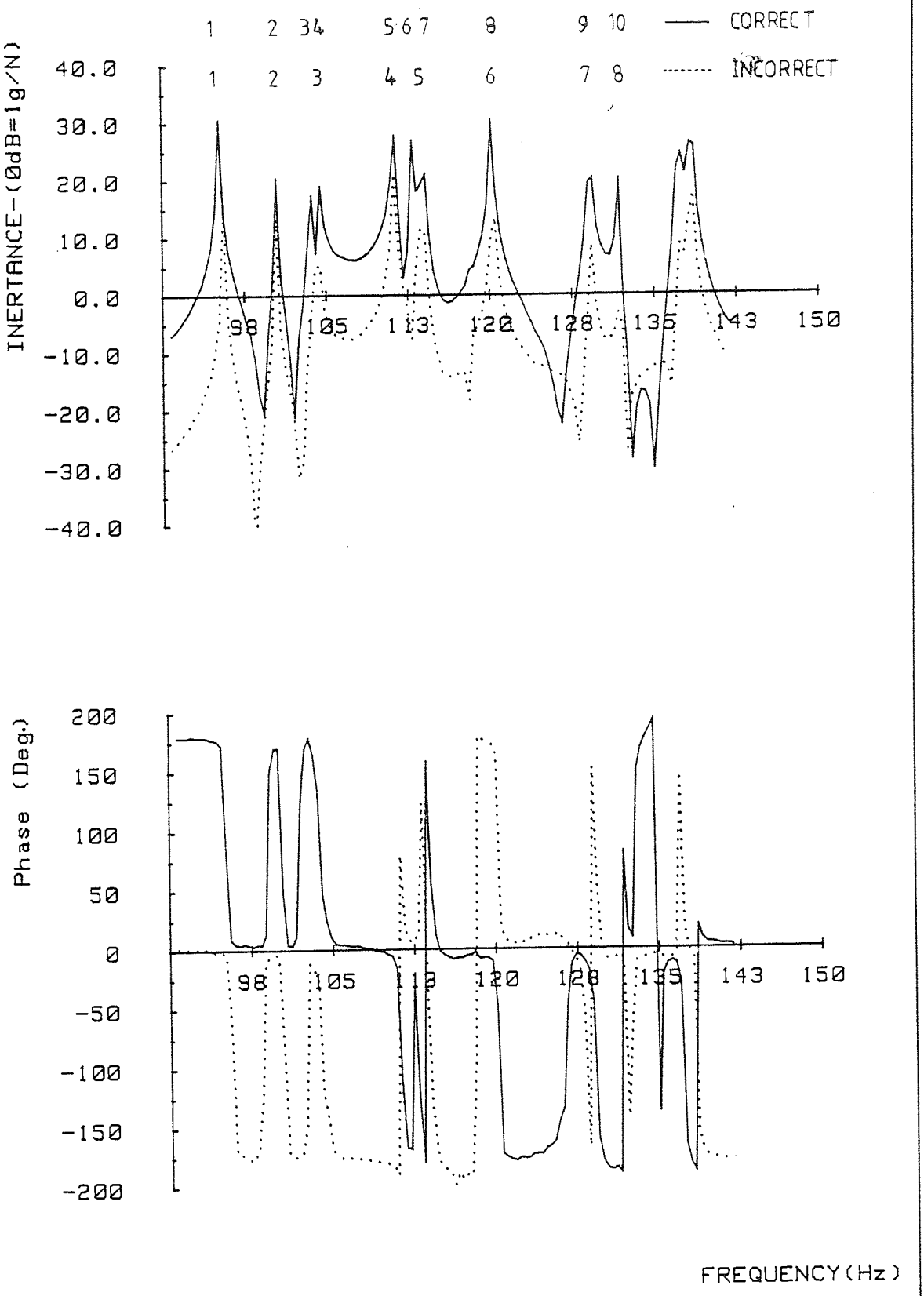

Fig.3.2 SHOWS THE INERTANCE PLOT FOR CLOSE RESONANCES

(2) Two groups of input data are read:

(i) Changes in frequencies for which the analysis will be done.

(ii) Data for plotting the undeflected structure.

(3) The desired number of measured frequencies and also the measured reduction in natural frequencies are input.

(4) A loop is set for the number of modes to be considered. For details of the execution of the algorithm for generating the defect location analysis, see Fig. (3.4).

(5) The method of defect location does not tolerate any mode changes equal to zero, if these modes are considered, then zero or negative changes are therefore set equal to 1/1000 of the minimum non-zero positive change, but if these modes are not required then it is necessary to proceed to the next mode.

(6) The error is calculated by using pairs of changes in frequencies for all modes. The total error is calculated by assuming a defect to be in a certain element. Total errors equal to zero are therefore made to 1/1000 of the minimum non-zero total error.

(7) The NPE is calculated which is an inverted and normalized value of the total error.

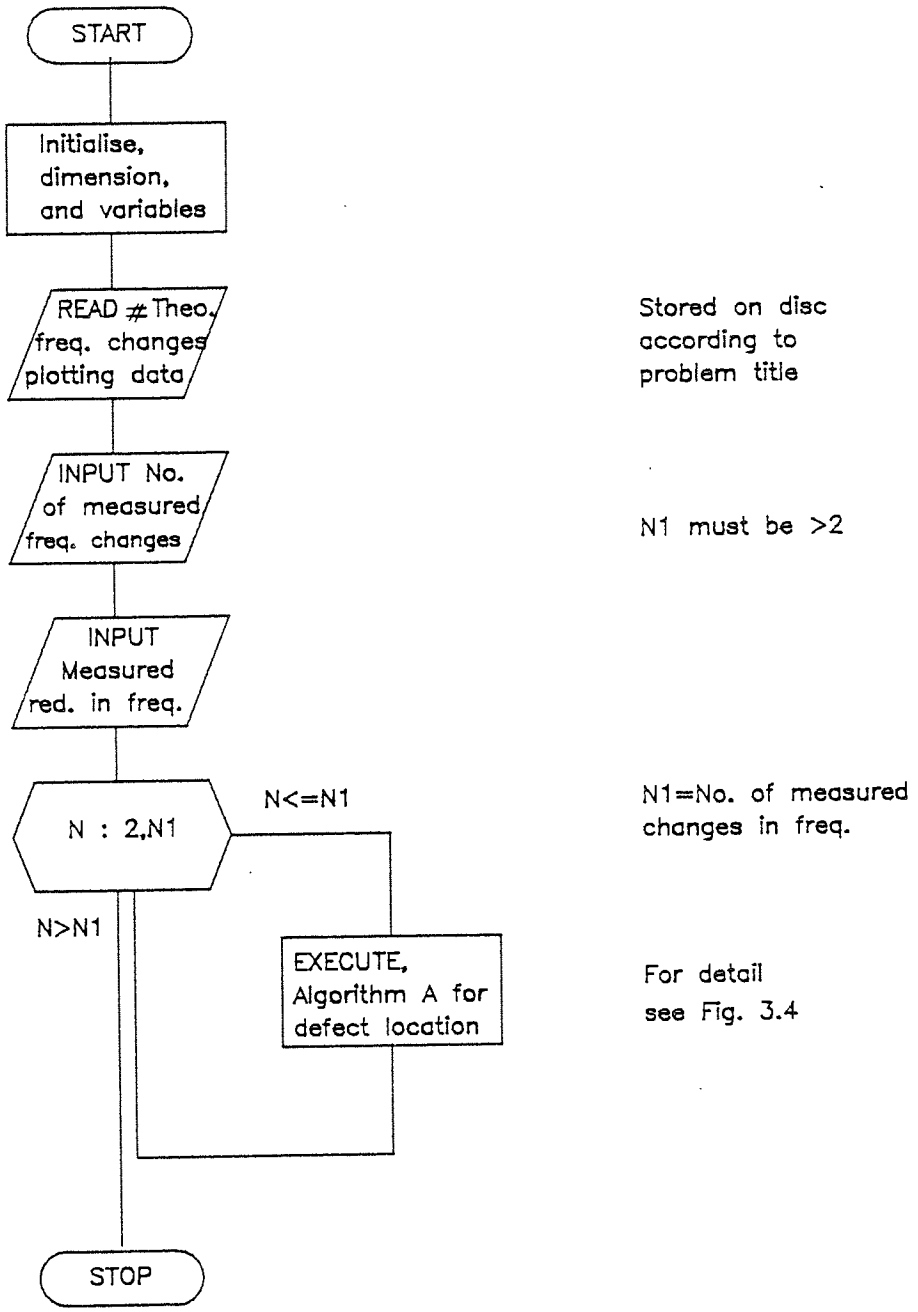

Fig. 3.3 FLOW CHART FOR DEFECT LOCATION OF PLANE AND SPACE FRAMES

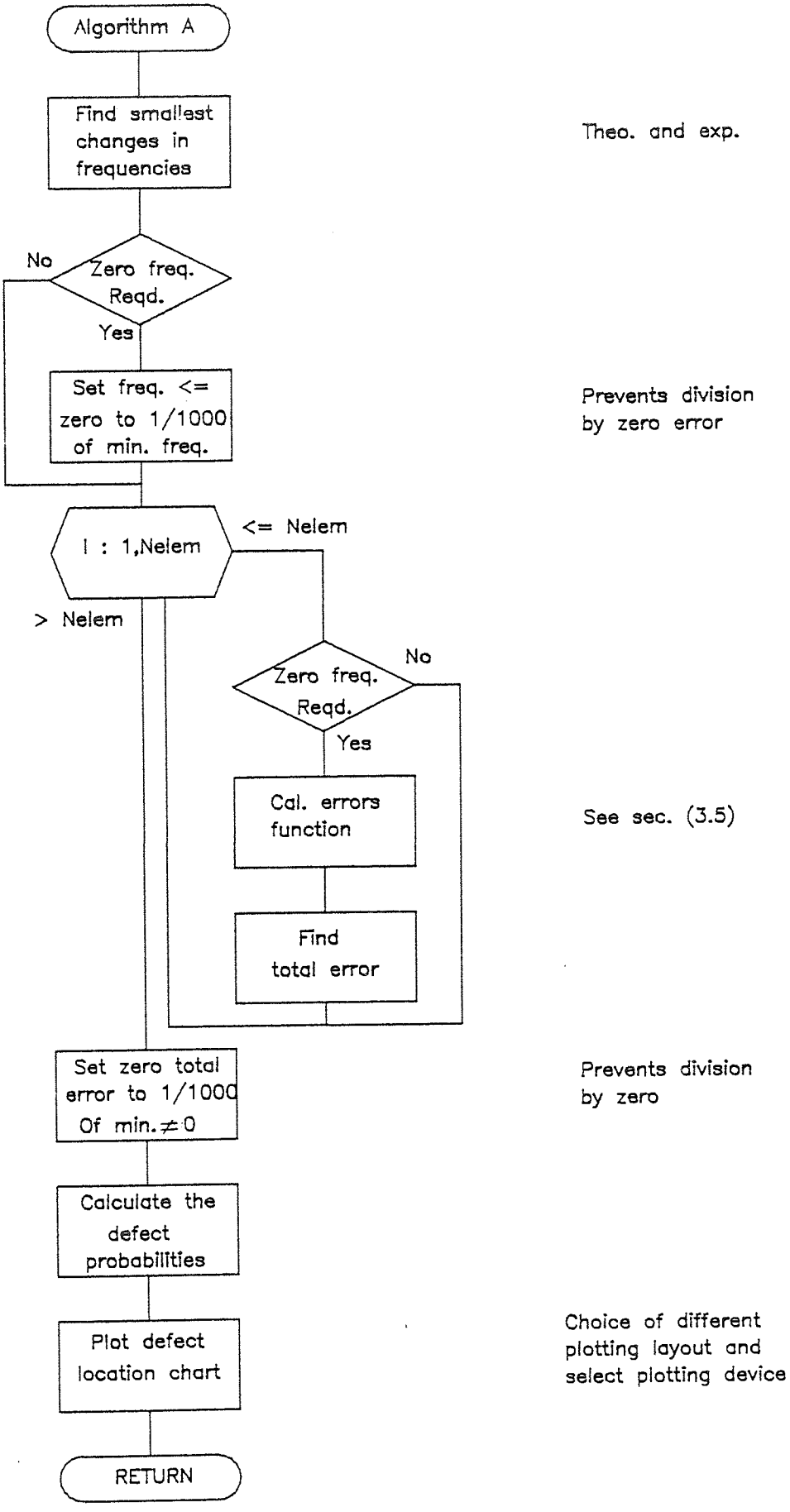

FIG. 3.4 FLOW CHART OF "ALGORITHM A" FOR DEFECT LOCATION

(8) Finally, the defect location chart is plotted. A choice of plotting layout and plotting device is given.

All input data to the programs should be in a consistent set of units.

With reference to the flow chart, see Fig. 3.5, the main steps in the program are listed below. The first five steps are the same as mentioned above with the exception of step 4.

5- The Log ratio of changes in frequencies are calculated, see equation (3.12).

6- The transformation matrix is calculated, see Appendix 1.

7- The Coefficient of determination $100R^2$ with and without β_o is calculated.

8- Steps 1 to 7 are repeated for each element in turn and the results are printed. Then a choice for plotting the defect location charts is given.

9- If a new mode is required, return to step 5 and proceed.

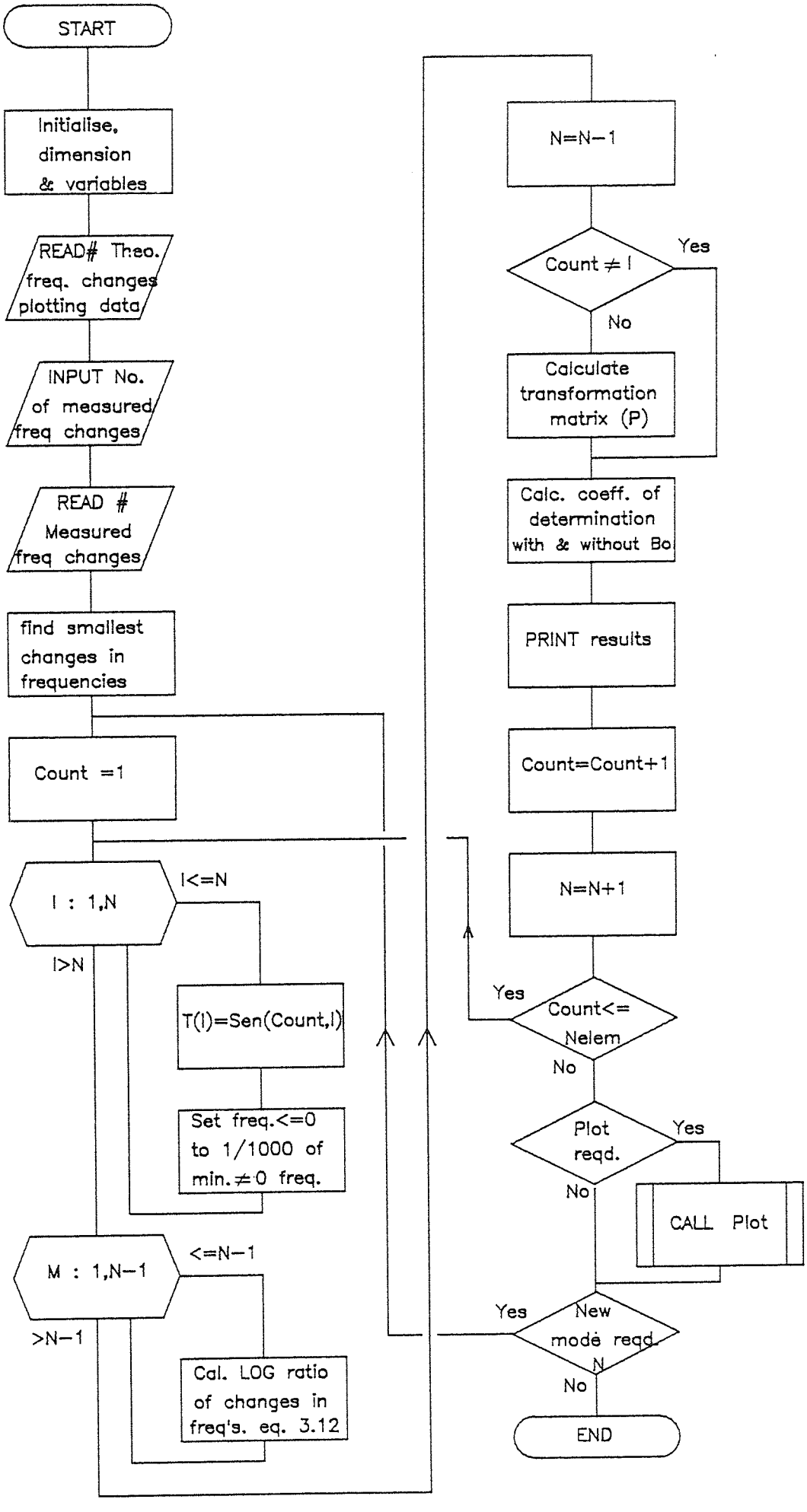

FIG. 3.5 FLOW CHART OF PROGRAM "SPGLS"

3.9 CLOSING REMARKS.

In the present work, the method used for locating damage in structural member required both the measured and theoretical frequency changes in the modes of interest. Four damage models were used for computing the pattern of the theoretical changes in frequencies. A comparison was then made of two statistical methods which were used to analyse these changes and to predict the most likely damage sites.

The statistical methods can be used to detect and locate damage without the need for physically examining the structure in a piece-wise manner. Computer programs were developed for applying these techniques to plane and space frames. The programs were constructed as a package to be used on a microcomputer.

It is concluded that there is no reason why this method should not be applied to a structure in practice. Also, the structure must be excited sufficiently for at least the first two or four natural frequencies in order to use either the Cawley-Adams or the new method respectively.

In the next chapter, a brief description is given of the dynamic analysis technique based on the finite element method, which was used in order to find accurate theoretical values of the changes in natural frequencies.

CHAPTER FOUR

FINITE ELEMENT ANALYSIS USING THE POLYNOMIAL DISPLACEMENT FUNCTION

4.1 INTRODUCTION.

As already discussed in the preceding chapter, the defect location method requires a knowledge of the theoretical changes in natural frequencies of a structure caused by hypothetical defects. These changes can be obtained from a detailed dynamic analysis of the structure.

A structure cannot be analysed dynamically as a whole due to its irregular shape. It is modelled by considering it as being built up of regular discrete elements consisting of rigidly or flexibly connected simple beams. In dealing with the treatment of structures as assemblages of beams, the individual behaviour of each element needs to be understood.

Finite element methods (FEM), which originated in the field of structural analysis, are firmly establised in civil engineering and widely used by mechanical engineers for the vibration analysis. A vast number of papers and books have been written on this subject, see Zienkiewicz (25,26).

The finite element method may be viewed as a piecewise Ritz method. It is preferable to other numerical methods (e.g. the finite difference method) when analysing the structural frame because of its versatility and flexibility of use. The application of the finite element method to frame vibration involves imagining the frame to be actually divided into a finite number of elements of finite (but not necessarily equal) length, and connected with each other through nodal

points. This concept has given rise to the name "the finite element method". The versatility of the method means that variations in element length can be taken into account easily without any additional difficulty.

The displacement function within each element must be assumed to have a suitable form and then the strain and kinetic energy of the element may be computed. Summation over all the elements yields the total energy of the whole structure. The assumed functions are frequently of a polynomial form which is chosen because of the ease with which the mathematics can be manipulated when formulating the equation of motion. In the case of dynamic analysis, this formulation leads conveniently to a linear eigenvalue problem (EVP), see (27,28), with which this chapter is concerned.

However, for the purposes of dynamic analysis an alternative is to use the exact displacement functions arising from the solution of the governing differential equations for beam vibration. As will be seen in the next chapter this approach offers certain advantages but has the disadvantage of leading to a non-linear EVP.

The solution of the linear EVP can be found by using well known techniques such as the QL-algorithm or Sturm´s sequence with bisection (29,30,31). The accuracy of the finite element model is improved by increasing the number of elements per member. A sufficient number of elements must be used in order to obtain an acceptable representation of the behaviour of

the structure under consideration. With the advent of high-speed electronic digital computers, the emphasis in engineering analysis has moved towards the development of versatile methods of evaluation which now enable structural engineers to use matrix algebra to examine problems which would otherwise be too large to tackle. Matrix based structural analysis is suitable for the use of routine methods of data preparation and standard programming techniques for computer solution.

Advantages of the finite element method include the ability to deal with structures with arbitary loading, including support conditions, and also the ability to model structures of arbitrary geometry. A further advantage of this method can be to model composite structures comprising of different structural components.

When the finite element method is employed, two stages must be considered. The first requires study of the individual elements into which the system is divided, while the second involves studying the assemblage of elements which represent the entire system. Thus, the outline of the finite element process may be summarized into five essential steps (32), which are as follows.

(I) Definition of the Finite Element Mesh.

The first step involves the process of discretising the structure into appropriate sub-regions.

(II) Selection of displacement models.

In this process, a suitable displacement function must be selected for a typical element which would lead to a finite number of degrees of freedom and would satisfy the boundary conditions of the system. In order to retain the bounding and convergance properties inherent in the Ritz procedure, it is necessary that the element interpolation functions should include the rigid body displacements and uniform strain states, and that they maintain displacement compatibility along the inter element and exterior boundaries.

(III) Formulating the discrete stiffness equation or equations of motion.

The strains at any point within the element may be expressed in terms of the element nodal displacements. The static equations of equilibrium can be obtained by using the principle of stationary total potential energy whereas the dynamic equations of motion are obtained by using Hamilton's principle.

(IV) Solution of the stiffness equation or the equations of motion.

The solution of stiffness equations lead to a set of simultaneous equations whereas the equations of motion in the free vibration case lead to an eigenvalue problem.

(V) Determination of the desired properties.

Once the nodal displacements have been determined, strain and stress can be calculated from the strain-displacement relationship and by Hooks law, respectively. The natural frequencies and mode shapes are then obtained by evaluating the eigenvalue problem.

The finite element method applied to vibration problems is now becoming well-known and the study of the vibrational behaviour of plane and space frame structures is assuming greater importance. One of the objectives of this thesis is to examine the potential for applying these techniques to the condition monitoring of complex and costly structures.

4.2 APPLICATION OF F.E.M. TO SPACE FRAME VIBRATION PROBLEMS.

4.2.1 Stiffness and Mass Matrices for a Beam Element.

In the analysis of frame structures it is assumed that the structure is composed of discrete members, as shown in Fig. (4.1a). In this respect, each of the constituent members is regarded as a beam, and so the beam theories of bending and torsion (33) apply. The effects of shear deformation and rotary inertia are neglected.

The simplest one-dimensional element is a uniform, straight beam. Such an element has been used when analyzing the space frame structure, as shown in Fig. (4.1c). For the convenience of computation, the local coordinate axes are chosen to be coincident with the principal axes of the beam, so that the centroid of the cross-sectional area is on the x-axis.

Four types of vibration for this simple element exist, namely, longitudinal vibration in x-direction, torsional vibration along the beam, flexural vibration in the xy-plane and flexural vibration in the xz-plane. Thus, it is possible to construct stiffness and mass matrices for the beam element from the submatrices arising from the longitudinal, torsional and flexural vibration equations. The stiffness and mass matrices are of order 12*12 for each element of the beam (34). In order to define the motion of the structure it would be necessary to establish the nodal displacements associated with all these elements. The total number of these nodal

displacements represents the number of degrees of freedom of the system which comprise:

(I) Axial displacements dx_1, dx_2

(II) Transverse displacements dy_1, dz_1, dy_2, dz_2

(III) Torsional angles θx_1, θx_2

(IV) Bending angles θy_1, θz_1, θy_2, θz_2

The positive direction of these displacements corresponds to the positive directions of the beam element axes and rotation shown in Fig. (4.1b), which are positioned at node 1, of Fig. (4.1c). The suitable polynomial displacement function for a one-dimensional element is of the form,

$$U^e(x) = \sum_{i=1}^{N} a_i * x^{i-1} \qquad (4.1)$$

where: a_i are arbitrary constant coefficients,

N the number of degrees of freedom.

The procedure involved in finding the beam element stiffness and mass matrices in tension, torsion and bending is as follows;

(I) Beam element in tension:

From equation (4.1), since the beam element in tension has two degrees of freedom, so the approximating function for the element displacement is represented as:

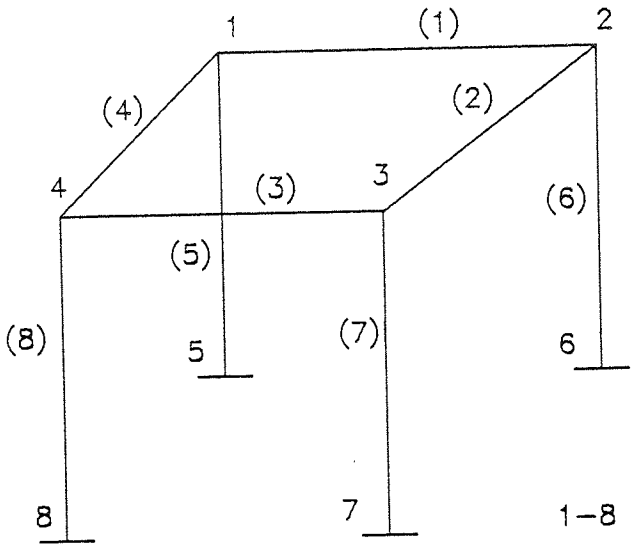

1–8 Represents node number

(1)–(8) Represents element No.

(a) Space Frame Structure

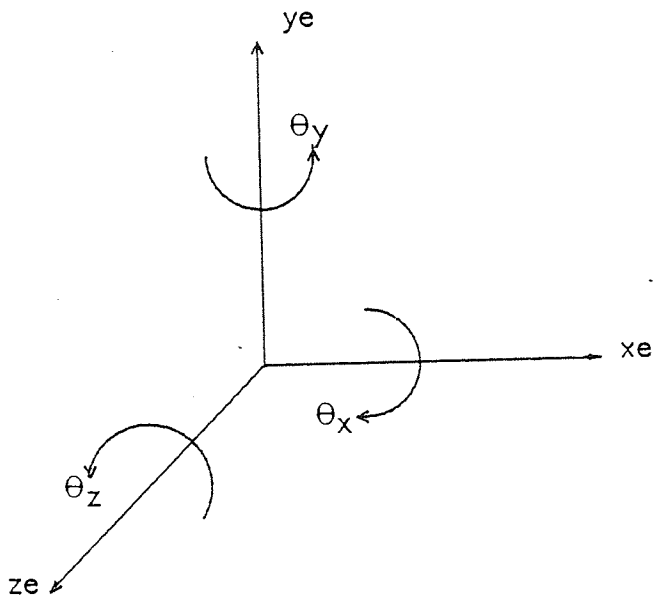

(b) Beam element axes

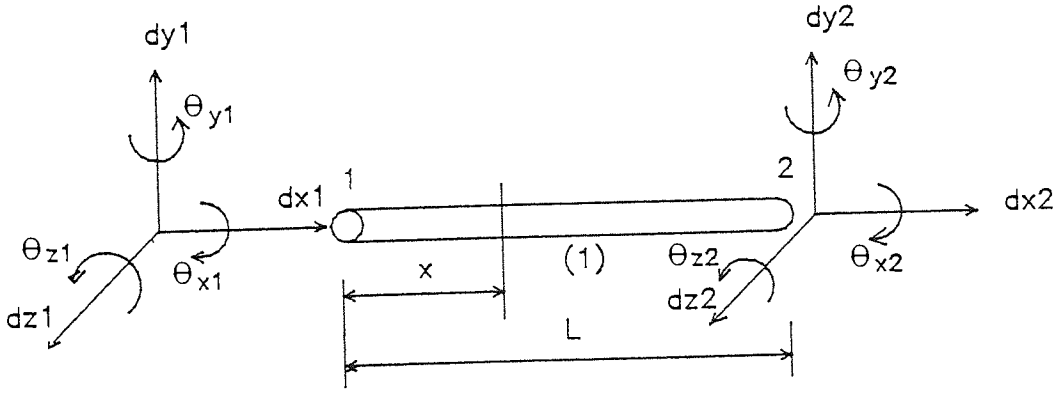

(c) Typical One–Dimensional Element

FIG. (4.1) ONE–DIMENSIONAL FINITE ELEMENT BEAM

$$U^e(x) = a_1 + a_2 x$$
$$= [f(x)]\ \{a\} \qquad (4.2)$$

By substituting the boundary conditions, x=0 for node 1 and x=L for node 2 in turn, into equation (4.2), we have

$$U^e(x) = (1 - x/L).dx_1 + x/L\ dx_2$$
$$= [(1 - x/L) \quad x/L] \cdot \begin{Bmatrix} dx_1 \\ \\ dx_2 \end{Bmatrix}$$
$$= [N_1(x)] \cdot \{d\}^e_o \qquad (4.3)$$

$[N_1(x)]$ is called the shape function for a beam in tension. $\{d\}^e_o$ is a vector of element nodal displacement.

For the whole element, e, the strain energy stored is

$$U^e = 1/2 \int_o^L \{\varepsilon\}^{e^t} [EA]\ \{\varepsilon\}^e dx \qquad (4.4)$$

where EA is the extensional rigidity.

The strains at any point within the element may be expressed in terms of the nodal displacements and can be found by a suitable differentiation of the displacements defined by equation (4.3), so that

$$\{\varepsilon\}^e = [\partial]\ [N_1(x)]\ \{d\}^e_o = [B]\ \{d\}^e_o \qquad (4.5)$$

where $\{\varepsilon\}^e$ is the element strain vector;

$[\partial]$ is a matrix of differential operators, and

$[B]$ contains appropriate derivatives of $[N_1(x)]$.

Hence

$$U^e = 1/2\ \{d\}_o^{e\,t} \left(\int_o^L [B]^t [EA]\ [B]\ dx \right) \{d\}_o^e \qquad (4.6)$$

which after manipulation, yields

$$U^e = 1/2\ \{d\}_o^{e\,t} EA/L \begin{bmatrix} 1 & -1 \\ & \\ -1 & 1 \end{bmatrix} \{d\}_o^e$$

$$= 1/2\ \{d\}_o^{e\,t} [K_1]^e \{d\}_o^e \qquad (4.7)$$

where $[K_1]^e$ is called the element stiffness submatrix for a beam in tension.

$$[K_1]^e = EA/L \begin{bmatrix} 1 & -1 \\ & \\ -1 & 1 \end{bmatrix} \qquad (4.8)$$

The kinetic energy of the element is given by integrating the triple matrix product $[N_1(x)]^t[\rho A]\ [N_1(x)]$, where ρ is the density of the material and A the cross sectional area. Then

$$T^e = 1/2 \int_o^L \{\dot{d}\}_o^{e\,t} [N_1(x)]^t [\rho\ A]\ [N_1(x)]\ \{\dot{d}\}_o^e\ dx$$

$$= 1/2\ \{\dot{d}\}_o^e [m_1]^e \{\dot{d}\}_o^e \qquad (4.9)$$

where $[m_1]^e$ is the element mass submatrix for a beam in tension. After carrying out the integration, equation (4.9) yields:

$$[m_1]^e = mL/6 \begin{bmatrix} 2 & 1 \\ 1 & 2 \end{bmatrix} \qquad (4.10)$$

where m is the mass per unit length.

(II) Beam element in torsion.

In the torsional vibration the nodal displacements can undergo rotations (θx_1 & θx_2) corresponding to twisting moments, each one having two degrees of freedom. The same procedure is followed as already described in (I) above. The strain energy U^e stored in a typical element is obtained by integrating the triple matrix product $\int_o^L [B]^t [GJ] [B]$ leading to

$$U^e = 1/2 \quad \{d\}_o^{e\,t} [K_2]^e \{d\}_o^e \qquad (4.11)$$

where GJ is the torsional rigidity of the beam cross section and $[K_2]^e$ is termed the element stiffness submatrix for the beam in torsion and is given by

$$[K_2]^e = GJ/L \begin{bmatrix} 1 & -1 \\ -1 & 1 \end{bmatrix} \qquad (4.12)$$

The kinetic energy of the element is found by integrating the triple matrix product $[N_2(x)]^t [\rho Jx] [N_2(x)]$, where Jx is the mass polar moment of inertia and $[N_2(x)]$ is the shape function for a beam in torsion, and after manipulation, the element mass submatrix is given by

$$[m_2]^e = mLJx/6A \begin{bmatrix} 2 & 1 \\ 1 & 2 \end{bmatrix} \qquad (4.13)$$

(III) Beam element in bending in the $(x_e\text{-}y_e)$ plane.

In this case, the nodal displacements can undergo both translation and rotational displacements at nodes 1 and 2 (dy_1, θ_{z_1} and dy_2, θ_{z_2}) respectively. The element must therefore have four degrees of freedom, see Fig. (4.1c). Since the number of terms in the chosen displacement model must equal the total number of degrees of freedom, (32), a suitable function is

$$U^e(x) = a_5 + a_6 x + a_7 x^2 + a_8 x^3$$
$$= [f(x)] \{a\} \qquad (4.14)$$

Proceeding as before

$$U^e(x) = [N_3(x)] \{d\}_o^e \qquad (4.15)$$

where $[N_3(x)]$ is the shape function for beams in bending in the $(x_e\text{-}y_e)$ plane.

The strain energy stored in an element is given by:

$$U^e = 1/2 \int_0^L EI_z \, (U^{e''}(x))^2 \, dx \qquad (4.16)$$

$$\text{where } U^{e''}(x) = [N_3''(x)] \{d\}_o^e = [B] \{d\}_o^e \qquad (4.17)$$

and EI_z is the flexural rigidity.

The element stiffness submatrix for beam elements bending in the $(x_e - y_e)$ plane is obtained from considering the strain energy in a typical element, and after carrying out matrix multiplication and the integration as before, is found to be

$$[K_3]^e = EI_z/L^3 \begin{bmatrix} 12 & 6L & -12 & 6L \\ & 4L^2 & -6L & 2L^2 \\ \text{Symm.} & & 12 & -6L \\ & & & 4L^2 \end{bmatrix} \qquad (4.18)$$

From the kinetic energy of an element the mass submatrix $[m_3]^e$ becomes:

$$[m_3]^e = mL/420 \begin{bmatrix} 156 & 22L & 54 & -13L \\ & 4L^2 & 13L & -3L^2 \\ \text{Symm.} & & 156 & -22L \\ & & & 4L^2 \end{bmatrix} \qquad (4.19)$$

(IV) Beam element in bending in the x_e-z_e plane.

In this case, the nodal displacements can undergo both translation and rotational displacements viz, dz_1, θy_1 and dz_2, θy_2 for nodes 1 & 2 respectively. By applying the same principles as before for strain and kinetic energies, the element stiffness and mass submatrices are respectively given as;

$$[K_4]^e = EI_y/L^3 \begin{bmatrix} 12 & 6L & -12 & 6L \\ & 4L^2 & -6L & 2L^2 \\ & \text{Symm.} & 12 & -6L \\ & & & 4L^2 \end{bmatrix} \qquad (4.20)$$

and

$$[m_4]^e = mL/420 \begin{bmatrix} 156 & 22L & 54 & -13L \\ & 4L^2 & 13L & -3L^2 \\ & \text{Symm.} & 156 & -22L \\ & & & 4L^2 \end{bmatrix} \qquad (4.21)$$

The displacement models, the stiffness and mass matrices associated with axial, torsional and bending loadings of an element have been presented separately. In three dimensional analysis the beam element will have 12 degrees of freedom, six at each node, as shown in Fig. (4.1c). Consequently, the three dimensional element stiffness and mass matrices in local coordinates will be denoted by assembling the element submatrices $[K_1]^e$ to $[K_4]^e$ and $[m_1]^e$ to $[m_4]^e$ in the order of the displacement shown in Fig. (4.1c).

The element stiffness matrix $[K]^e$ is given by equation (4.22) below;

$$
\begin{bmatrix}
\frac{EA}{L} & 0 & 0 & 0 & 0 & 0 & -\frac{EA}{L} & 0 & 0 & 0 & 0 & 0 \\
 & \frac{12EI_z}{L^3} & 0 & 0 & 0 & \frac{6EI_z}{L^2} & 0 & -\frac{12EI_z}{L^3} & 0 & 0 & 0 & \frac{6EI_z}{L^2} \\
 & & \frac{12EI_y}{L^3} & 0 & -\frac{6EI_y}{L^2} & 0 & 0 & 0 & -\frac{12EI_y}{L^3} & 0 & -\frac{6EI_y}{L^2} & 0 \\
 & & & \frac{GJ}{L} & 0 & 0 & 0 & 0 & 0 & -\frac{GJ}{L} & 0 & 0 \\
 & & & & \frac{4EI_y}{L} & 0 & 0 & 0 & \frac{6EI_y}{L^2} & 0 & \frac{2EI_y}{L} & 0 \\
 & & & & & \frac{4EI_z}{L} & 0 & -\frac{6EI_z}{L^2} & 0 & 0 & 0 & \frac{2EI_z}{L} \\
 & & & & & & \frac{EA}{L} & 0 & 0 & 0 & 0 & 0 \\
 & & & & & & & \frac{12EI_z}{L^3} & 0 & 0 & 0 & -\frac{6EI_z}{L^2} \\
 & & & & & & & & \frac{12EI_y}{L^3} & 0 & \frac{6EI_y}{L^2} & 0 \\
 & & & & & & & & & \frac{GJ}{L} & 0 & 0 \\
 & & & & & & & & & & \frac{4EI_y}{L} & 0 \\
 & & & & & & & & & & & \frac{4EI_z}{L}
\end{bmatrix}
$$

Symm.

Where: I_y & I_z Moment of inertia about y & z axes

A Cross sectional area,

E Young´s modulus of elasticity,

G Shear modulus of elasticity,

J Torsional constant.

The element mass matrix $[m]^e$ is given by equation (4.23) below:

$$\frac{mL}{420}\begin{bmatrix}
140 & 0 & 0 & 0 & 0 & 0 & 70 & 0 & 0 & 0 & 0 & 0 \\
 & 156 & 0 & 0 & 0 & 22L & 0 & 54 & 0 & 0 & 0 & -13L \\
 & & 156 & 0 & -22L & 0 & 0 & 0 & 54 & 0 & 13L & 0 \\
 & & & 140J' & 0 & 0 & 0 & 0 & 0 & 70J' & 0 & 0 \\
 & & & & 4L^2 & 0 & 0 & 0 & -13L & 0 & -3L^2 & 0 \\
 & & & & & 4L^2 & 0 & 13L & 0 & 0 & 0 & -3L^2 \\
 & & & & & & 140 & 0 & 0 & 0 & 0 & 0 \\
 & & & & & & & 156 & 0 & 0 & 0 & -22L \\
 & & & \text{Symm.} & & & & & 156 & 0 & 22L & 0 \\
 & & & & & & & & & 140J' & 0 & 0 \\
 & & & & & & & & & & 4L^2 & 0 \\
 & & & & & & & & & & & 4L^2
\end{bmatrix}$$

where:

m Mass per unit length

J´ Equal Jx/A

Jx Mass polar moment of inertia per unit length

4.2.2 TRANSFORMATION TO GLOBAL COORDINATES.

After calculating the stiffness and mass matrices, equations (4.22) and (4.23) respectively, for the individual elements into which the system is subdivided, particular reference is made to convenient local coordinates (x_e, y_e, z_e). However, before the assemblage [k] and [m] to the overall matrices, these matrices must be expressed in terms of the global coordinate system XYZ, see Fig. (4.2). This process of transformation from local to global coordinates is carried out through the transformation matrix [T] which consists of direction cosine submatrices [R] each 3*3. Since there are six nodal displacements at each node of the elements, see Fig. (4.1c), the matrix [T] is of the order 12*12 and expressed as

$$[T] = \begin{bmatrix} [R] & [0] & [0] & [0] \\ & [R] & [0] & [0] \\ \text{Symm.} & & [R] & [0] \\ & & & [R] \end{bmatrix} \qquad (4.24)$$

where [0] is a 3*3 zero matrix.

So, the element stiffness and mass matrices in global coordinates is given by,

$$[K]^e = [T]^t [K]^e [T] \qquad (4.25)$$

$$[m]^e = [T]^t [m]^e [T] \qquad (4.26)$$

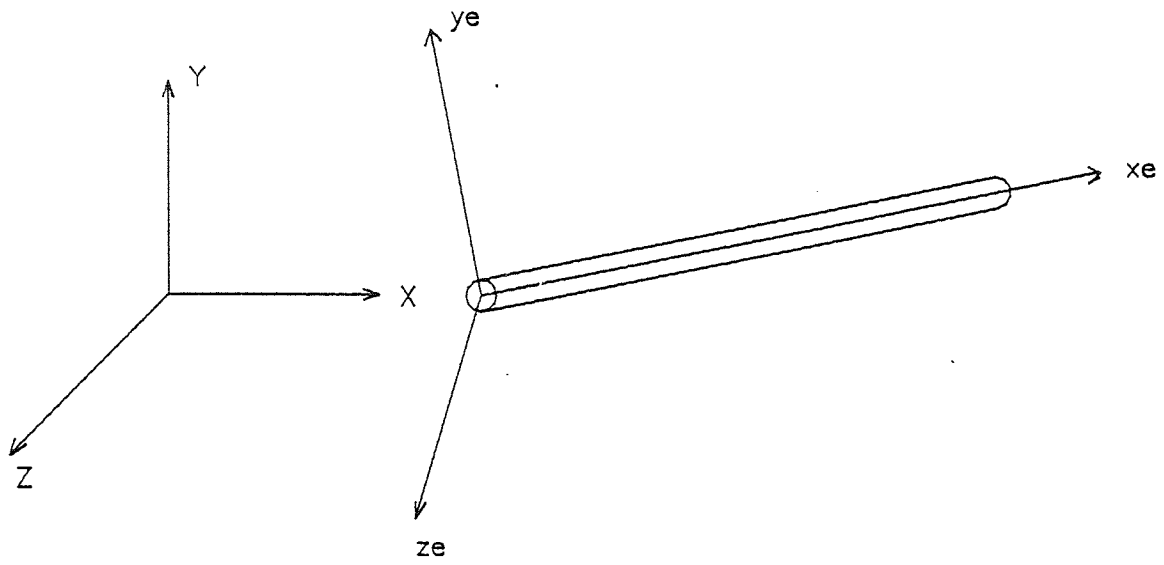

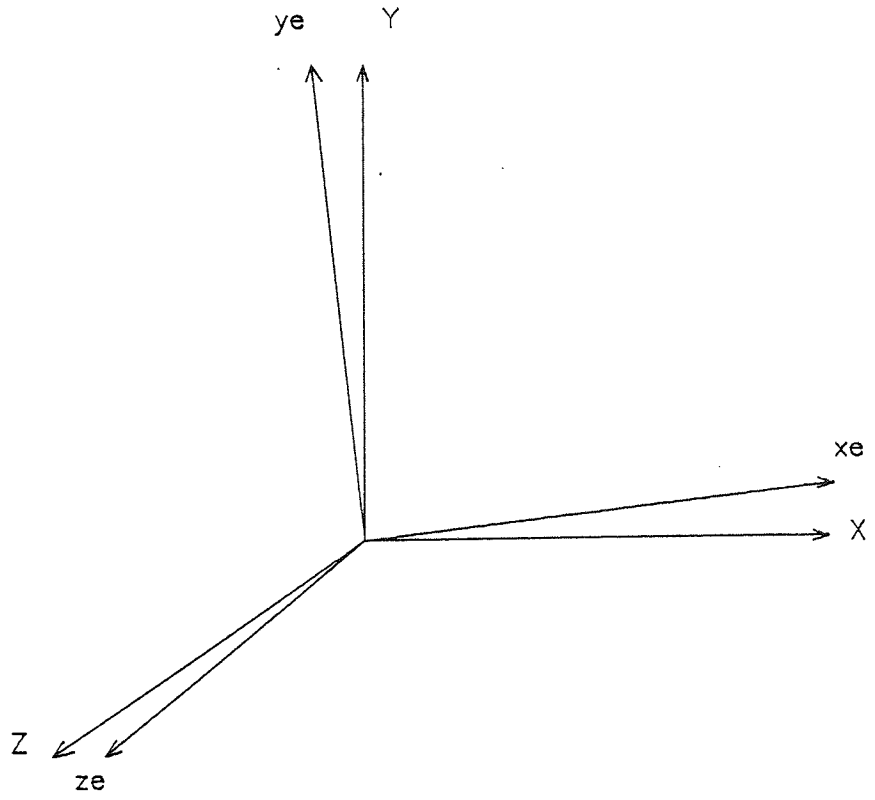

Where :

X,Y,Z	Refer to Global or Frame Coordinate
xe,ye,ze	Refer to Local Coordinate

FIG. (4.2) LOCAL AND GLOBAL COORDINATE SYSTEM

For a space frame member, the form of the rotation matrix [R] depends upon the particular orientation of the member axes. It is convenient to set up the matrix [R] in terms of the projections of the beam element on the structure axes. This is performed by imagining the beam element to be lying initially in the X-direction with its y_e and z_e axes coinciding with Y and Z axes. Three rotations are carried out to bring the element to its final position and the matrix [R] is constructed from the three rotation matrices, associated with these rotations. Consequently [R] may be expressed as:

$$[R] = [Ra].[Rb].[Rc] \tag{4.27}$$

Where [Ra], [Rb] & [Rc] are the rotation matrices associated with a rotation (a) about the x -axis, (b) about the z_e-axis and (c) about the y_e-axis respectively.

$$[Rc] = \begin{bmatrix} \cos(c) & 0 & \sin(c) \\ 0 & 1 & 0 \\ -\sin(c) & 0 & \cos(c) \end{bmatrix} \tag{4.28}$$

$$[Rb] = \begin{bmatrix} \cos(b) & \sin(b) & 0 \\ -\sin(b) & \cos(b) & 0 \\ 0 & 0 & 1 \end{bmatrix} \tag{4.29}$$

$$[Ra] = \begin{bmatrix} 1 & 0 & 0 \\ 0 & \cos(a) & \sin(a) \\ 0 & -\sin(a) & \cos(a) \end{bmatrix} \tag{4.30}$$

If (L) is the length of a beam element, and its projections in its final position on the X, Y and Z axes are Lx, Ly and Lz respectively, the rotation matrix is given by

$$[R] = \begin{bmatrix} R_{11} & R_{12} & R_{13} \\ R_{21} & R_{22} & R_{23} \\ R_{31} & R_{32} & R_{33} \end{bmatrix} \qquad (4.31)$$

Where:

$$R_{11} = Lx/L \ , \ R_{12} = Ly/L \ , \ R_{13} = Lz/L,$$

$$R_{21} = (-R_{11} * R_{12} * \cos(a) - R_{13} * \sin(a)) \ / \sqrt{(R_{11}^2 + R_{13}^2)}$$

$$R_{22} = \sqrt{(R_{11}^2 + R_{13}^2)} * \cos(a)$$

$$R_{23} = (-R_{12} * R_{13} * \cos(a) + R_{11} * \sin(a)) \ / \sqrt{(R_{11}^2 + R_{13}^2)}$$

$$R_{31} = (R_{11} * R_{12} * \sin(a) - R_{13} * \cos(a)) \ / \sqrt{(R_{11}^2 + R_{13}^2)}$$

$$R_{32} = -\sqrt{(R_{11}^2 + R_{13}^2)} * \sin(a)$$

$$R_{33} = (R_{12} * R_{13} * \sin(a) + R_{11} * \cos(a)) \ / \sqrt{(R_{11}^2 + R_{13}^2)}$$

Equation (4.31) gives the most common form of the rotation matrix employed in space frame analysis. However, this is not applicable when the beam centroidal line coincides with the Y-axis (vertical member). Therefore, vertical members are a special case, since there is no rotation about y_e-axis (through angle (c)). So that, the first rotation is through angle (b), which is about the z_e-axis and the second is through the angle (a) about the member x_e-axis. The rotation matrix [R] can then easily be obtained.

4.2.3 ASSEMBLY OF THE OVERALL MATRICES.

The next stage in the finite element analysis is to assemble the stiffness and mass matrices $[K]^e$ and $[m]^e$ of the individual elements to form overall stiffness and mass matrices for the entire discretised system. This is achieved by ensuring that the equilibrium and compatibility conditions are satisfied at all nodes within the discretised system (26).

The total strain energy stored in the whole structure is:

$$U = \sum_{e=1}^{n} U^e = \sum 1/2\{d\}_o^{e^t} [K]^e \{d\}_o^e \qquad (4.32)$$

Where n is the total number of elements in the assemblage and from (4.32), the element stiffness matrices are displayed as:

$$[\tilde{K}] = \begin{bmatrix} [K]^1 & 0 & . & . & . & 0 \\ 0 & [K]^2 & 0 & . & . & 0 \\ . & 0 & . & . & . & . \\ . & . & . & . & . & . \\ . & . & . & . & . & 0 \\ 0 & 0 & . & . & 0 & [K]^n \end{bmatrix} \qquad (4.33)$$

For the assemblage of the discrete elements, the displacements which have been matched at the nodes have to be compatible so that the displacement at any given node of the frame must be the same for all the elements connect to that node. So, the element displacements $\{d\}^e$ were related to the

displacements of the whole structure in generalised coordinates {q} as,

$$\begin{Bmatrix} \{d\}^1 \\ \{d\}^2 \\ . \\ . \\ \{d\}^n \end{Bmatrix} = [C].\{q\}$$

$$\{\tilde{d}\} = [C].\{q\} \qquad (4.34)$$

Where [C] is the compatible or connection matrix (32).

In every row of [C] there is only one non-zero element and its value is unity. The non-zero elements do not necessarily appear on the leading diagonal.

From equation (4.34) and (4.32), the assemblage of the stiffness matrix [K] for the complete structure would be,

$$[K] = [C]^t \ [\tilde{K}] \ [C] \qquad (4.35)$$

The assemblage of the mass matrix [M] for the complete structure is found from consideration of the total kinetic energy stored in the whole structure in a similar manner as [K].

$$[M] = [C]^t \ [\tilde{m}] \ [C] \qquad (4.36)$$

It should be noted that the structural stiffness and mass matrices are positive definite, symmetric in nature and square of an order equal to the number of degrees of freedom of the structure.

4.2.4 THE EQUATION OF MOTION FOR A COMPLETE FRAME.

The equation of motion for free undamped vibration of a dynamic system can be formulated by using Hamilton's principle (35), which considers the entire motion of the frame between two instants t_1 and t_2 and is therefore an integral principle in the form:

$$\delta \int_{t_1}^{t_2} (T-V)\, dt = 0 \qquad (4.37)$$

where T is the kinetic energy

V is the strain energy (V = U).

After substituting the values of T and V, (4.37), becomes

$$\delta \int_{t_1}^{t_2} 1/2 \left(\{\dot{q}\}^t [M] \{\dot{q}\} - \{q\}^t [K] \{q\} \right) dt = 0 \qquad (4.38)$$

After some manipulation, the equation of motion for the complete frame is obtained as,

$$[M] \{\ddot{q}\} + [K] \{q\} = 0 \qquad (4.39)$$

Since this form of equation arises in free vibration the

motion is harmonic and the displacement vector may be expressed as:

$$\{q\} = \{\hat{q}\} \sin(\omega t + \alpha) \tag{4.40}$$

where: $\{\hat{q}\}$ is the amplitude vector of harmonic motion

ω is the frequency of the harmonic motion in rad/sec.

α is the phase angle.

The equation of motion for the complete frame becomes:

$$([K] - \lambda[M]).\{\hat{q}\} = 0 \tag{4.41}$$

where $\lambda = \omega^2$

Equation (4.41), which is a general form of eigenvalue problem (36), which leads to a non-trivial solution only if

$$\left|[K] - \lambda[M]\right| = 0 \tag{4.42}$$

4.3 APPLICATION OF F.E.M. TO PLANE FRAME VIBRATION PROBLEMS.

4.3.1 Introduction.

Most engineering structures are assembled from elements connected together either by discrete or by continuous attachments. Although plane frames seldom exist as practical structures in isolation, nevertheless, many structures may be regarded as plane frames: the simplest model of a plane frame consists of discrete members of straight and uniform beams rigidly connected. Such frames are convenient for laboratory analysis since they have many of the features of the space frame but are generally simpler to analyse. In the present study, some of the initial experimental work was undertaken on plane frames.

The plane frame member is analysed as a combination of both axial and bending in the (x_e-y_e) plane; each element has six degrees of freedom, three at each node. The nodal displacements consist of three types, namely, the axial displacement (dx_1 and dx_2) along the member's centroidal axis (x_e -axis), the transverse translation in the direction perpendicular to the centroidal axis, (dy_1 and dy_2), and the rotations (θz_1 and θz_2) in the (x_e-y_e) plane and about the z_e-axis as shown in Fig. (4.1c). The usual assumptions employed in the simple beams theory are made: the effects of rotary inertia and shear deformation are neglected.

4.3.2 Stiffness and Mass Matrices for a Beam Element.

In a plane frame member, the procedure for obtaining stiffness and mass matrices for the extentional vibration and bending of the beam element in the $(x_e\text{-}y_e)$ plane is followed in exactly the same manner as already discussed for space frames in section (4.2.1). Consequently, the stiffness and mass matrices are then designated $[K_1]^e$, $[m_1]^e$ and $[K_2]^e$, $[m_2]^e$ for beams in tension and bending respectively.

$$[K_1]^e = EA/L \begin{bmatrix} 1 & -1 \\ & \\ -1 & 1 \end{bmatrix} \quad \& \quad [m_1]^e = mL/6 \begin{bmatrix} 2 & 1 \\ & \\ 1 & 2 \end{bmatrix} \qquad (4.43)$$

$$[K_2]^e = EI/L^3 \begin{bmatrix} 12 & 6L & -12 & 6L \\ & 4L^2 & -6L & 2L^2 \\ \text{symm.} & & 12 & -6L \\ & & & 4L^2 \end{bmatrix}$$

$$[m_2]^e = mL/420 \begin{bmatrix} 156 & 22L & 54 & -13L \\ & 4L^2 & 13L & -3L^2 \\ \text{symm.} & & 156 & -22L \\ & & & 4L^2 \end{bmatrix} \qquad (4.44)$$

As the system is linear, it is possible to combine the stiffness and mass matrices for extension and bending of the beam element, $[K]^e$ and $[m]^e$, each one having six degrees of freedom in local coordinates.

4.3.3 Transformation to Global Co-ordinates.

The $[K]^e$ and $[m]^e$ matrices must be transformed to global co-ordinates in a similar way to that explained in section (4.2.2) when discussing the space frame.

Plane frame rotations (a) and (c) about the x and y axes of the element are respectively equal to zero and the rotation matrix [R] can therefore be obtained with respect to the rotation (b) about the z -axis of the member, as illustrated in equation (4.29). The transformation matrix [T] must be of the order 6*6 and is expressed as:

$$[T] = \begin{bmatrix} [R] & [0] \\ [0] & [R] \end{bmatrix} \qquad (4.45)$$

4.3.4 The Equation of Motion for a Complete Frame.

The assembly of the overall matrices $[K]^e$ and $[m]^e$ and the equation of motion for the free undamped vibration of a plane frame can be obtained by following the same procedure for the space frame as explained in sections (4.2.3) and (4.2.4) respectively. The resulting equation of motion will be similar to equation (4.41).

4.4 SENSITIVITY ANALYSIS.

It will be recalled that the defect location method (section 3.3) requires the computation of a set of natural frequencies for the undamaged structure, and a further set when hypothetical damage has been introduced at each and every susceptible location, so that the changes in natural frequencies can be found. Thus, if there are ´n´ possible damage locations, it is necessary to solve ´n+1´ eigenvalue problems.

One possible way of modelling the damage to the structure (see (V) in section 3.4) is as a local decrease in the stiffness of one element. If this is done then it is possible, by using the sensitivity (perturbation) method of analysis (37) to demonstrate the sensitivity of the structure to damage in component characteristics and to avoid the need to resolve the EVP n times. This is done using the mode shapes of the undamaged structure determined from an initial dynamic analysis.

With reference to section (4.2.4), the eigenvalue equation (4.41) may be rewritten as:

$$([K] - \lambda[M]).\{q\} = \{0\} \qquad (4.46)$$

The damage model does not consider the mass of material removed by damage to be significiant, so that it is necessary to consider only the effect of a small change in stiffness.

This will cause changes in the eigenvalue λ and eigenvector $\{q\}$. Replacing K by $K+\delta K$, λ by $\lambda+\delta\lambda$ and q by $q+\delta q$, equation (4.46) becomes

$$\{([K]+[\delta K]) - (\lambda+\delta\lambda).[M]\}(\{q\}+\{\delta q\}) = \{0\} \qquad (4.47)$$

After multiplying out and neglecting second order terms, this gives:

$$([K]-\lambda[M])\{q\} + ([K]-\lambda[M])\{\delta q\} + ([\delta K]-\delta\lambda[M])\{q\} = \{0\} \qquad (4.48)$$

Examination of equation (4.46) shows that it is possible to rewrite equation (4.48) as

$$([K]-\lambda[M])\{\delta q\} + ([\delta K]-\delta\lambda[M])\{q\} = \{0\} \qquad (4.49)$$

and multiplying equation (4.49) by $\{q\}^t$

$$\{q\}^t([K]-\lambda[M])\{\delta q\} + \{q\}^t([\delta K]-\delta\lambda[M])\{q\} = \{0\} \qquad (4.50)$$

Since [K] and [M] are symmetric, then transposing equation (4.46) and post-multiplying by $\{\delta q\}$ gives

$$\{q\}^t([K]-\lambda[M])\{\delta q\} = \{0\} \qquad (4.51)$$

Now equation (4.50) becomes

$$\delta\lambda = \frac{\{q\}^t \ [\delta K] \ \{q\}}{\{q\}^t \ [M] \ \{q\}} \qquad (4.52)$$

The sensitivity of each natural frequency to changes in stiffness, $[\delta K]$, can therefore be computed from the mode shape vectors and the mass matrix of the undamaged structure.

$$Sen(x,i) = \sqrt{\lambda_i} - \sqrt{\lambda_i + \delta\lambda_i} \qquad (4.53)$$

Where: $Sen(x,i)$ is the reduction of natural frequency i due to a change in stiffness of element x.

λ_i is the original eigenvalue i.

$\delta\lambda_i$ is the change of eigenvalue i.

It is necessary to compute the changes in stiffness, $[\delta K]$, due to a defect at each element in the frame. The reduction in stiffness of an element is calculated simply by assembling the [K] matrix for a single element with the reduction in rigidity (stiffness) (15). Then

$$[\delta K] = - Red. \ [K]^e \qquad (4.54)$$

Where: Red. is the stiffness reduction factor, >0 and <= 1

$[K]^e$ is the element stiffness matrix.

This expression is readily evaluated using the stiffness subprogram from the dynamic analysis section (4.3.2). The stiffness subprogram will be discussed in section 4.6.4. The

reduction in each natural frequency due to damage at each element in the structure is calculated by means of equations (4.52) and (4.53).

4.5 EFFECT OF FLEXIBLY CONNECTED ELEMENTS.

In the previous sections, the dynamic behaviour of the structure was analysed by assuming that the members meeting at each joint were rigidly connected. Based on this assumption, the stiffness matrix of the structure can be computed, together with the mass properties of the structure in order to establish the dynamic characteristics of the structure.

Stevens (38) reported a method of representing some degree of partial fixity of the connections as illustrated in Fig. (4.3). A beam is shown, in Fig. (4.3a), to be hinged at end B but with varying degrees of fixity at support A. This method of representation involves imagining the beam to be extended past the support, as shown in Fig. (4.3b). The elastic stiffness of this hypothetical extension AA´ will determine the degree of end fixedness at support A. Variations in fixity may therefore be obtained by considering either various values of length (Lc) or the flexural rigidity of this hypothetical equivalent "connecting span". This method is relatively easy for a simple problem but difficulties do arise when larger structures are being considered.

In an investigation on a one-dimensional structure, Adams et al (17) represented the damage by using an axial spring which produces a local increase in the flexibility of the structure. Burgreen (39) also considered the effects of elastic supports on the free vibration of beams and also derived expressions that relate the end-fixity to the natural frequencies of the beam for an assumed support stiffness. He did not attempt to study the flexibility of any chosen node, whereas in the present work the elements are allowed to have both angular and transverse springs, thus allowing flexibility at their nodes. This method of representation seems to avoid the above difficulties and gives physically a more satisfactory picture of the real system involving a model of a frame in which the elements are assumed to be flexibly connected to a node. That is to say, the elements can rotate individually but there is some constraint in their relative movement. For example, if elements are hinged together, a partially restrained joint can be replaced by an equivalent system in which it is assumed that the two beams are connected by a rotational spring at the hinge.

Let us suppose that the elements of the frame are flexibly connected at the nodes by assuming the elements to be mounted with springs which have both transverse and angular stiffness. Fig. (4.4) shows how the elements are flexibily connected at the node with a torsional spring of stiffness K_t , axial and transverse springs of stiffness K_h and K_v, for horizontal and vertical movements, respectively.

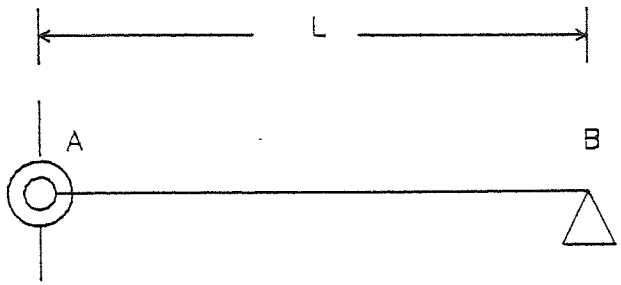

(a)

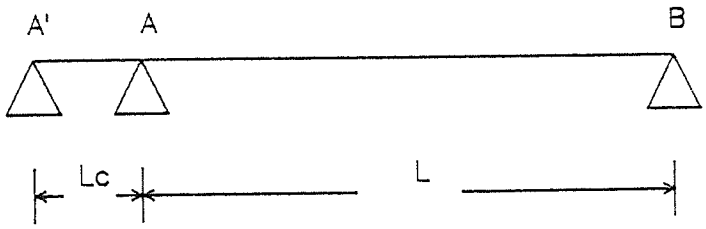

(b)

FIG. (4.3) BEAM WITH NON–RIGID CONNECTIONS

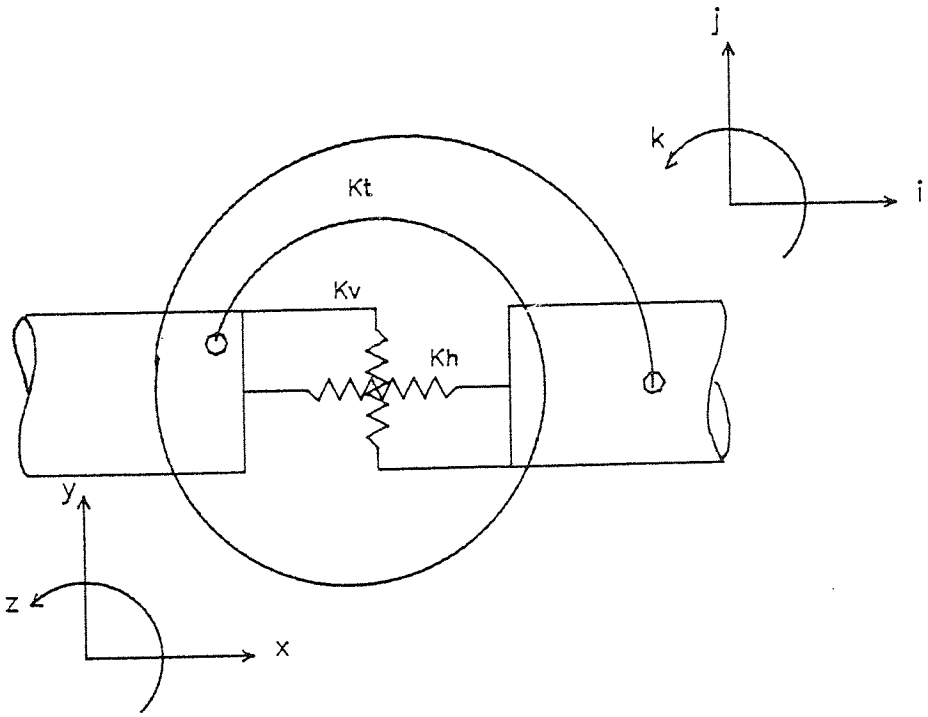

Where: i, j, k Is the spring's coordinates
x, y, z Is the node coordinates

FIG. (4.4) BEAMS WITH FLEXIBLE CONNECTION

Now the strain energy to be stored is:

$$U = \sum U \text{ beams} + \sum U \text{ springs} \qquad (4.55)$$

The linear and angular displacements of the springs must be described by coordinates i, j, k. The coordinates x, y, z will be used to represent the coordinates of the node, where the elements which are flexibly connected. since x, y, z are the linear and angular displacements of the rigidly connected element, the strain energy of the springs is given by:

$$\sum U \text{ springs} = 1/2\ K_h\ (q_x - q_i)^2 + 1/2\ K_v\ (q_y - q_j)^2 + 1/2\ K_t\ (q_z - q_k)^2$$

$$= 1/2\ K_h\ q_x^2 - K_h\ q_x\ q_i + 1/2\ K_h\ q_i^2 + 1/2\ K_v\ q_y^2 - K_v\ q_y\ q_j + 1/2\ K_v\ q_j^2 + 1/2\ K_t\ q_z^2 - K_t\ q_z\ q_k + 1/2\ K_t\ q_k^2 \qquad (4.56)$$

It was found that the effect of flexibly connected elements is merely an addition of spring stiffness into the assembled stiffness matrix. Additionally, three degrees of freedom are present in the non-rigidly connected nodes. In order to show the locations of spring stiffness in the overall stiffness matrix, equation (4.56) can be substituted in equation (4.55). Thus, the assembly stiffness matrix becomes

$$
\begin{array}{c|ccccccc}
 & x & y & z & \cdots & i & j & k \\
x & K+K_h & & & & -K_h & & \\
y & & K+K_v & & & & -K_v & \\
z & & & K+K_t & & & & -K_t \\
\vdots & & & & & & & \\
i & -K_h & & & & K+K_h & & \\
j & & -K_v & & & & K+K_v & \\
k & & & -K_t & & & & K+K_t
\end{array}
\qquad (4.57)
$$

Since the 'springs' are ficticious, they have no inertia and the kinetic energy of the elements is not affected. Any type of flexibly connected elements can be represented in this way. The number of degrees of freedom at the joint does not introduce additional difficulties in the representation of the structure or the logic of computation. This method is suited to the analysis by the finite element method of any frame structure. It is possible to estimate the spring stiffness at the joint by using beam theory in conjunction with experimental measurements of the model structure. This will be discussed in detail in section (6.9). The values so found for the spring stiffness (K_t, K_h, K_v) at the joint are then used in the dynamic analysis in order to obtain the stiffness matrix for the damaged structure under consideration.

4.6 COMPUTER IMPLEMENTATION.

4.6.1 Introduction.

In this section, the theory and methodology of solving the linear eigenvalue problem are presented in the form of computer programs. The ultimate objective of predicting the dynamic behaviour of plane and space frame structures can then be achieved through the use of the digital computer.

The discretization of any structure into finite elements normally leads to overall mass and stiffness matrices of large order. The solution of the resulting linear eigenvalue problem can be contemplated only through the use of a high speed digital computer, the core store size of which limits the complexity of the frame which may be analysed. In this section the programming techniques employed in predicting the dynamic behaviour of plane and space frame structures are described: these programs were implemented on the Hewlett Packard 9845B desk-top computer.

A suite of programs has been developed using the finite element method to analyse any arbitrary shape of plane and space frame comprised of straight and uniform elements which are allowed to have both angular and axial springs at their nodes. The programs also generate the generalized coordinates which describe the displacements of the nodes when the frame is vibrated. The amount of information requiring to be fed into the computer depends on the type of problem, the

complexity of the model, the sophistication of the program and the extent of the data required from the analysis.

Core store requirements are minimised by the use of established algorithms for the solution of banded and symmetrical matrices. The eigenvalue problem can be solved by various numerical methods: existing programs (40,41) were adopted to take into account the effect of the flexibly connected elements on the overall stiffness matrix.

Constraints on the structure must be imposed and those which act upon the frame must prevent it from rigid body motion and also from translations and rotations in any direction. The effect of a suppressed displacement described by a certain coordinate, j, is that the row j and column j in the stiffness and mass matrices are deleted.

The solution of the eigenvalue problem produced natural frequencies and natural modal shapes. The undeflected structure plot is a useful check as to whether the input data for the geometry and topology of the frame members is correct by labelling the nodes and elements. Also, a plot of a mode shape for a frame gives a good representation of its behaviour.

4.6.2 Solution of the Linear Eigenvalue Problem.

The first step required for solving the linear eigenvalue problem involves the conversion of equation (4.46) into the form of a standard EVP

$$[D]\{q\} = \lambda\{q\} \tag{4.58}$$

One way of reducing equation (4.46) to a standard form is to pre-multiply by $[M]^{-1}$ and let

$$[D] = [M]^{-1}[K] \tag{4.59}$$

where [K] and [M] are symmetric and both have the same bandwidth, but [D] is not necessarily symmetrical nor is it banded.

Alternatively Cholesky´s decomposition algorithm may be used to decompose the mass matrix [M] into the product of two matrices $[L][L]^t$, i.e

$$[M] = [L][L]^{-1}$$

where [L] is a lower triangular matrix. It is to be noted that the inverse matrices of [L] and $[L]^t$ are equal (28).

After some manipulation, equation (4.58) becomes

$$[A]\ \{U\} = \lambda\ \{U\} \qquad (4.60)$$

where: $[A] = [L]^{-1}\ [K]\ [L]^{-t}$ (Symmetrical but full matrix)

$$\{U\} = [L]^{t}\ \{q\}$$

This approach has the advantage that [A] remains a symmetric matrix, in contrast to [D]. [A] then is reduced to a tri-diagonal form by using Householder´s transformation (42). The method of solution depends on whether all the eigenvectors and/or eigenvalues are required, or whether all the eigenvectors and/or eigenvalues are in a certain interval of frequency or of a certain sequence. In the former case, the QL algorithm (31) was used in the plane and space frames: the tri-diagonal matrix [A] was decomposed into the product of a unitary matrix [Q] and an lower triangular matrix [L]. In the latter case, the Sturm sequence with bisection produced the eigenvalues but the eigenvectors were then obtained by inverse iteration.

4.6.3 Presentation of Input Data.

For both plane and space frame structures the input data to the programs can be divided into five categories. Each will be discussed in turn, below

1- Geometry.

The geometry can be described in one of two ways:

(I) By the cartesian coordinates of the nodes.

(II) By the local polar coordinates, the length and counter clockwise inclination to imagined x-axes of the elements. The elements are treated as vectors with start point node 1 and end point node 2 and the angle is input in degrees, in the case of plane frame programs. Calculation of the cartesian coordinates can then be performed and the nodal coordinate matrix Noco[I,J] results.

Where: J represents the nodes

I represents the coordinates,

I=1 for X-direction,

I=2 for Y-direction,

I=3 for Z-direction.

2- Topology.

This includes the element connections in which the two nodal numbers associated with each element are given, together with a property-group number representing the material properties of each element. The angle of rotation between the x-axis of the member and the X-axis of the structure is also required in space frame analysis. Thus, the element connection matrix

Elco[I,J] was formed, where Elco[I,J] is the global node number for node I (I= 1,2) of element J.

The geometry and topology provide sufficient information for which to calculate the number and length of the elements, the number of nodes and the number of property groups.

3- Material properties.

The use of property groups is employed purely to save re-entering the same string of data for elements possessing the same properties. Each property-group includes a cross sectional area, a moment of inertia about the Z-axis, Young´s modulus and the mass per unit length (or material density) for both plane and space frame. Additionally, a moment of inertia about the Y-axis, a torsional constant about the X-axis and a shear modulus is required for space frames. These properties are then arranged in one-dimensional arrays according to the property group and the element number.

4- Boundary conditions.

The structure is suppressed initially (is assumed to have no degrees of freedom) and then is able to release the nodes in the directions they are free to move. There must be at least one suppression in the X, Y and Z directions to prevent the frame, or parts of it, from rotating as a rigid body or acting as a mechanism. This also implies that the stiffness matrix will not be singular. The boundary conditions matrix Bc[I,J] is thus created,

Bc[I,J] = 1 is free to move in direction I, of node J

= 0 is fixed and cannot move in direction I of node J

The couplings matrix, Coup[I,J], the generalized coordinate number for the transformed local coordinate I of element J was then established. This implementation is presented as ,

IF Bc[K,Elco(J,I)] =1 THEN Coup[K+A,I] = Elco(J,I)*B-(B-K)

where: I = 1 TO Nelem, (Nelem = number of elements)

For each I : J = 1 TO 2 , Where A=0 if J=1, A=B if J=2

B = 6 For space frame and B = 3 for plane frame

For each J : K = 1 TO B

the value of zero is assigned to Coup[K+A,I] if Bc[K,Elco(J,I)] is zero (i.e. the freedom in any direction of node 1 or node 2 of a certain element is suppressed).

If an element is flexibly connected to a node, a separate generalized coordinate is required to describe the movement of each element which is flexibly connected to that node, since the elements will move independently of each other. However, if the movement of a node is released, there is already a coordinate describing the translation and rotation of the node. It is therefore only necessary to establish new coordinates. The new generalised coordinates are established when nodal stiffness is considered and can therefore start from a value which is defined by the maximum Nnode * B + 3, and increase by three for each element having nodal

stiffness. The coupling matrix now consists of numbers up to (Nnode * B + Neco), where Nnode is the number of nodes and Neco is the number of new generalised coordinates.

5- Nodal stiffness.

The frame was modelled to allow the elements to be flexibly connected to the nodes. If the element is flexibly connected to a node the spring stiffness has to be input for that element and node respectively. The final number of degrees of freedom (N) is calculated as:

N = N + Neco

Also the stiffness subprogram is able to order coordinate numbers from 1 to N. Nodal stiffness must be considered when assembling the stiffness matrix and this is easily done by the BASIC statement,

```
K[Coup(I*B-(B-K),H), Coup(I*B-(B-K),H)] = K[Coup(I*B-(B-K)
,H), Coup(I*B-(B-K),H)] + Nodal stiffness
```

When a node is free to move in any direction, the coordinate numbers for any of the rigidly connected elements at that node must be found and the nodal stiffness must be added, hence,

```
K[Coup(J*B-(B-K),G), Coup(I*B-(B-K),G)] = K[Coup(J*B-(B-K),
G), Coup(J*B-(B-K),G)] + Nodal stiffness

K[Coup(J*B-(B-K),G), Coup(I*B-(B-K),H)] = K[Coup(J*B-(B-K),
G), Coup(I*B-(B-K),H)] - Nodal stiffness
```

K[Coup(I*B-(B-K),H), Coup(J*B-(B-K),G)] = K[Coup(J*B-(B-K),
G), Coup(I*B-(B-K),H)]

where H=G=1 to Nelem

I=J=1 TO 2 (i.e. node 1 or 2 for each element)

B = 6 for space frame

B = 3 for plane frame

K=1 TO B

The user must provide all the above information as input data from the key board, in response to requests displayed on the computer VDU. Items in a string of data are separated by commas: the order of inputting the strings is arbitrary. The data input is printed out for checking and a correction sequence is available to amend the data. It is not possible to delete any node or element. As an additional measure to help avoid mistakes a checkplot may be drawn.

4.6.4 Structure of Computer Programs.

In this section, the general structure for the linear EVP programs is presented. In systematic programming, it is standard practice to sub-divide any large program into various routines, which are more or less independent. Implementation of these routines is most conveniently carried out by the use of subroutines or subprograms which may be called either once or several times during program execution. By using subprograms instead of subroutines the computer memory can be utilized more efficiently. In order to structure the main program logically, the calling of subprograms and the loading of programs must be in the optimum sequence. Memory is also conserved when local variables are dynamic and are re-allocated in other subprograms.

The general structure of the finite element package interaction is presented pictorially in Fig. (4.5). The program begins with an identification of the solution type, linear or non-linear EVP. The non-linear EVP will be described in detail in chapter 5. On identification of the problem as a linear EVP, execution proceeds with identification of the structure type. For a plane frame, program "LPFDI" is loaded, and for a space frame program "LSFDI".

The structure of computer package is represented in Fig. (4.6). On completion of the solution for the linear plane

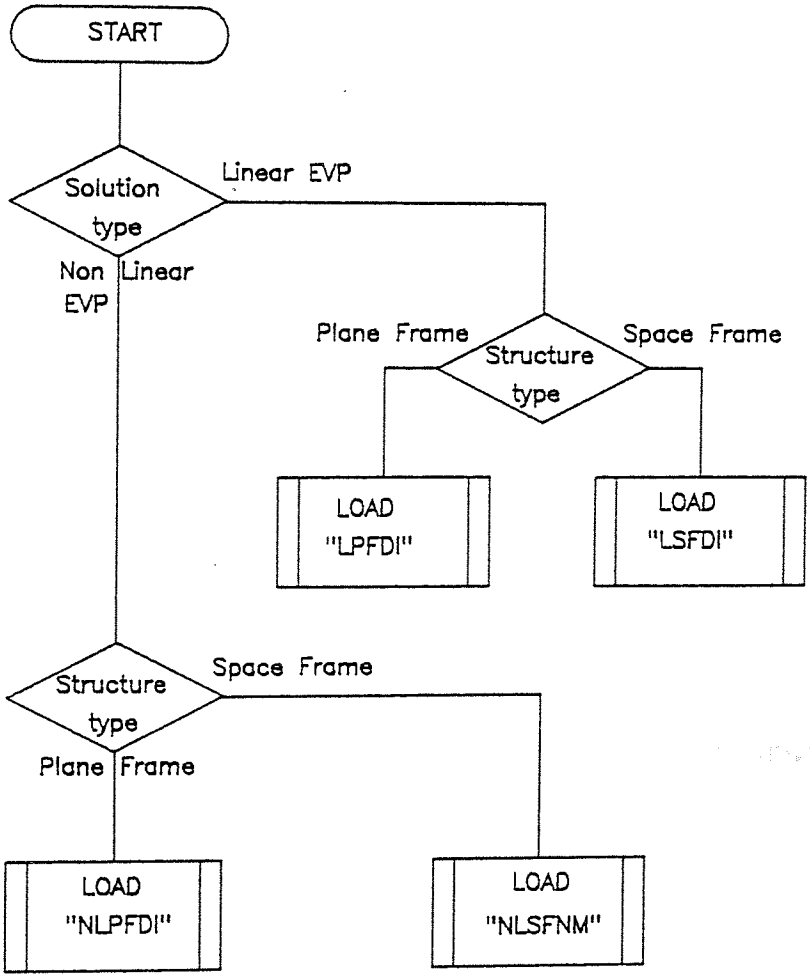

FIG. (4.5) FLOW CHART OF PROGRAM "START1"

frame data input processes, execution progresses with the loading of program "STMASE", which calculates the stiffness, mass and sensitivity matrices. The next program down the execution tree "PFTRAN", transforms the eigenvalue equation to the standard symmetric tridiagonal form using Cholesky´s decomposition and Householder´s transformation. During this stage, the user is prompted for the required solution type and depending on which is chosen, branching occurs with the loading of programs "PFQL", "PFEV" or "PFEVVE". The first program (PFQL) calculates all the eigenvectors and/or eigenvalues by using the QL algorithm. The second (PFEV) calculates the eigenvalues in a certain interval or of a certain sequence by using Sturm´s sequence with bisection. The final (PFEVVE) calculates the eigenvalues with the eigenvectors in a certain interval of frequency or of a certain sequence by using Sturm´s sequence with bisection and inverse iteration.

The program "LPFDI" enables the generation and editing of the datafile which will be accessed by the main simulation program "START1". The flow chart describing "LPFDI" is shown in Fig. (4.7). The first process is to define the dimensions of the arrays and variables, and to ´common´ variables (which allows the transfer of variables and arrays when another program is loaded). The next process requires an input datafile name which checks the status of the filename. If the filename has been assigned to a program, another filename is prompted, otherwise execution continues. If the filename is that of an existing datafile, the data is first read before

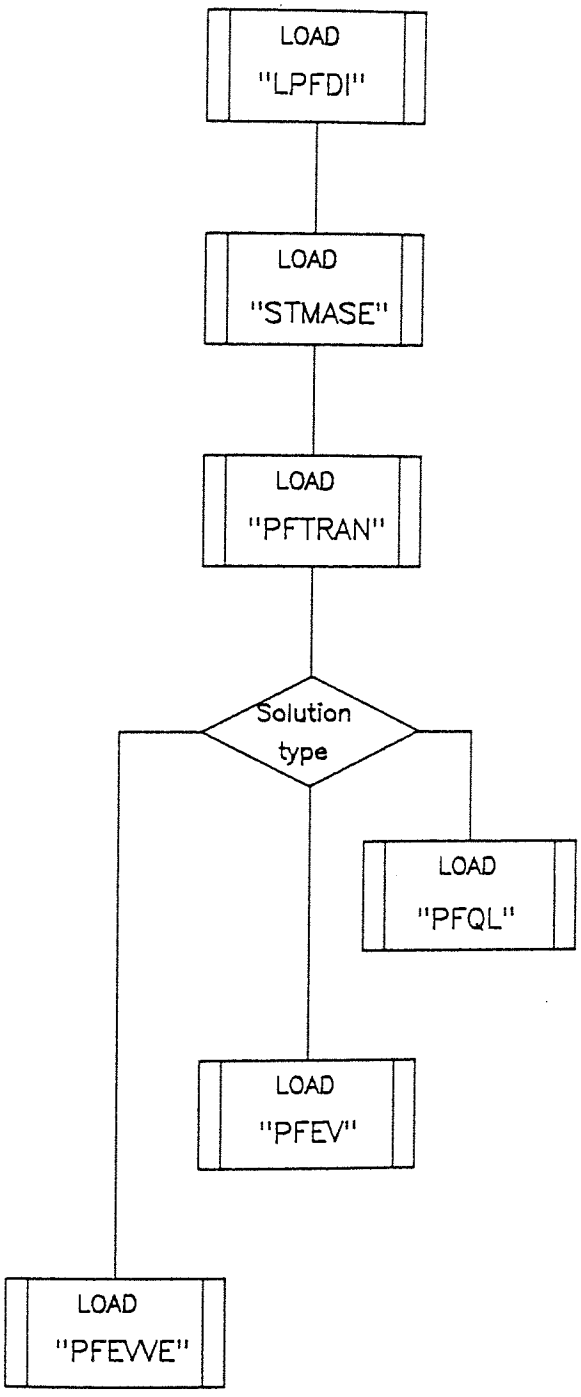

"Linear Plane Frame Data Input"
To generate datafile

To calculate STiffness, MAss
and SEnsitivity matrices

"Plane Frame TRANsformation"
Select solution type & transforms
to symmetric standard form
Using Cholesky decomposition
and Householder transformation

"Plane Frame QL–algorithm"
Calculates all eigenvalues
using QL–Algorithm

"Plane Frame EigenValue"
Calculates eigenvalues in
a certain interval or of a
certain sequence, Using Sturm's
Sequence with Bisection

Calculates eigenvalues with
eigenvectors in a certain
interval of Freq. or of a
certain sequence

FIG. (4.6) STRUCTURE OF COMPUTER PACKAGE FOR PLANE FRAME,
USING LINEAR EVP

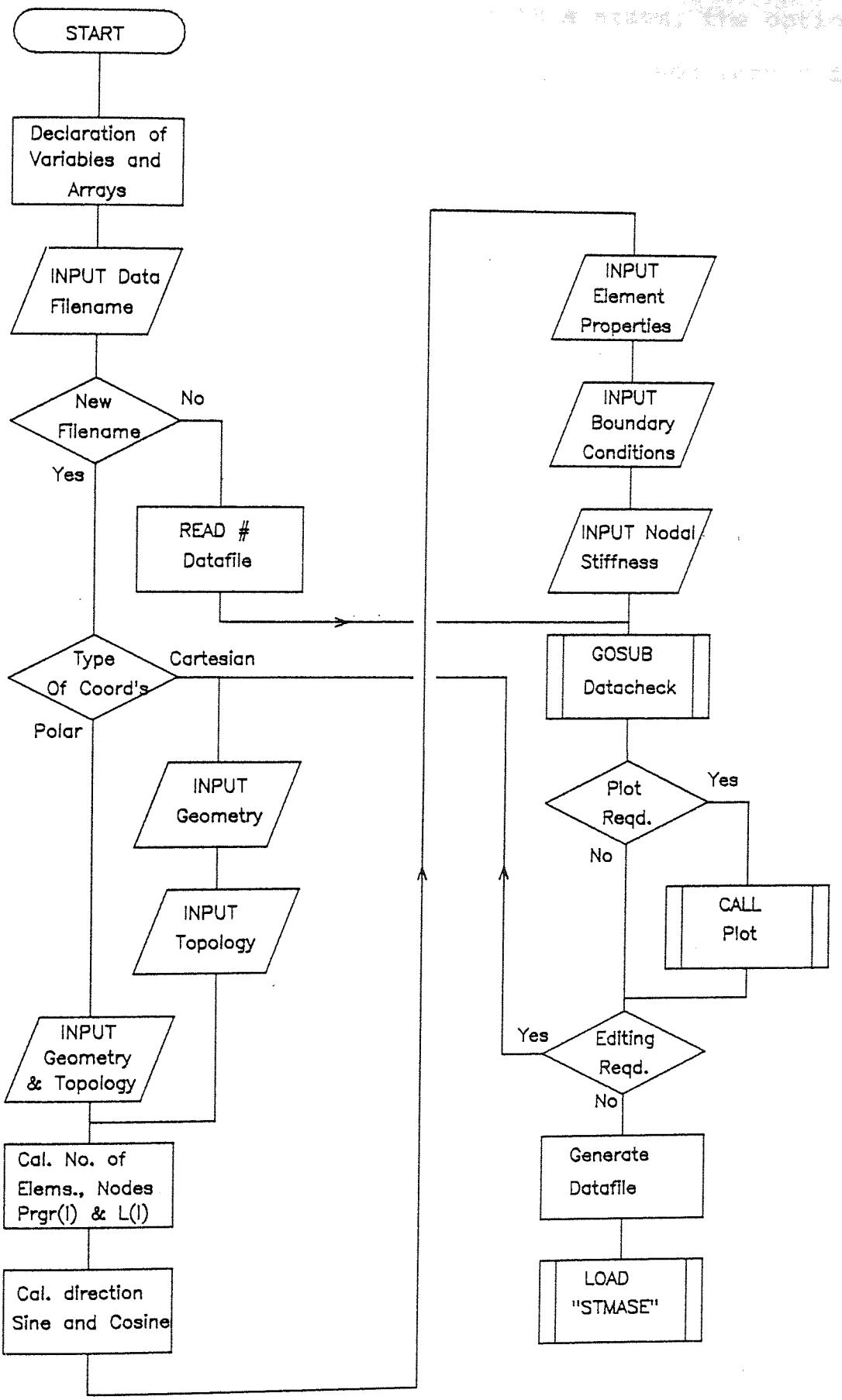

FIG. (4.7) FLOW CHART OF PROGRAM "LPFDI"

proceeding with the datacheck. After this stage, the option of displaying the data is permitted. If this is not required, the program continues. Here, another branching allows the option of editing existing data. If no editing is required, the current data is written out to mass-storage. The program "STMASE" is then loaded, while still preserving the variables in common memory.

For the case of a new datafile, the program branches, depending on the type of coordinate system selected (either cartesian or polar). Program execution continues with the appropriate input of element properties, boundary conditions and nodal stiffness, prior to the datacheck. The program flow after this stage is similar to that when an existing datafile was selected.

The program "STMASE" consists of four subprograms as shown in Fig. (4.8). Of these, "Stiffness" and "Sensmat" will be described in detail. These subprograms contain the computer implementation of the sensitivity analysis (as explained in section 4.4).

The subprogram, "Stiffness", shown in Fig. (4.9), begins with the declaration of variables and arrays. The first branch if the sensitivity analysis is required which case the subprogram "Elem.stiff." is ´called´ and executed. On return, the matrix element stiffness ´Keg´ is assigned to Knode, and then executing returns to the calling program "STMASE". For the case when sensitivity is not required, a loop is set

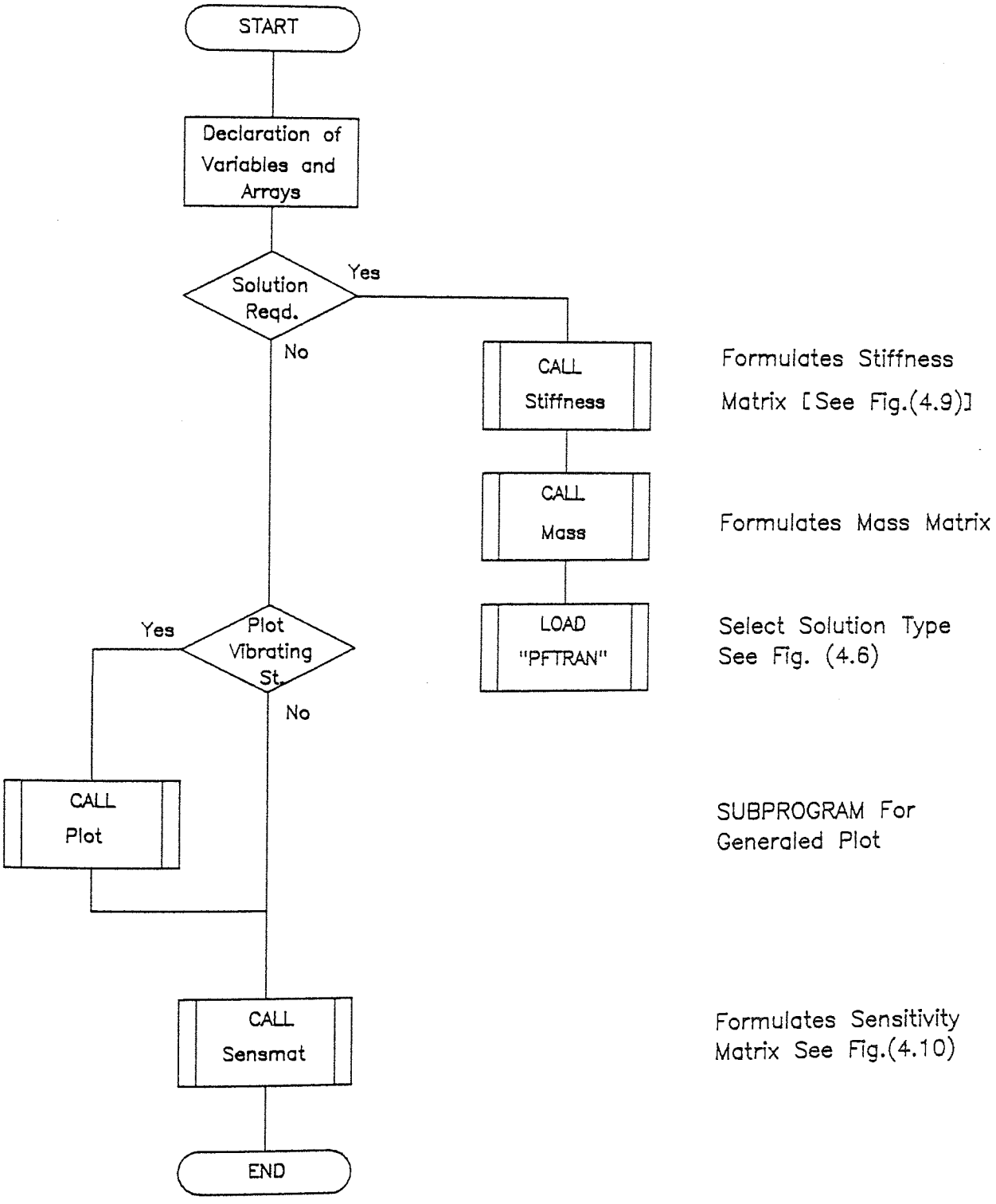

FIG. (4.8) FLOW CHART OF PROGRAM "STMASE"

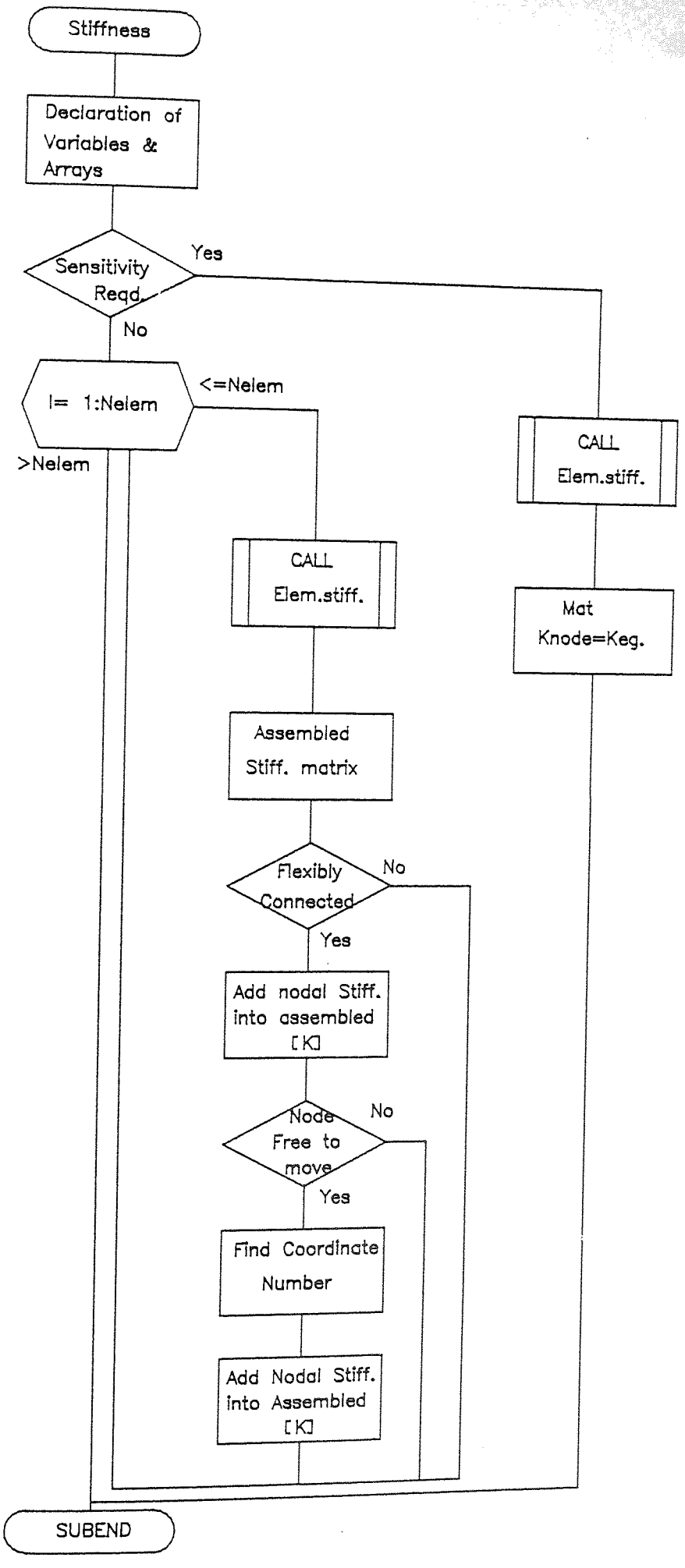

FIG. (4.9) FLOW CHART OF SUBPROGRAM "Stiffness"

depending on the number of elements (Nelem). For each element, the element stiffness is generated by calling subprogram "Elem.stiff.". Further execution assembles the overall stiffness matrix. The other branches depend on whether either end of the current element is flexibly connected to a node. Where the element is flexibly connected and the node is constrained, the program returns and generates the element stiffness for the next element, otherwise the subprogram continues by adding the nodal stiffness into the appropriate positions of the assembled stiffness matrix, having first found the coordinate numbers for any of the rigidly connected elements.

Subprogram "Sensmat":

This subprogram, shown in Fig. (4.10), assembles the necessary sensitivity matrix (i.e. frequency changes) for a later defect location analysis and begins with the necessary declaration of arrays and variables. If the perturbation analysis is not required, the subprogram returns to the calling program, otherwise program execution progresses along one of two branches, depending on the method of analysis selected. The sensitivity matrix is either obtained by a calculation sequence of frequency changes determined by the analyst (method 1), or from the use of the perturbation analysis, see equation 4.53 (method 2).

The perturbation analysis computes the changes in the natural frequencies when each element in turn is assumed to have reduced stiffness along its whole length. Method 1 can be

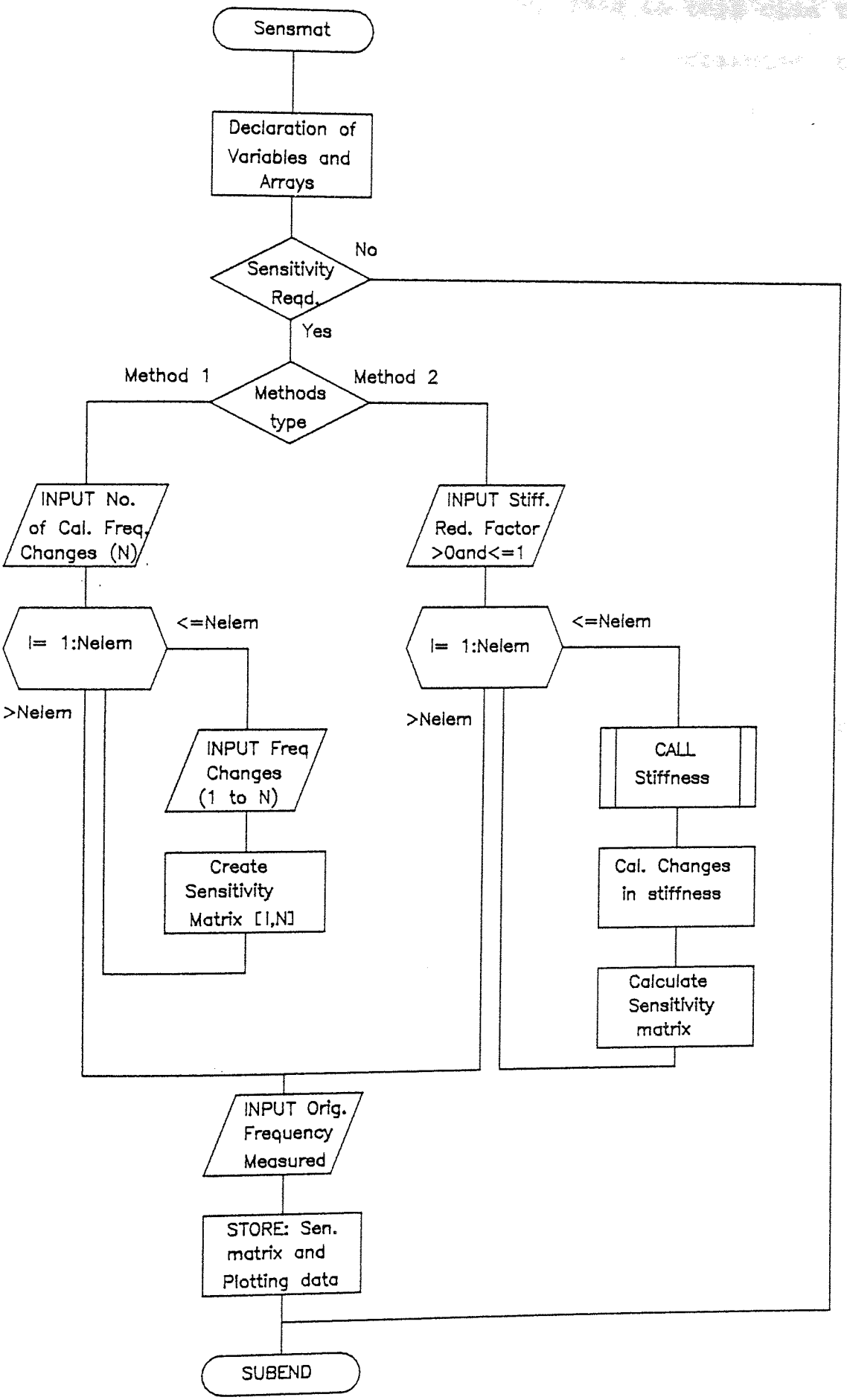

FIG. (4.10) FLOW CHART OF SUBPROGRAM "Sensmat"

used, if method 2 is not required, then in this case the analyst can construct his own method of obtaining the sensitivities as explained in section (3.4) and feed to the computer. After this, proceed to execute the input of the original measured frequencies if required. Then, the sensitivity matrix and the plotting data are stored in the mass-storage device.

With reference to the structure of the computer package Fig. (4.11), on completion of the solution for the linear space frame data input processes, the first program "LSFDI" performs two main functions. The first is that of data input and verification. Data verification is achieved by means of a graphical output of the undeflected structure. The data input procedure is similar to that for program "LPFDI" as explained earlier. Successful completion of the first stage leads to the next function, which is the generation of the mass, stiffness and sensitivity matrices.

Execution progresses with the loading of program "SFTRAN", which the user is prompted for the required solution type, and depending on which is chosen, also the coordinates system will be calculated. The next program down the execution tree "SFTRNC", transforms the eigenvalue problem to the standard symmetric tridiagonal form, using Cholesky´s decomposition and Householder´s transformation. During this stage, branching occurs with the loading of either program "SFQL", "SFEV" or "SFEVVE" depending on the solution types as explained in the plane frame.

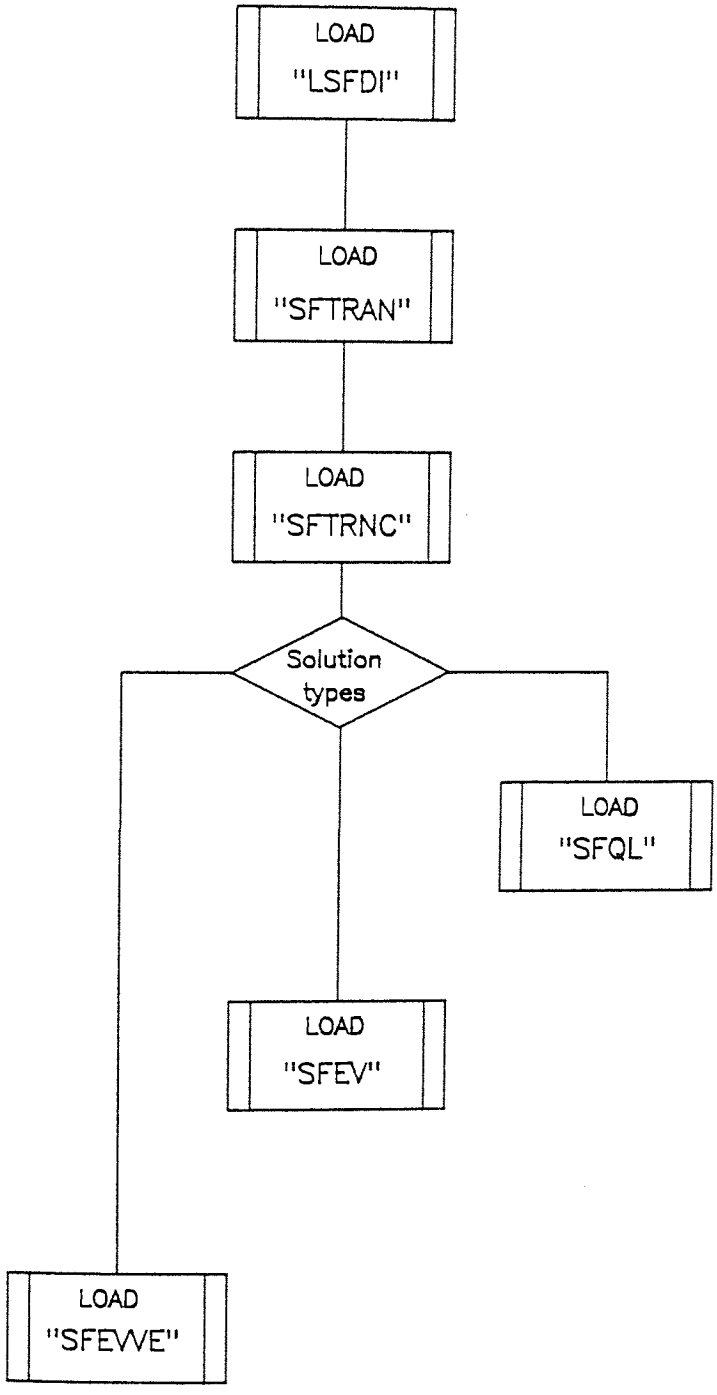

Generate data and calculate the stiffness, mass and sensitivity matrices

Select solution types

Transform to symmetric standard form using Cholesky decomposition and Householder's transformation

Calculate all Eigenvectors and/Or Eigenvalues, Using QL–Algorithm

Cal. a sequence of Eigenvalues Or Eigenvalues in a certain interval, using Sturm's sequence with Bisection.

Cal. Eigenvalues With Eigenvectors in a certain interval of Freq. Or of a certain sequence, using Sturm's sequence with Bisection

FIG. (4.11) STRUCTURE OF COMPUTER PACKAGE FOR SPACE FRAME USING LINEAR EVP

4.7 CLOSING REMARKS:

In the present investigation, the finite element method was chosen as a tool to predict the natural frequencies and associated mode shapes of plane and space frame structures, since it is the most powerful method available. The mathematical formulation, using the assumed polynomial displacement function, leads to the establishment of frequency independent mass and stiffness matrices. The solution of the resulting linear EVP has been summarised in order to clarify a description of the development of a computer program which has been implemented on the HP9845B desk-top computer. Using this program it is possible to represent complex structures composed of many elements, flexibly connected at their nodes and to carry out a perturbation analysis of the structure.

It was observed that the maximum number of eigenvalues is equal to the number of degrees of freedom in the structure. The greater the number of elements used to represent a given structure, the more accurate become the results and the greater the number of eigenvalues that can be obtained.

Because one element per member is not sufficient for the solution of the linear EVP to be within acceptable limits of accuracy, the next chapter will describe an infallible method of finding all natural frequencies, using the exact displacement functions for the elements, rather than approximate ones.

CHAPTER FIVE

FINITE ELEMENT ANALYSIS USING THE EXACT DISPLACEMENT FUNCTION

5.1 INTRODUCTION.

The previous chapter was devoted exclusively to the vibration of a distributed system leading to a linear EVP; in this chapter a method of analysis will be presented which leads to the solution of a non-linear EVP.

An important requirement in the dynamic analysis of structures is to employ an adequate accuracy of computation to ensure that the natural frequencies and modes are obtained with reasonable finite element discretization, even for the higher modes. For more complex structures, this inevitably requires automatic computation so that an accurate and reliable algorithm is essential. This may be accomplished by the use of exact rather than approximate displacement functions for the elements, obtained from the solution of the differential equations governing the free vibrational behaviour of structural components. When applied to a frame structure, the resulting non-linear eigenvalue problem is solved by a straightforward and infallible method which converges on as many of the natural frequencies of vibration as may be required.

The method was developed for rigidly jointed plane or space frames. In this analysis each important node can be flexibly modelled using a spring at that position. Members of the frame are treated as being continuous and uniform rather than an approximately equivalent lumped-mass system. It follows that each member of the frame, and hence also the frame

itself, has an infinite number of degrees of freedom so that there are an infinite number of natural frequencies for the frame. With this method it is possible to calculate how many natural frequencies lie below any chosen frequency without determining them and hence converge on any required natural frequency to any specified accuracy.

The matrices for an exact solution are frequency dependent and form a non-linear eigenvalue problem. As the methods of solution which are presented for a linear eigensystem are inapplicable, the determinant method must be invoked. With the property of the sturm sequence and the treatment of asymptotic poles, the determinant method has been proved efficient and reliable. The differential equation and general solution for the flexural and extensional vibrations of a uniform straight beam have been presented by many investigators, for example Wittrick et al (43), Williams et al (44, 45) and Richards et al (46). Basci et al (47) also reported that the influence of rotatory inertia on the frequencies of vibration is rather small, even for higher frequencies. In this application the effects of shear deformation and rotatory inertia were ignored.

The non-linear EVP is suitable for the computer analysis of structural vibration as it is based on the systematic use of the dynamic stiffness matrix.

5.2 APPLICATION OF F.E.M. TO PLANE FRAME VIBRATION PROBLEMS.

5.2.1 Exact Displacement Functions.

Any plane frame member exhibits two basic modes of vibration, namely flexural and extensional. First, let us consider a beam in flexure.

The transverse displacement at any point x is a function of x and t, denoted by y(x,t). The governing differential equation of motion for a prismatic beam in the general form is given by:

$$EI\ \partial^4 y/\partial x^4 + m\ \partial^2 y/\partial t^2 = 0 \qquad (5.1)$$

where m is the mass per unit length ($m = \rho A$), ρ is density and A is the cross sectional area.
EI is the flexural rigidty (E is Young´s modulus of elasticity and I the moment of inertia).

Letting

$$y = V(x)\ \sin\ (\omega t + \varphi) \qquad (5.2)$$

where φ is the phase angle, V(x) is a function of x only and ω is the angular frequency of harmonic motion.

Using separation of variables method, equation (5.1)

simplifies to :

$$d^4V(x)/dx^4 - \lambda^4 V(x) = 0 \qquad (5.3)$$

where: $\lambda^4 = \left(m/EI\right)\omega^2$. (5.4)

The solution of equation 5.3 gives;

$$V(x) = c_1 \sin \lambda x + c_2 \cos \lambda x + c_3 \sinh \lambda x + c_4 \cosh \lambda x \qquad (5.5)$$

Now, consider the beam in extensional vibration: assuming that the axial displacement is U(x,t), then the governing differential equation of motion for a uniform beam is given by:

$$EA\,\partial^2 U / \partial x^2 = m\,\partial^2 U / \partial t^2 \qquad (5.6)$$

Letting

$$U(x,t) = u(x) \sin (\omega t + \varphi) \qquad (5.7)$$

and using separation of variables method, equation (5.6) reduces to:

$$d^2u / dx^2 + \beta^2 u = 0 \qquad (5.8)$$

where: $\beta^2 = \left(m / EA\right) \omega^2$ (5.9)

The general solution of equation (5.8) gives:

$$U(x) = c_5 \sin \beta x + c_6 \cos \beta x \qquad (5.10)$$

In equations (5.5) and (5.10) c_i (i=1 to 6) are arbitrary constants. These equations represent the exact displacement functions and results obtained from them will be independent of element subdivision. The displacement at any point x is evaluated in terms of circular and hyperbolic expressions. It may also be noted that the transverse and longitudinal displacements are mutually independent of each other, but the relationship between the two frequency parameters is given by:

$$\beta = \lambda^2 \sqrt{I / A} \qquad (5.11)$$

5.2.2 Stiffness and Mass Matrices.

The procedure used for obtaining the stiffness and mass matrices for the beam element in bending and in tension is exactly the same as in the case of the displacement polynomial function, already discussed in the previous chapter. The equation for the slope at any point in the element is obtained by differentiating equations (5.5) and (5.10) and by substituting the boundary conditions respectively. The vector of element nodal displacements {u} is given by:

$$\begin{Bmatrix} u_1^e \\ u_2^e \\ u_3^e \\ u_4^e \\ u_5^e \\ u_6^e \end{Bmatrix} = \left[\begin{array}{cccc|cc} 0 & 1 & 0 & 0 & & \\ \lambda & 0 & \lambda & 1 & \multicolumn{2}{c}{[0]} \\ S & C & Sh & Ch & & \\ \lambda C & -\lambda S & \lambda Ch & Sh & & \\ \hline & & & & 0 & 1 \\ \multicolumn{4}{c|}{[0]} & \sin\beta L & \cos\beta L \end{array}\right] \begin{Bmatrix} c_1 \\ c_2 \\ c_3 \\ c_4 \\ c_5 \\ c_6 \end{Bmatrix} \qquad (5.12)$$

where: $S = \sin \lambda L$

$C = \cos \lambda L$

$Sh = \sinh \lambda L$

$Ch = \cosh \lambda L$

This may be written more concisely as:

$$\{u\}_o^e = [A] \{c\} \qquad (5.13)$$

Equation (5.13) is inverted and shape function [N] obtained for the flexural and extensional vibration. The second derivative of equation (5.5) is then required to be substituted in the expression for strain energy, Equation (4.16), after matrix multiplication and integration, the frequency dependent stiffness and mass matrices for a plane frame member are then given by (5.14) and (5.15):

$$[K] = \left[\begin{array}{c|c} [K_f]_{4*4} & 0 \\ \hline 0 & [K_e]_{2*2} \end{array}\right] \qquad (5.14)$$

$$[m] = \left[\begin{array}{c|c} [m_f] & 0 \\ 4*4 & \\ \hline 0 & [m_e] \\ & 2*2 \end{array}\right] \qquad (5.15)$$

where:

$$[K_f] = \lambda EI \begin{bmatrix} k_{11} & k_{12} & k_{13} & k_{14} \\ & k_{22} & k_{23} & k_{24} \\ \text{Symm.} & & k_{33} & k_{34} \\ & & & k_{44} \end{bmatrix}$$

Details of the elements of matrix K_f (K_{11} to K_{44}) are given in Appendix 4.

$$[K_e] = \beta EA \left[\begin{array}{cc|cc} \dfrac{\beta}{2\sin^2\beta L} & + \dfrac{\cos\beta L}{2\sin\beta L} & \dfrac{-\beta^2\cos\beta L}{2\sin^2\beta L} & - \dfrac{1}{2\sin\beta L} \\ & & & \\ \hline & & \dfrac{\beta}{2\sin^2\beta L} & + \dfrac{\cos\beta L}{2\sin\beta L} \\ \multicolumn{2}{c|}{\text{Symm.}} & & \end{array}\right]$$

$$[m_f] = \lambda EI \begin{bmatrix} m_{11} & m_{12} & m_{13} & m_{14} \\ & m_{22} & m_{23} & m_{24} \\ \text{Symm.} & & m_{33} & m_{34} \\ & & & m_{44} \end{bmatrix}$$

Also, details of the elements of matrix m_f (m_{11} to m_{44}) are given in Appendix 4.

and

$$[m_e] = EA \begin{bmatrix} \dfrac{\beta}{2\sin^2\beta L} - \dfrac{\cos\beta L}{2\sin\beta L} & \dfrac{-\beta^2\cos\beta L}{2\sin^2\beta L} + \dfrac{1}{2\sin\beta L} \\ \text{Symm.} & \dfrac{\beta}{2\sin^2\beta L} - \dfrac{\cos\beta L}{2\sin\beta L} \end{bmatrix}$$

5.2.3 Dynamic Stiffness Matrix.

The dynamic stiffness matrix $[D_s]$ is formulated from the stiffness and mass matrices by the equation

$$[D_s] = [K] - \omega^2 [M] \qquad (5.16)$$

The dynamic stiffness matrix is simpler than its constituent matrices, [K] and [M]. Referring to section (4.2.1), the element stiffness and mass matrices is given by:

$$[K] = \int_0^L [B]^t [D_i] [B] \, dx \qquad (5.17)$$

$$[m] = \int_0^L [N]^t [\rho A] [N] \, dx \qquad (5.18)$$

where $[N] = [f(x)] [A]^{-1}$ and [B] is obtained by differentiating [N].

Substitution of equations (5.17) & (5.18) into equation

(5.16), yields:

$$[D_s] = [A]^{-1^t} \left(\int_0^L [J]\, dx \right) [A]^{-1} \qquad (5.19)$$

The matrix [J] for the element in bending is given by:

$$[J_b] = -2EI\lambda^4 \begin{bmatrix} 0 & 0 & -S_1 S_2 & -S_1 C_2 \\ & 0 & -C_1 S_2 & -C_1 C_2 \\ \text{symm.} & & 0 & 0 \\ & & & 0 \end{bmatrix}$$

and for the element in tension

$$[J_e] = EI\lambda^4 \begin{bmatrix} C_3 & -S_3 \\ -S_3 & -C_3 \end{bmatrix}$$

where: $C_1 = \cos \lambda x$, $S_1 = \sin \lambda x$

$C_2 = \cos \beta\lambda x$, $S_2 = \sin \beta\lambda x$

$C_3 = \cos 2\beta x$, $S_3 = \sin 2\beta x$.

After carrying out the integration of [J], direct triple matrix multiplication will produce the dynamic stiffness matrix :

$$[D_s] = \left[\begin{array}{c|c} [D_{sf}] & 0 \\ \hline 0 & [D_{se}] \end{array}\right] \qquad (5.20)$$

where:

$$[D_{sf}] = \frac{\lambda EI}{1-CCh} \begin{bmatrix} \lambda^2(SCh+CSh) & \lambda SSh & -\lambda^2(S+Sh) & -\lambda(C-Ch) \\ & (SCh-CSh) & \lambda(C-Ch) & -(S-Sh) \\ \text{Symm.} & & \lambda^2(SCh+CSh) & -\lambda SSh \\ & & & (SCh-CSh) \end{bmatrix}$$

$$[D_{se}] = \frac{\beta EA}{\sin \beta L} \begin{bmatrix} \cos \beta L & -1 \\ -1 & \cos \beta L \end{bmatrix}$$

5.2.4 Transformation to Global Coordinates.

Having acquired the values of $[D_s]$ for the individual elements into which the system is subdivided, the next step is to assemble these to form an overall matrix for the entire discretised system. The transformation matrix [T] for the plane frame member was obtained and is illustrated in section (4.3.3). The transformed dynamic stiffness matrix in global coordinates is thus given by:

$$[D_{sg}] = [T]^t [D_s] [T] \qquad (5.21)$$

From these member equations the overall dynamic stiffness matrix of the frame, D, can be assembled in exactly the same way to obtain the overall stiffness matrix described in chapter 4. The natural frequencies then correspond to the

values of ω, the circular frequency, which satisfy the matrix equation:

$$[D]\{q\} = 0 \qquad (5.22)$$

Where $\{q\}$ is the vector of the amplitudes of the nodal displacement and $[D]$ is a function of ω.

5.3 APPLICATION OF F.E.M. TO SPACE FRAME VIBRATION PROBLEMS.

In order to construct the dynamic stiffness matrix for the structure, the procedure is performed in a similar manner to that for the plane frame, which has already been discussed in section (5.2) and in the preceding chapter. For further details see (48,49).

The space frame member may vibrate in any combination of four types of vibration, namely, longitudinal vibration in the x-direction, torsional vibration along the beam, flexural vibration in the xy plane and flexural vibration in the xz plane. When the member is vibrating at a frequency ω, then it is approximated by a straight member as shown in Fig. (4.1c), representation of the beam element taking into account all six possible translations and rotations at each node. The dynamic stiffness matrix for the element consists of 12*12 dimensional arrays. The governing equations of motion for vibration with boundary forces have been obtained as follows.

(I) Longitudinal Vibration:

$$EA\, d^2u / dx^2 + \rho A \omega^2 u = 0 \qquad (5.23)$$

With boundary conditions, $u(0) = dx_1$ and $u(1) = dx_2$, the solution is given by:

$$u(x) = c_1 \cos \psi x + c_2 \sin \psi x \qquad (5.24)$$

where:

$$\psi^2 = \left(\rho A / EA\right) L^2 \omega^2 \qquad (5.25)$$

(II) Torsional Vibration:

$$GJ\, d^2\theta / dx^2 + \rho I \omega^2 \theta = 0 \qquad (5.26)$$

With boundary conditions $\theta(0) = \theta_{x1}$ and $\theta(1) = \theta_{x2}$, the solution is given by:

$$\theta_{(x)} = c_3 \cos \gamma x + c_4 \sin \gamma x \qquad (5.27)$$

where:

$$\gamma^2 = \left(\rho I\, L^2 / GJ\right) \omega^2 \qquad (5.28)$$

(III) Flexural Vibration in xy Plane:

$$EI_z\, d^4V / dx^4 - \rho A \omega^2 V = 0 \qquad (5.29)$$

With the boundary conditions $V(0) = dy_1$, $V(1) = dy_2$,

$V'(0) = \theta_{z1}$ and $V'(l) = \theta_{z2}$, the solution is given by:

$$V(x) = c_5 \cos \lambda_z x + c_6 \sin \lambda_z x + c_7 \cosh \lambda_z x + c_8 \sinh \lambda_z x \qquad (5.30)$$

where:

$$\lambda_z^4 = \left(\rho A L^4 / EI_z\right) \omega^2$$

(IV) Flexural Vibration in xz Plane:

$$EI_y \, d^4W / dx^4 - \rho A \omega^2 W = 0 \qquad (5.31)$$

With the boundary conditions $W(0) = dz_1$, $W(l) = dz_2$, $W'(0) = \theta_{y1}$ and $W'(l) = \theta_{y2}$, the solution is given by:

$$W(x) = c_9 \cos \lambda_y x + c_{10} \sin \lambda_y x + c_{11} \cosh \lambda_y x + c_{12} \sinh \lambda_y x \qquad (5.32)$$

where: $$\lambda_y^4 = \left(\rho A L^4 / EI_y\right) \omega^2 \qquad (5.33)$$

5.4 THE SOLUTION OF THE NON-LINEAR EVP.

5.4.1 Introduction.

The frequency dependent matrices for structural members are constructed from consideration of the solution to the equations of motion. The overall frequency dependent matrices are formed by a conventional assembling process. The non-linear EVP thus obtained may be solved by the Sturm sequence technique and the treatment of asymptotic poles. The determinant method has been proved both efficient and reliable.

In general, the solution will be in terms of transcendental functions and the dynamic stiffness matrix of the member; therefore the dynamic stiffness matrix will be a transcendental function of frequency ω. The natural frequencies are usually those for which the determinant of the overall dynamic stiffness matrix is zero. Several of these natural frequencies may be close together or coincident, while others may correspond to the case where the eigenvector is zero (q=0). Also, as $|D|$ is now a highly irregular function of ω, any trial and error method may fail to recognise the roots since this involves computing $|D|$ and observing when it changes sign. These problems can be completely overcome by the use of an algorithm, (43), which enables the precise determination of the number of natural frequencies lying below any chosen frequency, without determining their actual values. Furthermore, this will

usually reduce the number of iterations needed, leading to a saving in total computation time. The converging process on the various natural frequencies can be completely automated, with no possibility of missing any natural frequencies of the structure.

5.4.2 Sturm Sequence.

This method was originally designed for the solution of polynomial problems, and has proved to be applicable to the non-linear eigensystem (43). In the case of the non-linear EVP for free vibration analysis, the extra calculation involved in determining the Sturm sequence is not significant when compared with the total computational time. A detailed example of Sturm´s Sequence is given in (50).

The solution of the non-linear EVP, to obtain the natural frequencies by the Sturm sequence technique, requires information on the values of determinant [D] and the number of changes of sign of the leading diagonal of [D] at various values of ω. This will be carried out after the Gaussian elimination process of triangularizing the matrix [D] into its upper triangular form. A property of a Sturm sequence is that the number of changes of sign between consecutive terms of the sequence is equal to the number of roots of the determinant lying below the chosen value of ω, that is to say, the number of natural frequencies which are less than the chosen value.

5.4.3 Sign Count.

From equation (5.22), the characteristic equation is written as:

$$|D| = 0 \qquad (5.34)$$

where $[D] = [K] - \omega^2 [M]$

The symmetry of the matrix ensures that its characteristic values are all real; if the matrix is non-singular, none of the characteristic values are zero. The simplest and most economical way of computing the sign count is to convert [D] into an upper triangular form, $[D]^{\triangledown}$, using a Gaussian elimination process without row interchanges. The determinant, $|D|$, is then the product of the leading diagonal elements of $[D]^{\triangledown}$. The important feature is that the number of changes in sign between consecutive terms of the sequence is a reliable means for identifying the order of the natural frequencies. The method simply substitutes the process of checking the sign of the leading elements of $[D]^{\triangledown}$ for the process of multiplying all these elements together.

The number of negative characteristic values, represented by the sign count of [D] and denoted by the symbol s{D}. It could be argued that the sign change method may break down if any of the leading diagonal elements of $[D]^{\triangledown}$ are zero, and as a result, the Gaussian elemination method would fail. To remedy this, it is necessary to choose a slightly different

value of frequency and repeat the process until the condition is avoided (43,44). The process of undertaking a sign count involves no more additional time than the evaluation of a determinant.

5.4.4 Asymptotic Pole Algorithm.

In free vibrations, the eigenvalues of the system are the values of ω which satisfy equation (5.22) and correspond to the natural frequencies. Let us suppose that $[D(\omega)]$ is evaluated at $\omega = \omega_t$, where ω_t is a trial value. It has been shown by Wittrick et al (43) that the asymptotic pole algorithm may be merged with the sign count algorithm using the equation :

$$n = n_o + s\{D(\omega_t)\} \qquad (5.35)$$

where n is the number of eigenvalues of the structure which are exceeded by ω_t and (n_o) represents the number of eigenvalues which would still be exceeded by ω_t if all the degrees of freedom corresponding to {q} were suppressed.

This action has the effect of isolating each member of the frame so that (n_o) can be calculated from:

$$n_o = \sum_{i=1}^{N} n_m \qquad (5.36)$$

where N is total number of elements in a structure

and n_m is number of eigenvalues of a member with its end clamped exceeded by ω_t.

From equation (5.20), the element of $[D_{sf}]$ and $[D_{se}]$ will be equal to infinity when either

$$1 - \cos \lambda L \cosh \lambda L = 0 \qquad (5.37)$$

or

$$\sin \beta L = 0 \qquad (5.38)$$

The roots of these two equations are solutions for a clamped-clamped structural member. The roots of (5.38) are clearly $\beta L = i\pi$ $(i=1,2,3,.....)$ and thus $\beta = i\pi / L$. The number of these roots exceeded by a given value of ω_t is n_e, where

$$n_e \text{ highest integer} < (\omega_t L \sqrt{m/EA}) / \pi \qquad (5.39)$$

or $$n_e = \beta / \pi$$

$$\beta^2 = (mL^2 / EA)\, \omega_t^2$$

Similarly, from equation (5.37), the number of roots exceeded by the value of λ corresponding to the given value of ω_t, is given by,

$$n_b = i - .5\,[1 - (-1)^i \text{ sign } (1 - \cos\lambda \cosh\lambda)] \qquad (5.40)$$

where i is the highest integer $< \frac{\lambda}{\pi}$

$$\lambda^4 = (mL^4 / EI)\, \omega_t^2$$

m mass per unit length

L member length

EI flexural rigidity

EA extensional rigidity

For the plane frame structure,

$$n_m = n_e + n_b \tag{5.41}$$

For the space frame structure,

$$n_m = n_e + 2n_b + n_t \tag{5.42}$$

where n_t is the highest integer $< \left(\omega_t L / \pi\right) \sqrt{\rho I_p / GJ}$

ρI_p is the torsional inertia per unit length

(ρ is density and I_p polar moment of inertia)

and GJ is the torsional rigidity.

5.4.5 Convergence Procedure.

The key to converging on a given natural frequency is a knowledge of the number of natural frequencies exceeded by any trial value of ω_t . A simple but effective method for converging on a specified natural frequency for example, the rth, is as follows:

First of all, try a large value of ω_t and see if the corresponding value of n is less than r, ω_t is taken as a lower bound, ω_l , and ω_t is doubled successively until n >= r, when ω_t becomes an upper bound, ω_u. If, on the other hand, the n >= r then $\omega_u = \omega_t$ and ω_l is taken as zero. Once ω_u and ω_l have been established, a new value of ω_t is obtained from the equation,

$$\omega_t = (\omega_u + \omega_l) / 2 \qquad (5.43)$$

and becomes a new value of ω_l if n<r, or otherwise a new value of ω_u . This method can be converged to any specified accuracy. The next eigenvalue is then found in basically the same way by using the values of n and ω_t which have already been obtained and stored.

5.5 Description of the Programs.

Computer programs employing the algorithm described in the preceding sections were implemented on the Hewlett Packard HP9845B desk-top computer.

A flow diagram is given in section (4.6.4) see Fig. (4.5). Execution proceeds after selection of the non-linear EVP to identify the structure type, either plane or space frame. For the plnae frame, program "NLPFDI" is loaded. For the space frame, program "NLSFNM" is loaded.

The program "NLPFDI" (Non-Linear Plane Frame Data Input) is designed to perform two main functions; data input and verification. The process is fundamentally similar to that described in section (4.6.3). Data verification is achieved by means of a data list or graphical output for an undeflected structure.

Execution progresses with the loading of program "NLDYST", an acronym "Non-Linear DYnamic STiffness". The user is prompted for the required solution type, and depending on which is chosen, the natural frequencies and the modal shapes will be calculated to the required accuracy. If the plots of the modal shape are required, the program "NGRAPH" is loaded. The plotter device can be a VDU, a Benson plotter or the HP9872A plotter. All the calculations using those programs were performed with full precision.

Another computer program was used for plane frame structures. This program was originally developed in Fortran by Williams et al (45) for calculating the natural frequency. Then, the program was translated to HPL language to implement on the HP9825B desk-top computer and modified for the purpose of the present work. The program has the facility of performing consecutive runs automatically and reading data off the mass-storage device as and when required. This enables the modelling of damage in a number of members.

Also, an equivalent space frame program in Fortran has been developed by Howson (49). The program was translated to HP enhanced BASIC, to run on a HP9845B computer and then modified to suit the present investigation. The program "NLSFNM" (Non-Linear Space Frame Natural frequency and Modal shape) calculated both the natural frequency and modal shape.

5.6 COMPARISON BETWEEN THE USE OF APPROXIMATE AND EXACT DISPLACEMENT FUNCTIONS.

Having already discussed the linear and non-linear EVP, a comparison will be made between them as methods for obtaining the natural frequencies and associated modes of vibration, and also the changes in the natural frequency caused by simulated damage.

The eigenvalues obtained from the solution of non-linear EVP are exact, depending only on the user´s specified accuracy.

Brevity of coding is another advantage. In this method only one element per member is required to describe the system, so that the working size of the matrices involved is smaller than of the linear EVP. Execution speed is rather slow although this could be improved by taking into account the bandwidth of the dynamic matrix. It is believed that the use of a compiler would have a greater effect on the non-linear EVP, thus resulting in a better execution speed. Node numbering in this case becomes important and a general rule is to choose a numbering which minimizes the greatest difference between the node numbers at the ends of any member. A disadvantage of using the exact displacement function is that in order to compute changes in frequency caused by simulated damage, the perturbation analysis cannot be used; it is necessary to resolve the EVP for the damaged structure.

Exact methods developed throughout the years are mostly applicable to relatively simple structures and boundary conditions. On the other hand, with advances in the finite element method and improved computational algorithms, more accurate predictions of the free vibration characteristics of complex structural systems have become a realizable goal.

The main advantage of the linear EVP is the high speed of execution. Another advantage is the use of the perturbation analysis to compute changes in frequency without the need to resolve the EVP. The method will, in most cases, lead to the need to manipulate large order matrices, which is uneconomic

in computing memory, and requires a large amount of data preparation and extensive storage. Furthermore, no recommendation can be given as to how many elements per member should be used; the accuracy of the solution increases as the number of elements increases. The limitation of the available operating system was that the maximum number of degrees of freedom may not exceed 72. For the solution of the linear eigenvalue problem it is insufficient to employ one element per member if the natural frequencies are to be determined with acceptable accuracy.

It should be emphasized that the above comparisons are based on experience gained when using these algorithms implemented on a microcomputer. It can be concluded that, if few modes are required, then the non-linear EVP will always provide a reliable solution without a time penalty and this should be preferred. If all the modes are required, then the decision depends on whether the prime consideration is execution speed, in which case the linear EVP is more successful, or accuracy of solution, in which case the non-linear EVP is the one to choose.

5.7 Closing Remarks.

In this chapter, the theory of the finite element method using the exact displacement functions and the solutions of the governing differential equations of motion for the element has been discussed. The frequency dependent dynamic stiffness matrix was obtained and the resulting non-linear EVP solved using determinant based methods, namely the sign count algorithm. This algorithm identifies a root of the solution using the concept of the Sturm sequence.

The solution methods described have been employed to determine the natural frequencices and modal shapes of large rigidly jointed plane and space frames within the core store of a small computer. The programs were modified, to take account of the effect of flexibly connected elements. One element per member proved sufficient for the solution and enabled convergence on any required natural frequency to any specified accuracy.

In the next chapter, development of the experimental measurement techniques and the instrumentation required will be discussed.

CHAPTER SIX

INSTRUMENTATION AND DEVELOPMENT OF EXPERIMENTAL TECHNIQUE

6.1 INTRODUCTION.

This chapter outlines the development of the measurement techniques and the instrumentation required for measuring the natural frequencies and mode shape, before and after the structure is damaged. The natural frequencies are obtained from the measurement of inertance of the laboratory model structures.

In the past, analogue systems have been used to monitor and control experimental work in the vibration field, but such techniques have limitations in their flexibility, accuracy and ability to process data. Significant progress has been made in recent years with the introduction of digital computers for data analysis and also as controllers for experimental research.

Signals from transducers fixed to the test structure will be in analogue form (i.e. continuous function of time) and, depending on the transducer, detect either the structural response or the input force. Hence, analogue to digital (A to D) conversion is required. Commercially available Frequency Response Analysers (FRA) and Spectrum Analysers (SA) carry out this and other functions, and these devices are discussed later in this chapter.

The problem which faces the experimenter is how to excite the system, measure the response and present the derived information in a clear and concise manner. Also, the

linearity of systems must be checked, because in the finite element analysis it is assumed that the structure behaves in a linear elastic fashion, as is almost always the case in structures if the amplitude of vibration is small. These problems will be discussed in detail in this chapter.

The vibration characteristics of structure in the linear elastic properties can be described by means of the frequency response function. This function may be determined experimentally by measuring the ratio of the response of the structure to the exciting force at various frequencies. Response is usually measured by accelerometers and so inertance may be expressed directly in terms of the measured quantities. The frequency response function is normally presented graphically, the function being expressed in terms of magnitude and phase or in terms of real or imaginary parts.

Structural natural frequencies may be measured by applying steady-state, random or shock loads to the structure. If random or shock loads are used then in this case it becomes necessary to determine the Fourier transforms of the response of the structure and the input force.

Using the steady state method, the structure is excited by a sinewave of constant amplitude and frequency. When the steady state response has been achieved, the amplitude and phase of the response with respect to the excitation is noted. Many papers and text books on this topic have been published (see

Kennedy et al (51), Ewins (52) and Bishop & Johnson (53) in which the methods of measuring frequency response required for the vibration analysis are discussed. The steady state method has been refined by the introduction of computer control (54) and incremental frequency response measurements may now be made automatically through chosen frequency ranges. Such automation is considerably simplified if a programmable digital synthesiser and a micro-computer are available. It is then readily possible to adjust the sweep rate to correspond with the attainment of steady conditions at each frequency of excitation. The sweep sine and random tests are discussed in more detail in this chapter.

The shock or transient method of excitation is attractive because the test time is very short. Interest in transient testing, as a technique applied to structures arose from the development of the digital computer and spectrum based data analysis systems using the Fast Fourier Transform (FFT). The basic method has been described by White (55) who has also discussed the choice of forcing function. A method of exciter attachment was investigated by Holmes et al (56). While Cawley et al (57) describe a method for improving the accuracy of the natural frequency obtained from the Fourier transform of structural response to an impulse.

It is extremely difficult to control simple pulses, using either mechanical impact or electrodynamic force generators in order to achieve the desirable energy spectrum characteristics. Also, in a transient test, the level of the

response in each structural mode cannot readily be controlled by the operator. Because of this, the steady state method was used in the present investigation.

In order to be certain of valid data and consistent results when processing test data for frequency response information, instrumentation techniques were continually updated and improved during the course of the investigation.

6.2 VIBRATION INSTRUMENTATION.

The experimental apparatus used for the measurement of inertance or apparent mass is shown in Fig. 6.1. Tests were carried out under the control of the Frequency Response Analyser (FRA) or Spectrum Analyser (SA). Control signals passed via the power amplifier to the vibrator, regulating frequency and amplitude. The response was measured using piezo electric accelerometers and charge amplifiers, output signals from which were transmitted to an appropriate analyser and then connected to the HP9825B computer through the interface bus. Details of individual items of instrumentation are now discussed.

6.2.1 Vibrator and Amplifier.

In order to provide the exciting force on the structure, a Goodmans Industries Ltd, type 390A electrodynamic vibrator was used. The maximum frequency range for operation was 4.5

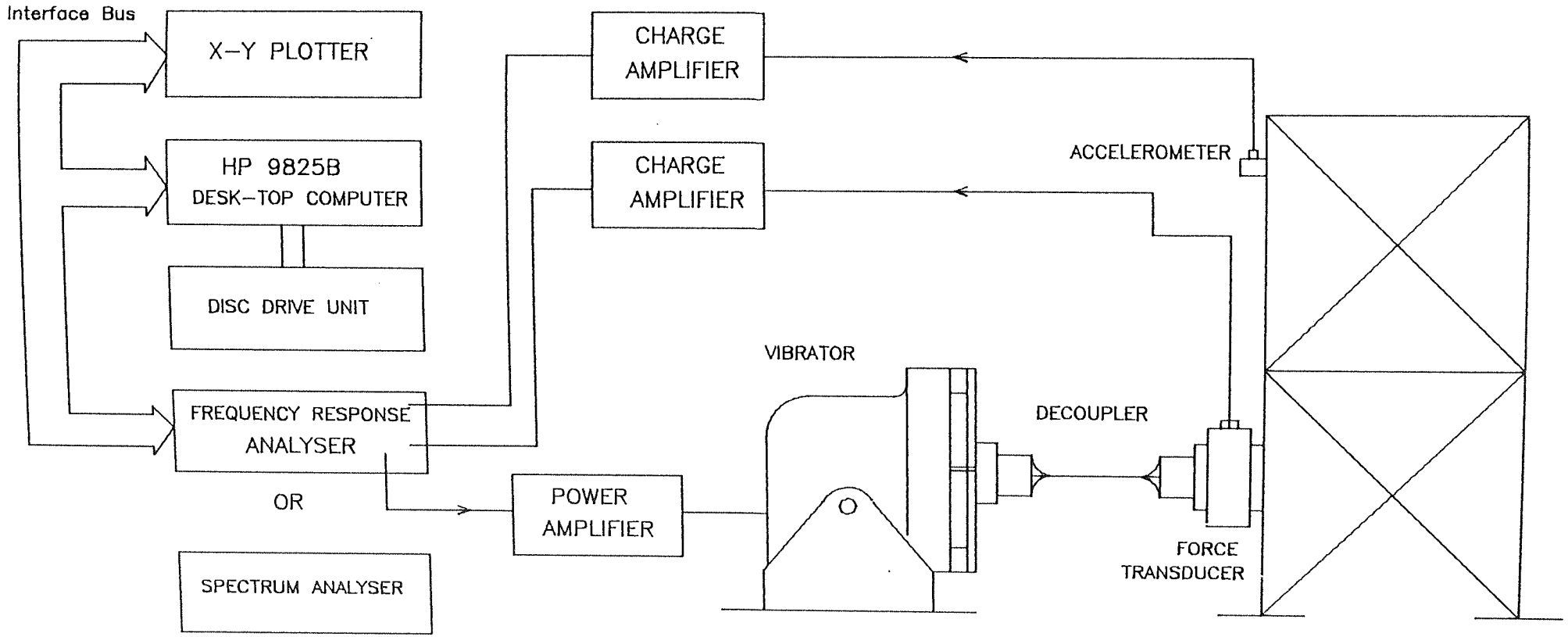

FIG. (6.1) INSTRUMENTATION FOR MEASUREMENT OF INERTANCE OR APPARENT MASS

KHz and the total permissable stroke was 0.5 inch.

The signal to drive the vibrator (generated by either an FRA or SA) was amplified by means of a Radford Electronics Ltd power amplifier type MA25 series 3, with maximum input 0.5 Volt (rms).

6.2.2 Transducers and Signal Conditioners.

In order to measure the input force function to excite the structure, a Bruel and Kjaer (B & K) piezo electric force transducer, type 8200 was used. This had a mass of 21 grams, force of 1KN tensile to 5KN compressive and a nominal charge sensitivity of 4 pC/N.

The response of the structure was measured by either B & K or DJ Birchal miniature piezo electric seismic accelerometers. These were chosen because they had a total mass of only 3.5 grams approximately with a nominal charge sensitivity of 3-4 pC/g with a resonance frequency of 32 KHz. These accelerometers were attached to the test structure using bees wax. Did they stay on?

It is important that the signals from both transducers are free from noise. Thus, low noise cables were used to transmit the signals to the charge amplifier. This charge amplifier used in the test was the model CA/04 manufactured by D.J. Birchall Ltd. This unit provided a sensitivity range of 1-100

pC/g, with output via a switched gain operational amplifier providing a 1 volt peak output for vibration levels of 1-300g was available for use.

6.2.3 Frequency Response Analyser (FRA).

The signals from transducers were analysed by a Solatron-Schlumberger Frequency Response Analyser, type 1172, using a correlation technique. A particular advantage of this machine is that it may be programmed to control the vibrator to carry out a sweep test by setting frequency limits and incremental frequency steps. The FRA was provided with a digital interface, enabling a computer to be used as a remote controller and data acquisition device. Thus, at each frequency investigated, the magnitude ratio and phase difference from the transducer signals were transmitted to the computer via the interface bus. The signal generator of the FRA had a range from 0.1 mHz to 9.999 KHz, with sine, square or triangular wave shape.

From the measurements of the force input and acceleration response the Inertance could be calculated. The FRA had a dynamic measurement range in excess of 80 dB and a feature to automatically select its measurement range from 10 mV to 100V in 20 dB steps. The sweep rate on the FRA could be altered by selecting values of the frequency step value, integration time and the measurement time delay.

6.2.4 Spectrum Analyser (SA).

A Hewlett Packard 3582A Spectrum Analyser provided all the advantages of a digital analyser FFT system. This Spectrum Analyser has two input channels and a frequency range of 0 - 25 KHz with a dynamic range of 80 dB. Inbuilt performance features of the instrument provide optimal solutions to the problems of low frequency spectrum analysis, thus allowing a greater flexibility in selecting the portion of the spectrum to be analysed. The available selection of frequency spans was found to provide exceptionally good frequency resolution. However, data acquisition time had to be increased to provide the required resolution when narrow spans were employed. For broader spans, data acquisition time was small and processing speed became the limiting factor.

The most significant additional measurement capabilities of the instrument resulted from having two input channels which operated simultaneously. Not only could independent input signals be examined for common characteristics, but also device input/output relationships could be evaluated. The instrument provided directly both amplitude and phase information about the transfer function of a structure. A built-in pseudo-random noise source could be used to drive the structure under test.

All of the measurement functions of the model 3582A were remotely programmable via the Hewlett-Packard Interface Bus (IEEE 488).

6.2.5 Controller and Data Aquisition System.

A Hewlett Packard 9825B computer was used as the processor around which an on-line laboratory controller and data analysis system. This desk-top computer was specifically designed for this type of application. It has a work space of 64 K bytes of random access read and write memory (RAM): the program language, HPL, is an interpreter type of language which is stored in Read Only Memory (ROM).

Peripheral devices connected to the computer included an X-Y plotter, a thermal printer and a mass-storage unit capable of storing up to one mega-byte. All devices were connected to the computer by means of a general purpose interface bus (IEEE 488). The function of this interface was to transmit the digital data back and forth between computer and peripheral devices via 8 data lines in an 8 bit parallel byte, serial mode. Fig. 6.1 shows the instrumentation for the measurement of inertance or apparent mass.

6.3 FREQUENCY RESPONSE RELATIONSHIP.

In structural testing, it is necessary to determine the frequency response, relating motion to applied force. The response is describable in terms of displacement, velocity, or acceleration. As reported by Salter (59) many different names are given to these relationships. According to the British Standard 3015 in 1976, the current definitions used

in frequency response testing, are:

1- Force / Displacement	Dynamic Stiffness
2- Displacement / Force	Receptance
3- Force / Velocity	Impedance
4- Velocity / Force	Mobility
5- Force / Acceleration	Apparent mass
6- Acceleration / Force	Inertance (In)

Receptance, mobility and inertance can be measured directly; from the response of the structure to a unit dynamic force applied at one point in the structure. But, dynamic stiffness, impedance and apparent mass are difficult to measure because the forces in the structure are due to a unit displacement, velocity or acceleration occurring at one point only in the structure. Thus, 1, 3 and 5 are usually derived from 2, 4 and 6 by matrix inversion.

In addition three other definitions describe the positions and directions of the measured force and response. For example, with respect to inertance:

(I) The point inertance is obtained by measuring the acceleration and the applied force at the same point and in the same direction.

(II) The transfer inertance is obtained by measuring the acceleration at any point other than that at which the force is applied.

(III) The cross inertance is obtained by measuring the

acceleration and the force at two different 'reciprocal' points, i.e., two inertance measurements are obtained by interchanging exciter and accelerometer positions.

It is apparent from the above that measurement of inertance would yield mobility and receptance via integration. The inertance relationship was chosen for use in the present work since acceleration was measured directly by accelerometers.

6.4 CALIBRATION TECHNIQUE.

Accurate calibration of transducers is essential if reliable and precise measurements are to be made. The force transducer and accelerometers used in the experimental work were checked for calibration and the gains of the charge amplifiers were adjusted to give the necessary voltage sensitivites. In carrying out the calibration the transducer together with a B & K standard accelerometer type 8305 was mounted on a vibrator and subjected to known levels of excitation over a range of frequencies.

The outputs from the charge amplifiers of the standard accelerometer and the transducer under calibration were fed either to FRA or SA, as desired. The method used to calibrate the force transducer required the measurement of the inertance of a known mass.

The frequency response characteristics of the transducer and

charge amplifier combination were plotted as shown in Fig's. 6.2 and 6.3. The graph of these figures shows that within the frequency range of interest the response is linear with zero phase shift. Further information on the calibration technique may be found in (60).

6.5 DESIGN OF MODELS TO REPRESENT FABRICATED STRUCTURES.

A structure whose components are all one-dimensional is usually called a framed structure. Such a frame as a whole usually exhibits either two or three-dimensional extensions. For the purpose of the present work a series of framed structures were used and the following factors borne in mind in choosing the design of each model.

1- The structure must have linear elastic properties, limiting the amplitude of vibration to small values.
2- For ease of construction and economy, its members should be made from standard size material that is readily available.

The experimental investigations of the vibration characteristics were carried out on a series of different model structures. These models were either plane or space frame structures. These structures could be excited at either one of two positions, one near the free end and the other near their mid-point, represented as points 1 and 2, thus enabling all the modes in the frequency range of interest to

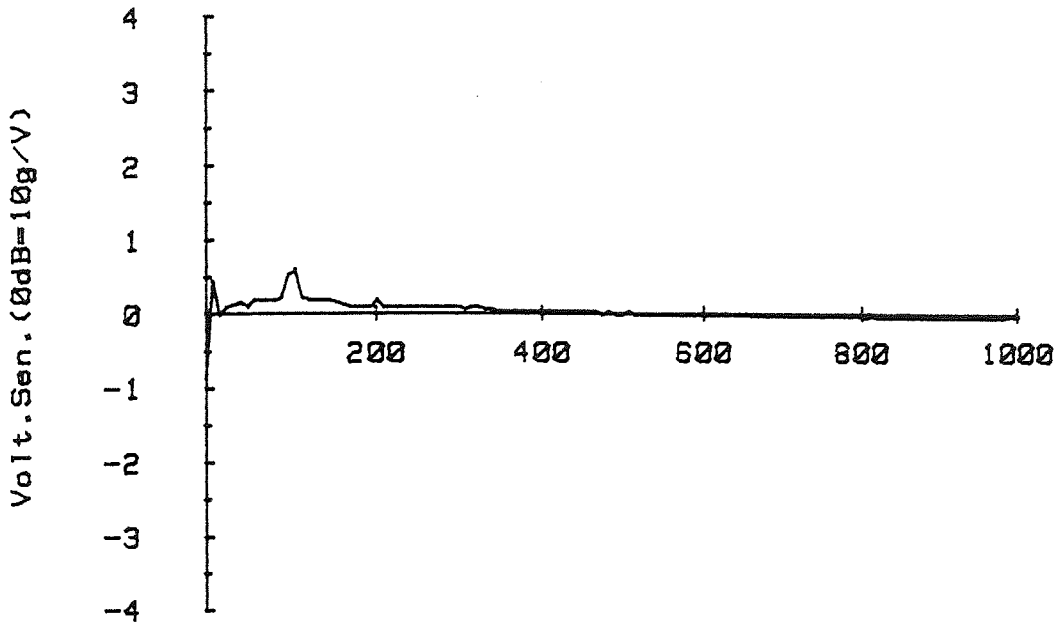

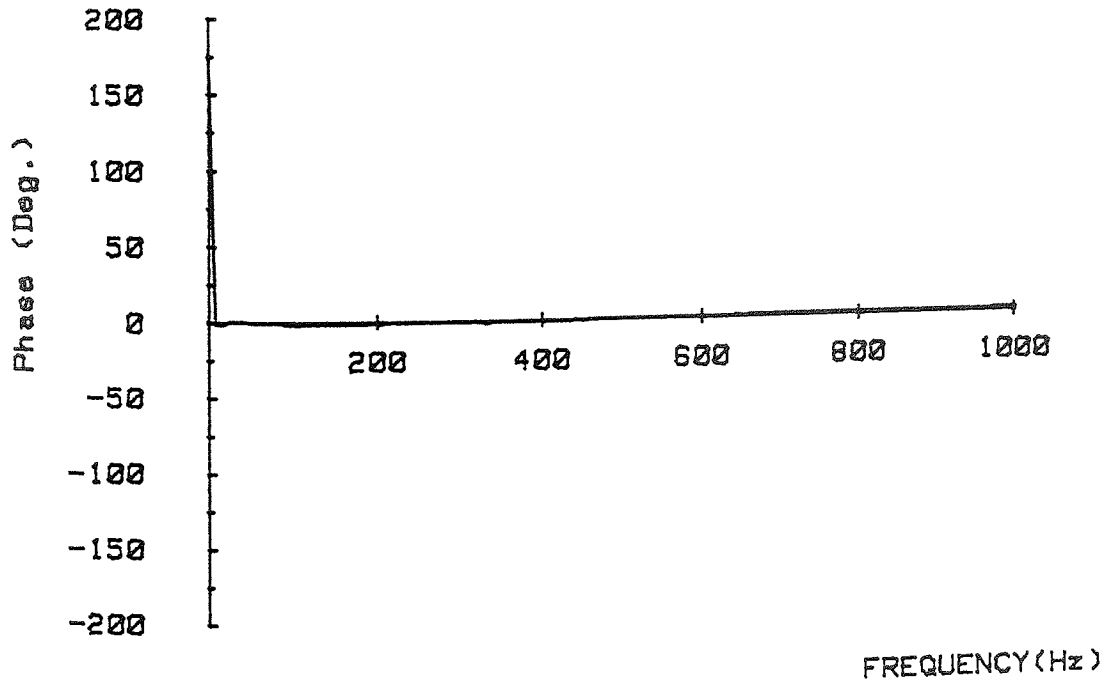

Fig.(6.2) CALIBRATION OF ACCELEROMETER

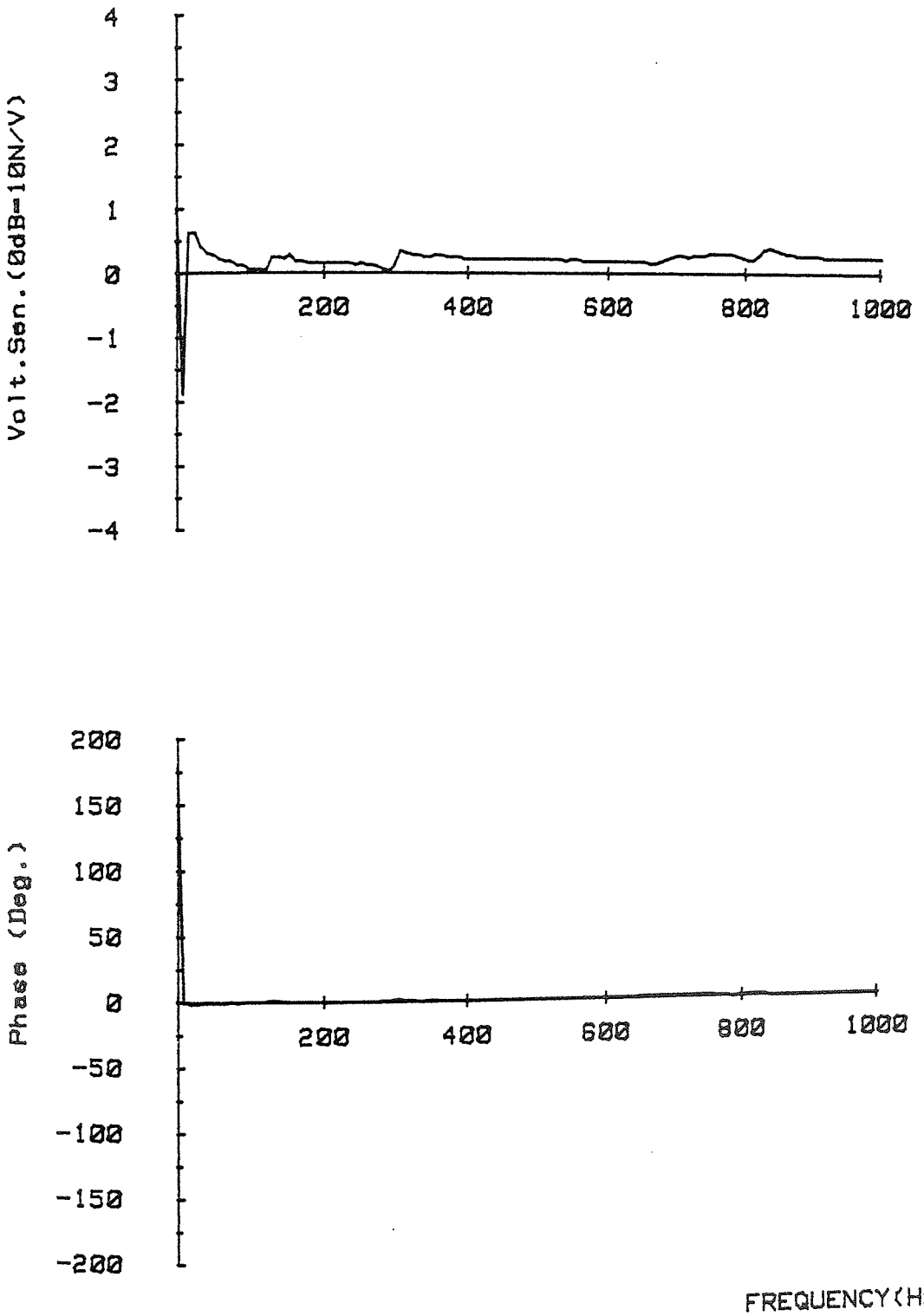

Fig.(6.3) CALIBRATION OF FORCE TRANSDUCER

be excited. In order to provide a degree of restraint, these structures were fixed to a large machine bed plate in such a manner so as to prevent motions; two translations and one rotation for a plane frame or three translations and three rotations for a space frame. Each structure will be discussed in turn.

1- Simple structure.

I- The cantilever.

The first structure to be investigated was the cantilever, as shown in Fig. 6.4. This was chosen as a starting point because a cantilever is one of the simplest structures: also, the characteristic functions representing normal modes of vibration are available (61,62).

2- Plane frame structures.

I- The symmetric cross-brace portal frame.

The first plane frame structure was a symmetric cross-brace portal frame, see Fig. 6.5, which consisted of nine members of different lengths made from a mild steel rectangular bar. This model was used to study the dynamic response and to establish the changes in natural frequencies of the structure due to partial and complete fracture. The locations of the accelerometer and damage positions are shown in Fig. (6.5a).

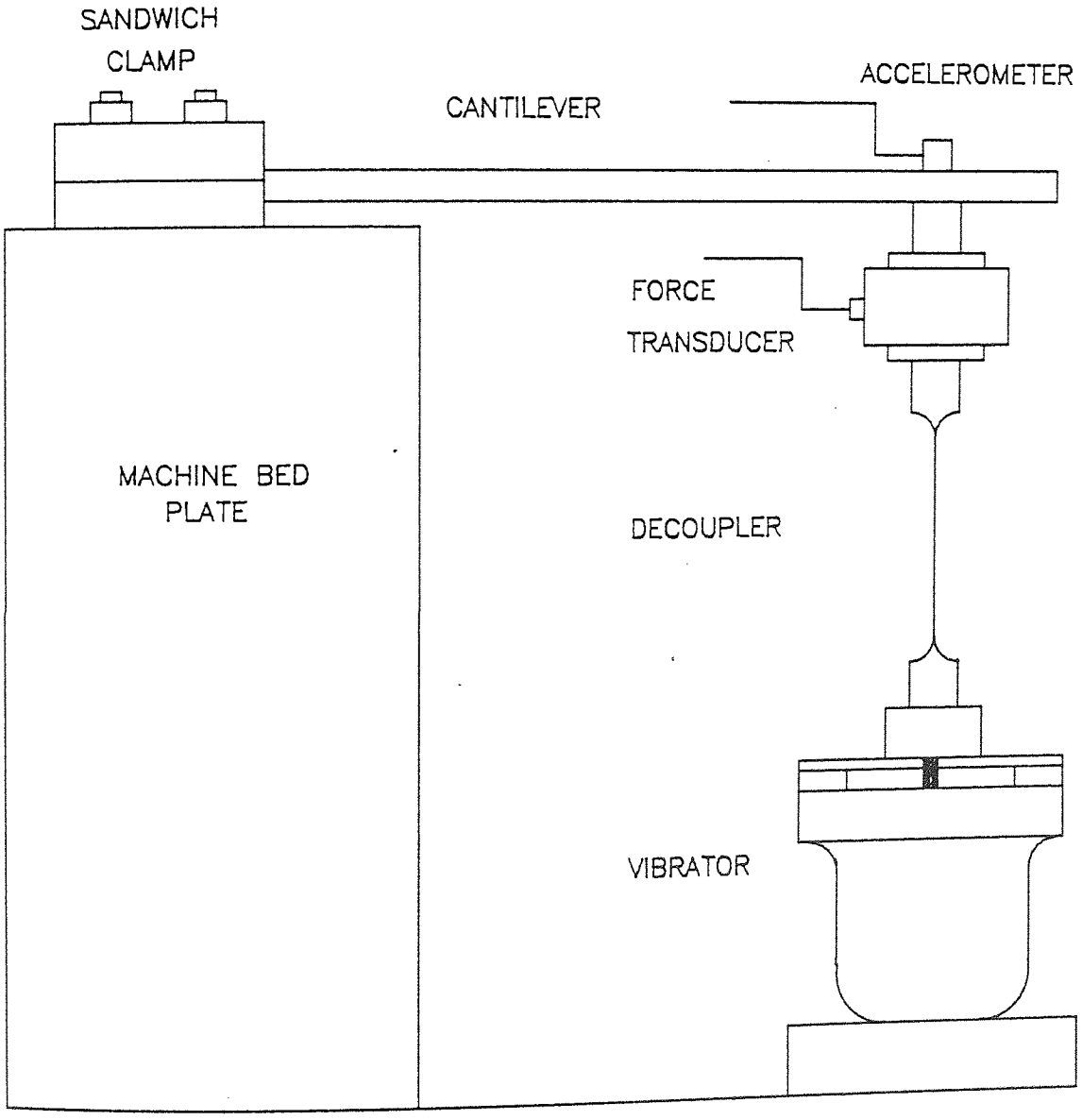

FIG. (6.4) EXPERIMENTAL SET-UP FOR CANTILEVER INERTANCE TESTS

II- The asymmetric cross-brace portal frame.

The second plane frame was an asymmetric cross-brace portal frame, see Fig. 6.6, which consisted of fourteen members of different lengths fabricated from a mild steel bar. This structure was more complicated than the first plane frame but had the same cross-sectional area. The locations of the accelerometer and damage positions are shown in Fig. 6.6.

III- The symmetric tower frame.

The third plane frame structure was a symmetric tower frame, see Fig. 6.7, which consisted of fourteen members fabricated from a mild steel rectangular section bar. This structure had a different cross-sectional area from that of structures I and II. The locations of the accelerometer and damage positions are shown in Fig. 6.7.

IV- The asymmetric tower frame.

The fourth plane frame model was more complicated than the other test structures. This model was an asymmetric tower frame consisting of twenty three members, each member having a rectangular cross-sectional area of the same dimensions as the preceding structure (III), see Fig. 6.8. The locations of the accelerometer and damage positions are shown in Fig. 6.8.

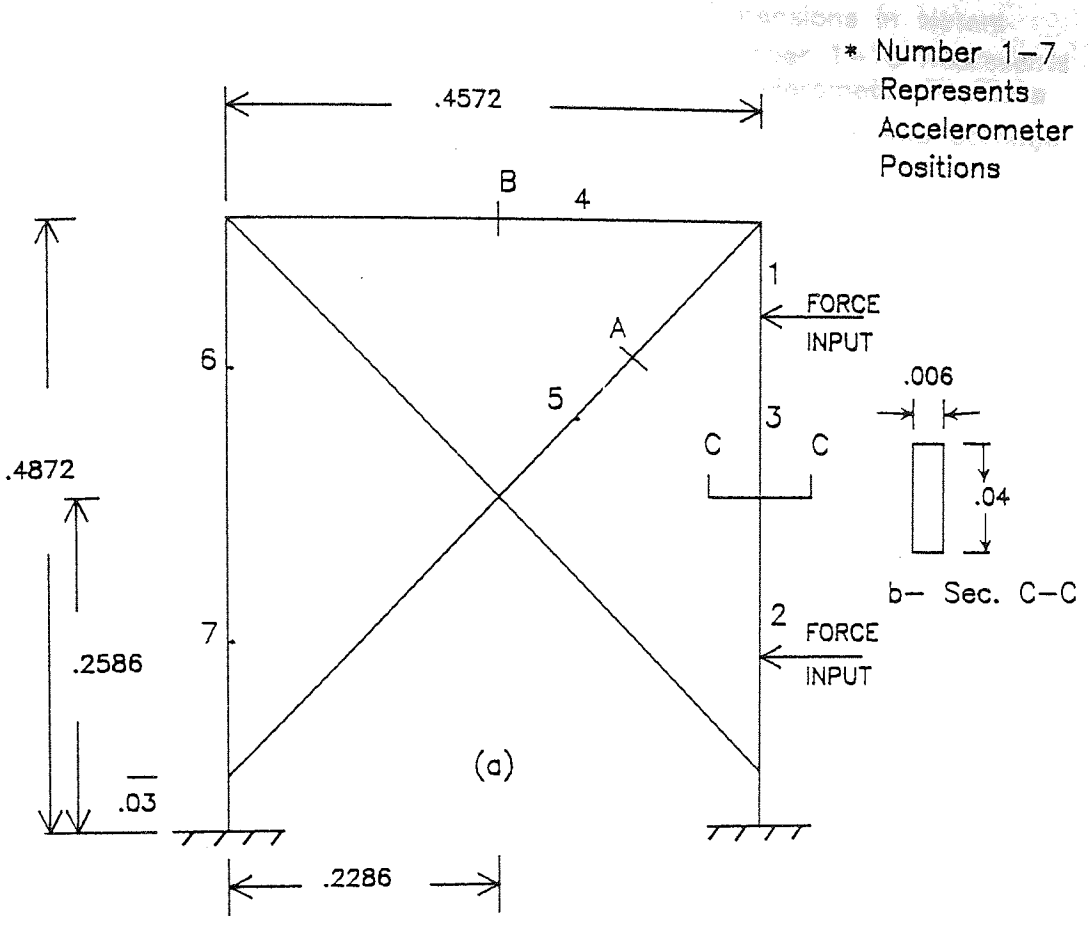

FIG. (6.5) SYMMETRIC CROSS-BRACE PORTAL FRAME

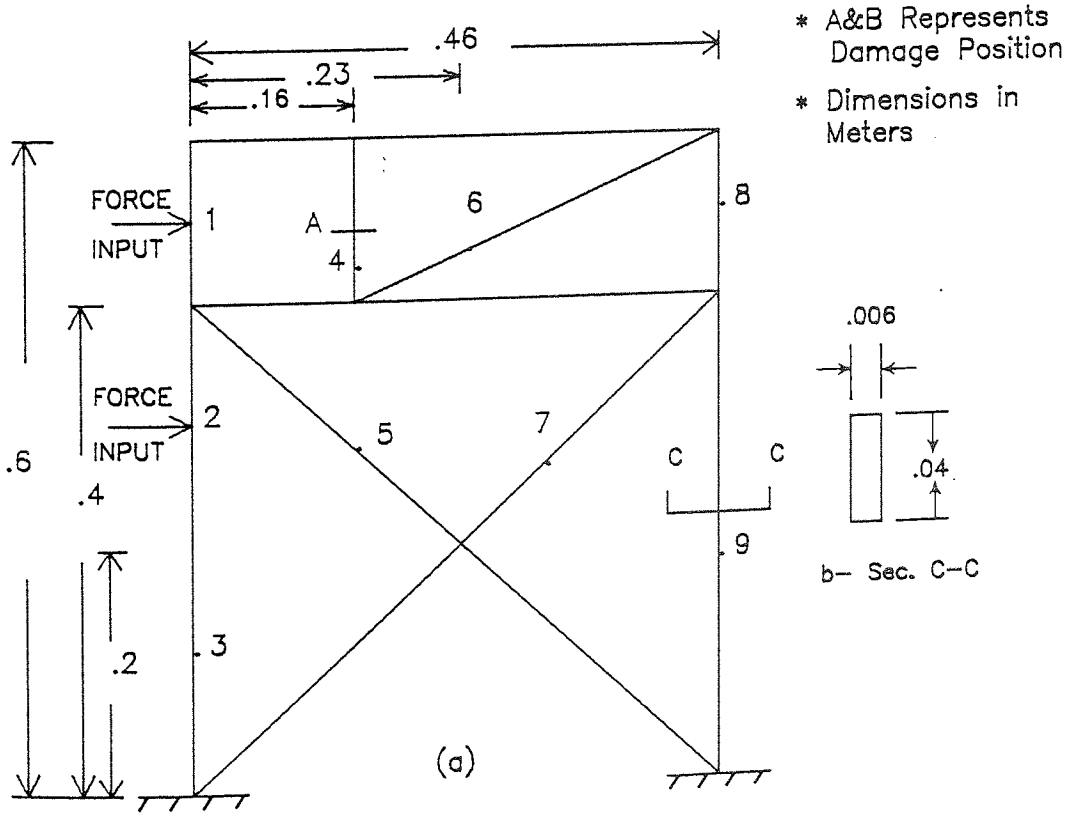

FIG. (6.6) ASYMMETRIC CROSS-BRACE PORTAL FRAME

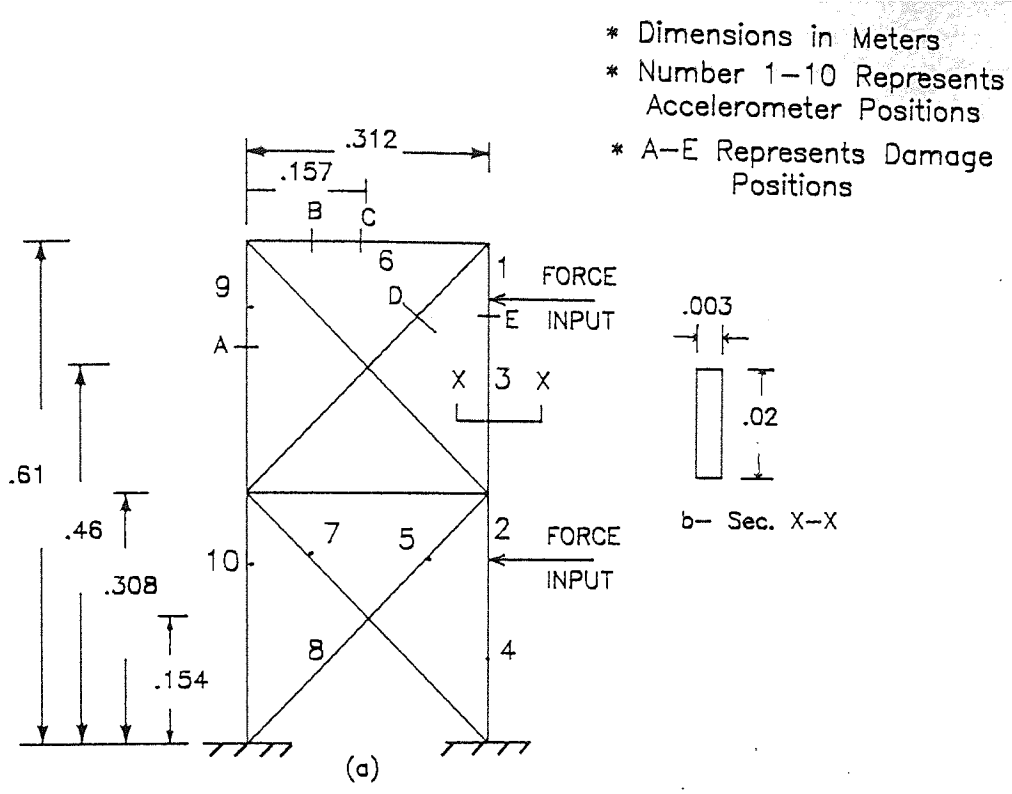

FIG. (6.7) SYMMETRIC TOWER FRAME

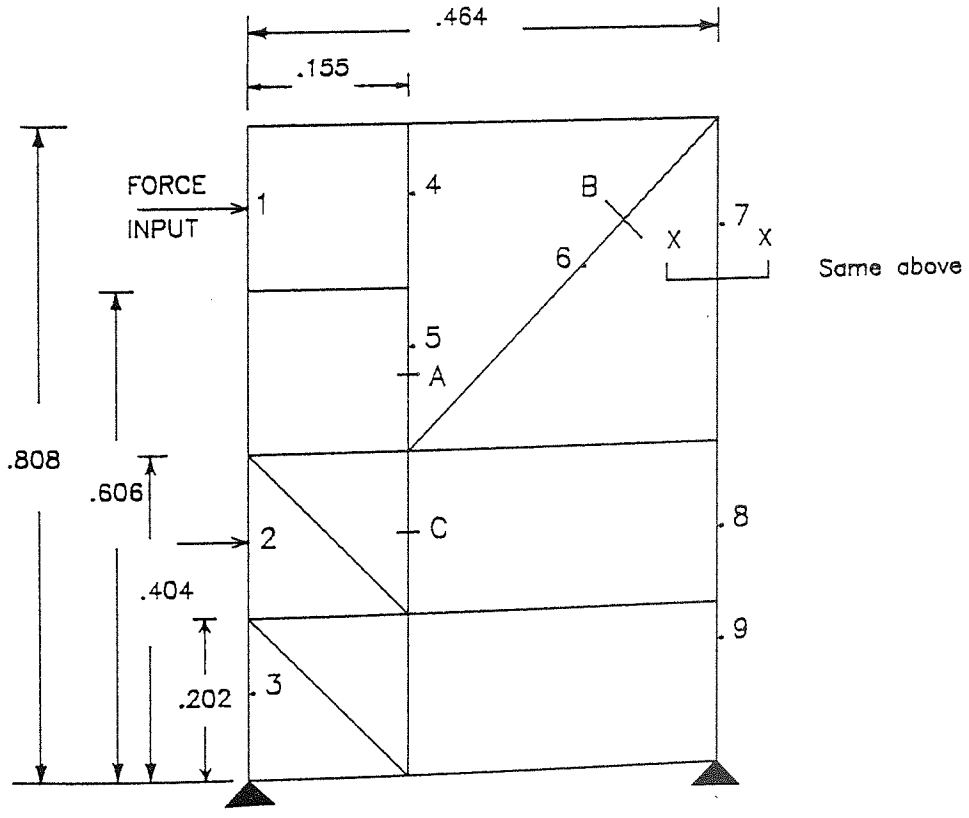

FIG. (6.8) ASYMMETRIC TOWER FRAME

3- Space frame structures.

Experimental investigation of the vibrational characteristics of more realistic structures were carried out on three space frame models fabricated from bright drawn mild steel which are as follows.

I- The space frame symmetric about both diagonals.

A general arrangement of the first model is shown in Fig. 6.9, including the accelerometer, vibrator and damage positions. Excitation was applied in either of two orthogonal horizontal directions, X and Z, as indicated. The structure was attached to the heavy steel bed through four plates (B), using three bolts through each plate. The structure consisted of four long steel columns (A) to which braces (C) were connected. The model was a symmetric space frame about both diagonals and consisted of twenty-four members, of common circular cross-sectionl area.

II- The space frame symmetric about one diagonal.

The second model was symmetric space about one diagonal. This structure was fabricated from the first model by removing one of the top corner members and inserting another member in the top diagonal, as shown in Fig. 6.10. The model then comprised twenty-two members.

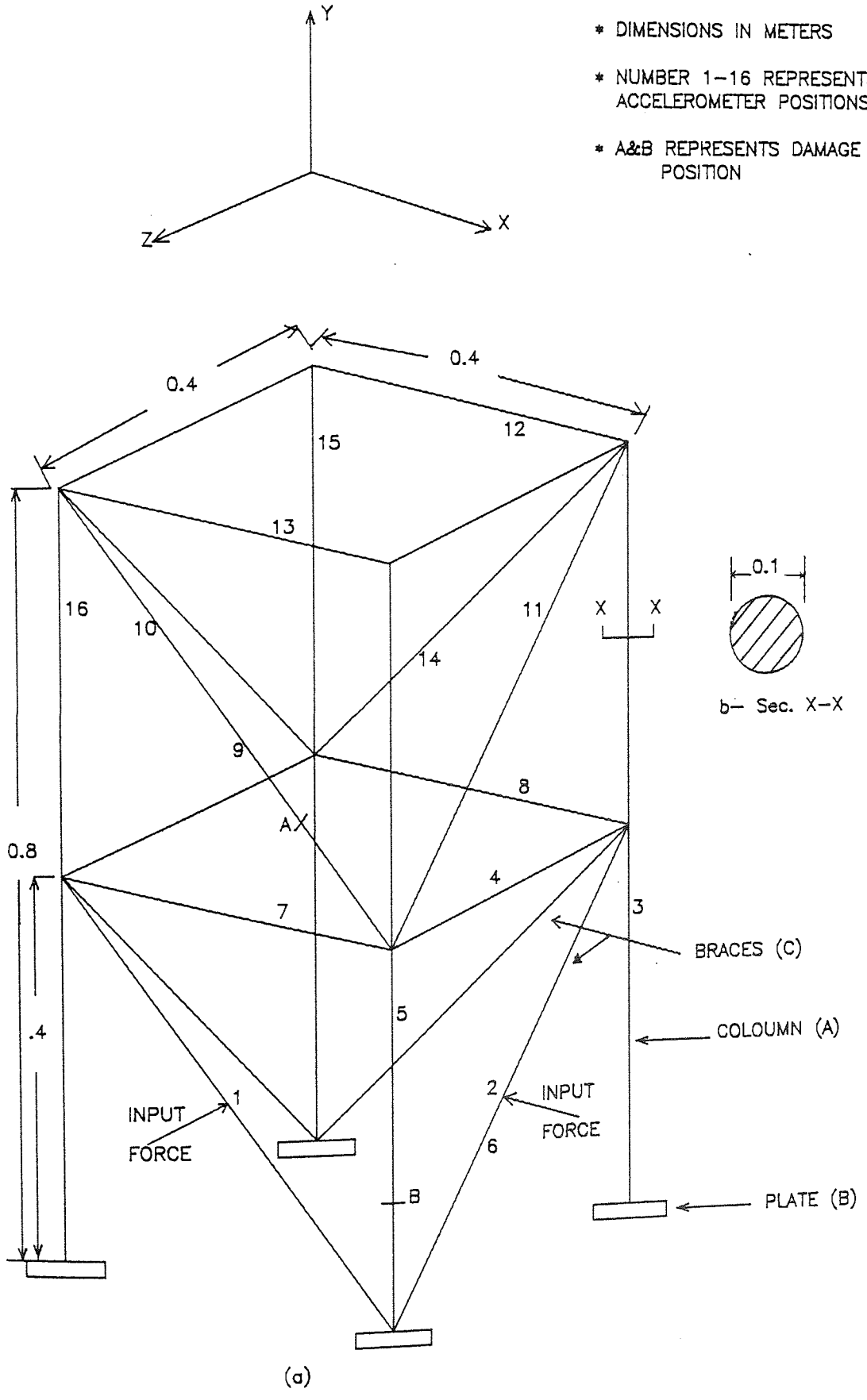

Fig. 6.9 SYMMETRICAL SPACE FRAME MODEL ALONG BOTH DIAGONALS

III- The asymmetric space frame.

The final space frame model was modified from the second model by the addition of a brace member in the XY plane as shown in Fig. 6.11. The model was now an asymmetrical space frame consisting of twenty-five members. The locations of the accelerometer and damage positions are shown in Fig. 6.11.

6.6 TESTING TECHNIQUES.

6.6.1 Test Procedure.

The development of the testing techniques used to measure inertance is now described. The objective of this section is to detail a test procedure which will give accurate values of the natural frequencies of a structure as well as indicating and recording changes in natural frequencies as the structures is damaged progressively.

The procedure requires that the structure under test be excited by a harmonic force and the response at various points of the structure be measured. In order that all test results may be compared meaningfully, the test procedure must establish homogeneous conditions throughout all phases of the experimental work. Thus, the method used for supporting the structure during each investigation should be simple to set up and must be reproducible. Also, it is essential to

* A&B REPRESENTS DAMAGE POSITIONS

* 1–17 REPRESENTS ACCELEROMETER POSITIONS

* SAME DIMENSIONS AS IN Fig. 6.9

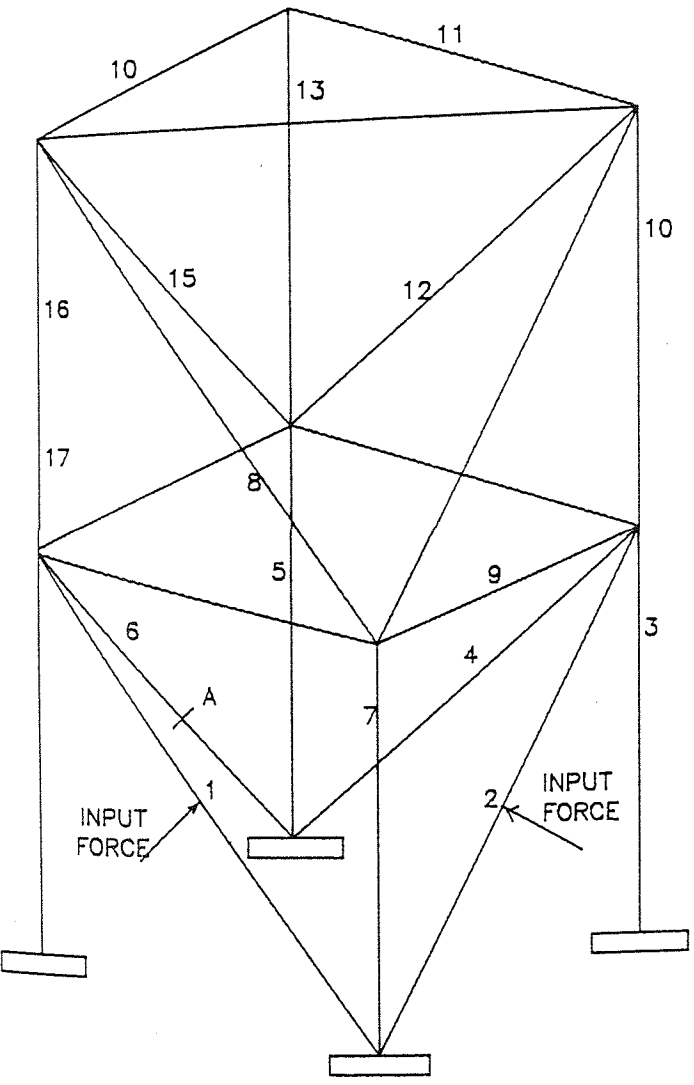

Fig. 6.10 SYMMETRIC SPACE FRAME MODEL ALONG ONE DIAGONAL

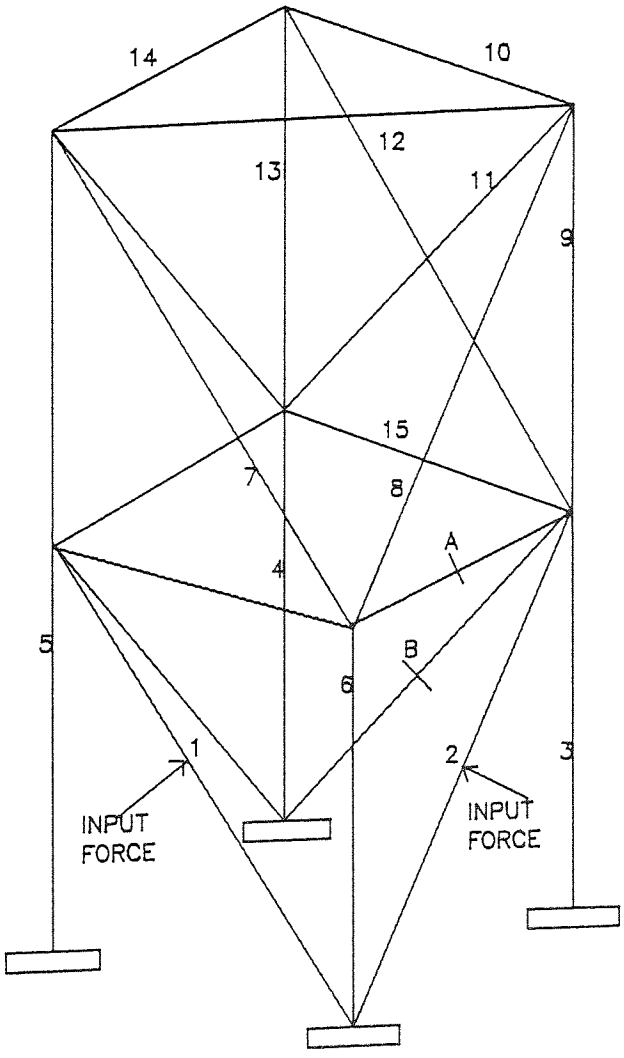

Fig. 6.11 ASYMMETRIC SPACE FRAME MODEL

minimise the number of any changes to the structure e.g. mass and constraint, in order to obtain accurate results. The transducer should be of small mass to have negligible effect.

An arbitrary choice of the point of excitation could lead to difficulties in producing the resonance at certain natural frequencies of the structure. For example, exciting the structure at a nodal point (point of zero amplitude of vibration) of a certain natural frequency would result in missing out the resonance at that natural frequency in the frequency response function. Thus, it is necessary to excite the structure at a point of maximum amplitude of vibration for a given frequency. It is also useful to change the position of excitation of a structure to excite the different modes of vibration. However, measurements are made either for a point inertance or for a transfer inertance.

A simple guide is given below which outlines the main points of the procedure to be followed when setting up and conducting the measurement of the frequency response function (63).

1- Suitable accelerometer and force transducer attachments are required for the structure.

2- An electro-dynamic exciter is required to provide sufficient force. This exciter is then connected to the structure by a decoupler to ensure minimal rotational

constraint.

3- Correct alignment of the exciter, connector, and force transducer assembly must be ensured.

4- The amplifier gains in both channels must be adjusted in order to use as much of the dynamic range of the analysis as possible.

5- Extraneous noise must be prevented.

Several methods exist by which inertance data may be measured experimentally. This can be done by using periodic or non-periodic random excitation. In this work only the basic sinusoidal and periodic random excitation technique will be described in detail.

Sweep Sine Test.

In this particular form of testing, the structure is excited by a harmonic (sinusoidal) force generated by a electro-dynamic shaker. A mechanical force is generated at the command frequency which is then applied to the test structure through the force transducer. The response is detected and measured using the piezo-electric accelerometer. All the transducer signals are amplified and fed into the analyser which measure the amplitude and phase of each signal. The force and response signals are filtered to allow only the excitation frequency component to be measured.

Frequency of excitation is slowly swept through the range of interest in order to allow time for the structure under test to reach the steady state of vibration and for the data analysis system to make accurate measurements. Currently, in a digital analysis system the excitation frequency is gradually increased in small steps, the force is allowed to find its own level and phase measurements between the force and response signals are performed digitally. The sweep sine method of testing is generally considered to be the most accurate method of testing but unfortunately proves to be time consuming. As this technique was suitable for controlling one experiment at a time with a single accelerometer, it was necessary for the test to be repeated with different appropriate accelerometer positions.

Random test.

The structure is excited by a periodic random varying force which is band limited and in that bandwidth has a continuous spectrum with components at all frequencies. This will, in turn, excite a response with a continuous spectrum and using a suitable analyser the ratio of the force and response can be obtained over the frequency range required. This process is now performed digitally by using the FFT spectrum analyser. The advantage of using random excitation is that this is a faster method of testing, especially if a "quick look" is required in the frequency range of interest. If very accurate results are required this advantage is reduced.

6.6.2 Decoupler Design.

It is necessary for the model structure under investigation to provide the freedom of translation and rotation of the structure. An important part of the investigation concerned the perfecting of a measurement techniques which allowed the structure to rotate freely without any restraint being imposed by the attachment of the vibrator while ensuring that a pure force was transmitted to the structure, i.e. no restraining or any associated moments.

The use of a decoupler assembly has several advantages. The possible misalignment of the vibrator, may give rotational strain acting on both the vibrator and force transducer to produce not only errors in the inertance measurement but the possibility of serious damage to the vibrator and transducer. A further advantage of the decoupler is that it prevents the transmission of large moments caused by misalignment.

The simplest way of preventing the vibrator from introducing rotational restraint is to connect it to the structure via a decoupler assembly, which is stiff in the direction of excitation, but flexible in all other directions. To optimise the design of the decoupler a cantilever structure was coupled with different decouplers of various diameters and lengths. The inertance measured using each design of decoupler was then compared with the theoretical value: the optimum performance was obtained from a decoupler made from 1mm diameter of piano wire shown in Fig. 6.1. The force

transducer was attached directly to the structure.

It was noted that if the structure under investigation had a high stiffness then the effect of the contact stiffness between the transducer and the structure might lead to errors in the low frequency measurements (64).

6.7 EXCITATION AND MONITORING OF THE STRUCTURAL RESPONSE.

6.7.1 Method of Excitation.

It is essential to ensure that the method of excitation excites the structural response above background noise levels, excites the structure over the whole frequency range under examination, but avoiding a level of excitation which would drive the structure into a non-linear or overload type of behaviour.

The type of excitation may be extremely important. Hence, random or sinusoidal excitation may be absolutely necessary for certain types of structures, whereas, impact excitation may often be more appropriate for other types. As previously mentioned, an arbitrary choice of the point of excitation could lead to difficulties in producing the resonance at certain natural frequency of the structure.

To determine the inertance of the structure the input force must be monitored. This was achieved by mounting the force

transducer on the electro-dynamic shaker which was attaching to the structure via a decoupler. The effect of exciter attachment on the accuracy of measured inertance has been investigated (56). In the present tests three types of exciter attachment were used depending on the type of structure and the type of excitation, as shown in Fig. 6.12. The design illustrated in Figs. 6.12a and 6.12c were used for periodic excitation through all the tests for plane and space frame structures, respectively, but Fig. 6.12b was used for the periodic impulse. The use of the electro-dynamic shaker proved to be satisfactory but it was necessary to ensure that the attachment to the decoupler was aligned accurately. This system was adopted for all the tests described here, but in other situations, it may be preferable to use one of the other methods.

6.7.2 Inertance Measurements.

It was found that only the plot of inertance gives the true frequency response function even when a constant voltage or current is supplied to the shaker, so that measurement of the response alone gives an inaccurate representation of the natural frequencies. Thus, measurement tests were carried out on the structures in order to investigate the natural frequencies of the first ten modes by obtaining the structural response to sinusoidal excitation inputs. These natural frequencies were obtained from the inertance plot of different points on the structure. In other words these

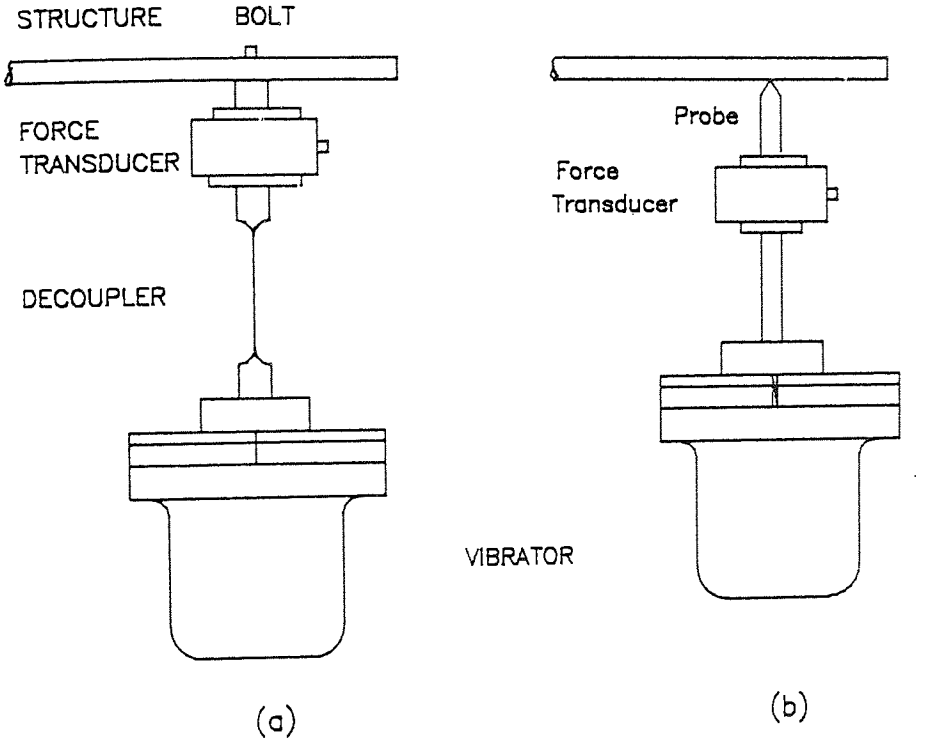

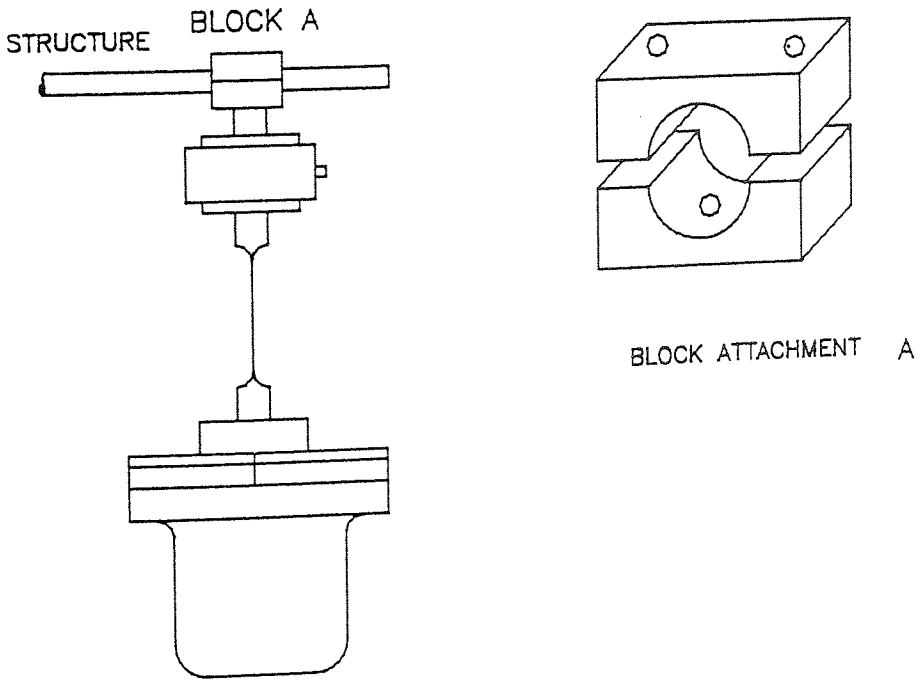

FIG. (6.12) METHODS OF EXCITER ATTACHMENT

measurements can be made at a single point on the structure.

Since inertance is the acceleration response at one point due to a unit excitation force at the same point or other specified points in the structure. If the force is applied at point j and then the response is measured at i,

$$In_{ij} = Ac_i / F_j \qquad (6.1)$$

Where:

Ac_i is the acceleration at i, (i=1,2,3,...,n)

F_j is the force at j, (j=1,2)

In_{ij} is the transfer inertance between coordinates i&j

If all the direct and transfer inertance for a structure is obtained, equation (6.1) can be written in matrix form as:

$$\begin{bmatrix} In_{11} & In_{12} \\ In_{21} & In_{22} \\ . & . \\ . & . \\ In_{n1} & In_{n2} \end{bmatrix} \begin{Bmatrix} F_1 \\ F_2 \end{Bmatrix} = \begin{Bmatrix} Ac_1 \\ Ac_2 \\ . \\ . \\ Ac_n \end{Bmatrix} \qquad (6.2)$$

$$[In]\{F\} = \{Ac\} \qquad (6.3)$$

Pre-multiplication of equation (6.3) by the inverse [In] gives

$$\{F\} = [In]^{-1}\{Ac\} \qquad (6.4)$$

The inverse inertance matrix is called the apparent mass matrix. Inertance is often expressed by using a logarithmic decibel scale, so that

$$\text{In (dB)} = 20\ \text{Log}_{10}(\text{Ac/F})\ \text{dB} \qquad (6.5)$$

For convenience, translational acceleration is expressed in terms of g (1g = 9.81 m/s^2) and force in Newtons (N). Typically, 0dB would be defined as an inertance of 1g/N. The reason for using this logarithmic format is to include the resonance peak in the dynamic range of the analyser. Thus, inertance data may be presented in two forms, either as plots of modulus against frequency and phase against frequency, or a vector diagram of the real component plotted against the imaginary component. The former presentation is the more useful if overall inertance levels are required for a wide frequency range.

Peak values of the inertance represent the condition of maximum response for the minimum excitation force i.e. a resonant condition. Thus, the natural frequencies are coincident with the resonant frequencies for a lightly damped structure, which is the condition for all the structures in this work.

In recent years, further developments in measurement technology have made it possible to achieve greater accuracy in experimental results so that data may now be used effectively not only for comparisons with theoretical

predictions, but also for predictive and analytical purposes, e.g. to measure the changes in natural frequencies due to the onset of damage.

6.7.3 Effects of Damage on the Inertance Measurements.

Where a structure has a series of natural frequencies or resonances, then these natural frequencies are changed, to a greater or lesser degree, if a member is damaged. These changes can be shown by plotting the inertance measurements before and after the structure is damaged. For a structure of given geometry, the amount and distribution of the changes in the frequencies varies according to the position of the damaged member within the structure and the extent of the damage. The characteristic of inertance is so fundamentally different when total failure occurs in a structural member, that progressive damage has been inflicted during the present tests to illustrate the gradual change in the shape of the inertance plots. If comparisons of the inertance measurements are made between the intact structure with those on the same structure after damage, then, the following three types of difference are found:

I- Difference of the inertance shape in the whole frequency range.

II- Difference in the amplitude of inertance at resonance and anti-resonance frequency.

III- Difference in natural frequency.

Occasionally, it was discovered that the frequency of one mode would increase slightly after damage was inflicted. This could have been due to the fact that the overall reduction in the strain energy of the system was less than the reduction in kinetic energy, due to the presence of the damage, but this is not the case for each individual mode. Another possible reason for the increase might be an error in the initial frequency readings. Since it was found that the damage model (e.g. a saw cut) provided clearance thus allowing the structure to vibrate up and down about the axis of the cut, sometimes resulting in noise affecting the inertance measurement.

6.8 EFFECTS OF TEST PROCEDURE AND CONFIGURATION ON THE INERTANCE MEASUREMENTS.

A series of tests was developed to establish the effects on the inertance mesurements of varying the test procedure and the test configuration. The number of additions and constraints to the structure was kept to a minimum in order to obtain accurate measurements and the transducers were of small enough mass to have a negligible effect. It would be possible to include the effect of the transducers into dynamic analysis, but this would add unnecessary complications and uncertainties to the program.

Any additions made to the structure have to be rigidly

attached, so that the nature of the response is not affected by such additions. For example, if the attachments are not rigid then the effect can be compared to that of additions to a spring-mass system. Inaccuracies associated with the measurements of changes in frequencies can arise from changes in the environment, e.g. the effect of temperature on the frequency depended on the type of material used. However, for the materials employed in the present work, it was found that the effect of temperature on the frequencies was negligible.

The following tests were used to investigate the effect of the inertance of the structure.

Repeatability.

1- The sweep tests were performed before and after dismantling and remaking the decoupler connections at varying periods. There was no noticeable effect on the inertance measurement.

2- A series of sweep tests was performed and repeated on two identical structures to determine the effects of constructional tolerances. It was noted that there was little difference in some modes on the measurement of the natural frequencies. The results of this test will be shown in chapter eight.

3- It was noted that by measuring the transfer inertance there was no effect on the inertance of the structure.

Sweep Rate.

The sweep rate of the FRA can be altered to improve the smoothness and accuracy of the inertance curves by judicious selection of frequency step value, integration time and measurement delay. Also it was noted that changing the sweep direction to decreasing the frequency had little effect on the measurements.

In order to indicate how sensitive the results were to changes in test configuration, the cross inertance must be compared for each of these tests. When a concentrated mass was added to the system (mass of the transducers) no significant difference on the cross inertance and resonance frequencies was found. Neither was inertance affected by altering the vibrator stiffness or by adding mass to the moving parts.

Generally contact stiffness, i.e. the stiffness of the contact between the vibrator and structure, became significant when measuring the frequency response of those 'mass like' systems which themselves, had a high stiffness. As a result, the method of connecting the vibrator to the structure was designed so that the force transducer was fixed directly to the structure. The contact stiffness, K, is a function of the contact area, and is estimated in [63] to be,

$$K = 2ER/(1-\upsilon^2) \qquad (6.6)$$

Where E and ν are the modulus of elasticity and poisson's ratio respectively, and R is the radius of a contact area.

6.9 MEASURING STIFFNESS AT A CRACK.

As explained in chapter three, the crack was modelled in the form of a spring positioned at a node that corresponded with the position of a crack. A series of experiments was performed in order to obtain values for the equivalent stiffness of a particular section of the cantilever. In these tests the load was applied at the free end of the cantilever, where the deflection was measured, initially without the crack and repeated with increasing crack depth.

This method of representation seemed to give a logical and more satisfying picture of a partial crack. It is imagined that an appropriate spring is included at a crack position to account for stiffness at that point. This method is suitable for the analysis of any frame structure using the finite element method.

An expression for the fictitious spring stiffness K at a crack can be made from experimental and theoretical considerations. Theoretically, using the elementary theory of beam and experimentally, using static structural analysis

methods to obtain, in terms of the applied load the corresponding deflections. Figure (a) below shows representation of the cantilever beam with a spring of stiffness K positioned at point A. By the elementary theory of beam bending, the bending moment (BM) at a point x along beam is given by:

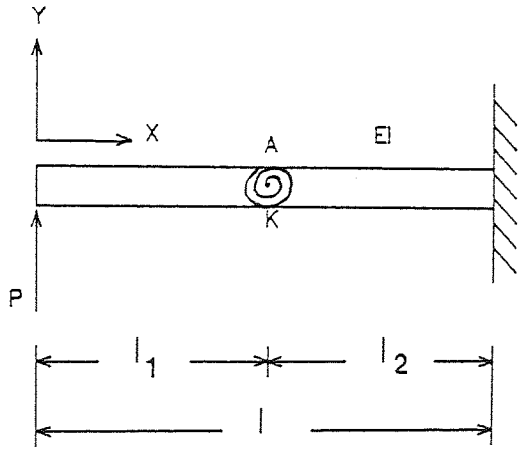

Fig. (a)

When $0 < x < l_1$,

$$EI\ Y'' = BM = Px \tag{6.7}$$

Where $Y'' = d^2Y/dx^2$

Integrating once,

$$EI\ Y' = (Px^2/2) + C_1 \tag{6.8}$$

Integrating again, gives

$$EI\ Y = (Px^3/6) + C_1x + C_2 \tag{6.9}$$

When $l_1 < x < l_2$,

$$EI\ \bar{Y}'' = Px \tag{6.10}$$

Integrating twice, gives

$$EI\ \bar{Y}' = (PX^2/2) + C_3 \qquad (6.11)$$

$$EI\ \bar{Y} = (Px^3/6) + C_3x + C_4 \qquad (6.12)$$

Boundary conditions, to evaluate C_1 to C_4 are,

At $x = l_1$, $\overset{+}{Y} = \bar{Y}$ and $BM = K\ (\overset{+}{Y}' - \bar{Y}') = Pl_1$

At $x = (l_1 + l_2)$, $Y = 0$ and $Y' = 0$

Substitution of these boundary conditions into equations (6.8) to (6.12), will yield C_1 to C_4.

To find the tip deflection (Ymax) at x=0 , equation (6.9) becomes

$$Ymax/P = ((l_1 + l_2)^3/3EI) - l_1^2/K \qquad (6.13)$$

or

$$K = \frac{l_1^2}{((l_1 + l_2)^3/3EI) - Ymax/P} \qquad (6.14)$$

Equation (6.14) can not be used in general because it depends on boundary conditions and lengths. The value of Ymax/P can be found from the experimental results. This value was measured for the undamaged and damaged structure with various horizontal and vertical cut depths. Three beams were examined and the value of Ymax/P was measured in turn. The first beam,

of length l_1=0.3m, was damaged by cutting horizontally at the top surface. The second and third beams of lengths l_2=0.15m and l_3 =0.2m respectively, were damaged by cutting vertically on both sides. Solution of the equation (6.14) will therefore yield the stiffness Kx and Ky which will be dependent upon the applied force. Similarly, the torsional spring stiffness Kt can be found (58). Figure 6.13 shows a plot of the equivalent spring stiffness K against the percentage of the crack depth for various cross sectional areas. As can be seen from the results of this figure, that when the percentage of the crack depth increased, the spring stiffness will decrease.

6.10 LINEARITY CHECKS OF A STRUCTURE.

The maximum exciting force to which a structure is exposed in service must lie within the elastic range of response and this range should be linear. The force to which the model structures could be subjected was restricted by the maximum output of the power amplifier used. The value of this input force was altered by changing the gain of power amplifier from within the software.

The theoretical analysis has been based on the assumption that the structure should behave as a linear elastic system. The adequacy of this assumption was verified on all the experimental tests: linearity checks were performed on each structure.

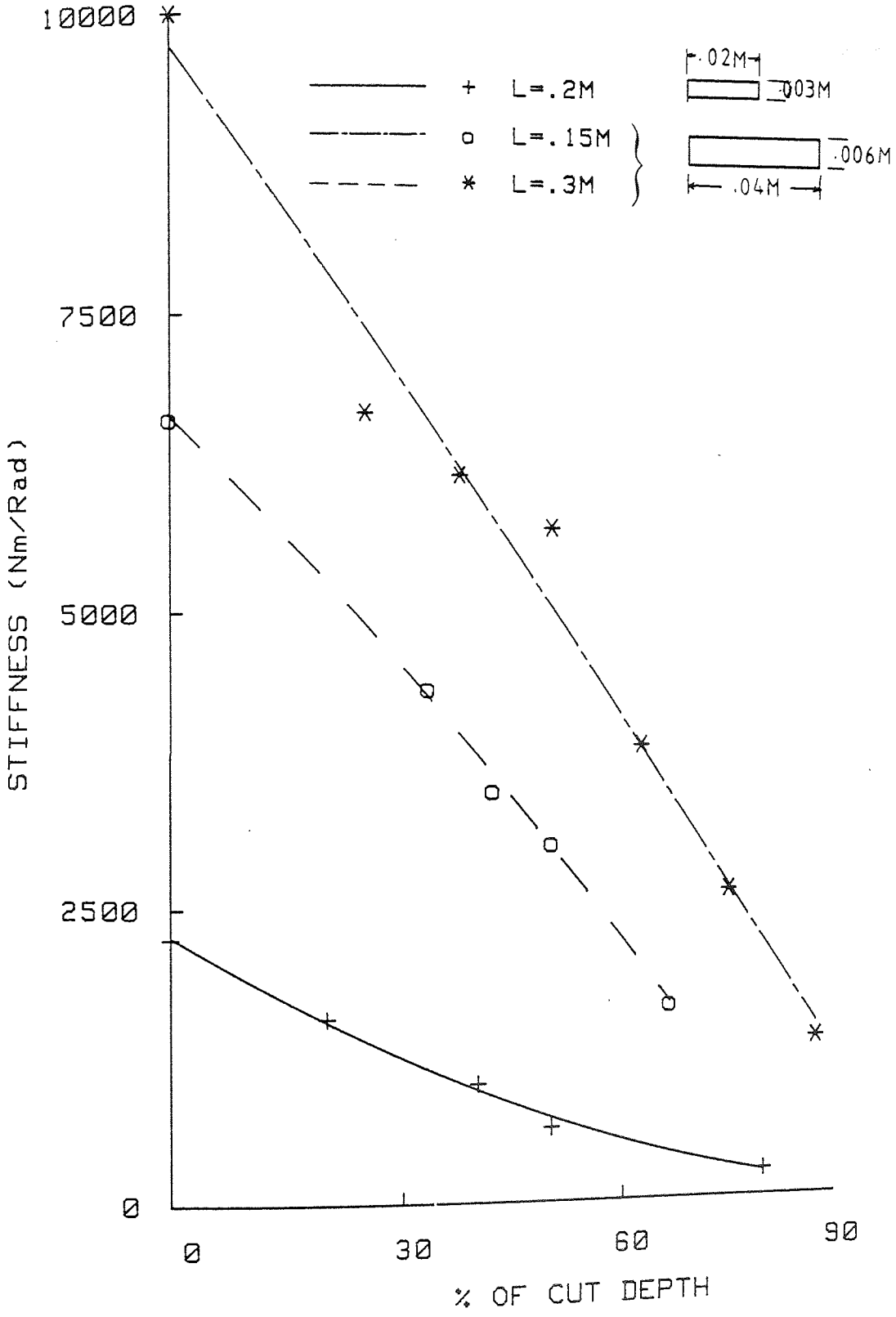

Fig.(6.13) SPRING STIFFNESS AND CUT DEPTH

The linearity of the structure under test was checked by carrying out the inertance measurement many times with different power amplifier gain settings. If the structure is linear then the inertance will be unaffected. The first voltage level was set in such a way that the peak forces were close to the maximum to which the structure or equipment could be safely subjected. The second level was set at a much lower value. Fig. 6.14 shows the typical inertance obtained from such a test. The results validate the supposition that the structure was linear elastic within the range of the forces being used in the investigation.

A second verification of linearity is to compare the reciprocal cross inertance measurements (In12 and In21), which will be identical for a linear elastic system. Fig. 6.15 shows close the agreement obtained when this technique was applied. Should a discrepancy arise the curves would not be coincident and this would indicate either a non-linear system or inadequate experimental procedure.

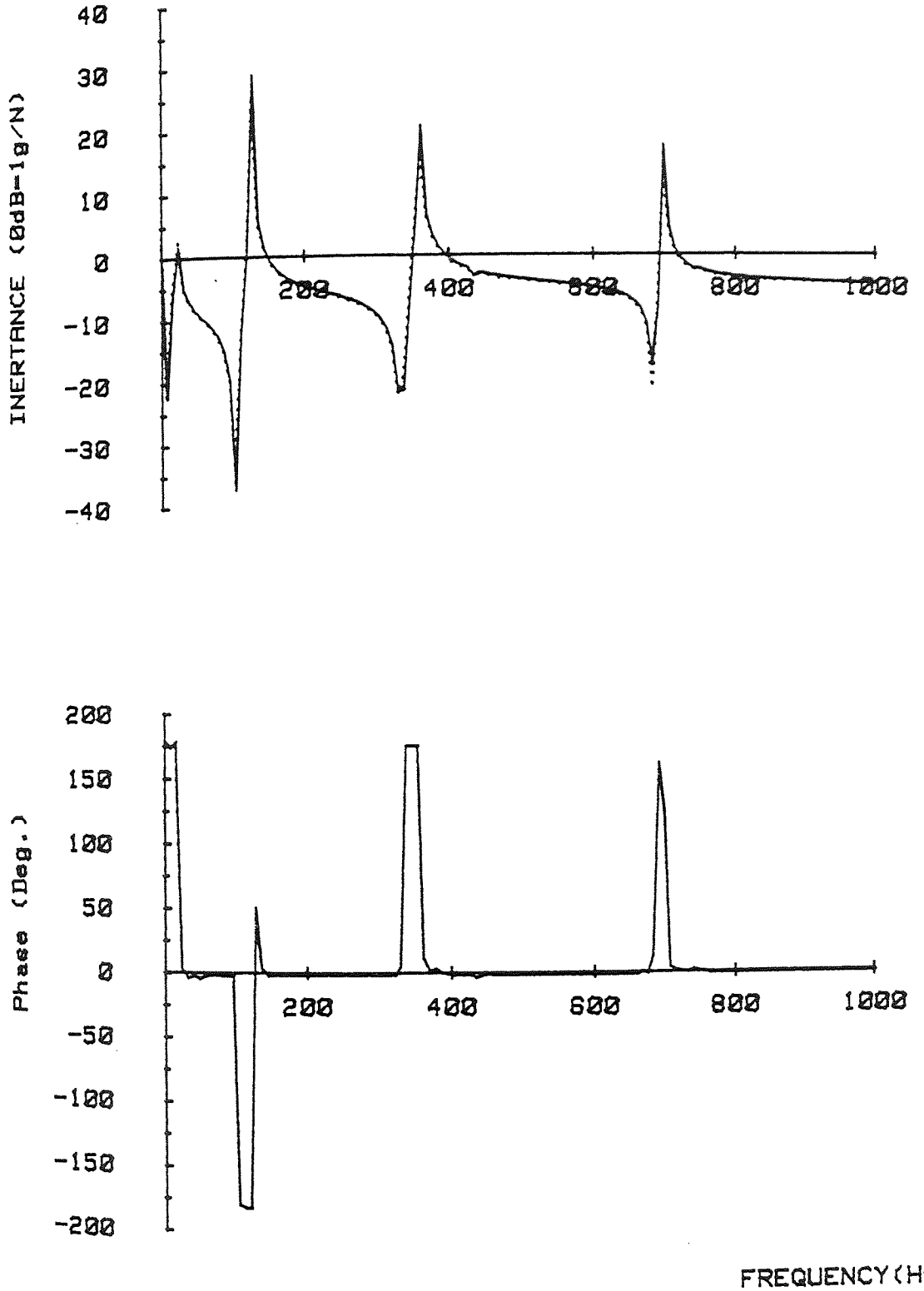

Fig.(6.14) LINEARITY CHECKS FOR In11

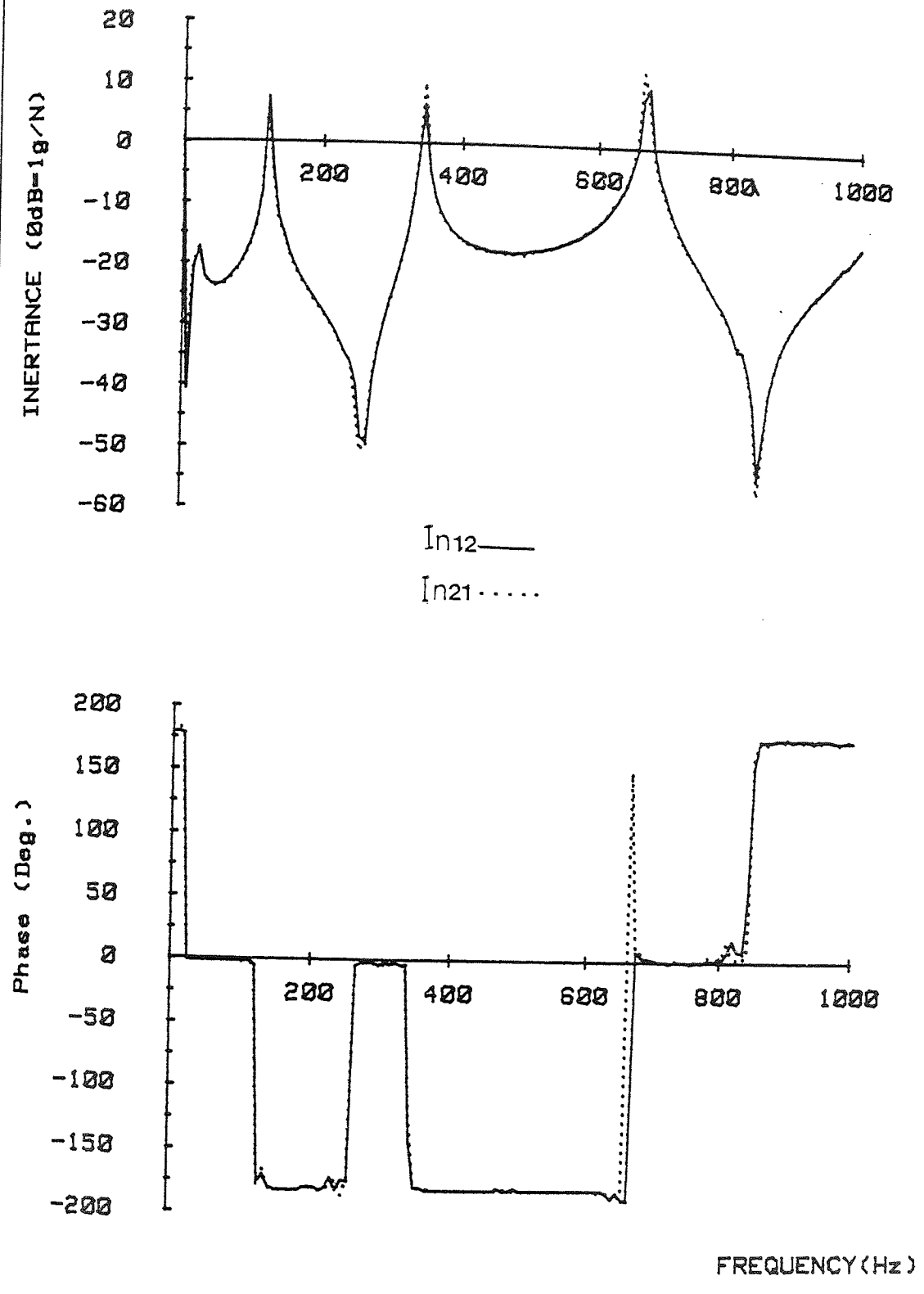

Fig.(6.15) CROSS INERTANCE In12 & In21

6.11 MEASUREMENT OF THE MODE SHAPE.

The experimental investigations described above were mainly concerned with the plot of the inertance against frequency and the location of the natural frequencies of the structure, which correspond to peaks in the magnitude ratio and sudden changes in the phase angle. The second stage of the experimental investigation was to study the mode shape of the structure. The instrumentation used in exciting the structure and monitoring the response was that shown in Fig. 6.1 except that the computer was disconnected and the analyser controlled locally from its own key board. However, in these tests a second accelerometer was used for the purpose of phase measurement and the force transducer was not in operation.

Although the finite element analysis represents the structures as a series of connected elements. Each beam member of a frame is actually a continuum. As such, measurement of its amplitudes of vibration have to be made at many closed points in order to produce a true form of the modal shape. Both linear and angular displacements (or amplitudes) can be calculated from the theoretical analysis. In the present work experimental measurements were restricted to linear displacements only, which introduced an added difficulty in the plotting of the experimental modal shape. Throughout the modal shape tests, the position and manner of attaching the vibrator to the structure was unchanged from the sweep test experiments. The oscillator generator signal

was adjusted in such a manner that the frequency of oscillation was the same as that of the natural frequency of interest.

Responses were measured by two piezo-electric accelerometers fed selectively to the charge amplifier and analyser. One of these accelerometers was used as a reference, fixed at one point, while the other measured the system´s response at different positions on the structure. This gave a direct comparison of amplitude and phase between the fixed and the moving accelerometers, thus enabling mode shapes to be determined at a resonant frequency.

Comparisons between experimental results and theoretical predictions will be presented in chapter eight.

6.12 EXPERIMENTAL REPRESENTATION OF DAMAGE.

The structure could be damaged in a controlled manner using any one of the following techniques.

1- Saw cut damage.

In this method a hack saw cut (0.7mm or 0.5mm thickness) is used to represent damage to the structural member. This was not considered as an ideal method for modelling a crack, but it had the advantage that it was not necessary to dismantle the structure and thereby risk disturbing the boundary

conditions on each and every occasion. Another important consideration was that the extent of damage, as represented by the depth of cut was easily to control. A further advantage of representing damage in this way is that it was much simpler to produce than the genuine fatigue crack and has, by necessity, been widely used in these experiments for complicated structures and inaccessible members.

Damage was represented in all tests carried out either by putting two saw cuts on opposite sides, or by a single saw cut into one surface of a structural member. The position and depth of cut was varied in a series of tests designed to examine the frequency changes.

2- Fatigue Crack Damage.

As no form of saw cut represents a very realistic form of damage, two methods were used to initiate and propagate fatigue cracks.

a) Using the Amsler vibrophore fatigue machine.

In this method, a 25.6 mm depth fatigue cracks was propagated at 140mm from the fixed end of a 480mm long cantilever model of cross section 40*6mm, using a 20KN Amsler vibrophore fatigue machine capable of producing sinusoidal waveforms, as shown in Fig. 6.16a. The model was polished to a 400 grade surface finish: a V-notch was made at an angle of 60 degrees, with a cut depth of 2mm as a starter crack point and the

model was loaded in "three point bending". Disadvantages of this method is that it is not possible to propagate fatigue cracks in complicated structures, e.g. space frame. Also, the boundary conditions are disturbed on each occasion when modifications are made. Furthermore, it was not possible to induce a complete crack.

b) Using a vibrator to propagate a crack.

A more suitable method was designed to initiate and propagate fatigue cracks at any position on a complicated structure without disturbing the boundary conditions on each occasion. An advantage of this method was that the propagation of the crack was easily controlled to any depth and it was possible to induce a complete failure of the member.

Initially, a V-notch is made on the chosen beam, using a hack saw, then the vibrator is connected at a position which is not a node point. The vibrator is then driven at a specified natural frequency and as the crack is propagated, the oscillator generated signal is adjusted: to obtain maximum fatigue rate.

This method was used successfully, to propagate a crack through forty percent of the cross-sectional area, as shown in Fig. 6.16b. This crack was then extended for complete failure at position "B" (Fig. 6.11).

3- Using the Spark Erosion Machine.

Another method for generating a crack involved the use of a spark erosion machine. Damage resembling the nature of a crack was created by using a copper tungsten shim of .005 inch thickness. Propagation of the damage was again easy to control and this method could be used on simple plane frame structures, see Fig. 6.7 position C. Figure 6.16c shows the successful generation of partial cracks. Disadvantages of this method are that the size of structure is limited by the capacity of the spark erosion machine and that the boundary conditions are disturbed on each occasion when modifications are made.

4- Other methods.

Different methods which could be used for generating 'damage' depended on the type of structure and material. One possible method is to notch a beam and bend it so that the notch is on the tension side. A crack will form, and the beam can then be ground back in order to obtain a straight beam. This method is not practical for the portal frame structures.

It was not possible to examine the effect of crushing or creep damage on the natural frequencies because of difficulty in inducing these on structures other than simple specimens.

An attempt was also made to generate the damage using a dilute acid, e.g. Nitric acid. A notch was made using a hack

a- Using the Amsler vibrophore fatigue machine

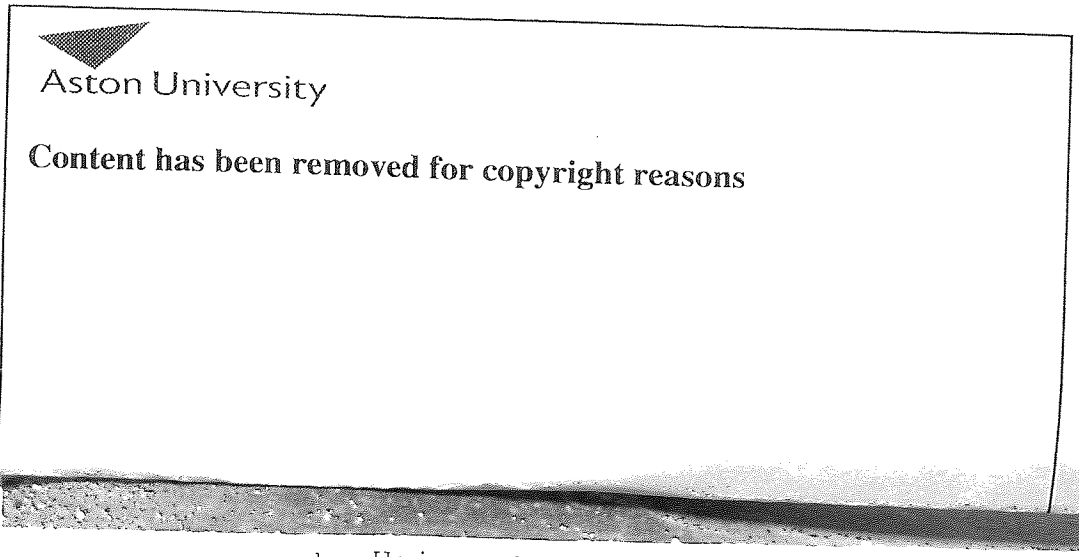

b- Using the vibrator

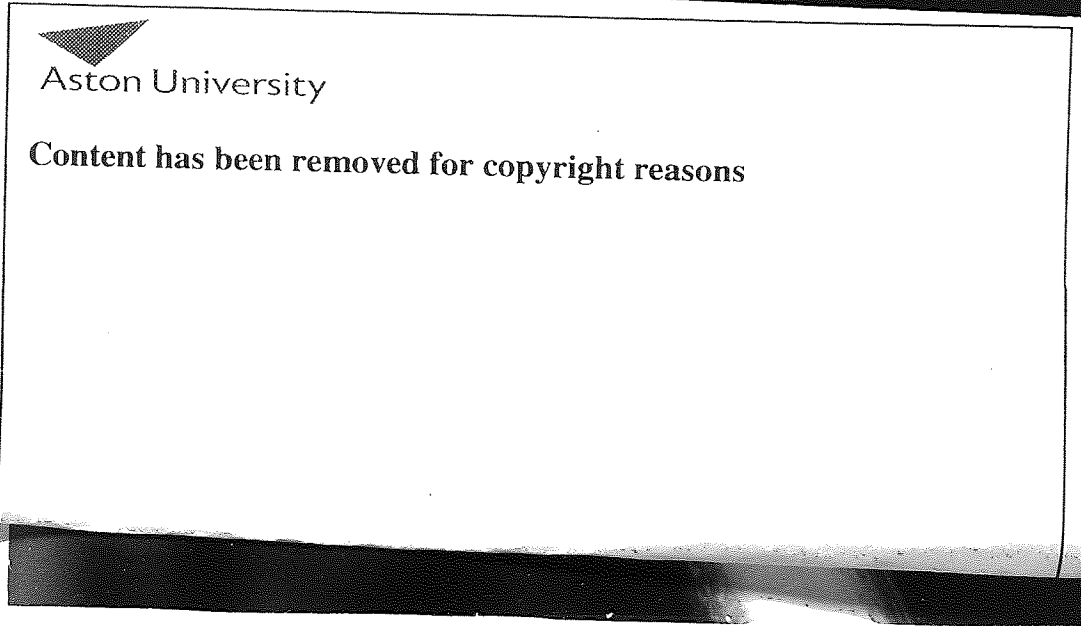

c- Using the spark erosion machine

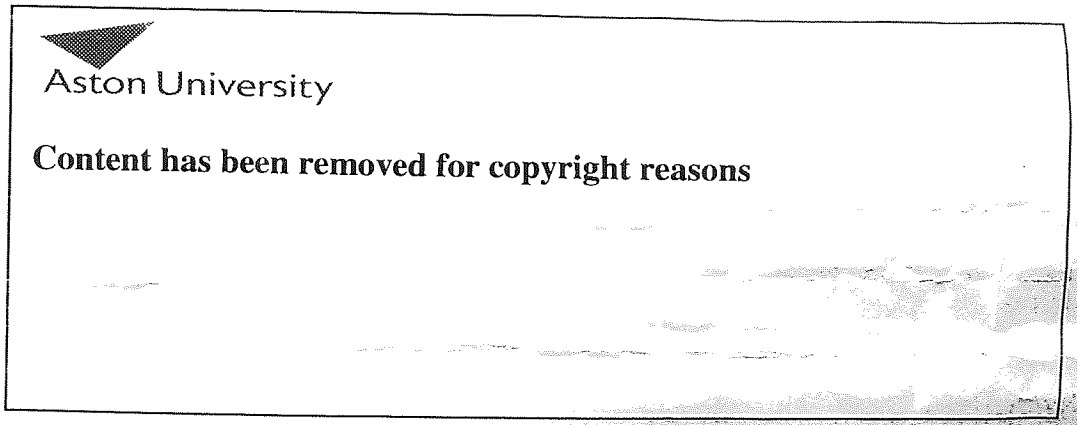

saw; acid was applied and the structure was then vibrated at one of its natural frequencies. This method was unsuccessful. A further attempt at crack generation using thermal shock was also unsuccessful.

6.13 THE COMPUTER PROGRAMS.

In order to monitor the natural frequencies of structures, the vibrational analysis programs were incorporated into a series of routines for on-line control of the tests and data acquisition, using the Hewlett Packard desk-top computer HP9825B in conjunction with either the frequency response analyser or spectrum analyser. These programs were also used to plot the inertance and phase data.
These programs are summarised below.

1- FRAST (Frequency Response Analyser Sweep Test).

This program allows the computer to control a Solatron FRA and to perform a typical frequency sweep test for inertance measurement. The sweep generator, analyser and other functions may be programmed remotely by the computer. The measured inertance values were transmitted to the computer memory from where they could be output, either in a tabulated or graphical form, showing the inertance and phase as a function of the frequency. Typical outputs will be seen in chapter eight. A more detailed description may be found in

(60). It was necessary to enter the following control data from the keyboard.

i- The frequency range (minimum and maximum) and frequency step value.

ii- The desired operating and displayed voltages and the desired output wave form.

iii- The desired measurement mode.

iv- The integration time.

v- The measurement time delay between successive incremental steps of frequency.

Each of these parameters has an ASCII code corresponding to various storage locations in the analyser.

2- SAPLT (Spectrum Analyser Plot).

This program allowed the computer to control the HP3582A Spectrum Analyser and to transfer data from the analyser to computer. The program interrogates the analyser switch setting automatically and duplicates the display onto the HP9872A plotter. In addition, the program offers the option of storing the data onto the mass-storage device. The program is self-contained in that all the necessary plotting and data parameters are obtained from the analyser.

3- The programs SAPLT and FRAST display the amplitude and phase data as functions of the frequency. These programs were modified to permit the display of the same data in the form

of a Nyquist plot. The Nyquist representation is quite suitable for detecting close resonances: these programs are called NSAPLT and NFRAST respectively.

6.14 CLOSING REMARKS.

In this chapter the development of the instrumentation and measuring techniques required to obtain the experimental data of an extremely high quality have been discussed. The inertance testing techniques which have been described constitute a powerful tool for the experimental investigation of structural vibration. This inertance represents the true frequency response function and other forms of the frequency response function can be obtained.

The test procedure requires mechanical contact between the vibrator and structure; a decoupler is used to achieve the freedom of the structure from rotational constraint. Three design of exciter attachment have been used depending on the type of structure and excitation.

One of the first major decisions to be made was that of crack representation. Four methods have been discussed for generating damage in structural members, depending on the type of structure and damage. Each of these methods will be used and the choice of the best model will be discussed in chapter eight. Changes in natural frequencies due to minor structural damage could be easily and accurately measured and

the validity of this technique was confirmed as a means of structural inspection for primary damage.

Both theoretical and experimental results will be discussed in the following chapters.

CHAPTER SEVEN

STUDY OF THEORETICAL CHANGES IN THE SPECTRUM OF NATURAL FREQUENCIES

7.1 INTRODUCTION.

Theoretical results obtained using the analysis described in chapters four and five are presented in this chapter. These results are used again in chapter nine when the location of structural defects is discussed.

The relationship between the stiffness characteristic of a structure and the variations of the natural frequencies and modal shapes of a structure is examined and the choice between approximate and exact dynamic analysis and damage modelling is discussed. Initially, this study is applied to a simple structure such as a cantilever, then it progresses to work on symmetric and asymmetric plane frame structures and finally to more complicated space frame structures.

A series of predictions is presented to show the effect on the natural frequencies of the structure when important parameters of the system are varied. These parameters included damage location, extent of the damage and boundary conditions. To investigate the theoretical changes in the natural frequencies, the damage models used are those already discussed in Section 3.4. To investigate the appropriate boundary conditions to be used for prediction an experiment was conducted on a plane frame for use in comparison with the theoretical results, see section 7.3.

7.2 COMPARISON BETWEEN APPROXIMATE AND EXACT DYNAMIC ANALYSIS.

In this section the linear and non-linear eigensystems as methods of obtaining the natural frequencies of a structure are compared.

As discussed in earlier chapters, alternative numerical methods are available to solve the problem of structural vibration. Unless the exact displacement functions are used, the accuracy of the computed frequencies depends mainly on the number of elements used to represent each member of the structure and on the nature of the assumed displacement functions. An improved approximation is obtained when the members are subdivided into more elements. Thus, in a structure analysed using many small elements, the lower modes of vibration obtained from the linear EVP are close to the exact solution.

Several tests were carried out in order to compare the accuracy of approximate solutions obtained by solving the linear EVP. The comparison was achieved by increasing the number of elements in each member and comparing the result with the exact solution obtained from the non-linear EVP. Three finite element discretizations for exact and approximate solution were used to analyse the plane frame shown in Fig. 7.1a. In the exact solution, 9 elements were required to describe the frame geometry, and in the approximate solution, 19 elements (45 dof) and 12 elements (24 dof) were considered. A similar study was undertaken in

the analysis of the tower frame shown in Fig. 7.1b. In the exact solution, 14 elements were used and the result was compared with the approximate solutions using 14 elements (18 dof), 26 elements (54 dof) and 30 elements (66 dof).

It may be observed from Fig. 7.1a, that even with a coarse discretization, for example with 12 elements, the results compare very favourably with the exact values up to the third modes, but decrease in accuracy towards the higher modes as discretization is reduced. Since the first ten modes are used in the damage location analysis it was decided to use the non-linear EVP. Whilst the solution is slower far fewer elements are used: the size of the matrices involved is smaller and a more complicated structure can be analysed despite the limited memory of the desk-top computer.

7.3 EFFECT OF BOUNDARY CONDITIONS.

In a theoretical analysis, it is convenient to assume that the boundary conditions are either pinned or fixed, but in practice these conditions are never completely satisfied; the actual behaviour of the supports corresponding to something between a hinged and a fixed point.

In order to investigate the boundary conditions, it was necessary to make a comparison between the theoretical predictions by assuming both fixed and pinned end conditions with the experimenatl natural frequencies of the first ten

(a)

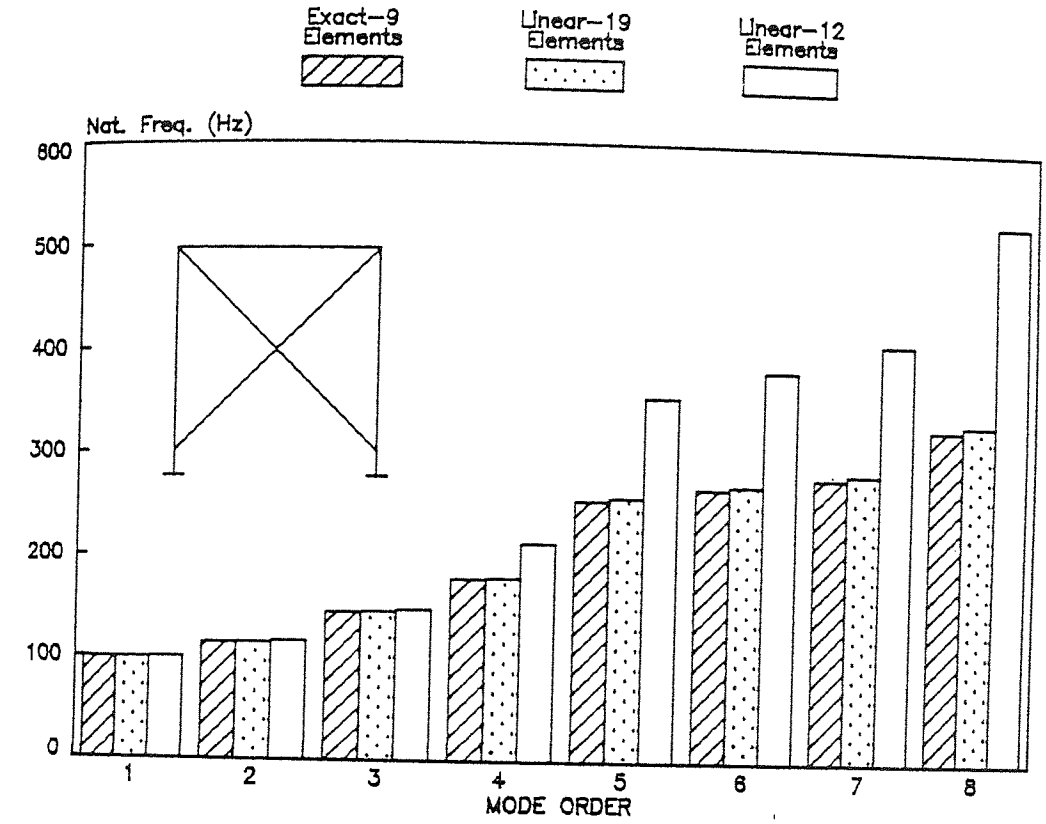

(b)

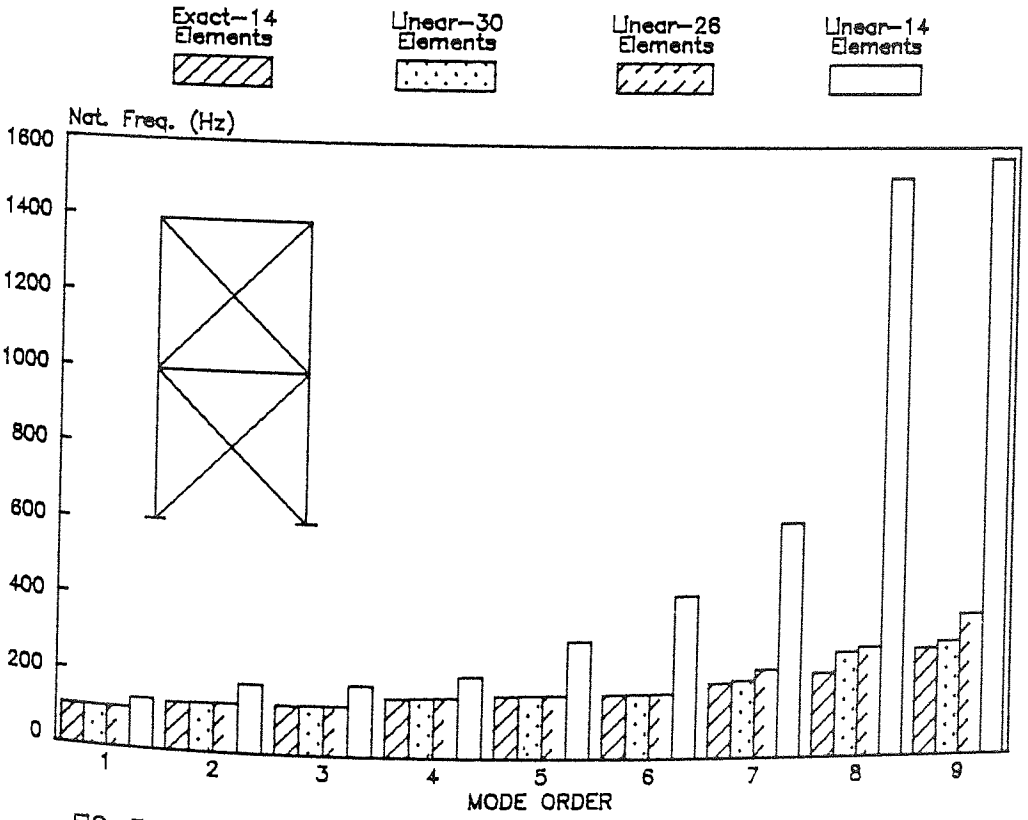

FIG. 7.1a–b COMPARISON BETWEEN THE EXACT AND APPROXIMATE NATURAL FREQUENCIES

modes of the tower structure. Referring to Fig. 7.2a, it can be seen that the difference between the theoretical fixed end condition and the experimental frequencies was relatively small. The differences between the pinned end condition and the experimental results was always greater than the difference between the fixed end and the experiment.

A comparison was made using both fixed and pinned ends conditions for a damaged and undamaged structure and the changes in the natural frequencies are shown in Table 7.1. It can be concluded that there is a significant difference in both the frequencies and in the frequency changes between the fixed and pinned boundary conditions. A similar conclusion was found when the damage was simulated at other positions.

In order to illustrate the effect of boundary conditions on the damage location procedure the tower structure was analysed assuming both fixed and pinned boundary conditions. The percentage change in the natural frequency caused by the simulated damage assumed pinned boundary conditions is shown in Figs. 7.2b-c and for the fixed boundary condition will be shown in Figs. 7.8a-b. The effect of the boundary conditions on the damage location is described in chapter nine.

Thus, it may be concluded that the correct choice of boundary condition is of great importance and, based on the evidence of Fig. 7.2a, only fixed end conditions were employed in the analysis of all other structures examined in this thesis.

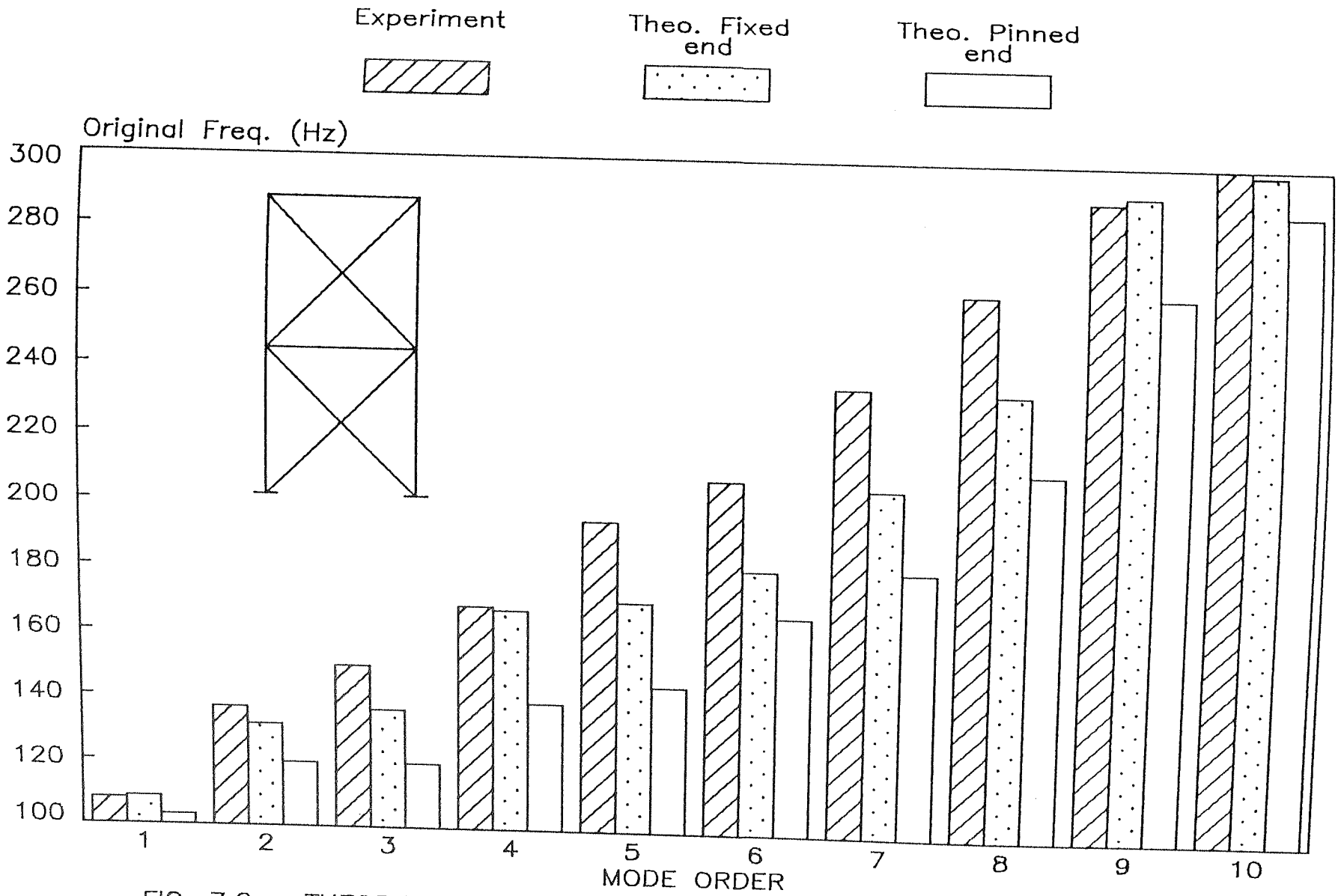

FIG. 7.2a THEORETICAL EFFECT OF BOUNDARY CONDITIONS ON FREQUENCIES

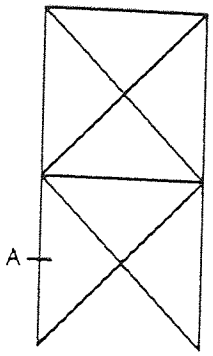

	Freqencies of fixed ends (Hz)			Frequencies of pinned ends (Hz)		
Mode order	Undamaged	Damaged at A	Frequency changes	Undamaged	Damaged at A	Frequency changes
1	105.2	83.2	22	103.1	64.7	38.4
2	126.7	106.2	20.5	119.7	82.9	36.8
3	131.03	108.8	22.23	119.8	107.7	12.1
4	155.5	126.7	28.8	139.3	119.3	20
5	164.4	138.2	26.2	145.2	136	9.2
6	168.4	158.9	9.5	167.4	142.8	24.6
7	197.6	167.4	30.2	181.7	167.2	14.5
8	222.1	194.0	28.1	211.7	183.4	28.3
9	283.7	221.9	61.8	263.1	209.7	53.4
10	290.6	262.8	27.8	287.0	261.5	25.5

TABLE 7.1 COMPARISON OF THEORETICAL FREQUENCIES BETWEEN FIXED AND PINNED BOUNDARY CONDITIONS

(b)

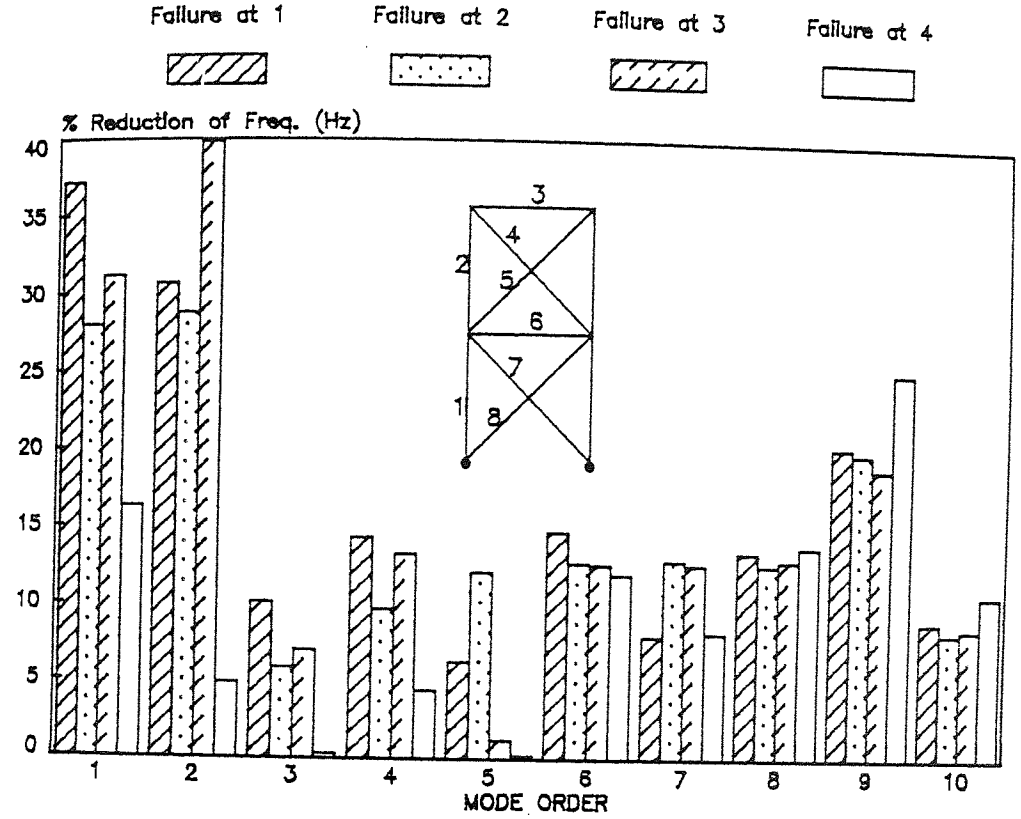

(c)

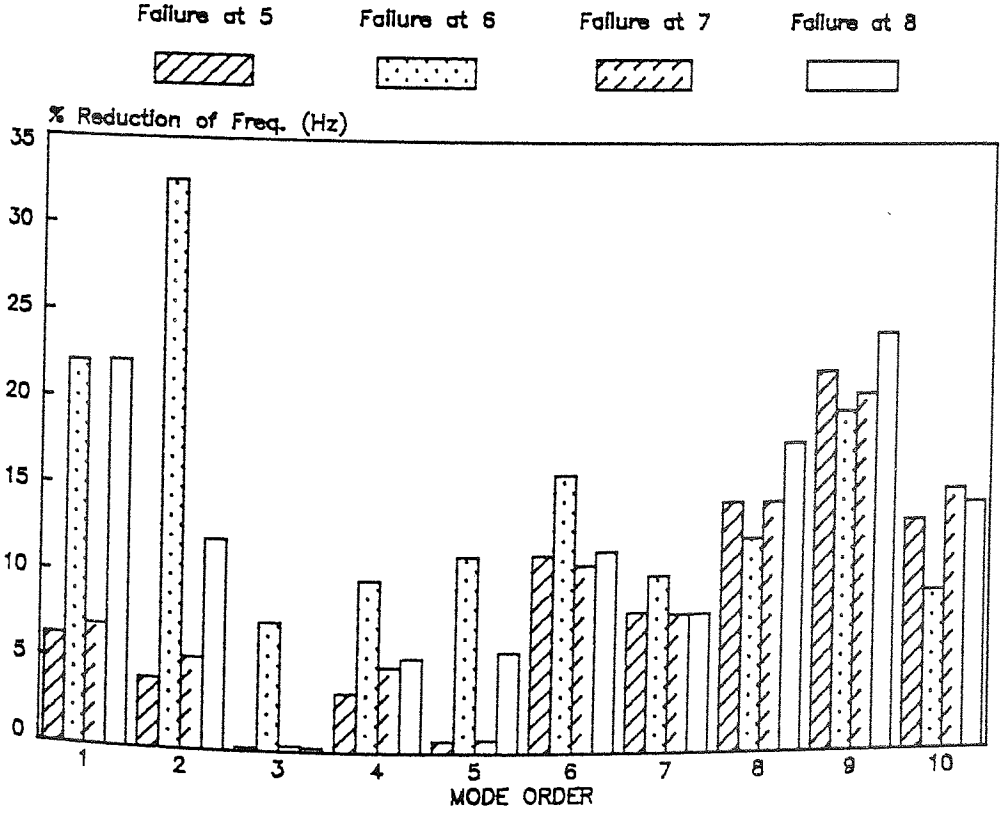

FIG. 7.2b–c THEORETICAL EFFECTS OF DAMAGE SITES (1–8) ON TOWER FRAME FREQUENCY (PINNED-END CONDITION)

7.4 EFFECT OF DAMAGE LOCATION ON A STRUCTURE.

Emphasis in this section has been placed upon the importance of the damage location with regard to the changes in natural frequencies of the structure: these frequency changes will be used later in the defect location analysis. Damages can be readily simulated by a computer model at any point along a structural member, as already explained in Section 3.4. Most of the complete damage was represented by the two-cantilever model. The structures themselves are assumed to have fixed boundary conditions.

Initially, theoretical natural frequencies were computed for an undamaged structure: these frequencies were then recomputed with partial or total damage simulated in one member. The above procedure was repeated with each of the members damaged in turn, using the non-linear EVP dynamic analysis program. For most of the structures the first ten natural frequencies were calculated.

7.4.1 The Cantilever Beam.

Preliminary predictions related to a cantilever beam of rectangular cross section were investigated. Damage was represented by reducing the cross-sectional area of a small element to simulate a narrow rectangular slot (0.01m wide) across the upper surface of the beam. The effect of this slot at various positions, (.1m, .2m, .3m and .4m from the clamped

end) was investigated. Fig. 7.3 shows a plot of the percentage reduction of the natural frequencies from their original values, damage being equivalent to a reduction of 25% in area. Fig. 7.4 shows the percentage reduction of the natural frequencies when the cross-sectional area is reduced by 60%.

When the damage is very near to the clamped end, a reduction in the fundamental frequency is clearly evident. A reduction in the cross-sectional area of the cantilever at positions 4, see Figs. 7.3 and 7.4, resulted in an increase of the frequency of the first mode but decreased the frequency in the other modes. From the same figures, it is observed that the damage at location 1 has no effect on second mode and damage at location 3 has no effect on first mode. In other words, the changes in the frequency spectrum due to damage depends on the position of that damage. As a result, this model of damage may not be suitable for use in the defect location analysis as no significant changes were predicted.

It was observed from the predictions that when the damage location was moved towards the free end, an increase in frequency occurred, indicating that the structure tends to behave as a shorter clamped-free beam. This observation was also made during vibration testing. The explanation might be that the element at position 1 is more heavily loaded than other elements. Physically, this means that although the present damage causes an overall reduction in strain energy of the system, it is less than the reduction in the kinetic

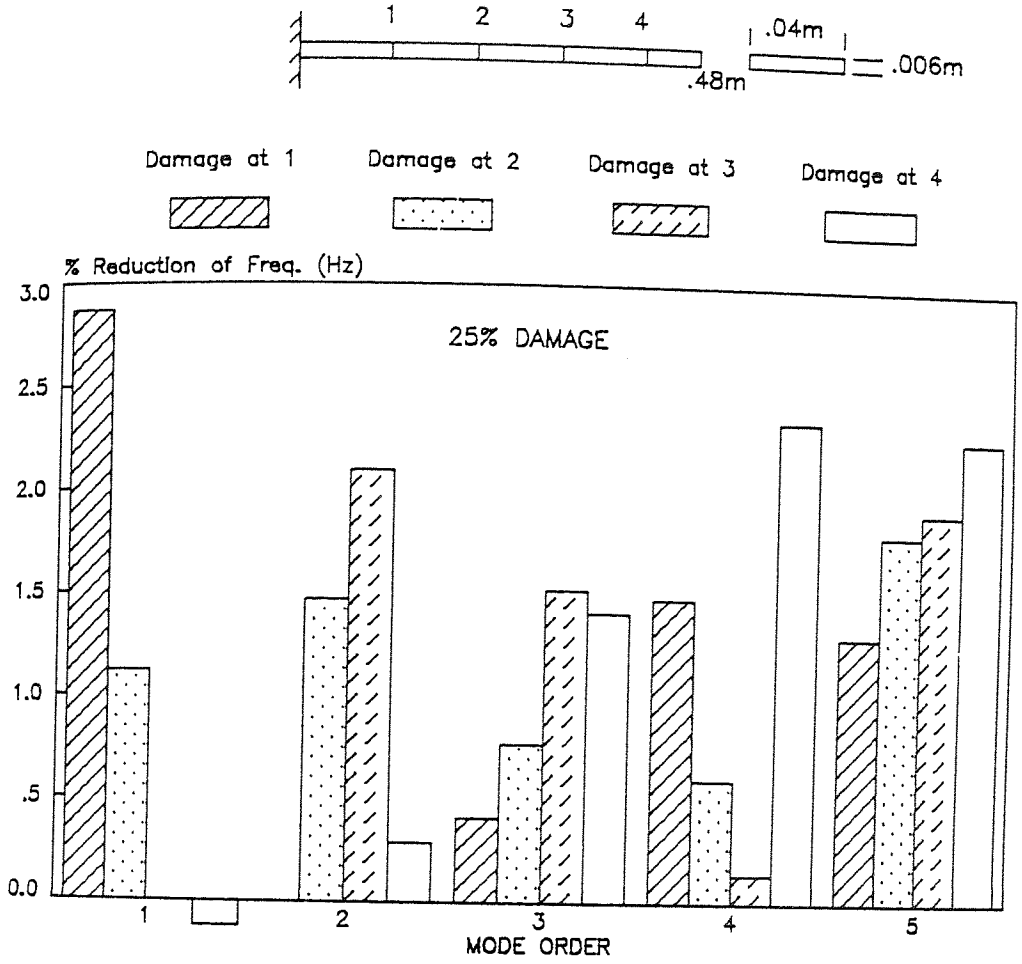

FIG. 7.3 THEORETICAL EFFECTS OF DAMAGE SITES ON CANTILEVER FREQUENCY (DAMAGE 25%)

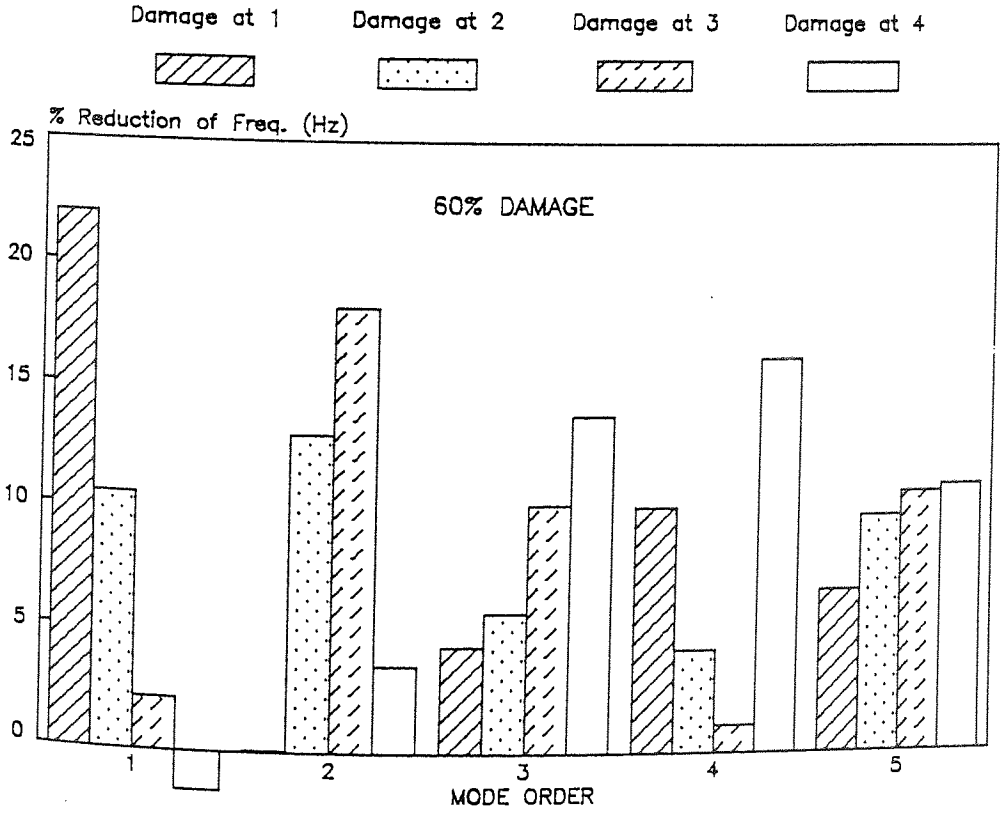

FIG. 7.4 THEORETICAL EFFECTS OF DAMAGE SITES ON CANTILEVER FREQUENCY (DAMAGE 60%)

energy, this is not necessarily true for each individual mode or position.

7.4.1.1 Effect of the extent of damage.

A further analysis was undertaken to examine the influence of the extent of damage at any given location on the natural frequencies of a cantilever beam. In general, frequencies reduced as the extent of damage increased, although the location of damage was also important. For example, it has already been shown that when damage is simulated at any position along the cantilever (Fig. 7.4) the frequency reduction corresponding to the first five modes with 60% damage higher than that predicted for 25% damage (Fig. 7.3).

Figure 7.5 is a plot of the percentage reduction of the original natural frequency against the percentage reduction in stiffness, for the first five modes. The reduction in stiffness was represented by a torsional spring model. This simulated 'damage' was located at 140mm from the clamped end of the cantilever model.

There is no significant reduction in frequency for any mode until damage exceeds 70% reduction in stiffness at a given position. From these predictions the first and third modes are more sensitive to the change in stiffness than the other modes for all degrees of damage.

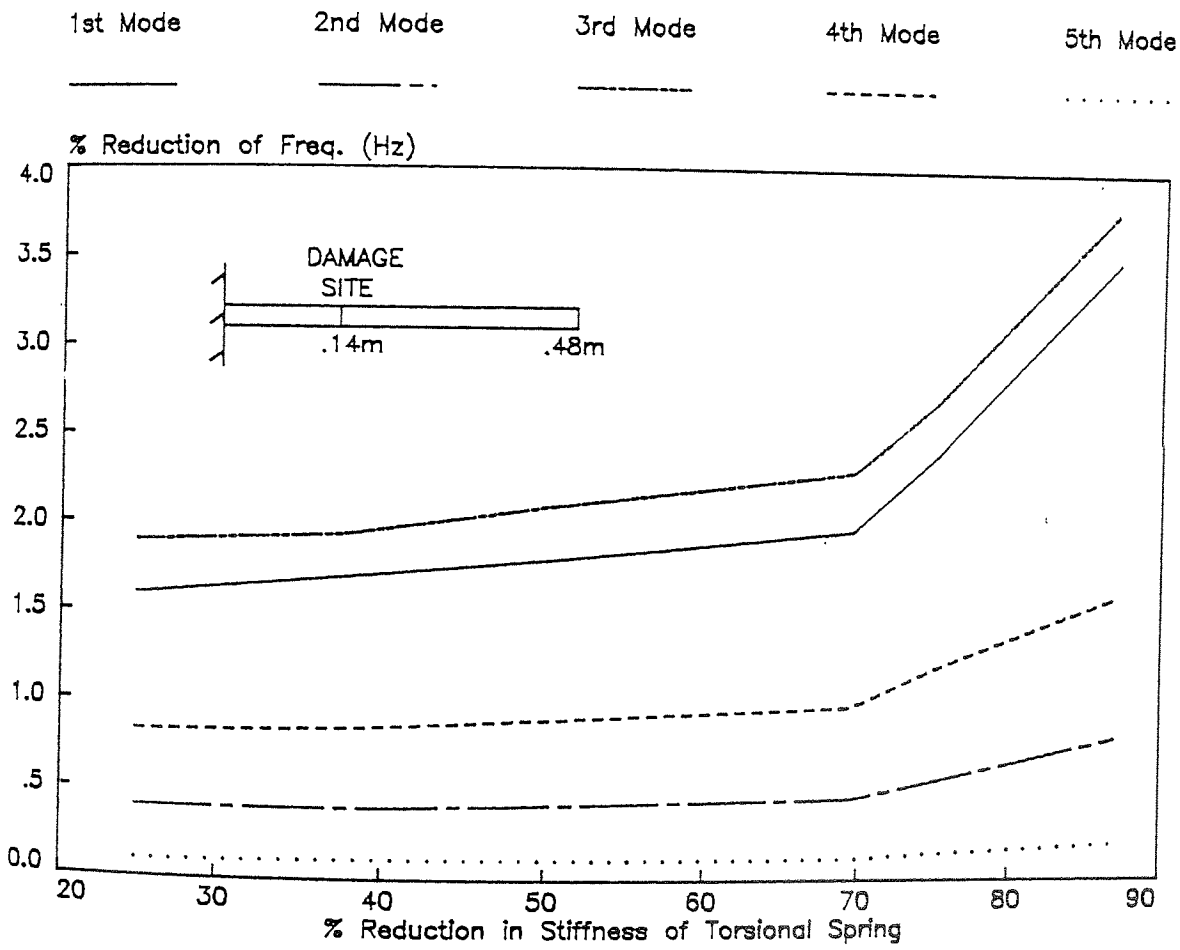

FIG. 7.5 THEORETICAL EFFECT OF DAMAGE SIZE ON NATURAL FREQUENCY OF CANTILEVER BEAM

Figure 7.6 compares the predictions of three different damage models by examining the percentage reduction of the first natural frequency of the cantilever beam as the location and extent of damage vary. For each model, the percentage reduction of the frequency from the original values is plotted against the percentage reduction in stiffness for the section.

1- Damage modelled as a reduction in rigidity.

It is evident that a reduction in the rigidity of the section at location 1, 2 and 3 of the cantilever beam will cause a decrease in the first mode, whereas a reduction in rigidity of the section at 4 and 5 will have virtually no effect on this frequency.

2- Damage modelled as a reduction in cross-sectional area.

In this case it can be seen that the reduction in the cross-sectional area of section 1, 2 and 3 has a similar effect to that produced by rigidity reduction, whereas a reduction in the cross-sectional area of section 4 causes an increase in the first mode. The physical explanation of this has already been discussed in section 7.4.1.

3- Damage modelled as a torsional spring.

For this model, it is evident that the location of a torsional spring at nodes 1, 2 and 3 has a significant effect

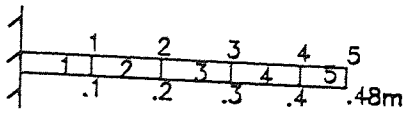

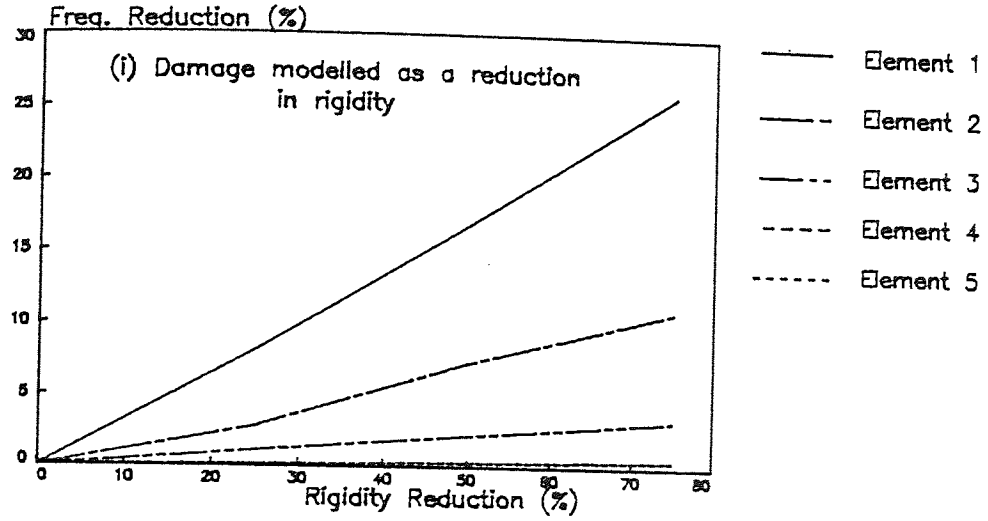

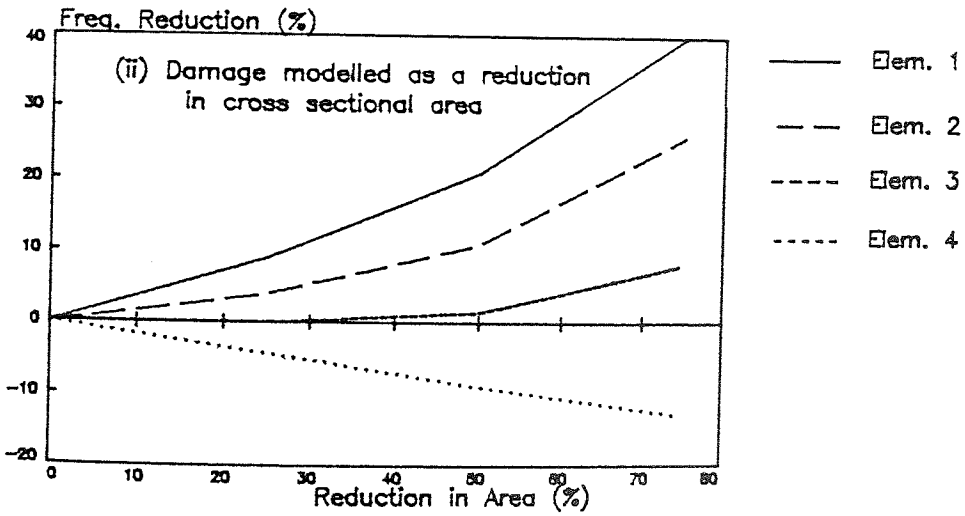

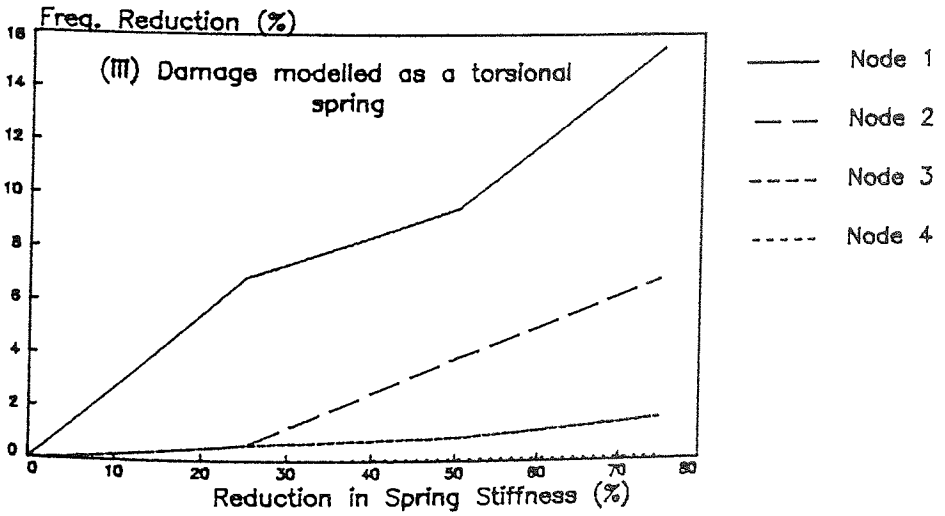

FIG. 7.6 THEORETICAL EFFECT OF DAMAGE MODEL, DAMAGE SIZE AND POSITION OF DAMAGE ON 1st MODE

on the first mode, whereas a spring at node 4 has an insignificant effect.

This reduction in frequency is predicted by each of the models. It can be seen that a higher frequency reduction is associated with a reduction in the stiffness of section 1 than with those of other sections.

7.4.2 The Cross-Brace Portal Frame.

Figure 7.7 shows the predicted effect of the location of damage on the frequencies of the cross-brace portal frame. These results are plotted in terms of the percentage reduction of the natural frequency caused by the complete failure. This failure was represented as the two-cantilever model described in section 3.4. Due to symmetry, it was necessary to simulate failure in the one half of the structure only. Failure was simulated at a position in the middle of each member.

All frequencies were reduced due to damage and in one case, a percentage change of over 42% was discovered at the second mode when the damage was located at position 2. Generally, the most affected mode of vibration depends on the position at which a member is damaged.

Also, complete failure was simulated at position 5 of the structure shown in Fig. 7.7. As a result, percentage changes

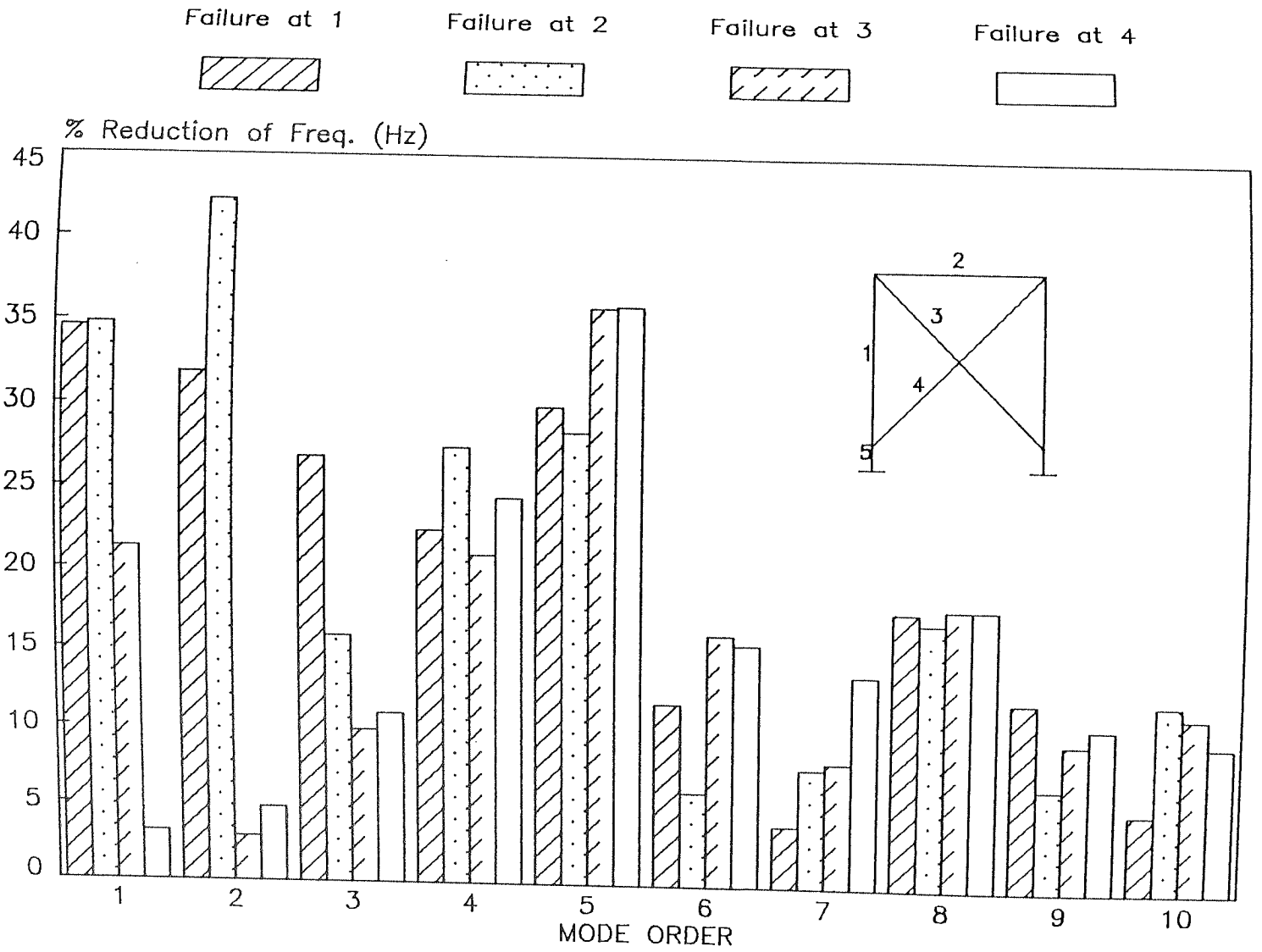

FIG. 7.7 THEORETICAL EFFECTS OF DAMAGE SITES (1–4) ON CROSS BRACE PORTAL FRAME FREQUENCY

at the first mode were greater than 92%, but the effect on higher modes was much less. This reduction in frequency was expected because the stiffer the structure, the higher would be its natural frequency. A much greater effect was obtained by breaking a main leg of the structure than by breaking any other brace.

7.4.3 The Tower Frame.

The effect of a complete failure in the middle of each member in turn on the first ten modes of the vibration of the tower frame is shown in Figs. 7.8a-b. Again, the failure was represented by the two-cantilever model. By breaking the members there is a significant effect on the frequencies and the magnitude of this effect is a function of the type and location of the damage.

The results show that the maximum reduction of the original natural frequency was greater than 43% when damage was simulated at position 3 for the second mode. It is also seen that the first mode frequency increases slightly, but the second mode frequency remains virtually unchanged when the damage is simulated at position 8.

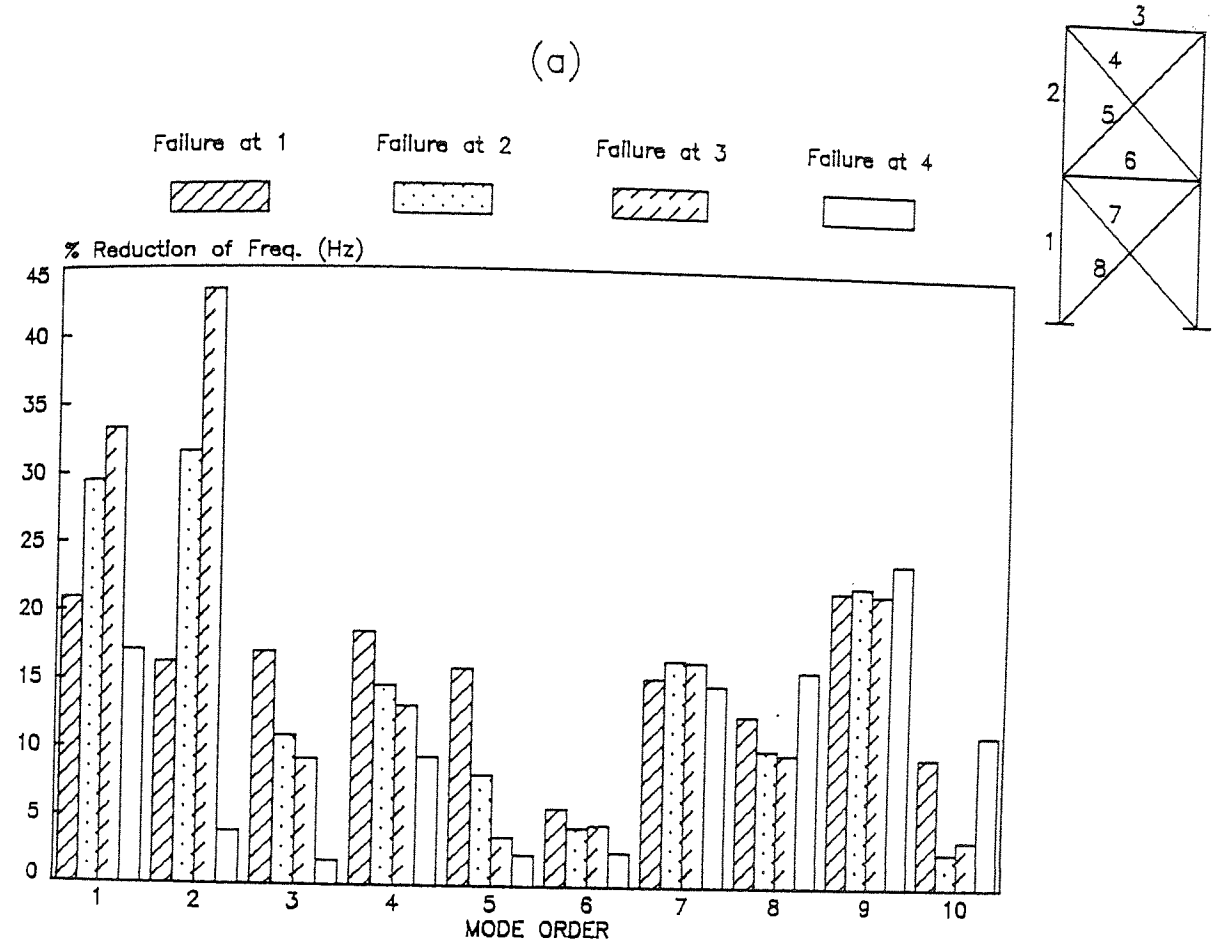

FIG. 7.8a–b THEORETICAL EFFECTS OF DAMAGE SITES (1–8) ON SYMMETRIC TOWER FRAME FREQUENCY

7.4.4 The Asymmetric Tower Frame.

Referring to Figs. 7.9a-f, the effect of damage location on the natural frequencies of an asymmetrical tower frame is shown. Damage was simulated as a complete failure in the middle of each member (positions 1 to 23). Results show that all frequencies were reduced and the maximum percentage reductions of over 77% were indicated at the first mode when damage was simulated at position 9. Also, it was noticed when damage was simulated at position 11, the effect on the frequency was smaller for all modes and smaller than that produced by any other damage positions, see Fig. 7.9c. This may give an indication that it would be difficult to detect any damage at position 11 from measurements, as this position was insensitive to the changes in frequency.

7.4.4.1 Effect of Damage Location at Any Point within a Member.

The effect on the natural frequency of the structure for different damage positions within the length of a given member was predicted for the asymmetric tower frame. The results were later embodied successfully into the defect location analysis and play an important part identifying both the damaged member and the location of damage within the member (see chapter nine).

Figures 7.10a-b show the percentage reduction from the

(a)

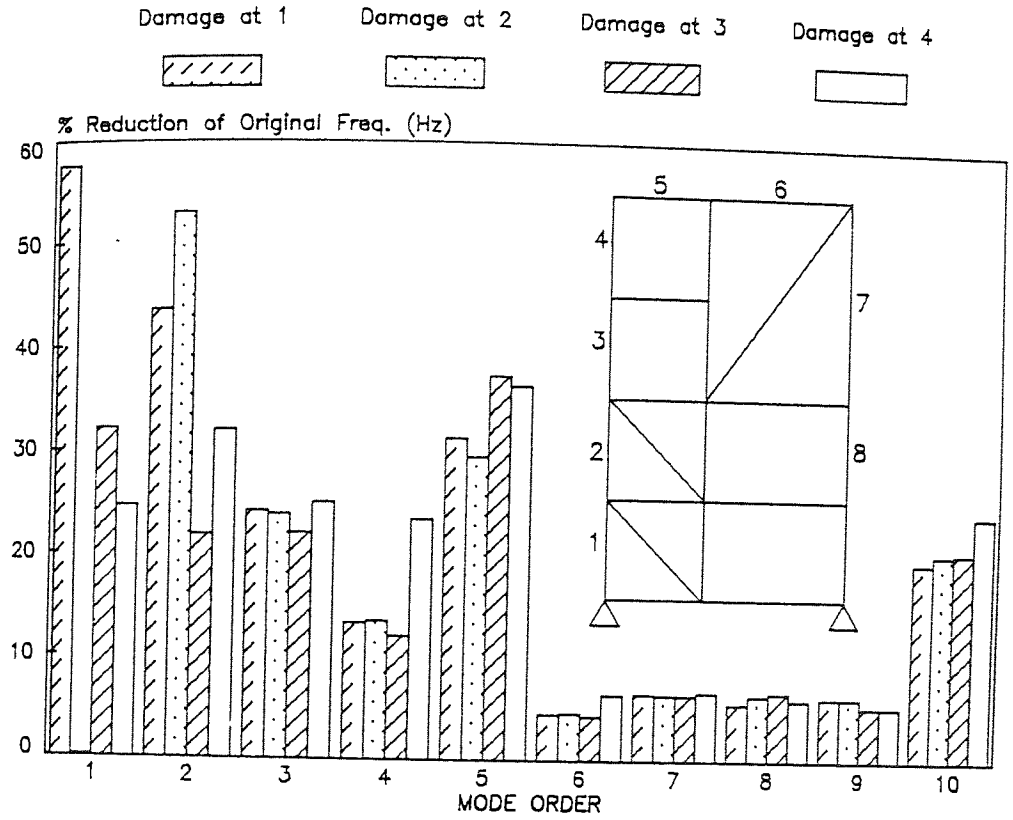

(b)

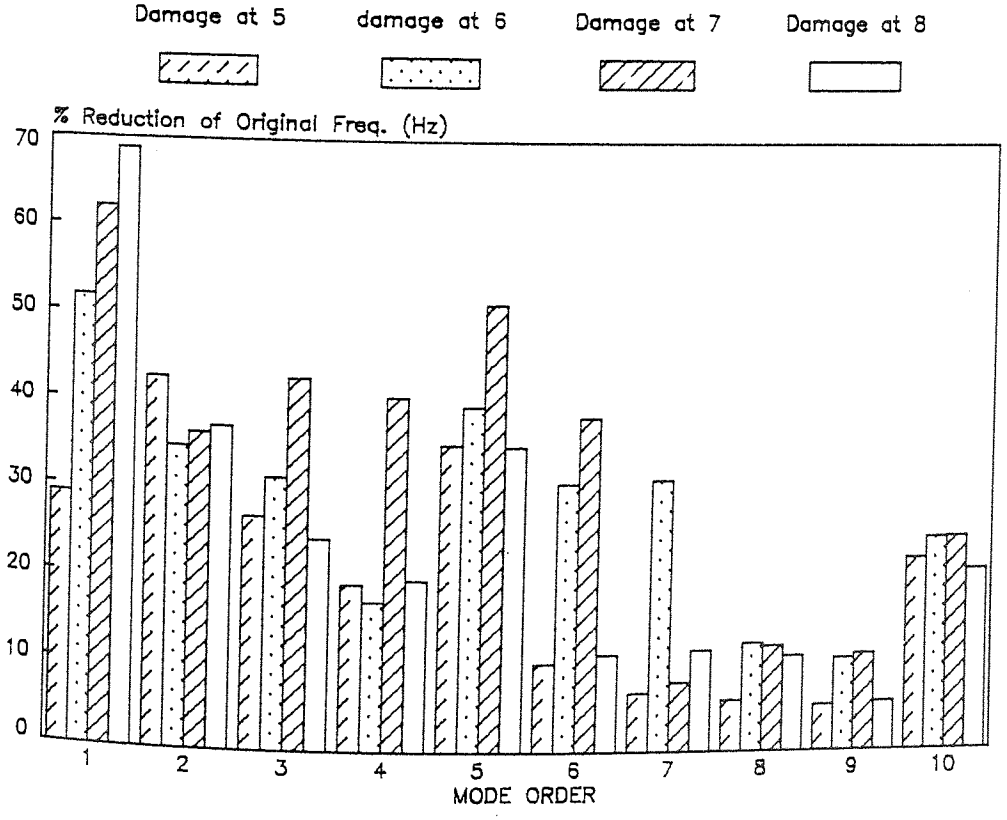

FIG. 7.9a–b THEORETICAL EEFECTS OF DAMAGE SITES (1–8) ON ASYMMETRIC TOWER FRAME FREQUENCY

(c)

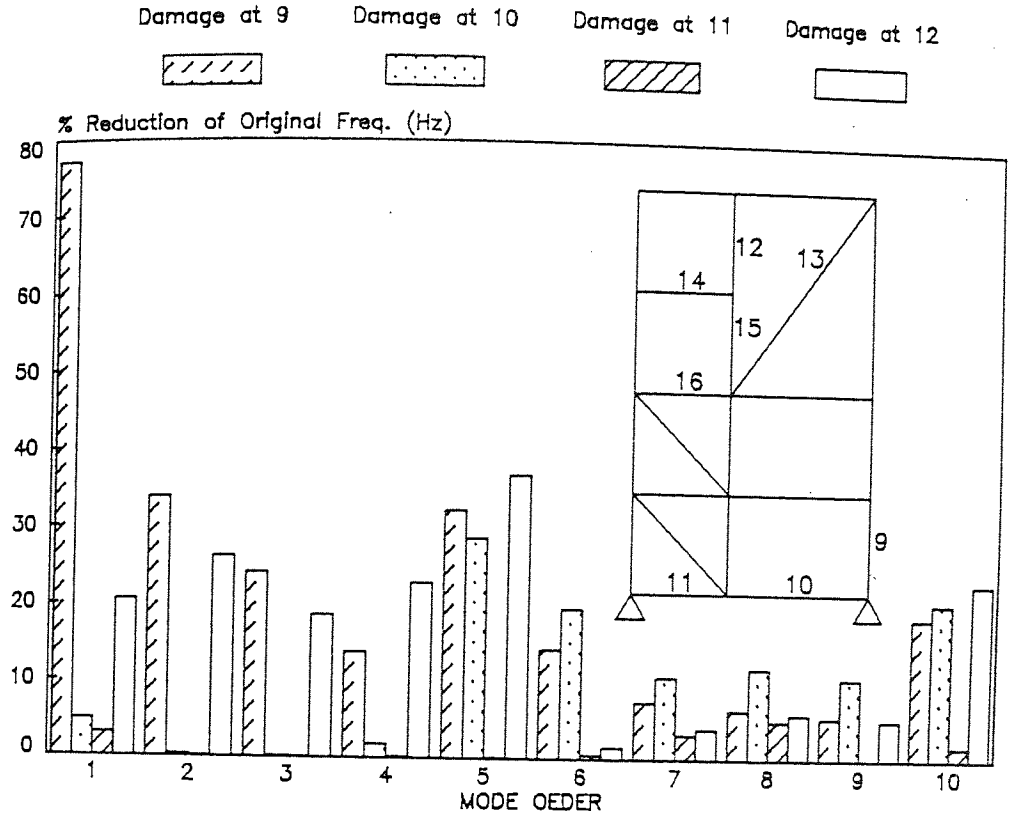

(d)

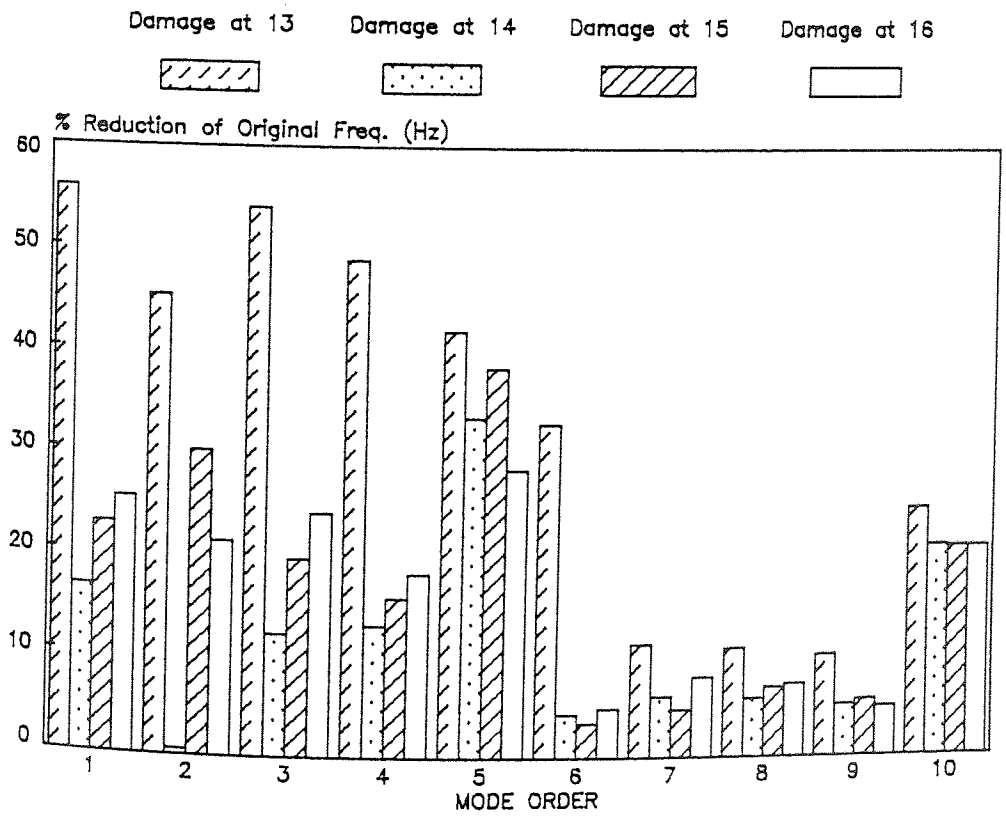

FIG. 7.9c–d THEORETICAL EFFECTS OF DAMAGE SITES (9–16) ON ASYMMETRIC TOWER FRAME FREQUENCY

(e)

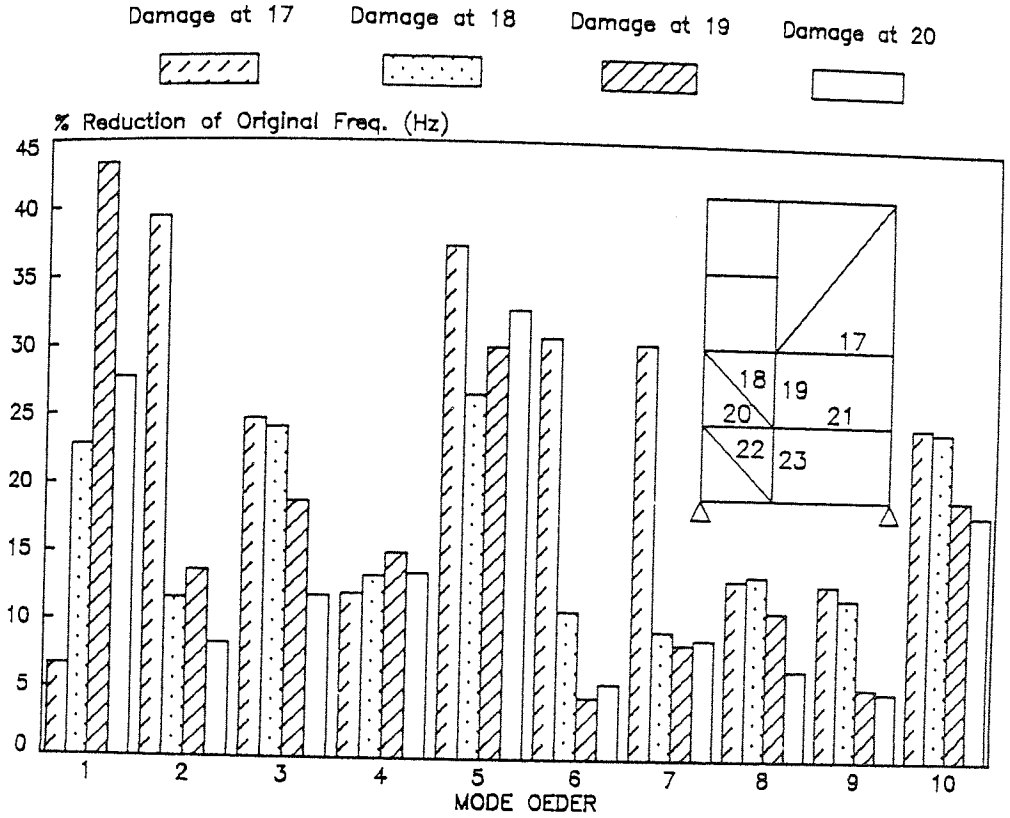

(f)

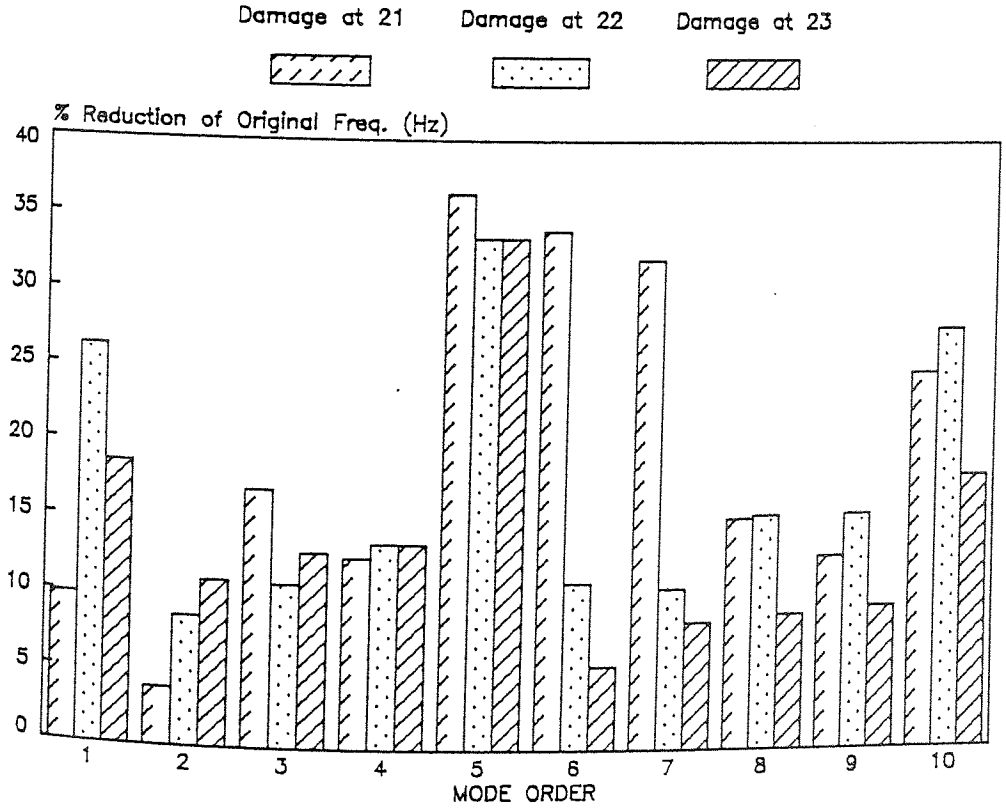

FIG. 7.9e–f THEORETICAL EFFECTS OF DAMAGE SITES (17–23) ON ASYMMETRIC TOWER FRAME FREQUENCY

original natural frequency in relation to the location of damage (x) on the principal diagonal member of the tower frame measured from end A (as a % of member length). The damage was simulated by the two-cantilever model.

It can be noted from the results of Fig. 7.10a, that the percentage reduction of the frequency of the first four modes varies between 20-80%. Figure 7.10b shows the range of the percentage frequency reduction for the 5th to 8th modes which lies between 10% and 40%. These results show that some modes are more sensitive to changes in frequency than others as the location of damage is varied. In other words, the percentage reduction in frequencies depends on the damage sites, but also on the mode order. For example, as shown in Fig. 7.10b the eight mode is insensitive to the frequency whenever damage is located in the member.

These figures also show that the percentage reduction in frequencies was identical for a given position of the damage on either side of the centre of the member. Thus it will be necessary to calculate the changes in natural frequency due to damage at different positions along each member of the structure, since this may help the defect location analysis to predict alternative location for damage within the predicted member. As a result of this finding most of the members in the plane frame structure and all the members in the space frame structure were 'damaged' at more than one position and the frequency changes were calculated.

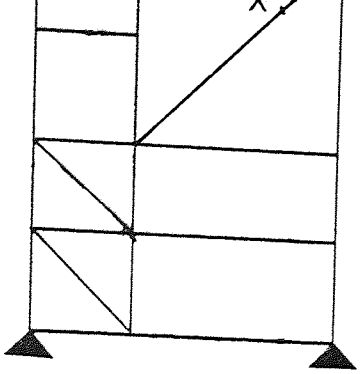

(a)

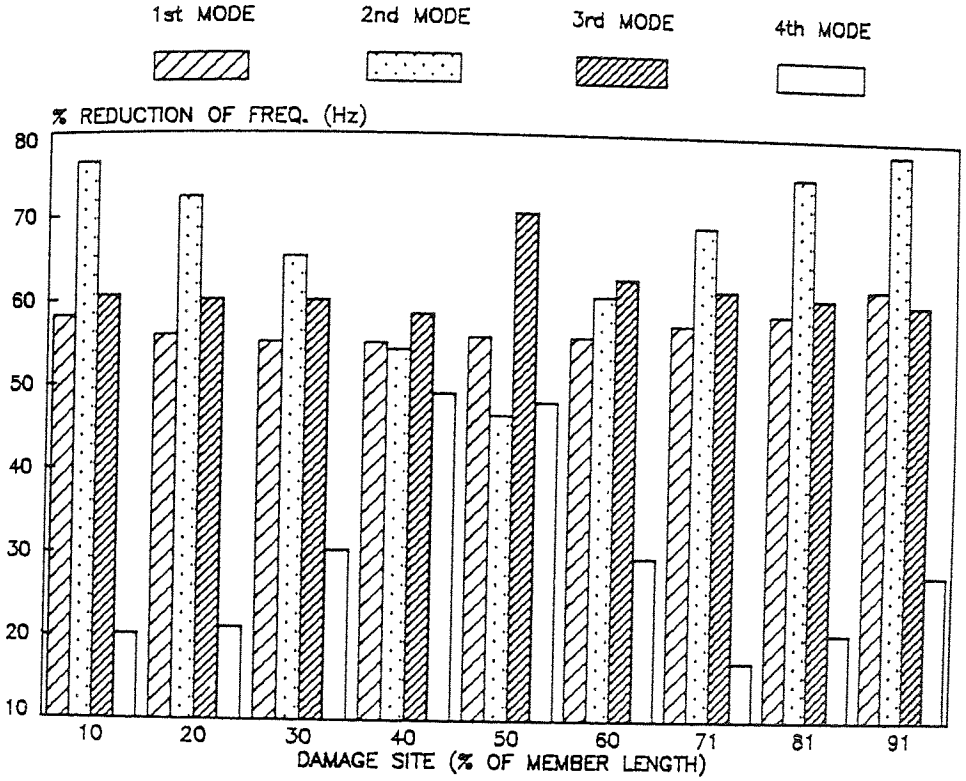

(b)

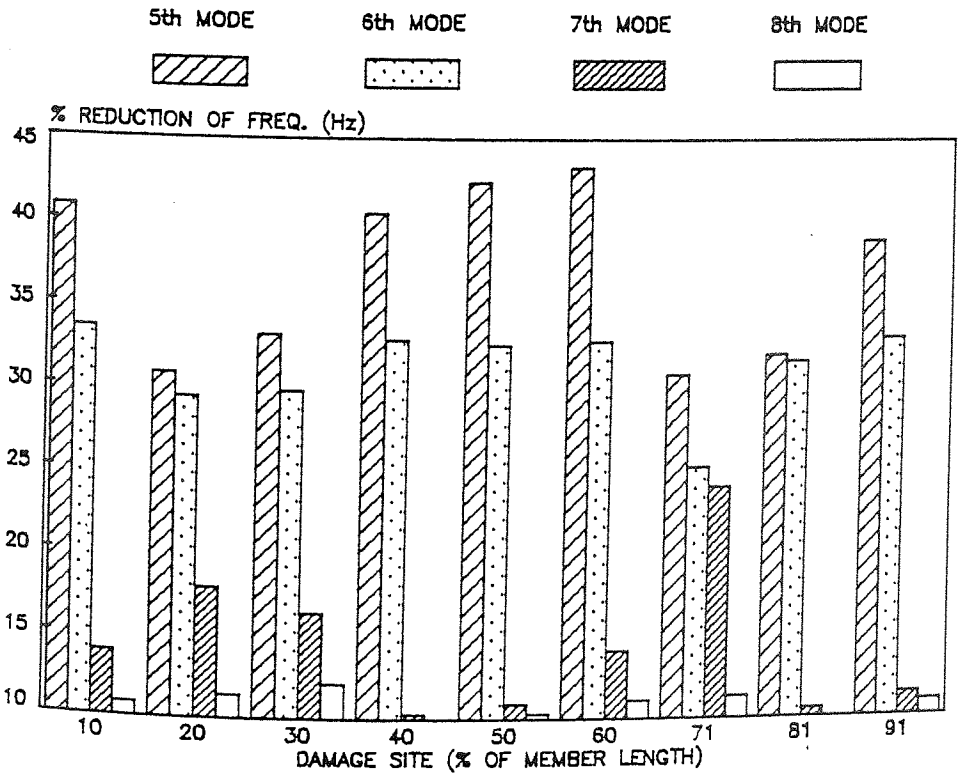

FIG. 7.10a–b THEORETICAL EFFECTS OF DAMAGE SITES WITHIN A MEMBER ON ASYMMETRIC TOWER FRAME FREQUENCY

7.4.5 The Asymmetric Cross-Brace portal Frame.

Results of an asymmetric cross-brace portal frame are plotted in terms of the percentage reduction in frequency caused by the simulated damage against the mode order. Referring to Figs. 7.11a-f, all the frequencies decrease except for the 10th mode where failure at position 1 showed a small increase. From fig. 7.11a it can be seen that complete failure at position 1 and 3 had little effect on any mode except the first and second mode which had a greater effect than failure positioned at 2 in the same member. Figure 7.11b shows the percentage reduction in frequency when the complete failure is located at position 6. A similar result is predicted for failure at position 7. It is also to be noted that the maximum percentage reduction of over 75% in the first mode arises when failure occurs at position 8.

The results of Fig. 7.11c show that complete failure at position 10 had a greater effect on frequency than failure at position 9 and 11 for all modes except the first and second. A comparison of the percentage reductions in frequency when the damage is located at positions 12 and 13 or 14 and 15, can be seen from Figs. 7.11c and 7.11d. Some of the modes had the same effect, while other modes had a different effect on the changes in frequency. Similar predictions can be found in Figs. 7.11e and 7.11f for failure at position 19-20, 21-22 and 23-24.

(a)

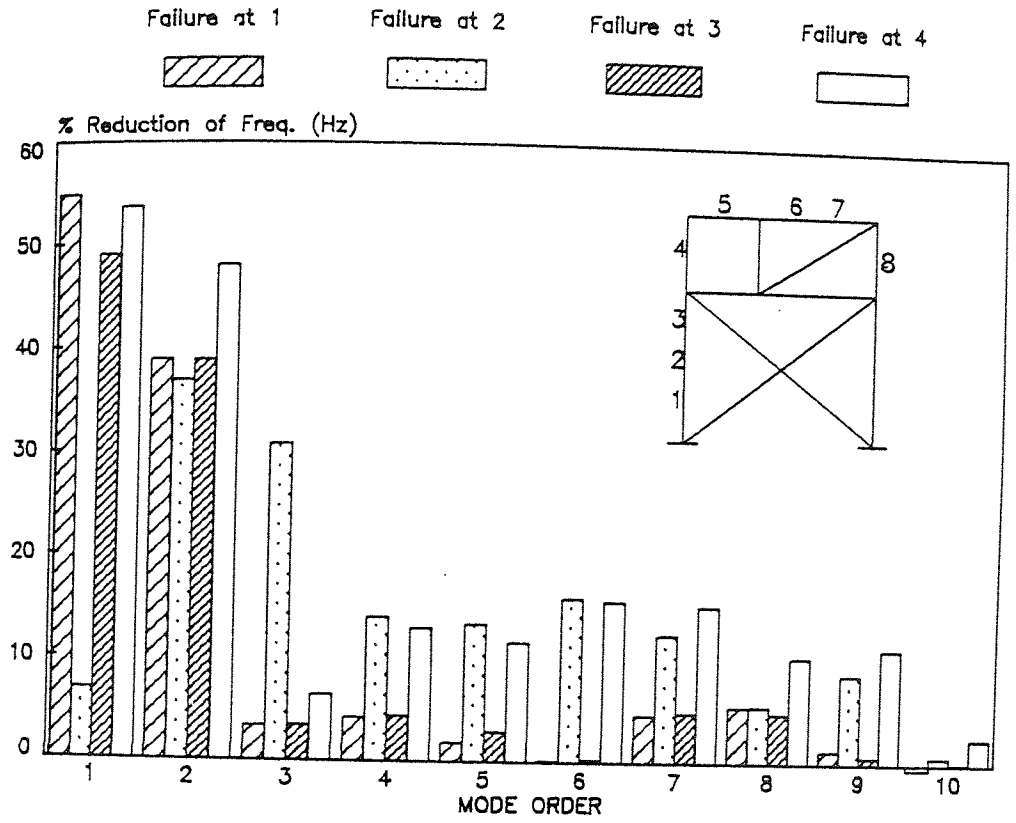

(b)

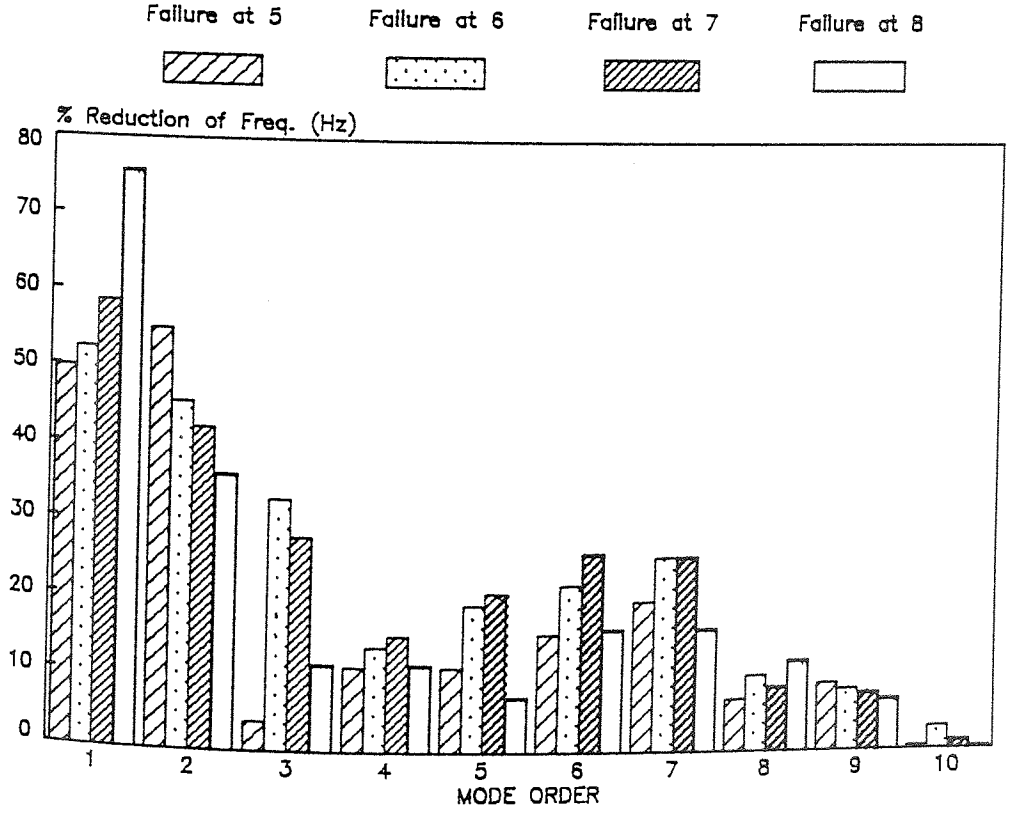

FIG. 7.11a–b THEORETICAL EFFECTS OF DAMAGE SITES (1–8) ON ASYMMETRIC CROSS BRACE PORTAL FRAME FREQUENCY

(c)

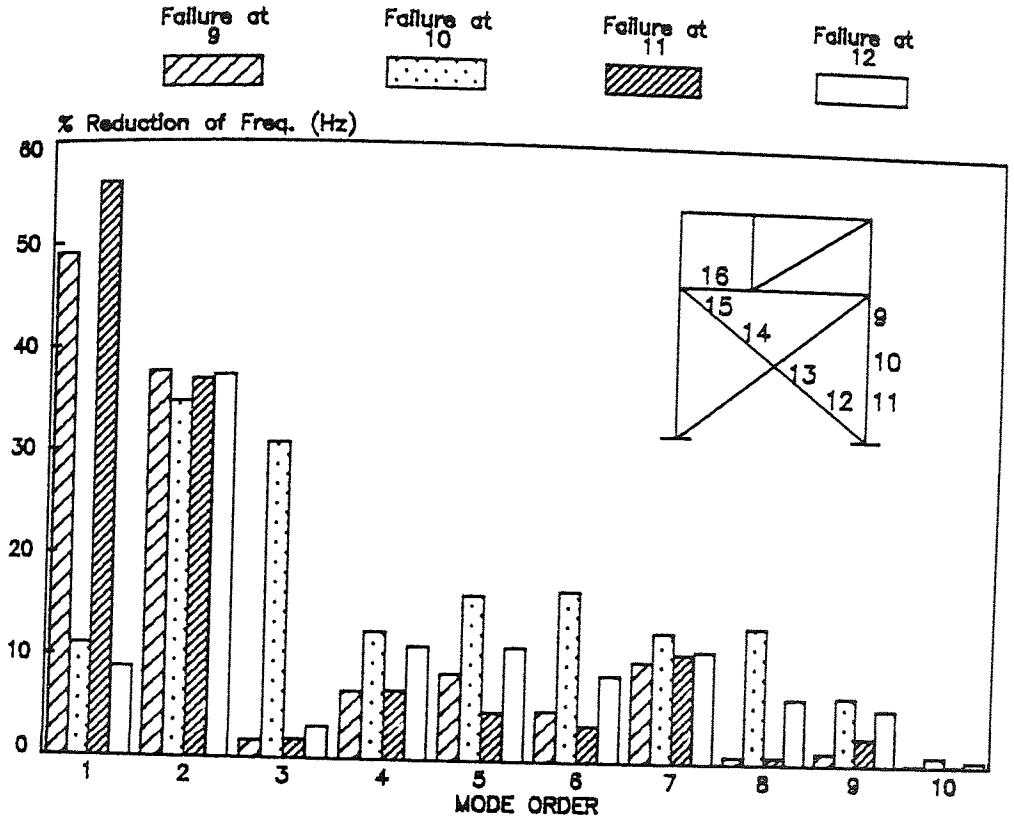

(d)

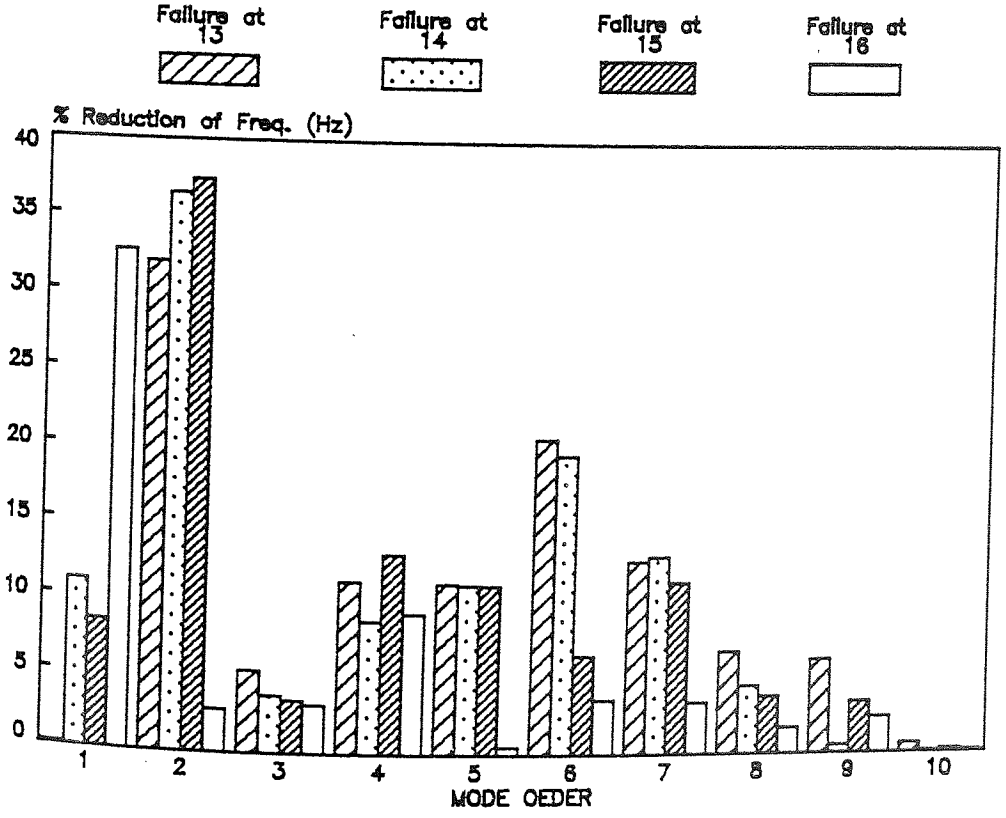

FIG. 7.11c–d THEORETICAL EFFECTS OF DAMAGE SITES (9–16) ON ASYMMETRIC CROSS BRACE PORTAL FRAME FREQUENCY

(e)

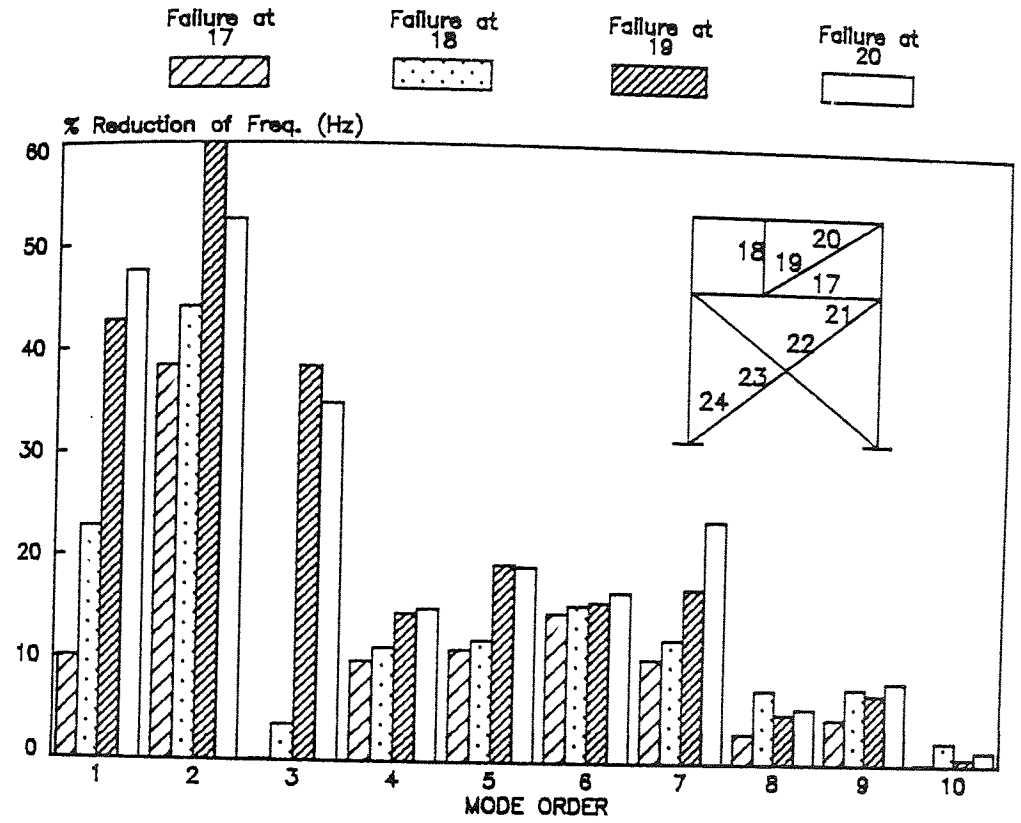

(f)

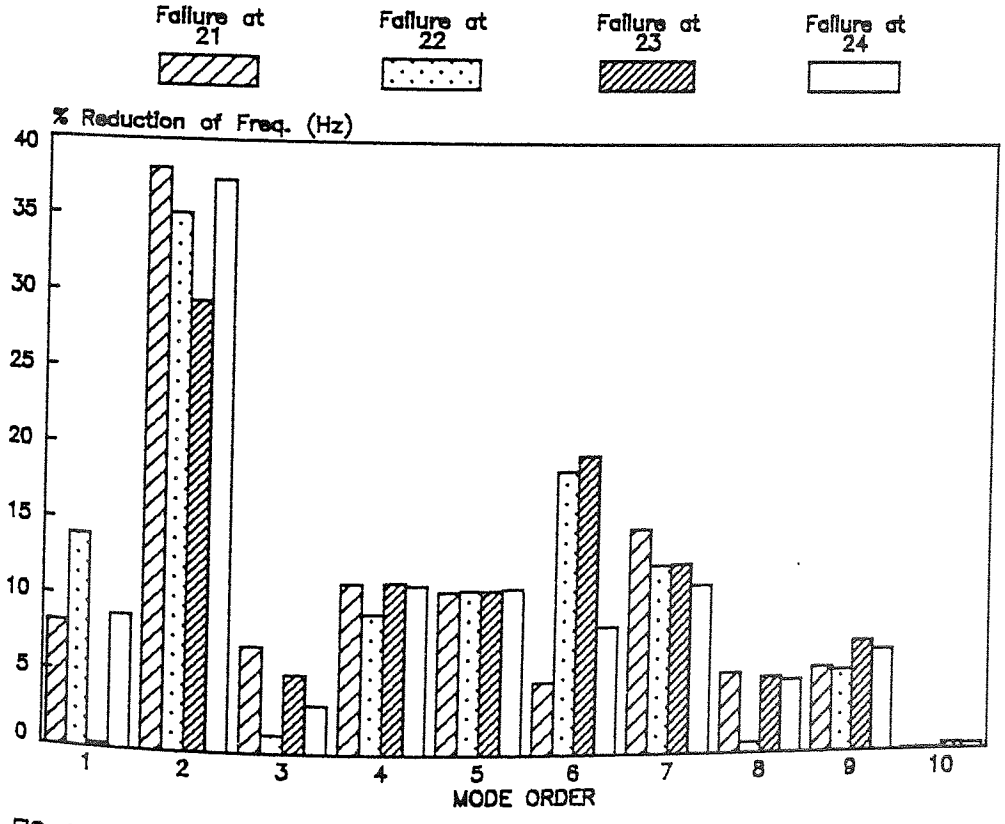

FIG. 7.11e–f THEORETICAL EFFECTS OF DAMAGE SITES (17–24) ON ASYMMETRIC CROSS BRACE PORTAL FRAME FREQUENCY

7.4.6 The Symmetric Space Frame About Both Diagonals.

a) Complete failure modelled by two cantilevers.

This structure was examined and, due to symmetry, each member in one quarter of the structure was 'damaged' in turn and resulting changes in natural frequencies were computed for complete failure, at quarterly intervals along the member: failure was represented by the two-cantilever model.

The results are plotted in Figs. 7.12a-f in terms of the percentage reduction in natural frequency against the mode order. These percentage changes are seen to be greater and more sensitive to position in the lower modes than the higher ones. Hence, the first modes produced the maximum percentage reduction in frequency for all damage locations (over 70%). Results from Fig. 7.12a indicate the sensitivity of the structure's natural frequency to complete failure at positions 1, 2 and 3 on the same member. It is shown that the damage at position 1 has the same effect as damage at position 3, and that both have greater effect than damage at position 2 for the majority of the modes considered. Similar predictions were obtained when damage was located at positions 4, 5 and 6.

By breaking the horizontal brace member, it was found that the percentage reduction in frequency had similar effects in some modes but a greater effect when the damage located at

(a)

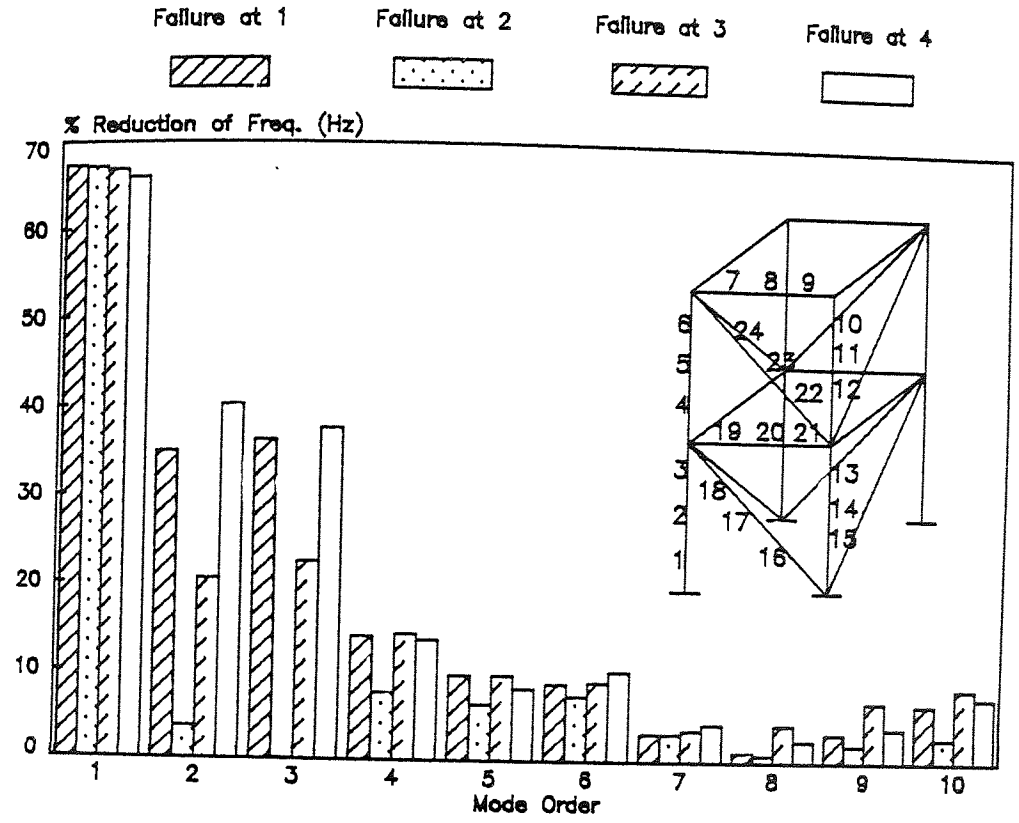

(b)

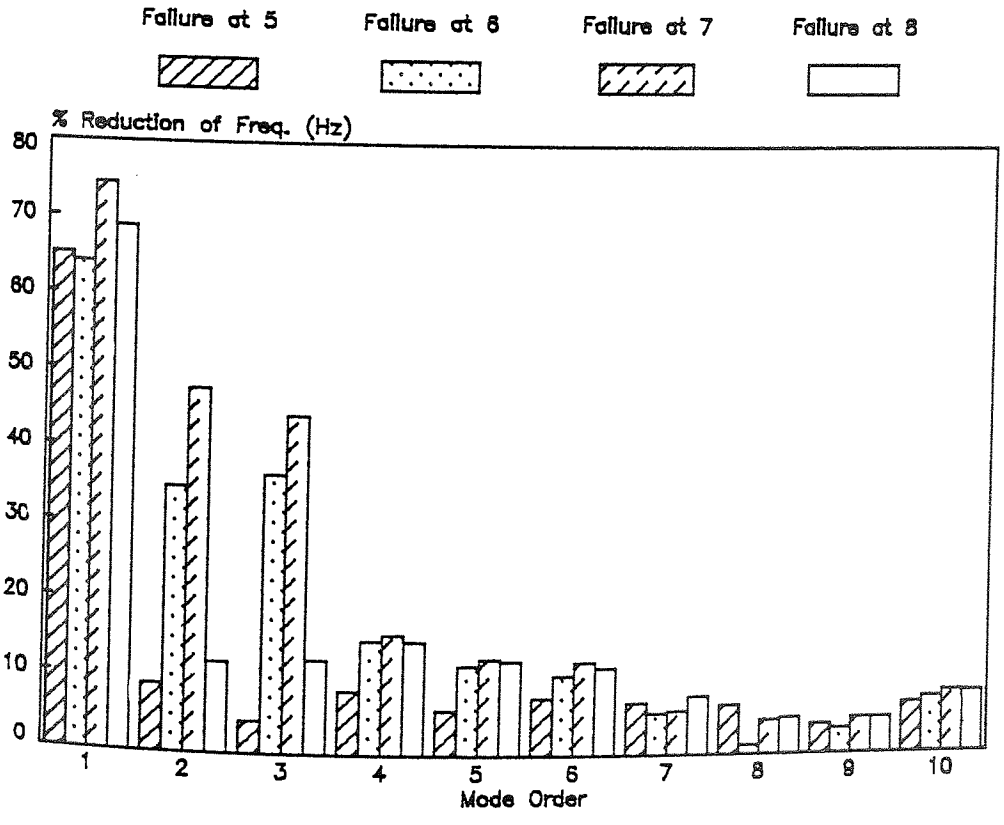

FIG. 7.12a–b THEORETICAL EFFECTS OF DAMAGE SITES (1–8) ON SYMMETRIC SPACE FRAME FREQUENCY

(c)

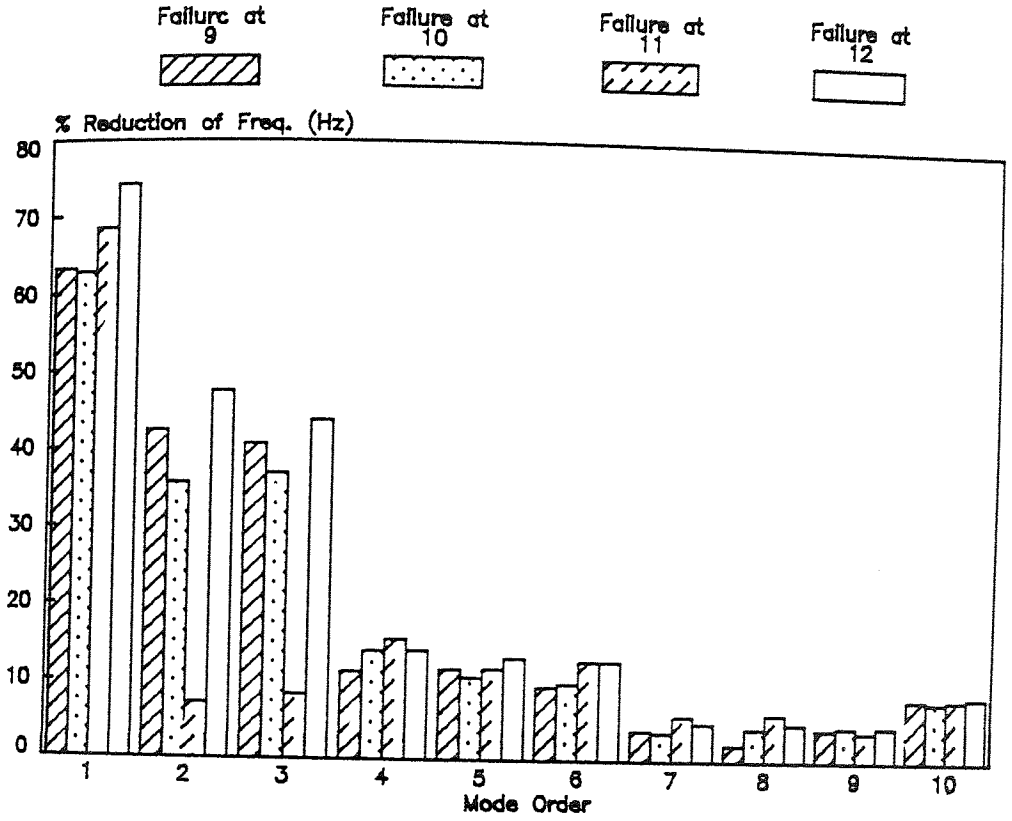

(d)

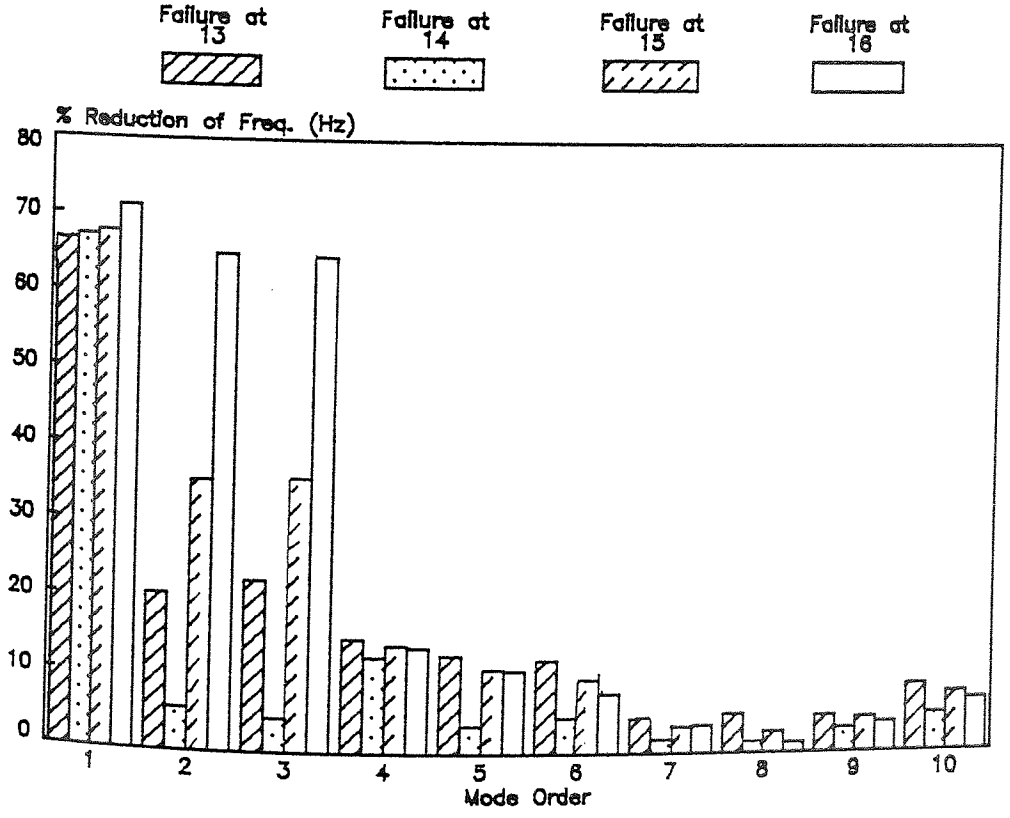

FIG. 7.12c–d THEORETICAL EFFECTS OF DAMAGE SITES (9–16) ON SYMMETRIC SPACE FRAME FREQUENCY

(e)

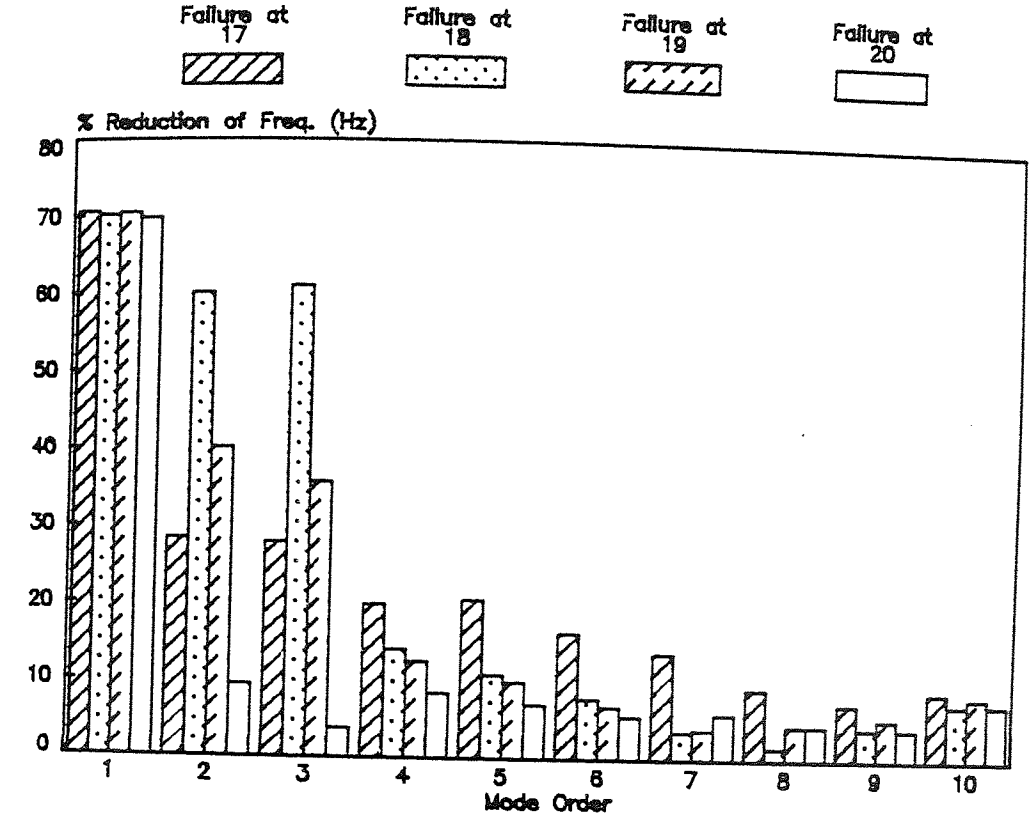

(f)

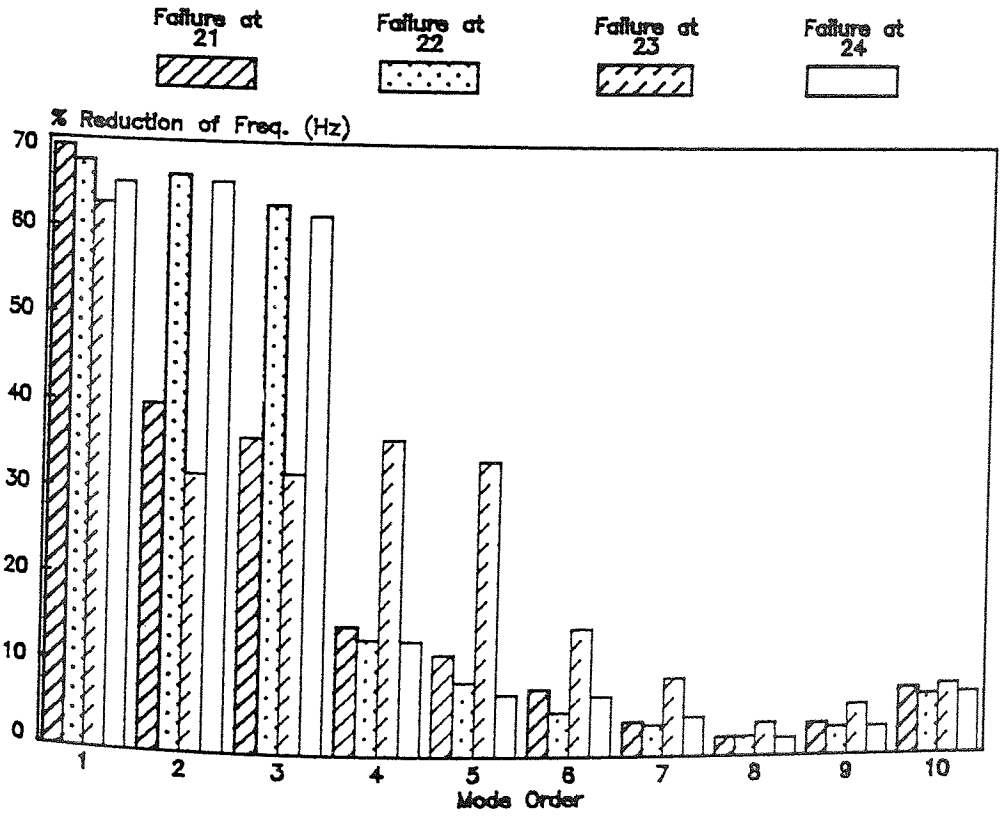

FIG. 7.12e–f THEORETICAL EFFECTS OF DAMAGE SITES (17–24) ON SYMMETRIC SPACE FRAME FREQUENCY

quarter points on the member than at the mid-point. Also, it is predicted that failure at the middle of the diagonal brace member is more sensitive to the frequency in most of the higher modes than the failure at the quarter points. These results are again suitable for incorporation into the defect location analysis.

b) Complete failure modelled by member removal.

Failure may be represented by the complete removal of one member from the space frame and the corresponding frequency changes predicted. This approach was applied to a frame which was symmetrical about both diagonals (see Figs. 7.13a-b). Due to symmetry, each member in one quarter of the structure was 'removed' in turn.

The predictions show the percentage reductions in natural frequencies of the first ten modes where the members marked 1-8 in Fig. 7.13a were removed in turn. The maximum percentage reduction of the first mode was greater than 69%. While for modes 2-9 no change greater than 5% is predicted. It is significant that these predictions for the effect of complete removal of a member show that the percentage reduction in the fundamental mode is so much greater than for other modes.

It is also observed that in high modes there can be small increases in natural frequencies caused by the removal of members. The reason for this is that in the structure, for

(a)

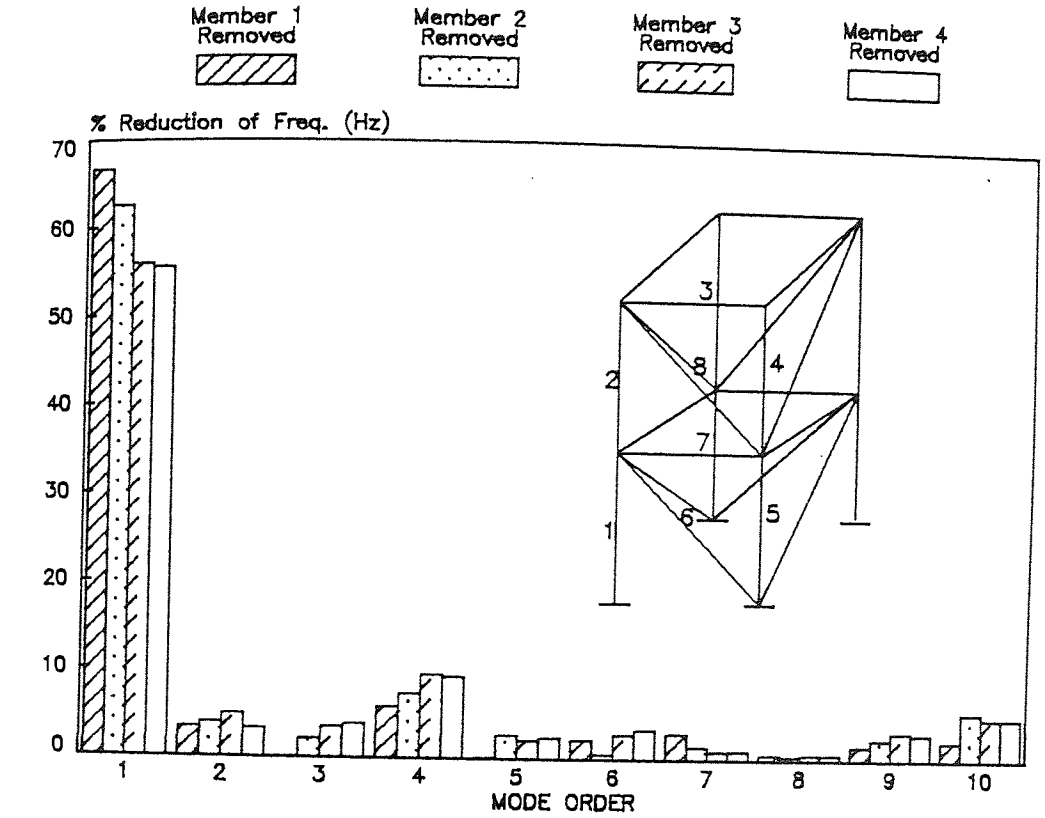

(b)

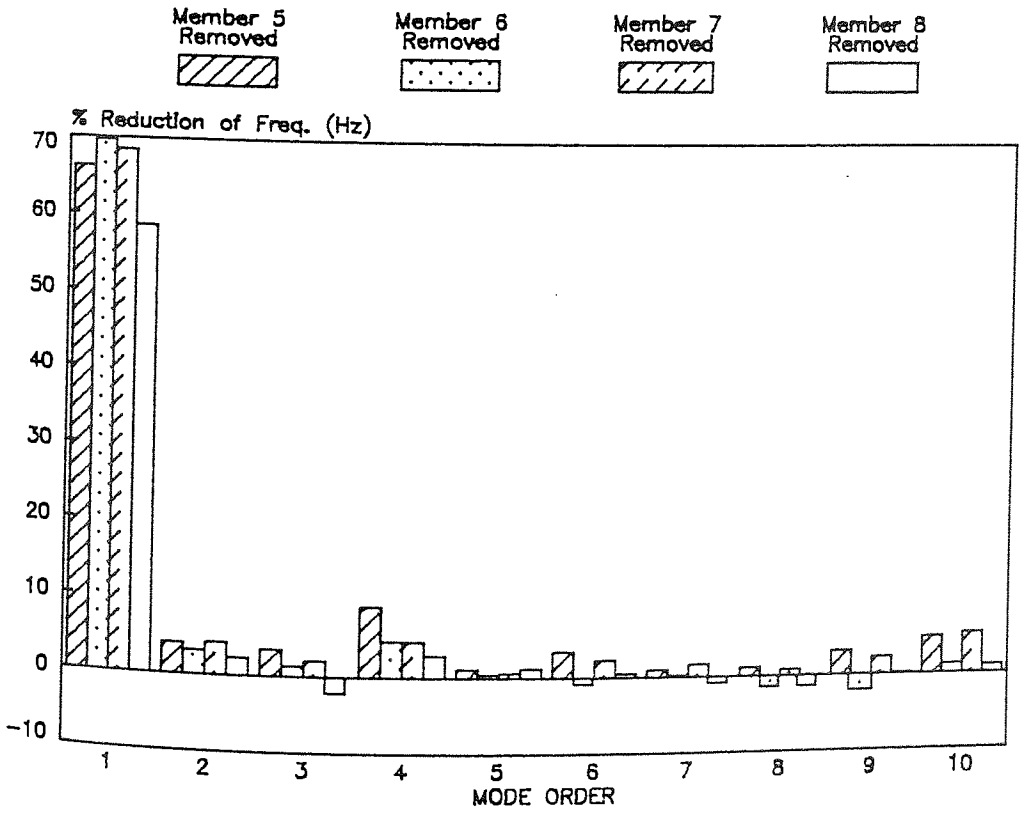

FIG. 7.13a–b THEORETICAL EFFECT OF MEMBER REMOVAL (1–8) ON SYMMETRIC SPACE FRAME FREQUENCY

any mode of vibration, the total kinetic and strain energy are made up of the corresponding energies of each individual member. The removal of a member, which for any mode contributes more to changes in strain energy than to kinetic energy, could result in a large reduction in frequency for that mode. By the removal of a member which, on account of its position, contributes less to kinetic energy than to strain energy, the result is an increase in frequency. In reality, the increase in frequency will never be as large as predicted, because a member failing at one end will still be hanging on by the other end and will still be contributing to some extent to the kinetic energy of the system.

7.4.7 The Space Frame Symmetric About One Diagonal.

The effect of the complete failure in the middle of each member on the first ten natural frequencies of a space frame symmetrical about one diagonal are shown in Figs. 7.14a-c. Failure was represented by the two-cantilever model and the frequency changes were calculated for each damage site in turn. These changes are used later in the defect location analysis. All the frequencies are reduced and the changes in the frequencies from the original are plotted.

It is observed from Figures 7.14b and 7.14c that breakage of the sixth and eleventh members has a larger effect on the first mode and a much smaller effect on the higher modes. Breakage of the twelvth member has the smallest effect on all

(a)

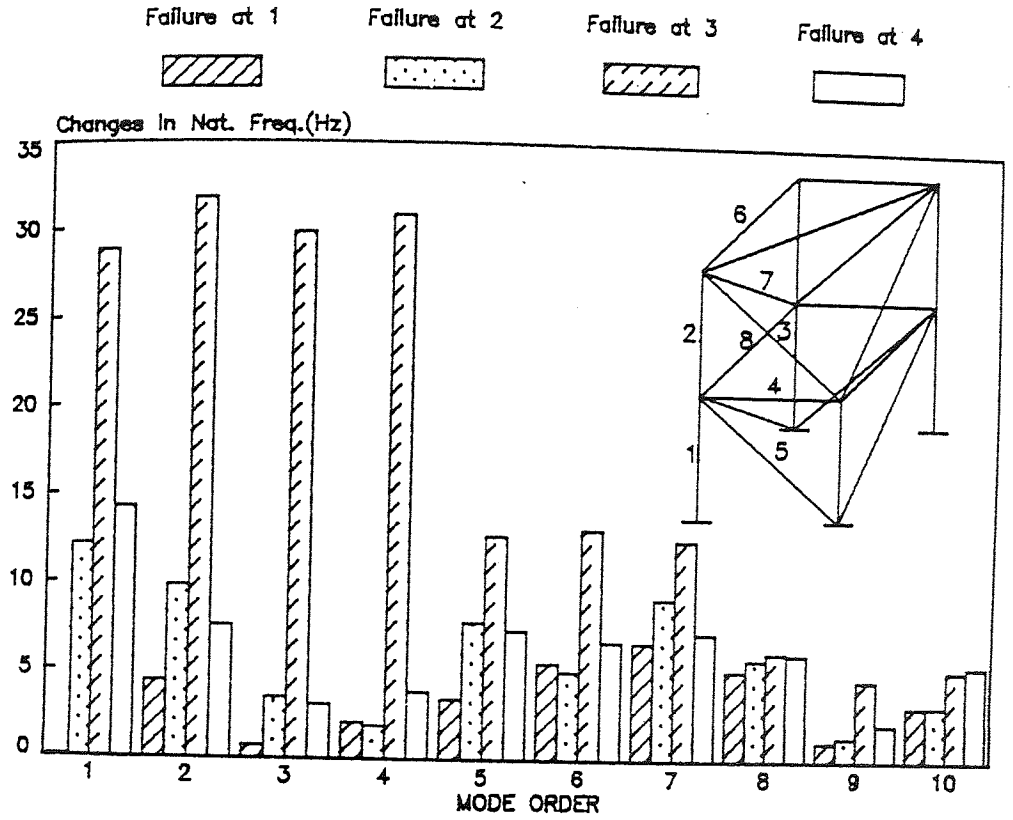

(b)

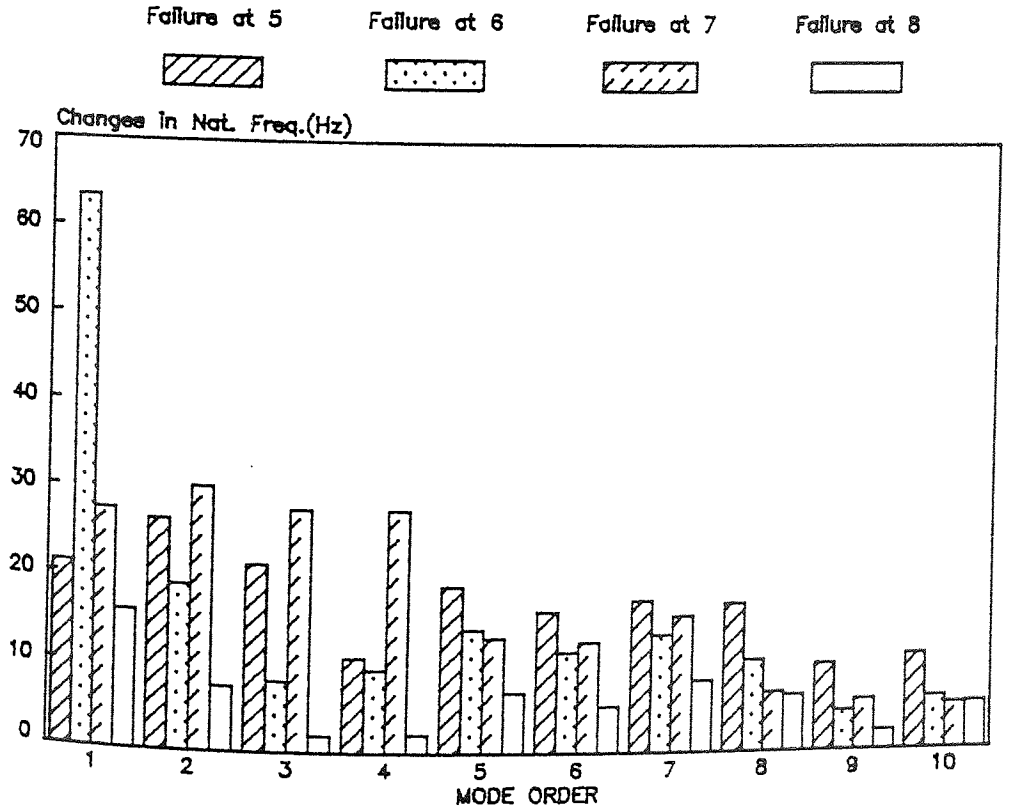

FIG.7.14 a–b THEORETICAL EFFECTS OF DAMAGE SITES (1–8) ON SYMMETRIC SPACE FRAME FREQUENCY–WITH ONE DIAGONAL

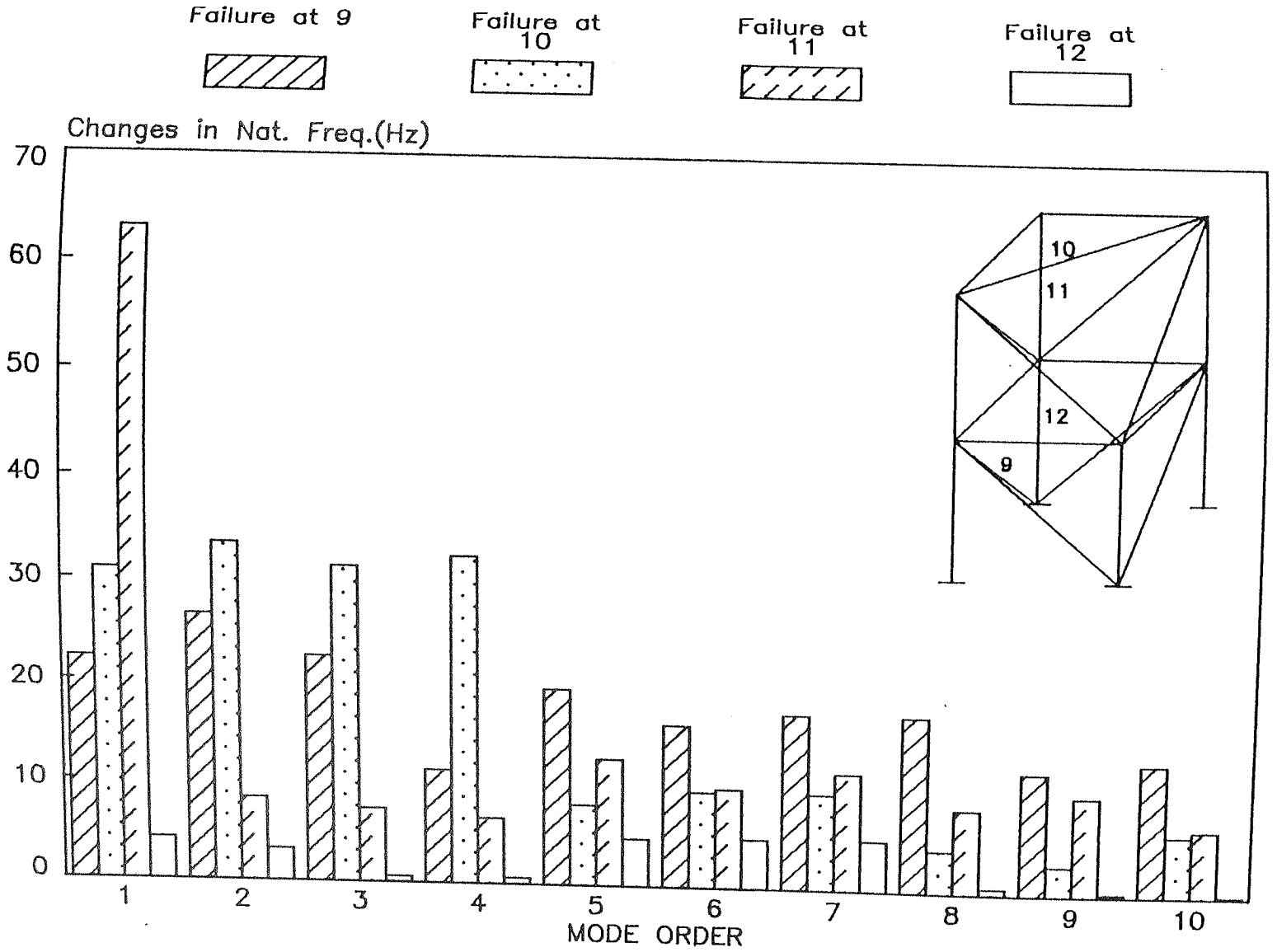

FIG. 7.14c THEORETICAL EFFECTS OF DAMAGE SITES (9–12) ON SYMMETRIC SPACE FRAME FREQUENCY–WITH ONE DIAGONAL

ten modes: the maximum percentage change was only 4.36%. Such a small change could be dismissed in an experimental investigation since it lies within the band of ±5% error which is normally anticipated. The predictions for this structure can be said to demonstrate the sensitivity of the system to damage location. It is evident, once again that some modes are more sensitive than others to the change in stiffness arising from damage.

7.4.8 The Asymmetric Space Frame.

The frequency changes brought about by failure in an asymmetrical space frame were investigated using the two-cantilever model, failures being located at the centre of each member in turn. The results of the investigation are shown in Figs. 7.15a-f.

It is found that once again many modes of vibration are insensitive to damage. The maximum percentage frequency reductions are greater than 66% for the first mode, where complete failure was simulated at position 3. It is also evident that percentage changes in frequencies are approximately 7%, when the location of the complete failure was in members 4-9, 14, 15, 17, 18, 20, 22 and 24, for all modes except for the first mode.

The simpler structures examined appear to show greatest sensitivity to damage, whatever the location. The more

(a)

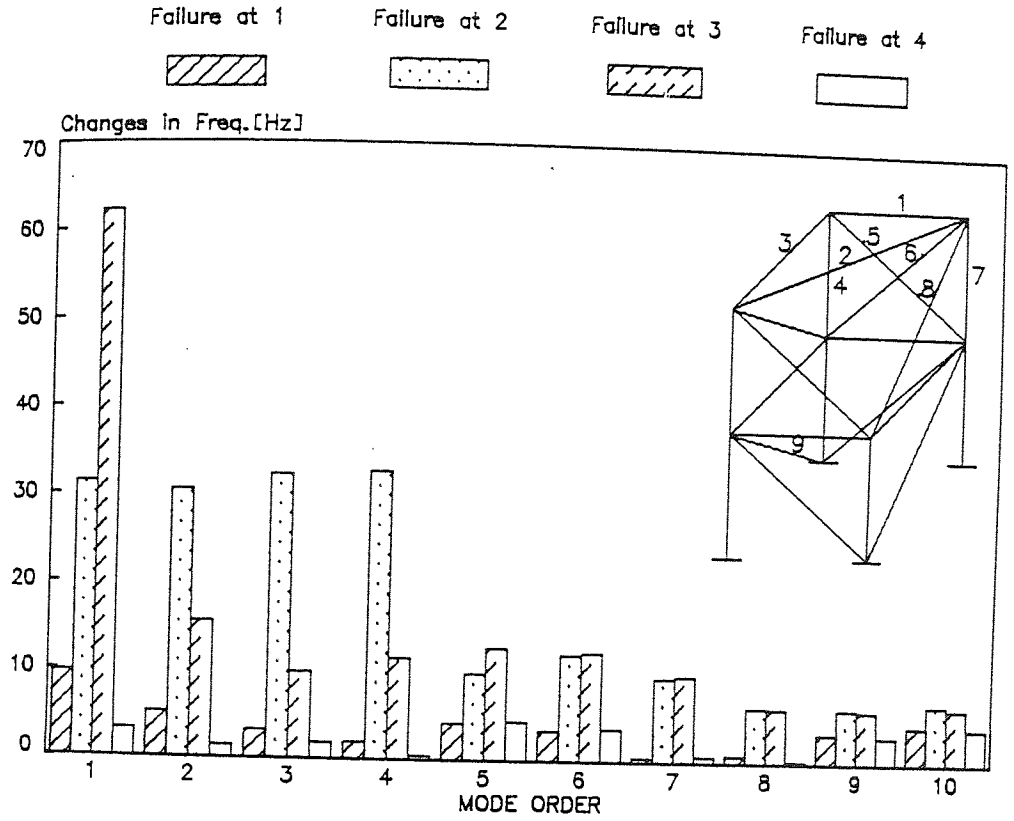

(b)

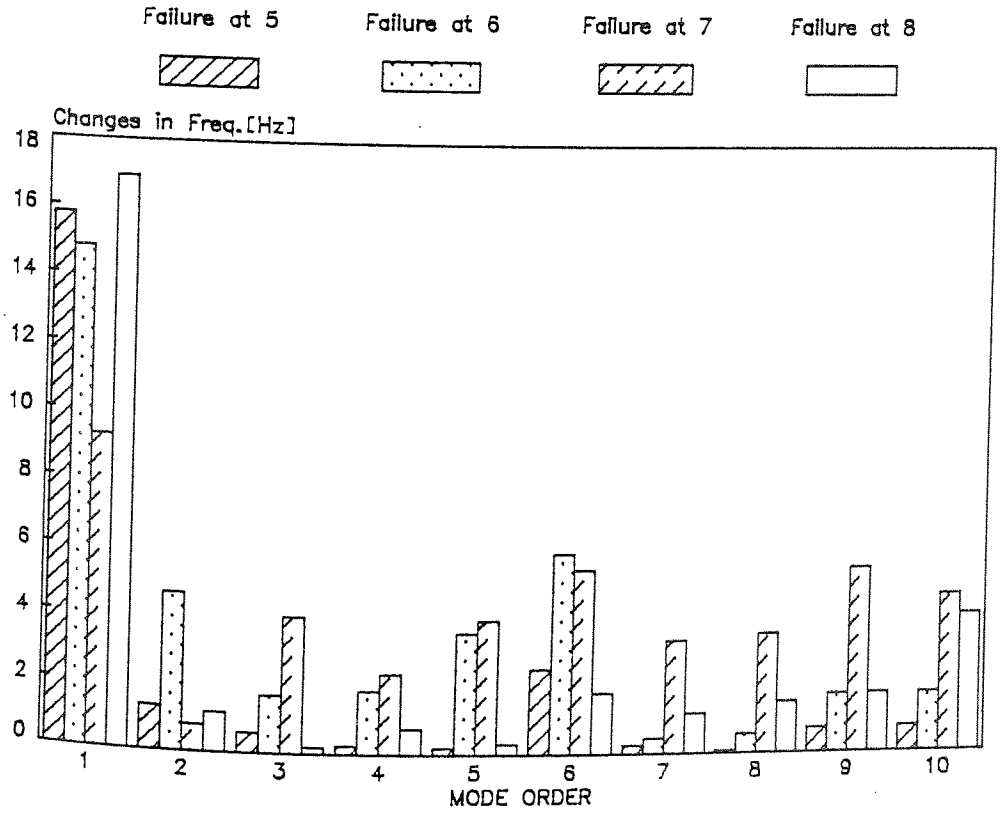

FIG.7.15a-b THEORETICAL EFFECTS OF DAMAGE SITES (1-8) ON ASYMMETRIC SPACE FRAME FREQUENCY

(c)

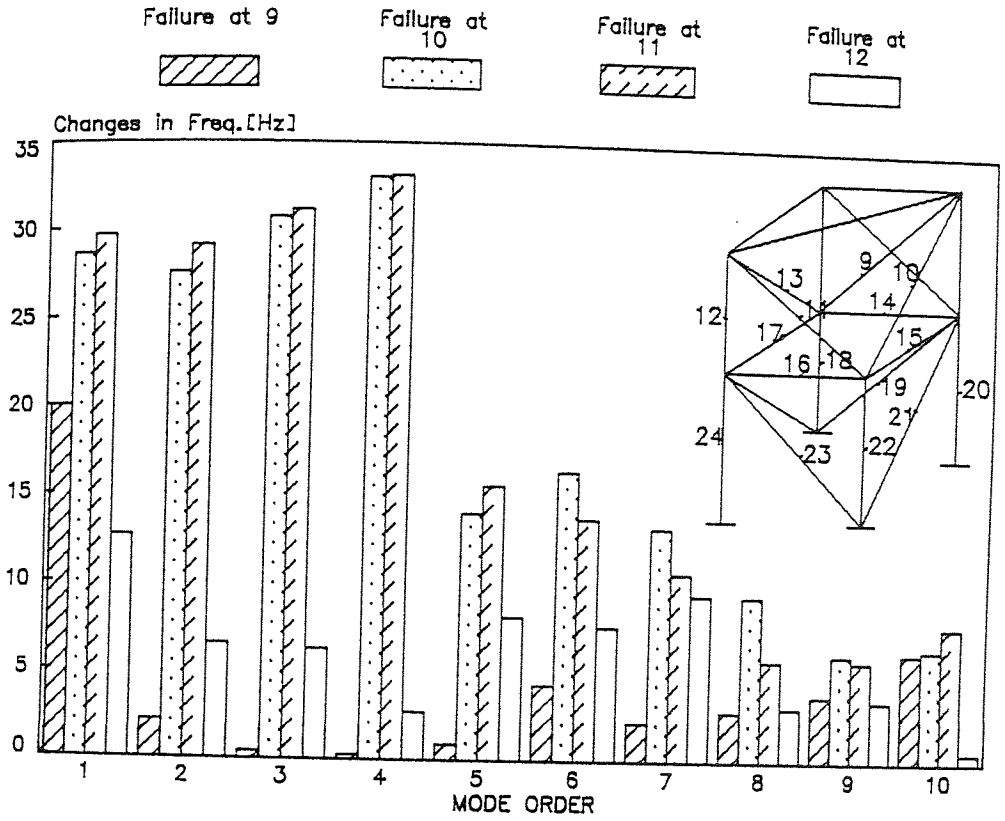

(d)

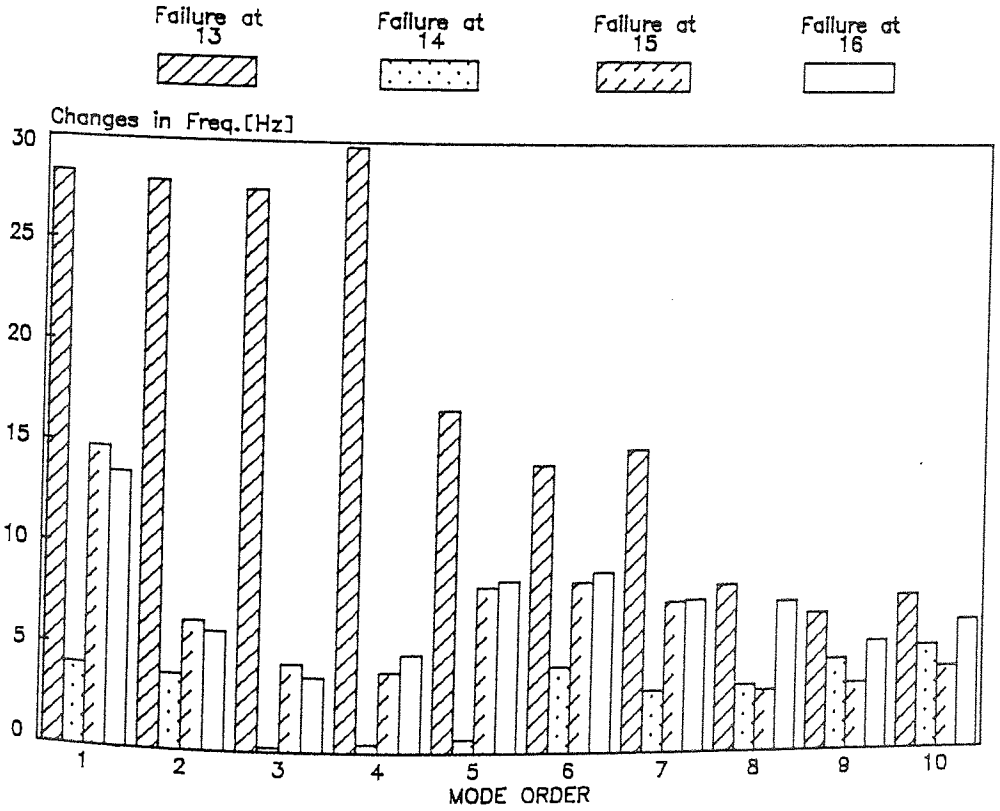

FIG.7.15c–d THEORETICAL EFFECTS OF DAMAGE SITES (9–16) ON ASYMMETRIC SPACE FRAME FREQUENCY

(e)

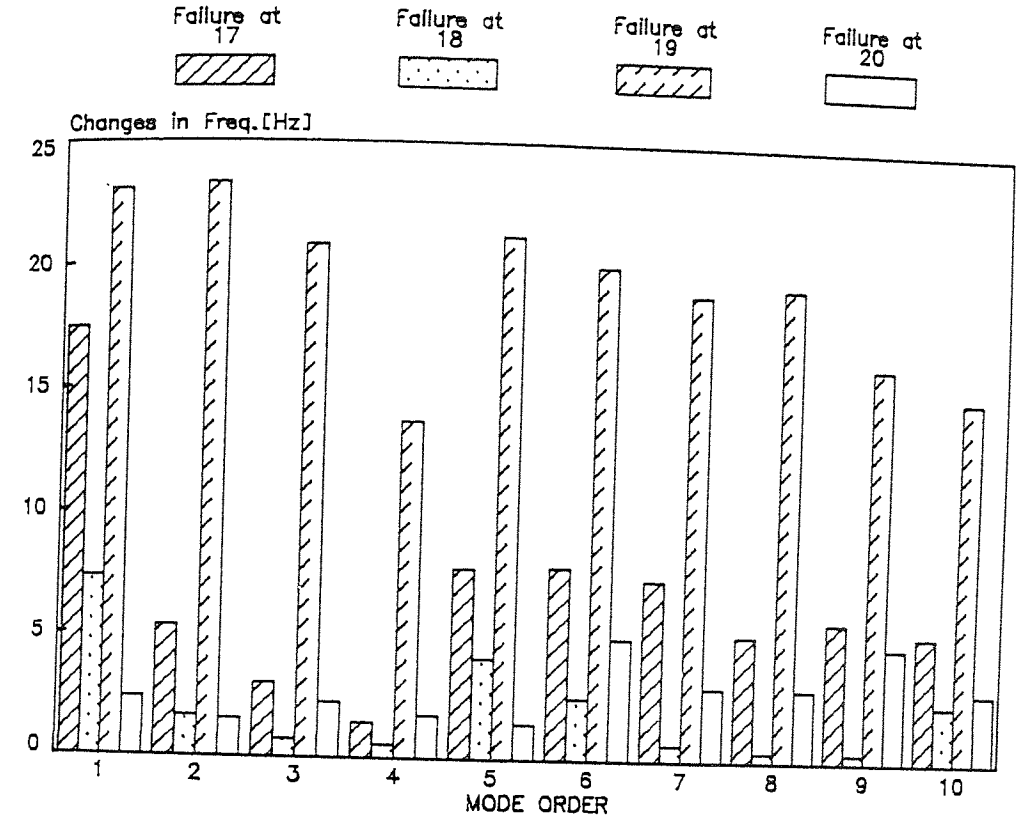

(f)

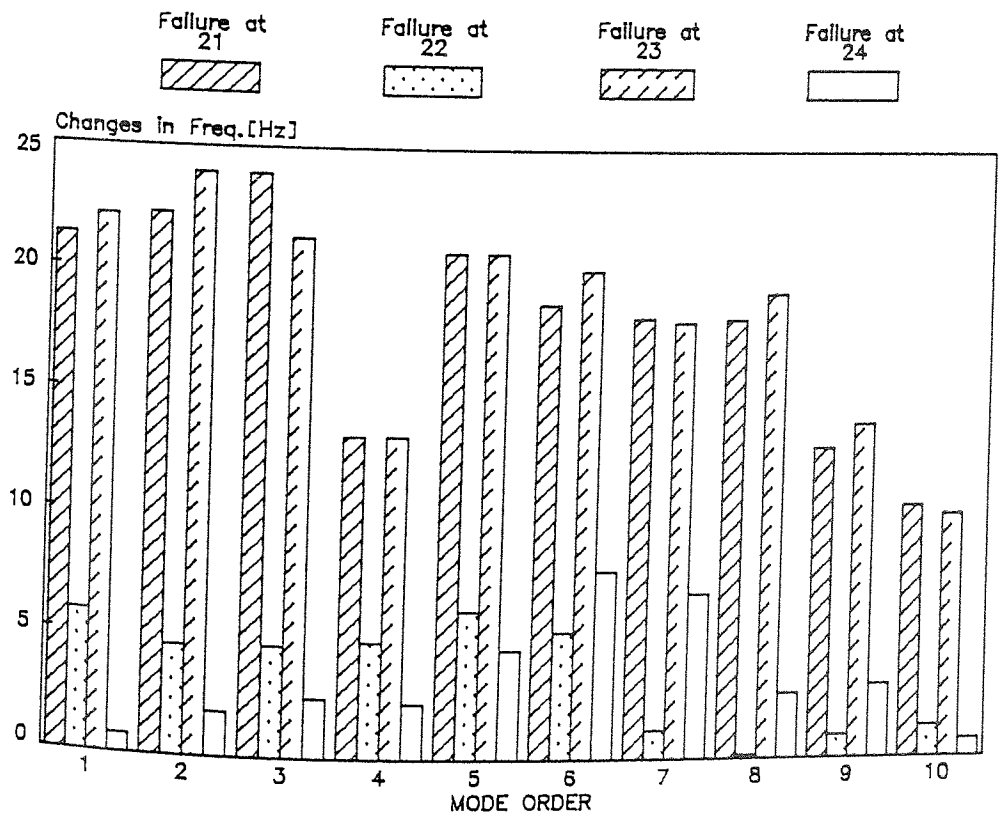

FIG.7.15e-f THEORETICAL EFFECTS OF DAMAGE SITES (17-24) ON ASYMMETRIC SPACE FRAME FREQUENCY

complex structures exhibit least change in the frequency spectrum when damaged: in particular, the asymmetric space frame predictions indicate that only the first mode is significantly affected.

In general, it is found that in the majority of structures, irrespective of their degree of complexity the lower modes are more affected by damage than the higher modes.

7.5 SYMMETRIC AND ANTI-SYMMETRIC MODES.

The symmetry of the frame about the centre line implies that the modes will be either of anti-symmetric configuration with no vertical displacement at the central joints or of symmetric configuration with zero horizontal displacement and rotation (53). The frequencies of the complete frame can therefore be obtained by calculating those for the symmetrical half-frame: this greatly reduces the computation time required and also enables a desk top computer of limited memory size to be used. The results predicted by this computation for an unbraced portal frame are shown in Table 7.2, from which it is apparent that there is an anticipated agreement between symmetric and anti-symmetric frequencies.

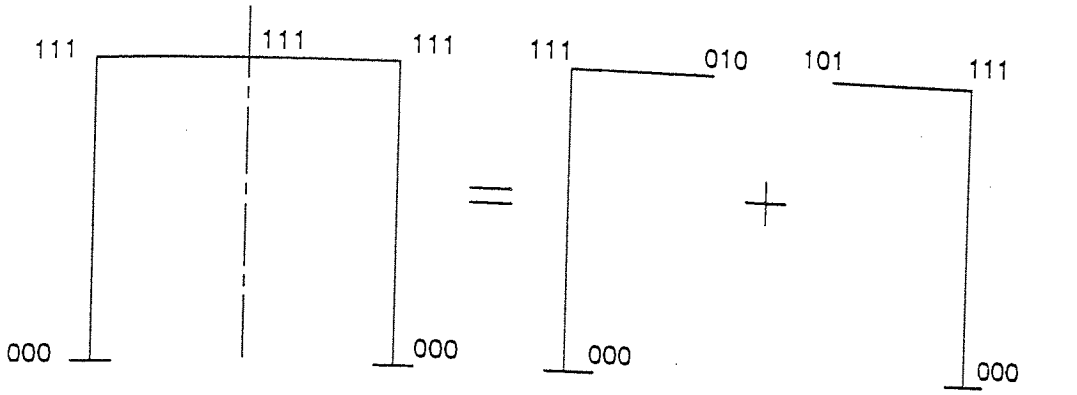

dof Represents Degrees of Freedom
1 Represents Freedom
0 Represents Suppression
010 Represents Y–Translation Only
A1 Represents First Anti–Symmetric Mode
S1 Represents First Symmetric Mode etc.

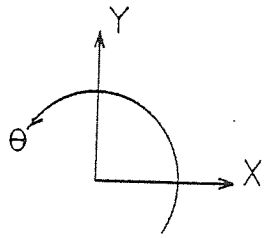

Half Frame		Whole Frame	
Symmetric	Anti–Symmetric	Frequency	Type
	24.99	24.99	A1
97.34		97.35	S1
	161.31	161.31	A2
173.8		173.8	S2
	347.27	347.27	A3
432.23		432.23	S3
	496.86	496.86	A4
745.55		745.56	S4
	895.58	895.57	A5

TABLE 7.2 SYMMETRIC AND ANTI–SYMMETRIC FREQUENCIES (Hz) OF PORTAL FRAME

7.6 CLOSING REMARKS.

In this chapter, sensitivity of the structure to damage has been investigated by examining the resulting changes in natural frequencies, due to the damaged member. The theoretical natural frequencies were predicted using the exact solution.

Mathematical models of several structures have been analysed to predict effects of the extent and position of the damage. The boundary conditions have also been examined. These various parameters affecting the dynamic characteristics of the structure were considered separately and their quantative effect on the natural frequencies was evaluated.

It has been observed that failure of a structural member may produce appreciable shifts in the natural frequencies of some modes and comparatively small shifts in others. These changes associated with the modes depend on relative changes in the strain and kinetic energies of the member.

All models which were used for representing damage yielded similar predictions from which it can only be concluded that the choice of model should be deferred until a comparison has been made with the experimental results for producing the defect location charts (chapter nine).

Correlation between experimental and theoretical results will be discussed in the next chapter.

CHAPTER EIGHT

CORRELATION BETWEEN EXPERIMENTAL AND THEORETICAL RESULTS

8.1 INTRODUCTION

It is essential that the frequency changes caused by damage can be measured readily and accurately, so that they can be used with confidence in the prediction of damage location by statistical analysis.

Tests were conducted on the range of structures analysed in chapter seven to establish the degree of correlation between predicted and measured frequency changes and thereby assess the viability of using frequency measurements as an non-destructive testing technique. Initially, this test was applied to a simple structure such as a cantilever, then progressing to work on symmetric and asymmetric plane frame structures and finally to more complicated space frame structures.

8.2 EFFECT OF EXTENT AND POSITION OF DAMAGE

A series of tests was performed on several structures which were damaged in different ways as already discussed in section 6.12. This damage was inflicted at different positions on the structure in order to monitor the changes in frequencies. On each occasion, the structure was repaired by welding and used again because it was impractical to build a new structure for each test. These frequencies of the structures were obtained from the measurement of inertance. The first ten modes are measured. Natural frequencies which

were below 1 KHz, were found to an accuracy of 0.5 Hz, and those above this were found to an accuracy of 1 Hz.

8.2.1 Tests on Cantilever Beam.

The first series of tests involved cutting with a hack-saw one side of a mild steel cantilever, 700*50*12 mm at 100mm from its fixed end. Further tests were then carried out with various cut depths on the upper surface of the beam, each cut going about 2mm, 5mm, 7.5mm, 8.5mm and 10mm of the way into the beam. In each case, the natural frequencies of the undamaged beam were measured and were later re-measured after further damage. Only the first five modes for the cantilever beam were measured as the higher modes was became difficult to measure with acceptable accuracy.

The results for this cantilever are shown in Table 8.1 and prove good agreement between the experimental natural frequencies and the theoretical predictions for the undamaged structure, the worst error in frequency being 5.7%. It is apparent that for all modes the reduction in frequencies becames higher as the extent of damage increases. But, it was found that the maximum percentage reduction was 41% in the fundamental frequency for a 10mm cut depth.

The natural frequencies of a second steel cantilever beam 480*40*6 mm were measured up to the fifth mode and the results compared with theoretical predictions obtained from

two different models; 1 and 2. Model 1 assumes that the end of the cantilever is fixed. Model 2 assumes that there is a torsional spring equivalent to 5% reduction in stiffness at the fixed end of the cantilever. Table 8.2 shows the comparison between the models and the experimental frequency. It was found that model 1 gave a maximum error of 8.4% while model 2 gave only 4.4%. While the discrepancy between the theoretical predictions is not large, the second model predicts the measured values more accurately. The cantilever was then subjected to fatigue using the Amsler fatigue machine to generate a crack 25.6mm deep at 140mm from the fixed end and the natural frequencies of the damaged cantilever were measured. The results are also shown in Table 8.2. Therefore, this model is considered to be closer to the experimental condition.

It is clear that from "% error 1" and "% error 2" in Table 8.2, these discrepancies are due to the effect of the non idealistic boundary conditions, and in addition, might be due to the effect of an added mass (transducers and decoupler) to the structure. It can be observed from Table 8.1 and 8.2, that the theoretical frequencies were higher than the experimental one.

Mode	Undamaged Freq. (Hz)			Exp. Changes in Freq. (Hz)				
	Theo.	Exp.	% Error	2mm Saw Cut	5mm Saw Cut	7.5mm Saw Cut	8.5mm Saw Cut	10mm Saw Cut
1	20.45	20.4	.24	.4	2.4	4.4	6.4	8.4
2	128.15	121	5.6	1	1	3	4	5
3	358.82	344	4.1	4	6	8	9	10
4	703.14	664	5.6	4	22	32	68	104
5	1162.4	1096	5.7	–	64	104	152	206

TABLE 8.1 EXPERIMENTAL CHANGES IN FREQUENCY DUE TO VARIOUS CUT DEPTHS IN A CANTILEVER BEAM

Mode	Undamaged Frequency (Hz)					Damaged Freq. (Hz)	
	Theo.		Exp.	% Error 1	% Error 2	Exp.	Exp. Changes
	Model1	Model2					
1	22.27	20.93	21.5	3.5	−2.7	19.38	2.12
2	139.56	132.03	127.78	8.4	3.2	126.36	1.42
3	390.78	371.42	361.79	7.4	2.6	348.26	13.53
4	765.77	730.85	702.75	8.2	3.8	694.64	8.11
5	1265.9	1212.5	1159.4	8.4	4.4	1139.8	19.6

TABLE 8.2 EXPERIMENTAL CHANGES IN FREQUENCY DUE TO FATIGUE CRACK IN A CANTILEVER BEAM

8.2.2 Tests on Symmetric Cross-Brace Portal Frame.

After having carried out some preliminary tests on cantilever beams, experimental studies on more a complex structure was required. Thus, a symmetrical cross-brace portal frame was the next structure to be tested, See Fig. 6.5. This structure was then damaged by a series of saw cuts. The first test involved the cutting on both sides, 10mm (50% of the cross sectional area), at position A, as shown in Fig. 6.5. The second cut was at the same site but a complete cut was made through the member. In both cases, the first nine modes were measured and the frequency changes produced by the damage are set out in Table 8.3.

As might be expected, these results show that the reduction in the frequencies increased as the damage size increased. Also, complete failure caused larger changes in frequency than the partial failure.

To continue with the test, this structure was then repaired by welding and the natural frequencies were again measured. Damage was applied in the form of a saw cuts with various depths at position B. Natural frequencies were measured for cuts of depth 10mm and 15mm on each sides of the member, corresponding to 50% and 75% reduction in cross sectional area, and also after the section had been completely severed at the same position. The results, together with the corresponding changes in frequency for the first nine modes,

are shown in Table 8.3.

It is apparent that the reduction in the frequencies increased as the damage size increased, although in the seventh mode the frequency increased as the extent of the damage increased. The reasons for this are already explained in section 6.7.3 and in the preceding chapter.

Changes in the inertance measurements with various cut depths of the cross-braced portal frame are discussed below. The first example represented the measured inertance (In21) for the virgin structure and for the cut depth of 15mm on both sides at position B as shown in Fig. 8.1a. The next example compares the inertance measurements for the virgin structure and for complete failure at site B as shown in Fig. 8.1b. From these figures it is seen that the inertance measurements exhibited radical changes in frequency when total failure occurred on the structure than the partial failure. Also, it can be seen that the seventh mode was inadequately excited during the tests.

8.2.3 Tests on Asymmetric Cross-Brace Portal Frame.

Inertance tests were carried out on the asymmetrical cross-braced portal frame structure, shown in Fig. 6.6. This structure was damaged by a saw cut, 2mm in depth 33% of the cross sectional area. The first saw cut was deepened in successive tests until the member was completely severed. In

each case the natural frequencies of the first ten modes were measured and the frequency changes were tabulated in Table 8.4. This table also shows the percentage of errors between the experimental and theoretical frequencies of the undamaged structure. A reasonable agreement is shown between the predicted and measured undamaged frequencies, the greatest frequency error was 6.3%. These errors are from variations in dimensions due to manufacturing tolerances, material operties, and the rigidity of welded joints, as well as the inaccuracies introduced by the finite element solution.

The percentage error between the experimental and theoretical frequencies for the damaged structure were also calculated. The maximum error was found to be 7.7% for the first mode and less than 5% for the other modes. These results have not been included, because they are not required in the statistical analysis.

Referring to both Table 8.4 and Fig. 8.2a, the frequency at the second and third mode was increased by the presence of the 2mm saw cut, but this produced little effect on the other modes. Again, Table 8.4 and Fig. 8.2b show that complete failure has a significant effect on the frequencies and this effect is different for each mode. It was noticed that the second mode had the maximum percentage frequency reduction of 43.7%. As might be expected, it was found that the changes in frequencies due to complete failure at position A, are more s ificant than these produced by partial damage.

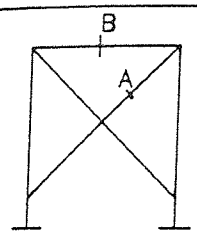

	1st Mode	2nd Mode	3rd Mode	4th Mode	5th Mode	6th Mode	7th Mode	8th Mode	9th Mode
	Undamaged Frequencies (Hz)								
	102	131	170	209	312	333	342	445	460
	Frequency Reductions (Hz)								
10mm Saw Cut at A	0.3	7.3	1.1	1	1.4	0.1	3.3	1.2	3
Complete Cut at A	18	4	27	48	122	87	42	86	87
After Welding Cut A	Undamaged Frequencies (Hz)								
	99	125	168	214	314	341	379	445	460
	Frequency Reductions (Hz)								
10mm Saw Cut at B	2.1	0.6	0.3	0.7	1	0.3	1.2	0.2	0.5
15mm Saw Cut at B	7.2	1.1	2.5	1	3.4	1	−7.5	1.4	1.7
Complete Cut at B	29	2.5	0.1	22.6	26.2	3.1	10.2	8.1	4

TABLE 8.3 MEASURED CHANGES IN FREQUENCIES OF CROSS PORTAL FRAME

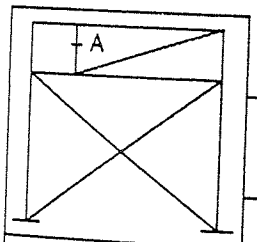

	1st Mode	2nd Mode	3rd Mode	4th Mode	5th Mode	6th Mode	7th Mode	8th Mode	9th Mode	10th Mode
	Undamaged Frequencies (Hz)									
Theoretical	108.47	172.97	179.56	201.83	224.5	265.06	302.59	318.85	339.71	340
Experimental	115.6	173.8	182	214	221.5	266	311	330	337	363
% Error	6.2	.48	1.3	5.7	−1.35	.35	2.7	3.3	−.8	6.3
	Frequency Reductions (Hz)									
2mm Saw Cut at A (33%)	0.1	−1.7	−2.6	2	4	1	5	4	8	0.3
Complete Cut at A	24.9	76	5.7	29.6	13.5	49.7	41.4	25.6	12.6	32.6

TABLE 8.4 MEASURED CHANGES IN FREQUENCIES OF ASYMMETRIC PLANE FRAME

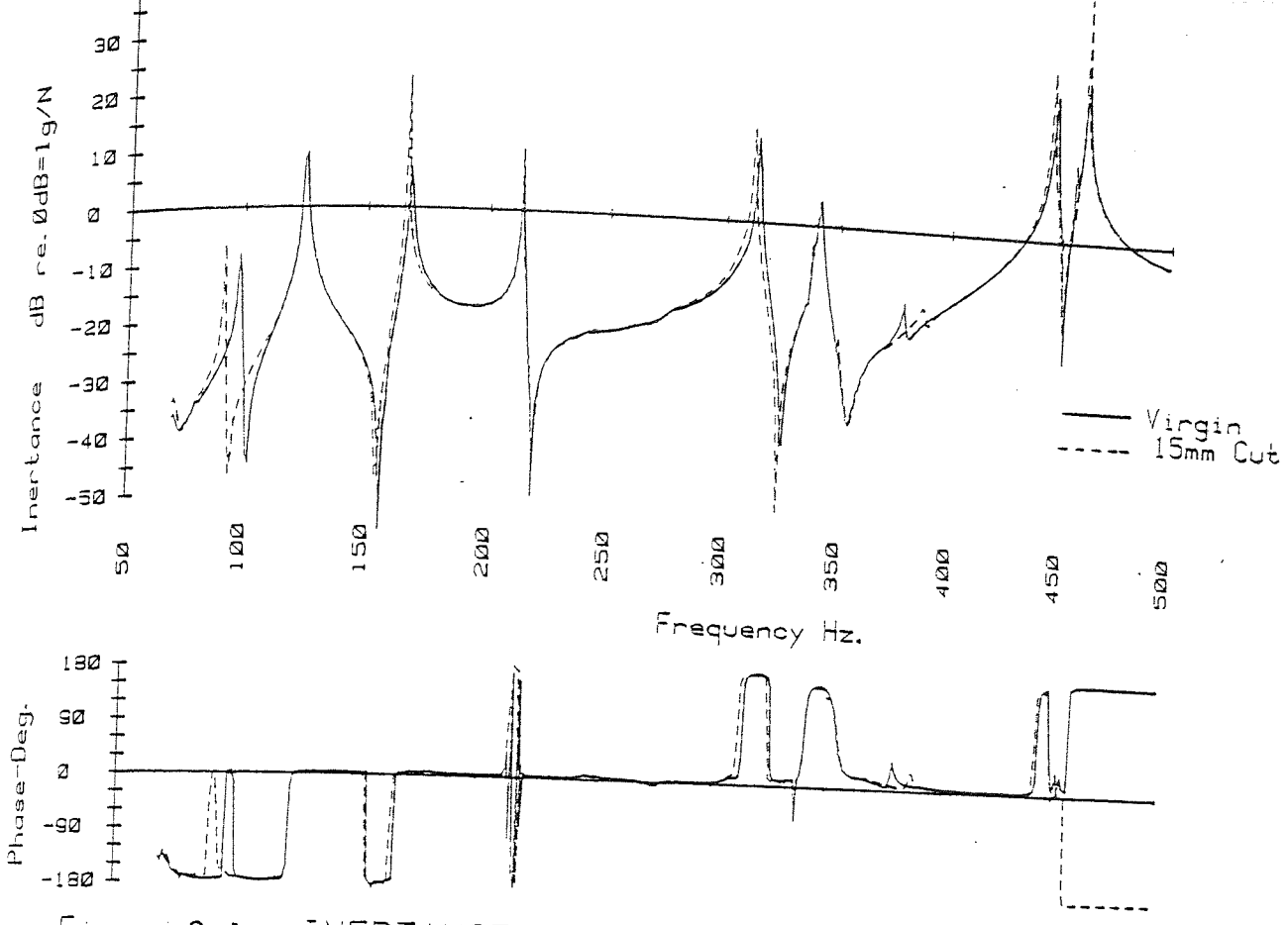

Fig. 8·1a INERTANCE OF VIRGIN AND 15mm CUT OF CROSS-BRACE PORTAL FRAME.

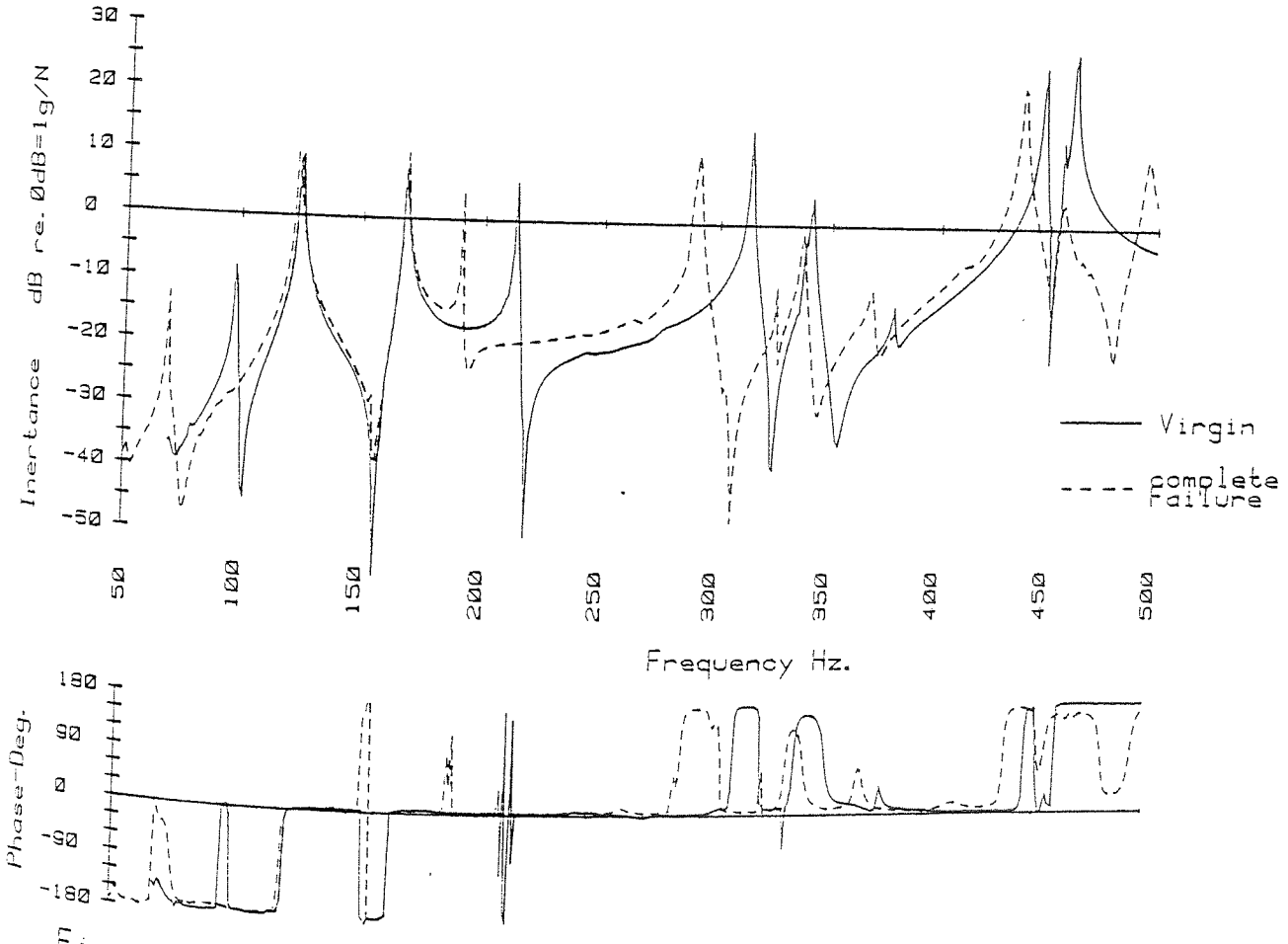

Fig. 8·1b INERTANCE OF VIRGIN AND COMPLETE FAILURE OF CROSS-BRACE PORTAL FRAME

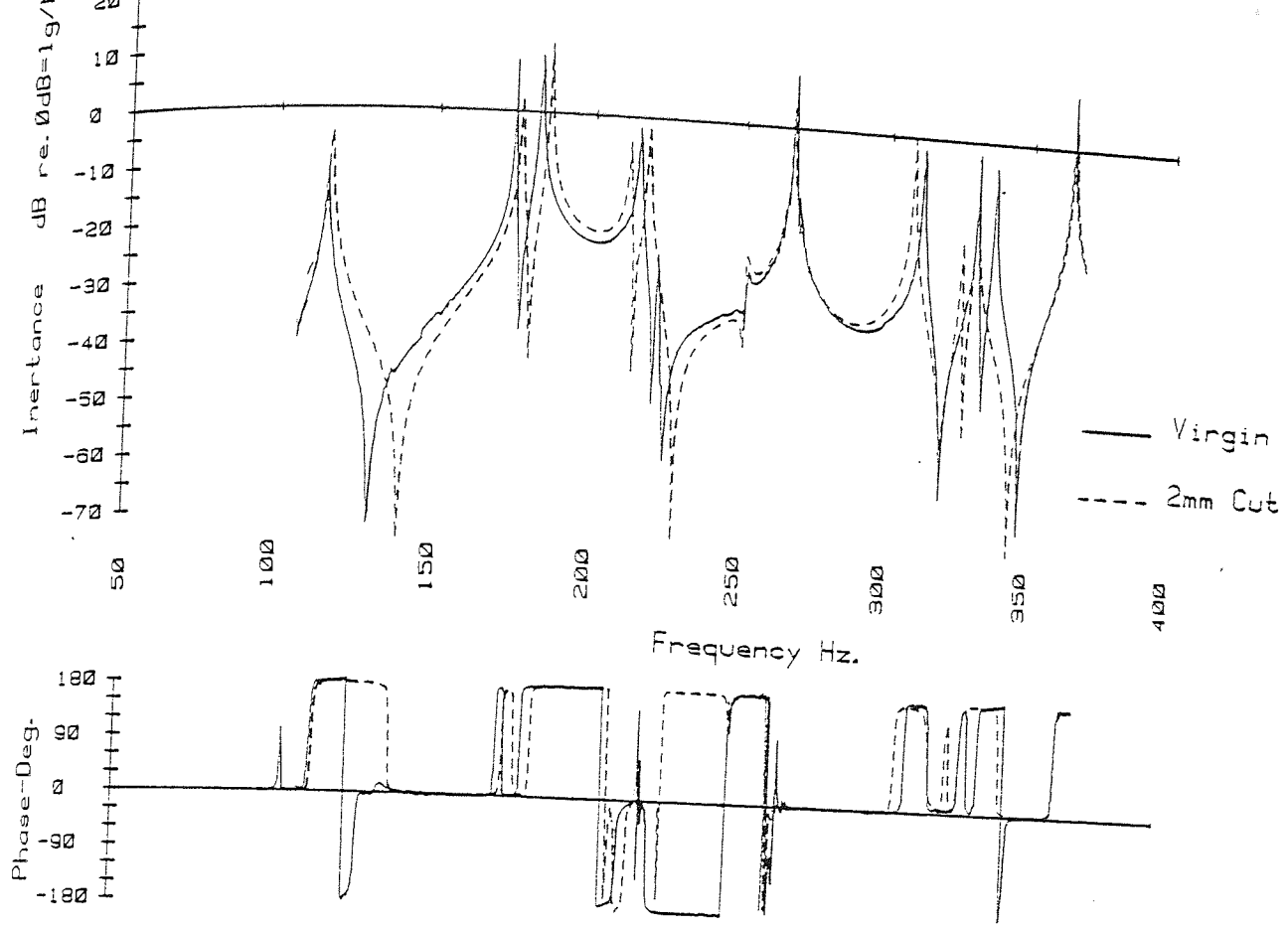

Fig. 8·2a INERTANCE OF VIRGIN AND 2mm CUT OF ASYMMETRIC CROSS PORTAL FRAME.

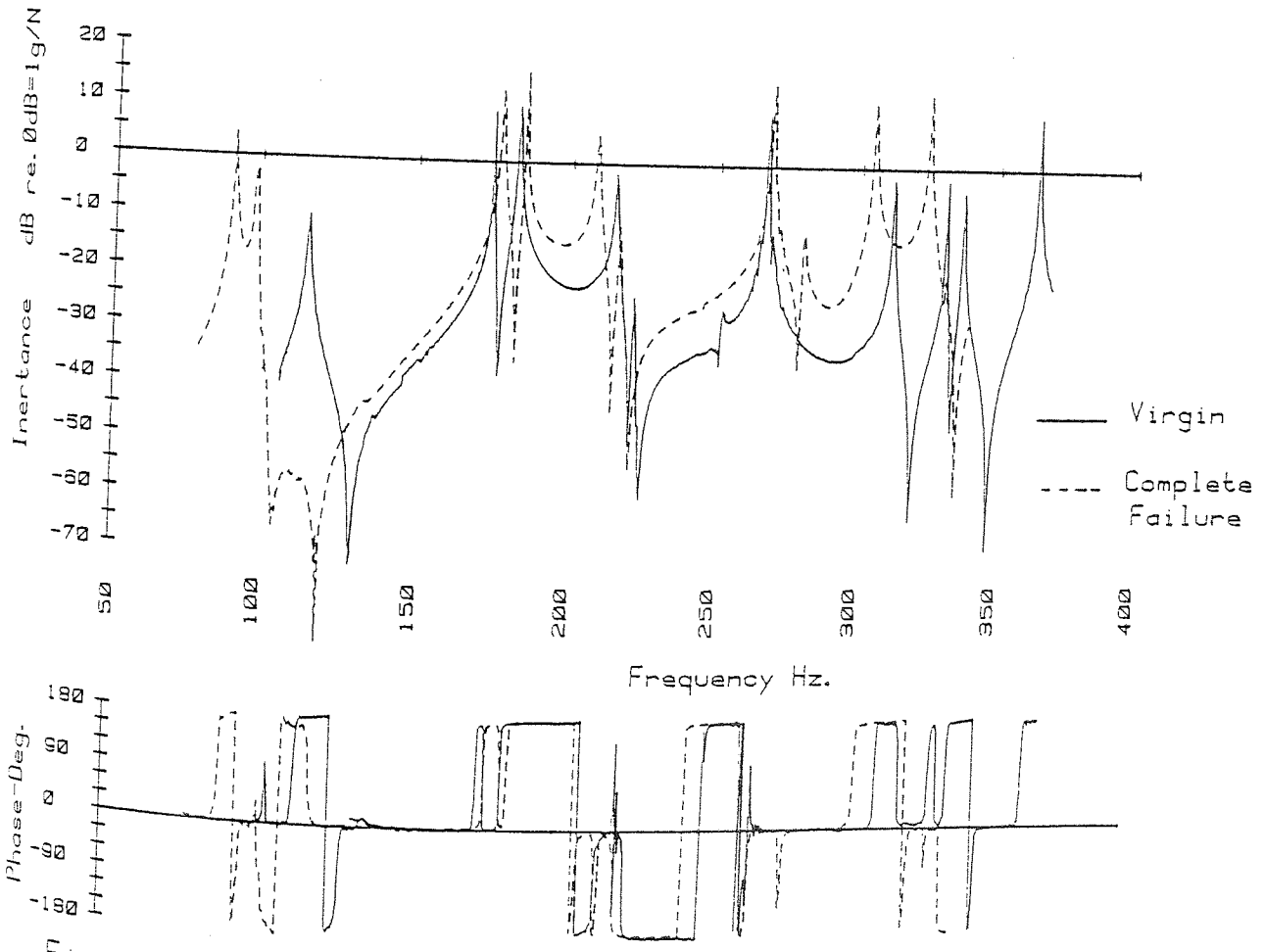

Fig. 8·2b INERTANCE OF VIRGIN AND COMPLETE FAILURE OF ASYMMETRIC CROSS PORTAL FRAME

8.2.4 Tests on Symmetric Tower Frame.

A series of tests was performed on the three identical symmetrical tower frames, each having the same dimensions (see Fig. 6.7) in order to study the differences between the experimental and theoretical frequencies which might arise from the following effects:

1- Boundary conditions.
2- Variations in dimensions due to manufacturing tolerances and distortion in the frame.
3- Local changes in the material properties.

The effect of these factors on the natural frequencies was studied separately on each frame in order to preserve the identity of each structure. Table 8.5 shows the comparison between the experimental and theoretical undamaged frequencies of the first tower frame together with the effect of increasing damage and of repair. It is revealed that for most modes the percentage errors are different for each case following a repair of damage at position C and D. These variations may be due to the effects 1, 2 and 3. Also, it can be seen that the experimental frequencies for the undamaged structure were affected each time the structure was welded.

The measured changes in frequencies due to partial and complete saw cuts at three different sites are also shown in Table 8.5. These frequency changes were produced by making

two saw cuts 5mm in depth on opposite sides of the member, at position D, and were found to be much smaller than those produced by complete failure at the same position. Thus, the structure is insensitive to the partial damage. Also, it can be seen that the second and third modes frequencies for the first complete cut were increased. The structure was then welded at cut D and the frequencies were again measured.

Damage was again caused in the form of saw cuts at another position (C) on the frame. An interesting observation in this case is that damage at position C had a significant effect on the frequencies of all modes. After welding cuts at positions D and C, the frequencies were re-measured. Finally, a third saw cut was made at position A, and the corresponding frequency reductions measured. These results are shown in Table 8.5.

Table 8.6 shows the measured changes in frequencies of the second symmetrical tower frame, of dimensions similar to the first structure. The percentage errors between the experimental and the theoretical undamaged frequencies was found to be much less than for the first tower frame. This was due to the improved boundary conditions and the deformation of the frame. Three complete saw cuts were made at the same position (E), 100mm from the free end of the structure. On two occasions the damage was repaired by welding after tests and the first ten natural frequencies were measured to find the reductions in frequencies. In each case following repair, the 'undamaged frequencies' of the

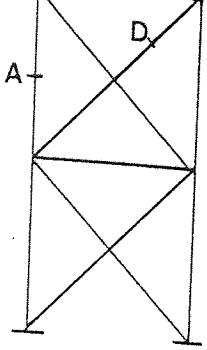

	1st Mode	2nd Mode	3rd Mode	4th Mode	5th Mode	6th Mode	7th Mode	8th Mode	9th Mode	10th Mode
	Undamaged Frequencies (Hz)									
Experimental	102	135	141	178	201	205	245	320	331	339
Theoretical	108.6	131.4	136.4	167.9	171.1	181.6	206.3	234.7	291.7	298.3
% Error	−6.5	2.7	3.3	5.7	14.8	11.4	15.8	26.6	11.8	12
	Frequency Reductions (Hz)									
5mm Saw Cut at D	0.4	0.1	0.1	0.4	0.5	0	1	0	1	0
Complete Cut at D	9	−4	−6	21	13	9	28	26	11	6
	Undamaged Frequencies (Hz)									
After Welding Cut D	92	136	150	164	189	210	244	294	304	311
% Error	−18	3.4	9.1	−2.4	9.5	13.5	15.5	20.2	4	4.1
	Frequency Reductions (Hz)									
Complete Cut at C	12.2	54.2	5.4	15.6	17	22	51.3	65.5	47	6
	Undamaged Frequencies (Hz)									
After Welding Cuts D & C	82.8	142.6	164	167	190.5	202	217	237.5	262.8	297
% Error	−31.2	7.9	16.8	−0.5	10.2	10.1	4.9	1.2	−11	−0.4
	Frequency Reductions (Hz)									
Complete Cut at A	2.8	40.6	34	10	9.5	18	21	28.5	40.8	40

TABLE 8.5 MEASURED CHANGES IN FREQUENCIES OF SYMMETRIC TOWER FRAME 1

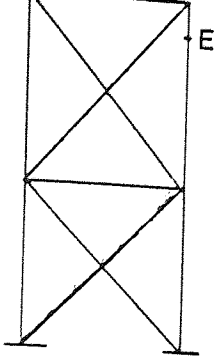

Mode Order	1st	2nd	3rd	4th	5th	6th	7th	8th	9th	10th
	Undamaged Frequencies (Hz)									
Experimental	108	136.6	150.2	169.3	195.6	208.4	236	263	290	300
Theoretical	108.6	131.4	136.4	167.9	171.1	181.6	206.3	234.7	291.7	298.3
% Error	−0.6	3.8	9.2	0.8	12.5	12.8	12.6	10.8	−0.6	0.6
	Frequency Reductions (Hz)									
1st Complete Cut at E	23	22.6	−1.5	7.7	21.6	1	19	23	41	11
	Undamaged Frequencies (Hz)									
After Welding Cut E	87.8	143	161	176.7	190	219	235.6	253	275	285
% Error	−23.7	8.1	15.3	4.9	9.9	17.1	12.4	18.3	−6	−4.7
	Frequency Reductions (Hz)									
2nd Complete Cut at E	26.8	57.4	47	24.7	18	42	22.6	29	31	37
	Undamaged Frequencies (Hz)									
After Rewelding Cut E	88	144.6	167	176	191.8	226	238	253	272	280.7
% Error	−23.4	9.1	18.3	4.6	10.8	19.6	13.3	7.2	−7.2	−6.2
	Frequency Reductions (Hz)									
6mm Saw Cut at E	0.1	0.6	1	0.15	−0.2	0.1	.02	1	.03	0.7
10mm Saw Cut at E	0.3	0.6	1	0.25	−0.2	0.2	2	1	0.2	0.7
15mm Saw Cut at E	0.4	2.6	1	0.4	3.8	0.3	2	3	6	8.7
3rd Complete Cut at E	27	58.6	53	24	20.5	48	24	25	30	32.7

TABLE 8.6 MEASURED CHANGES IN FREQUENCIES OF SYMMETRIC TOWER FRAME 2

structure were different to the values previously obtained. The frequencies of the first undamaged structure were found to be closer to the theoretical results than when the structure was welded and re-welded at cut E.

It is clear from Table 8.6 that the overall effect of damage results in a lowering of the frequencies. It was established that the partial damage of the members had an insignificant effect on the frequencies. Also, it can be seen that the third mode increased after the first saw cut, probably for the same reasons mentioned earlier in this chapter.

Table 8.7 shows the measured changes in frequency of the third symmetrical tower frame. This structure was slightly different in dimension and more accurately constructed than the first two structures. Also, the damage has been made using the spark erosion technique which is more representative of damage likely to be encountered in service. Cracks were eroded into the structure at position B, 120mm away from the left-hand free corner. The first crack was made to a depth of 1.5mm from the upper surface of the member, equivalent to an area reduction of 50%, and the first ten natural frequencies were measured. The member was then cut completely at this position and the measurements repeated. It was noted that the frequency reductions produced by the first crack were much smaller than those produced by total failure of the member, in spite of the fact that the damage was at a similar thickness and was at the same site. Therefore, it should be possible to use this damage as an indication of the

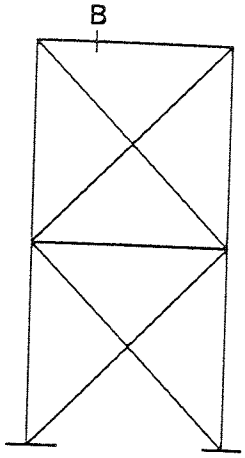

Mode Order	1	2	3	4	5	6	7	8	9	10
	Undamaged Frequencies (Hz)									
Experimental	111.4	137	140	161	187	191	214	252	323	333
Theoretical	107.8	130.1	132.7	156.7	166.3	171.4	203.3	229.3	293.6	300.2
% Error	3.2	5	5.2	2.7	11.1	10.3	5	9	9.1	9.8
	Frequency Reductions (Hz)									
1.5mm Crack Depth at B	1.2	0.4	1.8	3.6	2.4	1	−1	−1	24	28
Complete Crack at B	54.6	25.8	2.4	7.8	16.2	1	20.8	36.4	82.2	26

TABLE 8.7 MEASURED CHANGES IN FREQUENCIES OF SYMMETRIC TOWER FRAME 3

severity of damage.

8.2.5 Tests on Asymmetric Tower Frame.

The last plane frame structure to be tested is more complicated than those previously mentioned. A description of this structure is given in section 6.5. Damage was caused in the form of a series of saw cuts, (see Fig. 6.8), the first saw cut being 10mm in depth, (50% reduction of the cross sectional area) from one side of the member at position A and frequencies measured. The cut was then extended to sever the member and frequencies re-measured. After welding cut A, the frequencies of the repaired structure were measured. Damage was next caused at position B in the form of saw cuts to various depths. The first saw cut from one side of the member was 10mm in depth removing 50% of the cross section; the second cut was 15mm deep equivalent to a reduction of 75% in the cross section area. Finally, the member was completely severed. On each occasion the reductions in frequency were measured. These measurements are tabulated in Table 8.8, where it can be seen that the reductions in frequency are indicative of the extent of damage. Before welding cut B, another complete saw cut was made at position C in order to measure changes in the natural frequencies of the structure, not only with respect to the undamaged condition but also with respect to a state where more than one point in the structure is damaged.

Referring to Table 8.8, the frequency changes recorded were between the single failure at B and the double failure at B+C in case I and between the virgin structure and double failure case II. Table 8.8 indicates that the maximum percentage of error between both the experimental and theoretical undamaged frequencies for the first ten modes was 6.4%, which is an acceptable figure in engineering design practise.

8.2.6 Tests on Symmetric Space Frame about Both Diagonals.

Tests were also carried out on three dimensional structures in order to study the effect of the extent of damage and damage locations on the natural frequencies. The space frame symmetrical about both diagonals, described in chapter six, was damaged by the series of saw cuts, as shown in Fig. 6.9. The first cut was made in a Z-direction at position A (quarter of the way from the end of the diagonal) to a depth of 3mm into opposite faces of the diagonal member, equivalent to a reduction of 60% in cross section area. It was observed that this damage produced no significant change on the natural frequencies of the structure for any mode. Results of this test have not been included. The diagonal member was then severed completely at the same position (A) and the frequency reductions are shown in Table 8.9. Referring to this table, the maximum percentage of error between the experimental and theoretical frequencies of the undamaged structure was of the order of 5.6%. Also, it was noted that the reductions in the first, second and third modes were 66%,

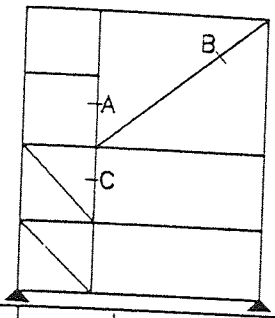

Mode Order	1	2	3	4	5	6	7	8	9	10
	Undamaged Frequencies (Hz)									
Experimental	23	58	76	88	129	134	142	149	166	199
Theoretical	22.4	54.4	72	82.4	125	130	139.2	148	156.1	197
% Error	2.6	6.2	5.3	6.4	3.1	2.9	2	0.7	5.9	1
	Frequency Reductions (Hz)									
10mm Saw Cut at A (50%)	1	0.4	0.2	0.3	10	4	8	7	17	33
Complete Cut at A	6	18	15	15	48	10	9	13	26	34
	Undamaged Frequencies (Hz)									
After Welding Cut A	22.7	58	76	88	128	132	140	150	166.8	199
% Error	1.3	6.2	5.3	6.4	2.3	1.5	0.6	1.3	6.4	1
	Frequency Reductions (Hz)									
10mm Saw Cut at B (50%)	−1	0.4	0.2	0.3	–	0.1	0.4	0.2	0.8	1
15mm Saw Cut at B (75%)	1	2	0.5	0.6	–	0.2	0.6	0.3	2.8	8
Complete Cut at B	12.6	31.4	34.2	42	47	38	11	16.2	24.3	49
CASE I : Frequency After Cut at B Taken as Undamaged Value CASE II: Virgin Frequency Taken as Undamaged Value										
CASE I, Compl. Cut at B & C	0.6	1.8	14.6	0.4	20.2	13.3	34.6	5.2	5.9	10
CASE II, Compl. Cut at B & C	13.2	33.2	48.8	42.4	67.2	51.3	45.6	21.4	30.2	59

TABLE 8.8 MEASURED CHANGES IN FREQUENCIES OF ASYMMETRIC TOWER FRAME

65% and 62% respectively, while higher modes showed frequency reductions of less than 10%.

Comparisons were also made between the experimental and theoretical frequencies for complete failure at A and the maximum percentage error was found to be 4.5%. Figure 8.3a shows the inertance plots for this structure before and after failure at A.

The structure was then repaired by welding and the frequencies were then measured. These results are compared with the theoretical frequencies in Table 8.9 and the maximum error between them is seen to be 5.9%.

Damage was then caused at position B (quarter of the way from the fixed end) by completely severs the member. The reduction in the frequencies of the first ten modes was measured and that of the first mode was found to be 67%, a value significantly greater than found for higher modes, as shown in Table 8.9. Figure 8.3b shows this reduction in the frequencies by plotting the inertance before and after failure at B.

The effect of the welding material on the natural frequencies of this structure was also investigated. The cut at position B was repaired using ´Araldite´ and the natural frequencies were again measured. These frequencies were then compared with the undamaged frequencies of the structure before the cut was made at B and it was noted that there was no

significant change in the natural frequencies for all modes.

8.2.7 Tests on Space Frame Symmetric About One Diagonal.

The second space frame to be tested was a model symmetrical about one diagonal, as already described in chapter six (see Fig. 6.10). Initially, the frequencies of the undamaged structure were measured: comparisons were then made between the experimental and theoretical frequencies. The greatest error in frequency was found in the tenth mode as 10.9% (see Table 8.10). The table also shows the frequency reductions produced by cutting the lower diagonal through 60% and 70% of the cross sectional area, and by severing it at position A, the mid point of the diagonal member.

Two conclusions may be drawn. In the first instance, with partial damage, the frequency spectrum of the structure was comparatively unaffected by the damage: the maximum percentage of the frequency reduction was only 7% in the tenth mode for the 70% cut and was much smaller in the other modes. The reduction in the frequencies increased as the extent of damage increased, thereby giving an indication of the severity of the damage. Also, Figs. 8.4a-c illustrate the change in the inertance plot due to 60%, 70% and complete failure at position A.

Mode Order	1	2	3	4	5	6	7	8	9	10
	Undamaged Frequencies (Hz)									
Experimental	98	102.5	105.9	112.4	114	117.2	118.5	121	130	133.8
Theoretical	97.2	100.3	102.9	113.1	114	116.8	117.9	118.8	122.7	128.9
% Error	0.8	2.1	2.8	−0.6	0	0.3	0.5	1.8	5.6	3.7
	Frequency Reductions (Hz)									
Complete Cut at A	65	67.1	66	13	7.1	3.6	2.6	3.3	11.3	11.3
	Undamaged Frequencies (Hz)									
After Welding Cut A	98.4	102.4	106.4	113.6	115.6	118	119.2	121.2	130.4	134
% Error	1.2	2.4	3.3	0.4	1.4	1	1.1	2	5.9	3.8
	Frequency Reductions (Hz)									
Complete Cut at B	66	36.4	39.2	15.6	11.8	8.6	5.6	5.2	11.4	14

TABLE 8.9 MEASURED CHANGES IN FREQUENCIES OF SYMMETRIC SPACE FRAME MODEL—WITH BOTH DIAGONALS

Mode Order	1	2	3	4	5	6	7	8	9	10
	Undamaged Frequencies (Hz)									
Experimental	95.4	98	107	112	115.2	119.2	121.3	125.2	126.4	138
Theoretical	93.2	99.1	99.14	101	109.3	112.5	117	117.5	119.4	122.8
% Error	2.4	−1.1	7.3	9.8	5.1	5.6	3.5	6.2	5.6	10.9
	Frequency Reductions (Hz)									
60% Cut at A	0.1	0	0.4	0.2	0.8	2	0.9	0.3	0.1	3.9
70% Cut at A	0.2	0.3	1.6	2.4	4	4.1	1.8	·3	0.5	9.8
Complete Cut at A	22	22.5	27.1	14	13.2	16.2	10.6	14.6	11.4	22.8

TABLE 8.10 MEASURED CHANGES IN FREQUENCIES OF SYMMETRIC SPACE FRAME MODEL—WITH ONE DIAGONAL

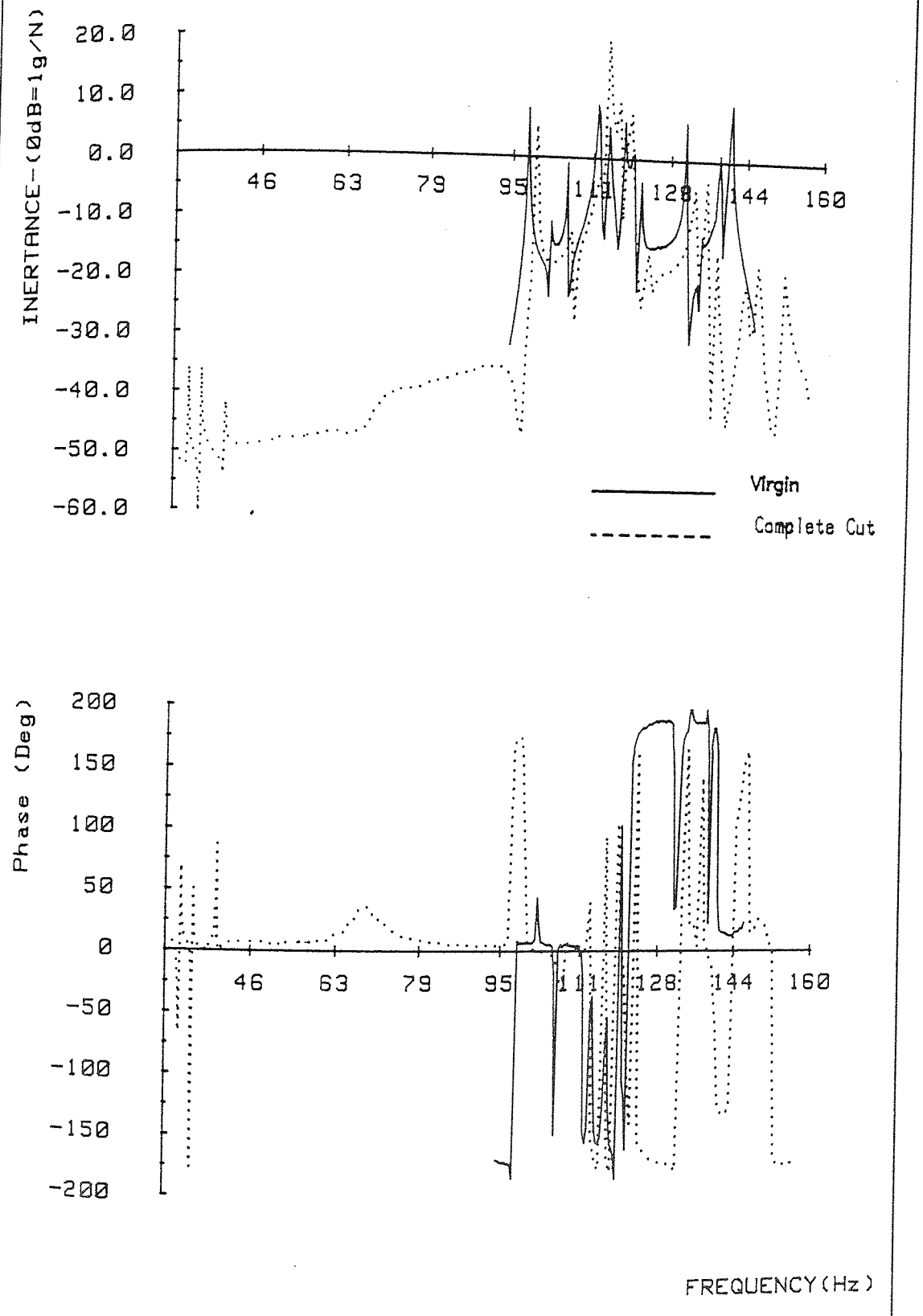

Fig.8.3a INERTANCE PLOT FOR VIRGIN AND COMPLETE CUT AT A OF THE SYMMETRIC SPACE FRAME

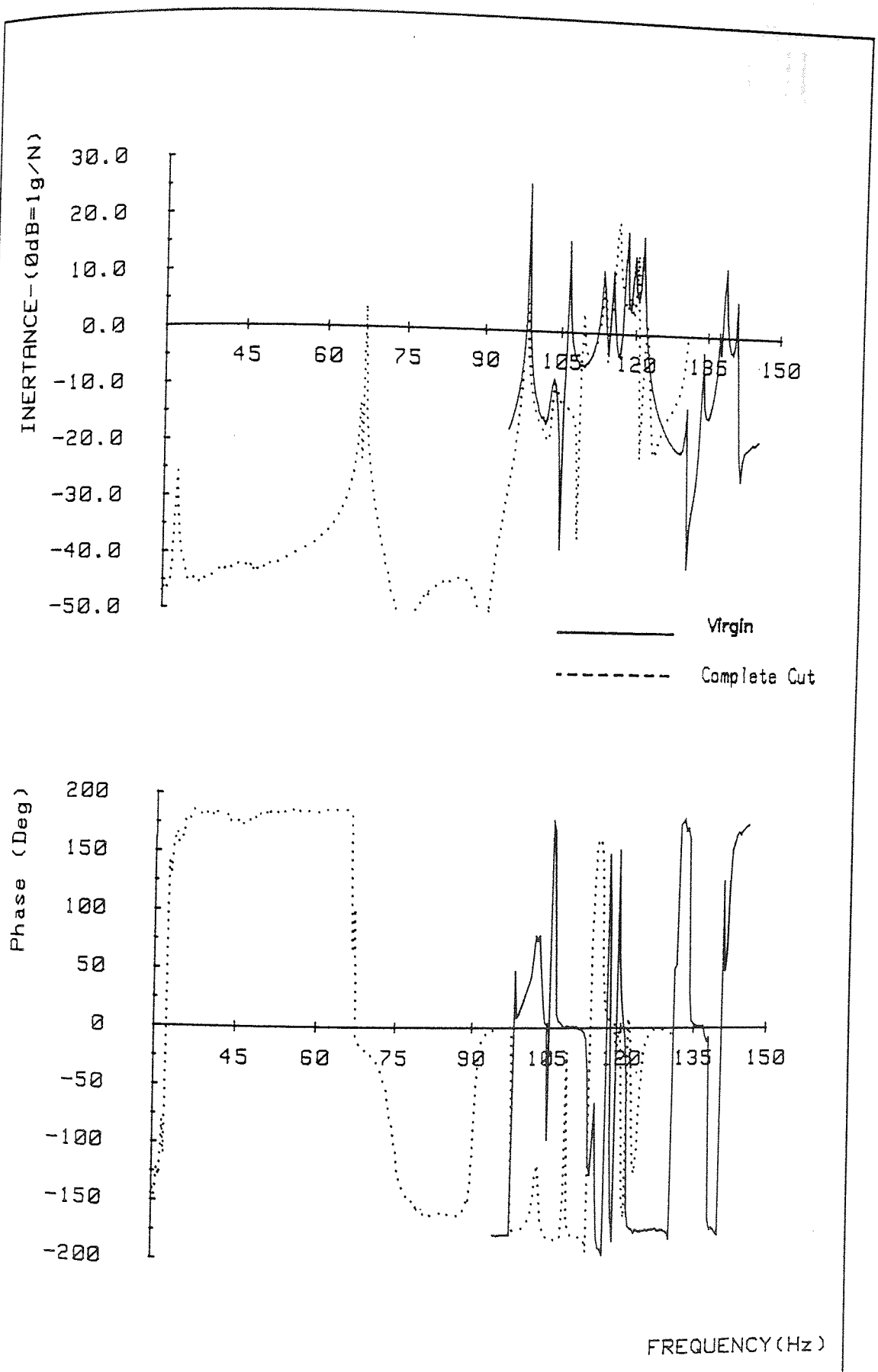

Fig. 8.3b INERTANCE PLOT FOR VIRGIN AND COMPLETE CUT AT B OF THE SYMMETRIC SPACE FRAME

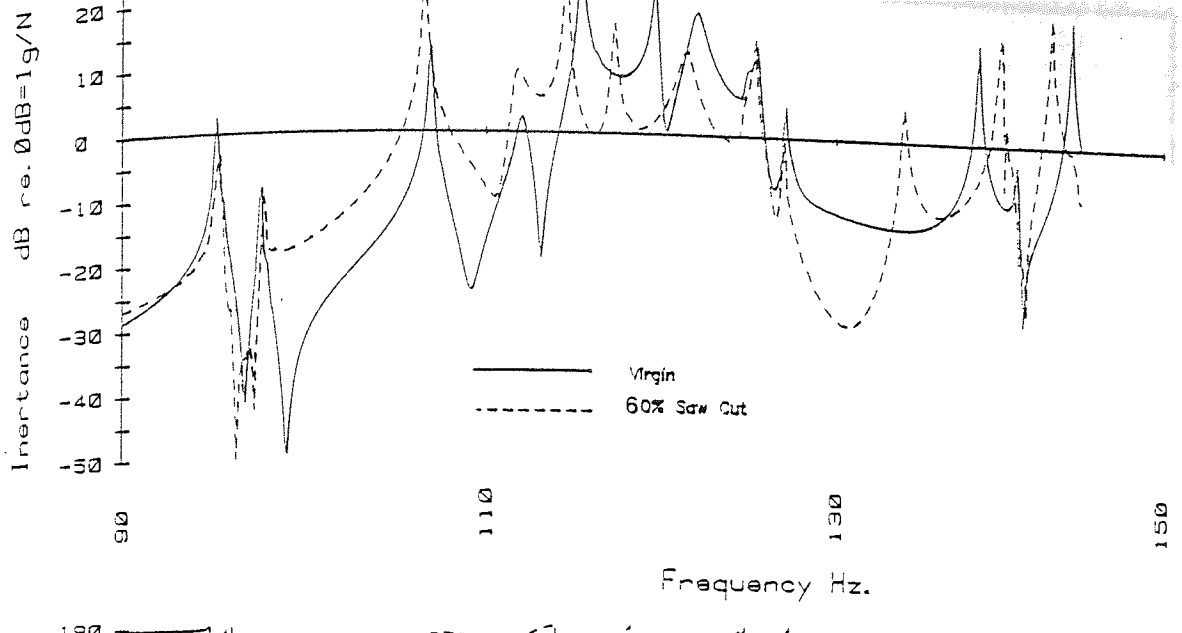

Fig. 8.4a INERTANCE PLOT FOR VIRGIN AND 60% SAW CUT AT A OF SYMMETRIC SPACE FRAME-WITH ONE DIAGONAL

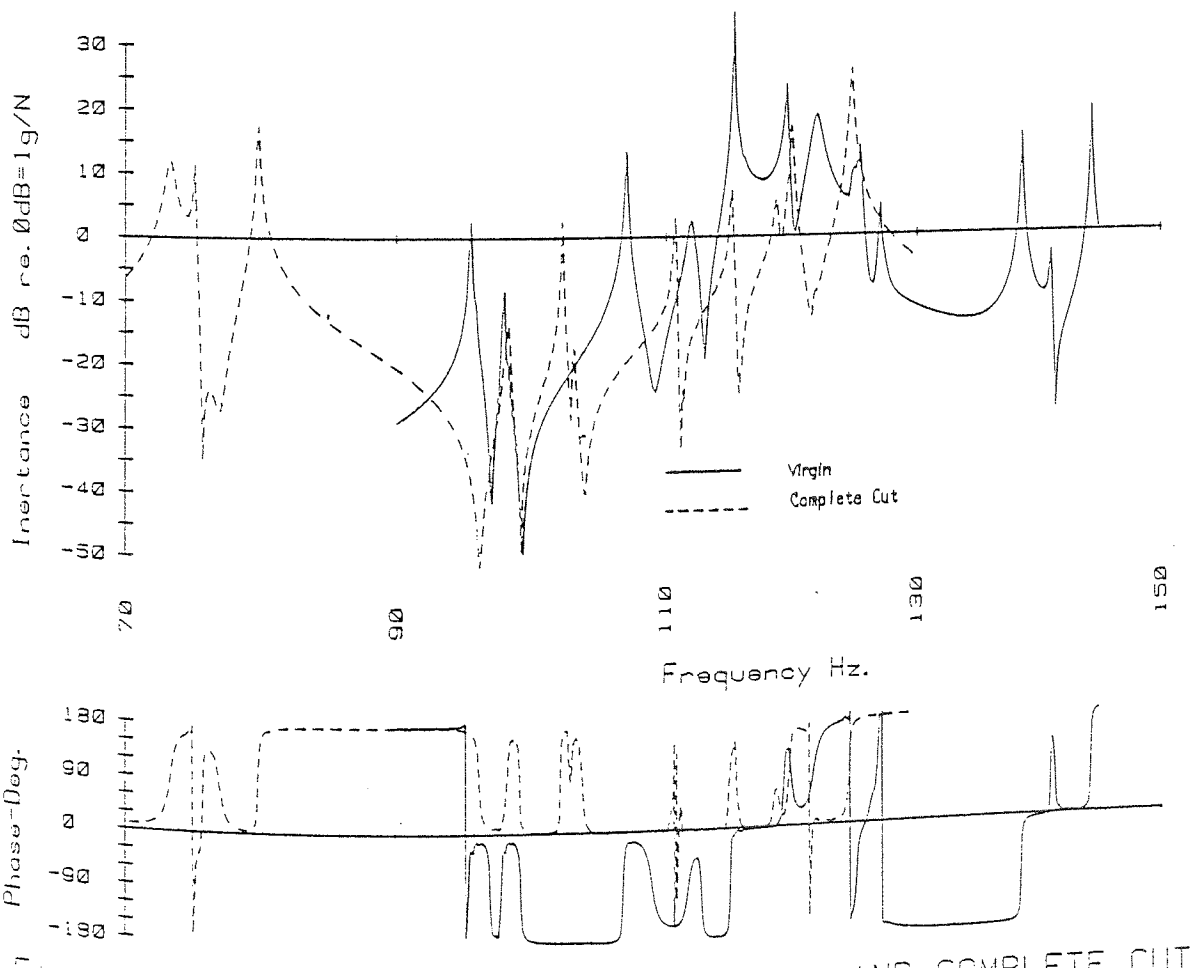

Fig. 8.4b INERTANCE PLOT FOR VIRGIN AND COMPLETE CUT AT A OF THE SYMMETRIC SPACE FRAME-WITH ONE DIAGONAL.

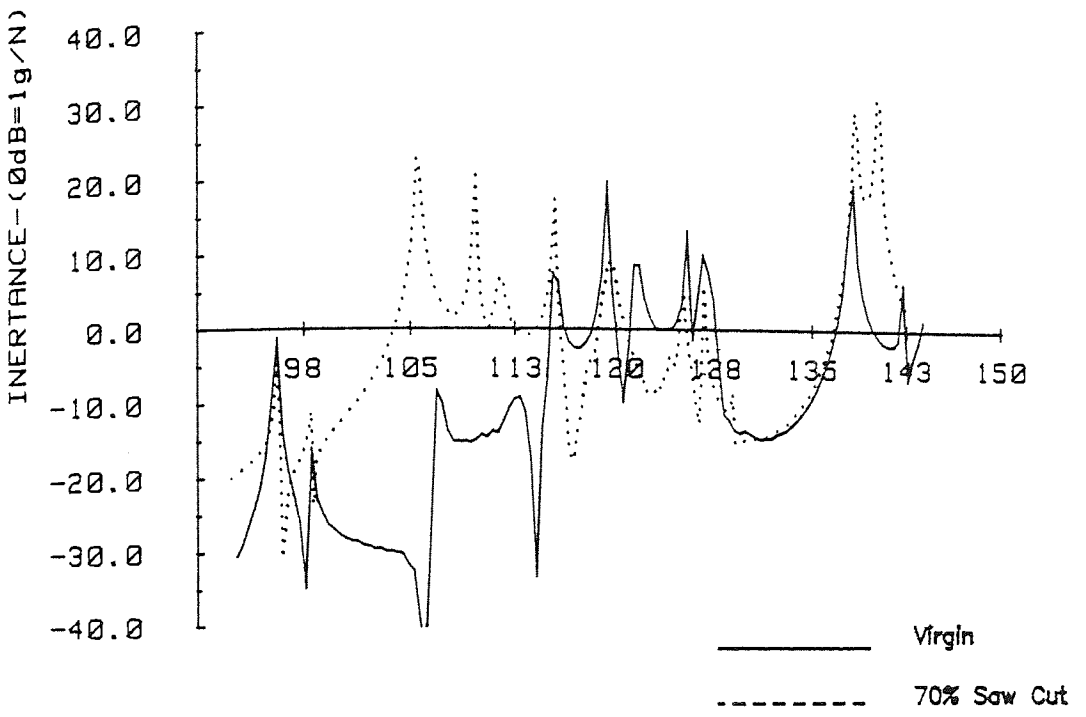

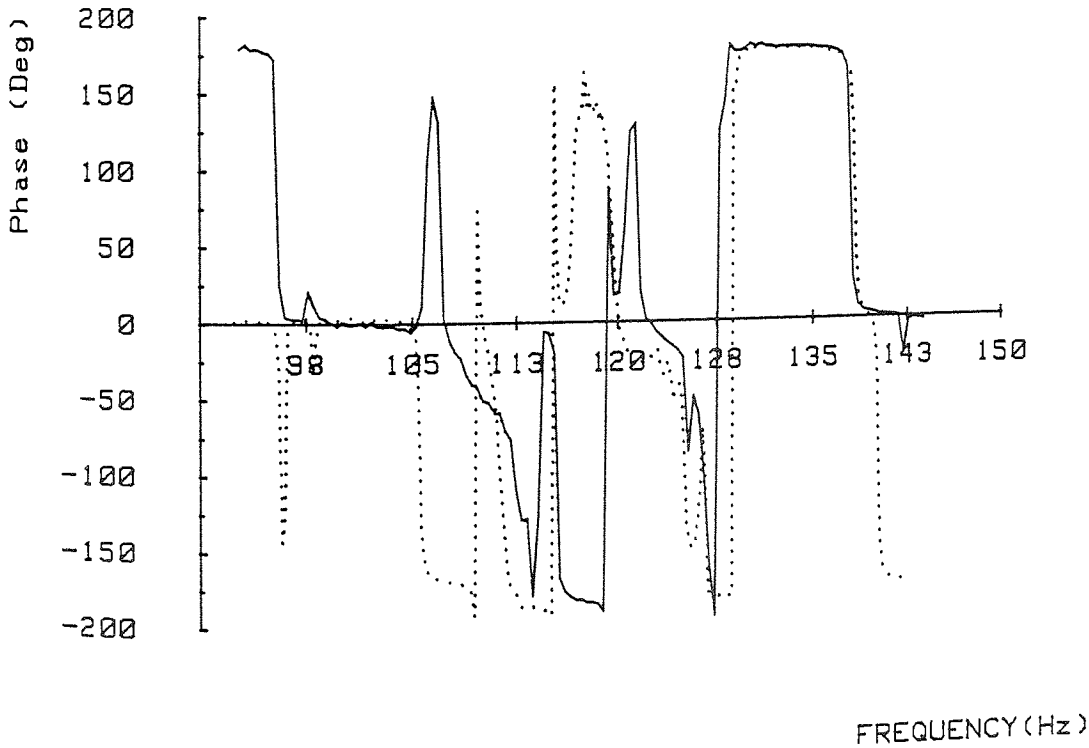

Fig.8.4 c INERTANCE PLOT FOR VIRGIN AND 70% SAW CUT AT A OF THE SYMMETRIC SPACE FRAME

8.2.8 Tests on Asymmetric Space Frame.

The third space frame to be tested was an asymmetrical model already described in chapter six (see Fig. 6.11). Table 8.11 shows the frequency reductions obtained when 70%, 90% and complete failure was produced at A (the mid point of the horizontal member). The percentage of error between the experimental and theoretical undamaged frequencies is shown, the maximum error being of the order of 6.3% for the fourth mode. It was found that the reduction in the frequencies increased as the damage size increased.

A further test was carried out after repairing the damage at A and the frequencies of the repaired structure were then measured. Damage was next caused at position B in the form of cracks, produced by a vibrator as described in section 6.12. This crack was located in one of the lower diagonals extended through approximately 40% of the cross sectional area. It can be seen from Table 8.11, that this structure is remarkably insensitive to a 40% crack at this position. The frequency reductions produced by complete failure at this position were also measured and are shown in Table 8.11.

Mode Order	1	2	3	4	5	6	7	8	9	10
	Undamaged Frequencies (Hz)									
Experimental	98.8	102	104.7	110.3	116.4	118	119.3	123.6	125.7	127
Theoretical	94.2	96.9	100.6	103.3	110.9	115.4	118	120.6	123.7	126.9
% Error	4.7	5	3.9	6.3	4.7	2.2	1.1	2.4	1.6	.08
	Frequency Reductions (Hz)									
70% Cut at A	0.4	0.2	1.1	1.2	2	0.4	0.2	0.4	1	−0.3
90% Cut at A	2.4	3.6	4.7	3.9	4.1	2.2	0.6	1.2	1.9	0.7
Complete Cut at A	20.4	7.7	7.3	9.5	10.8	10	5.3	5.6	4.5	3
	Undamaged Frequencies (Hz)									
After Welding Cut at A	95.6	100.4	104	111.2	115.6	117.2	120.2	128.4	131.6	134.8
% Error	1.5	3.4	3.3	7.1	4.1	1.5	1.8	6.1	6	5.9
	Frequency Reductions (Hz)									
40% Crack at B	0.8	1.2	0.1	0.6	0.23	0.6	0.7	0.3	0.01	12.8
Complete Crack at B	24	26	21	14	22.2	19.6	19	20.2	16	15.2

TABLE 8.11 MEASURED CHANGES IN FREQUENCIES OF AN ASYMMETRICAL SPACE FRAME

8.3 SUMMARY OF THE RESULTS

Good agreement has been shown between the experimental and theoretical frequencies with an average predictive error of the order of 10%. Errors are attributable to one or more of the following possibilities:

1- Non-ideal boundary conditions e.g. in the cantilever beam, the boundary conditions were by no means perfect, (between the fixed and hinged ends).

2- Flexibilities introduced by fabrication of the joints: the geometrical relation between the various elements at a joint was theoretically considered to be rigid.

3- Thermal stress and local annealing effects due to welding the structure: there was a small degree of distortion in the frame due to the heat from the welds and, certainly, local changes in the material properties e.g. the elastic modulus, would effect its flexibility and hence the frames frequencies.

4- Differences in material properties between the weld and the structure: it was assumed that the elastic modulus of the welding material was equal to the modulus of the structure.

5- Possible mechanical contact of both the vibrator and accelerometer with the tested model.

6- Neglect of rotary inertia and shear deformation of the element in the analysis.

7- Slight differences in dimensions of both the theoretical and actual model may occur.

8- Slight discrepancies in the representation of damage in both the theoretical and the experimental models.

Despite these possibilities, agreement between the measured and calculated frequencies is shown to be within normally accepted engineering tolerances.

8.4 COMPARISON BETWEEN THE THEORETICAL AND EXPERIMENTAL DAMAGE MODEL.

The aim of this section is to examine the accuracy of the theoretical damage model by testing the equivalent stiffness constants obtained in section 6.9, by comparing the natural frequencies both experimentally and theoretically, static deflection and modal shapes for the undamaged and damaged structure. The damage is represented theoretically by a spring stiffness and experimentally by local and symmetrical reduction in the cross sectional area of the member.

The first seven natural frequencies (both experimental and theoretical) of the portal frame in Fig. 8.5 with damage equivalent to 40% of the cross sectional area at position B,

are shown in Table 8.12. It can be seen that the percentage errors were found to be within 4.7%.

Mode order	1	2	3	4	5	6	7
Theoretical	24.8	95.1	160.1	171.4	344.8	428.1	493.3
Experimental	24	96	156	168	336	408	480
% Error	3.2	-.9	2.6	1.9	2.6	4.7	2.7

Table 8.12 Theoretical and Experimental Frequencies of Partial Damage of Portal Frame Model

Also, experimental static deflection tests were carried out on the portal frame with loads applied at points A and B respectively. Deflection was then measured at many points on the portal frame. Then, a comparison was made between the experimental static deflection and the theoretical modal shapes of the undamaged structure. It can be concluded that the modal shapes for first and second natural frequencies took the form of the static deflection configuration when the load was applied at A and B respectively. From these findings a similar comparison was made for the portal frame with a damage of 20% and 40% as shown in Figs. 8.5 and 8.6 respectively to determine the accuracy of the spring model.

Furthermore, theoretical static deflection shapes were computed for the frame being acted upon by a horizontal force at its corner and also by a central vertical force. It was found that the theoretical deflections for these mentioned

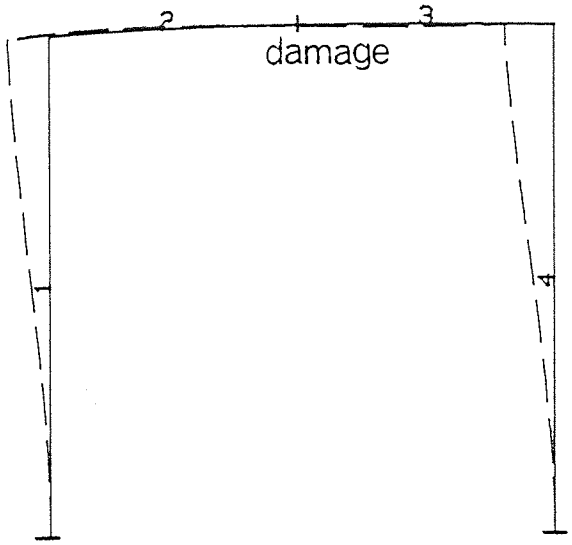

Theo. Mode Shape No. 1

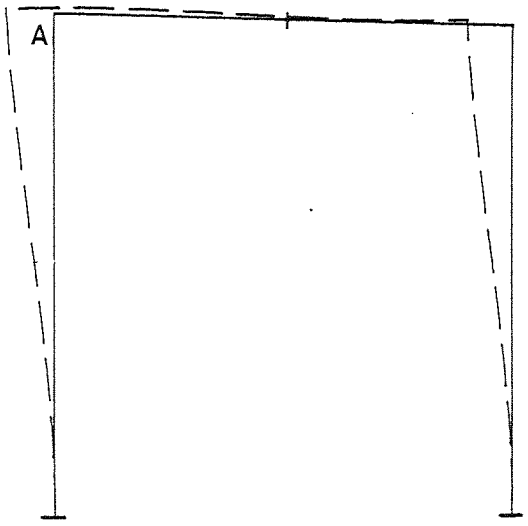

Exp. Static Deflection
Load at A

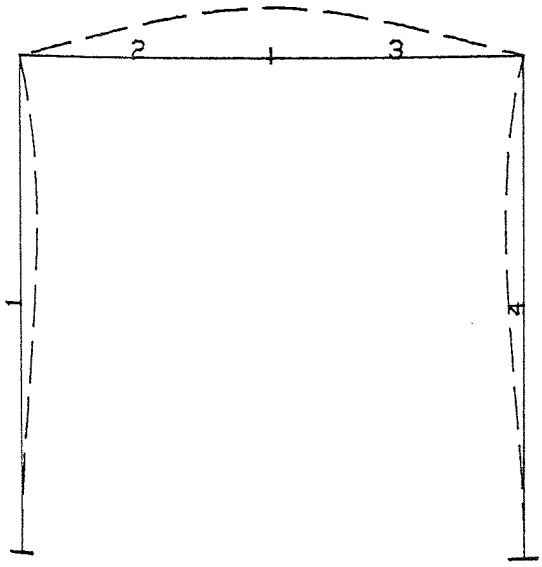

Theo. Mode Shape No. 2

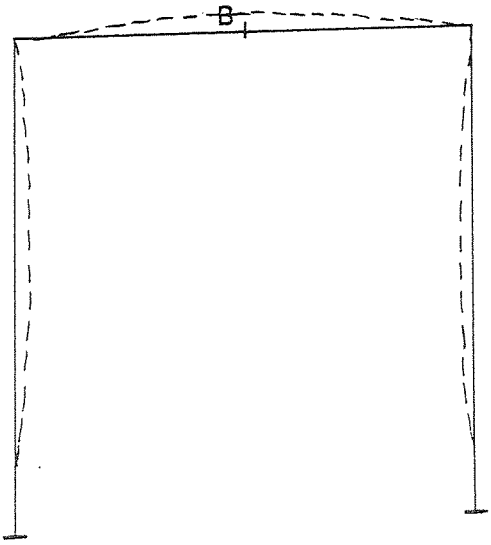

Exp. Static Deflection
Load at B

Fig. 8.5 COMPARISON BETWEEN DYNAMIC & STATIC DEFLECTION SHAPES FOR 20% DAMAGE MODEL

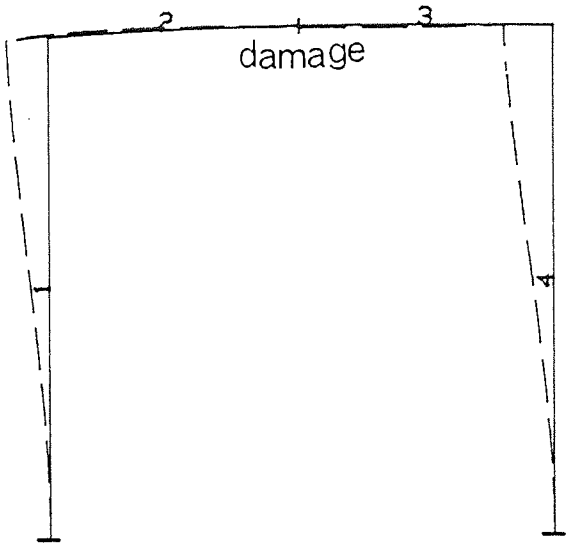

Theo. Mode Shape No. 1

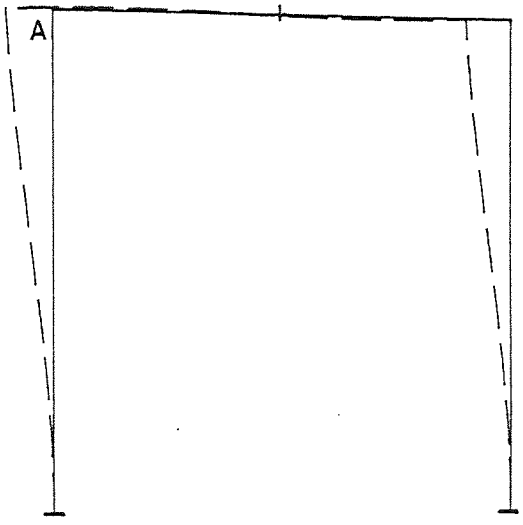

EXP. Static Deflection
Load at A

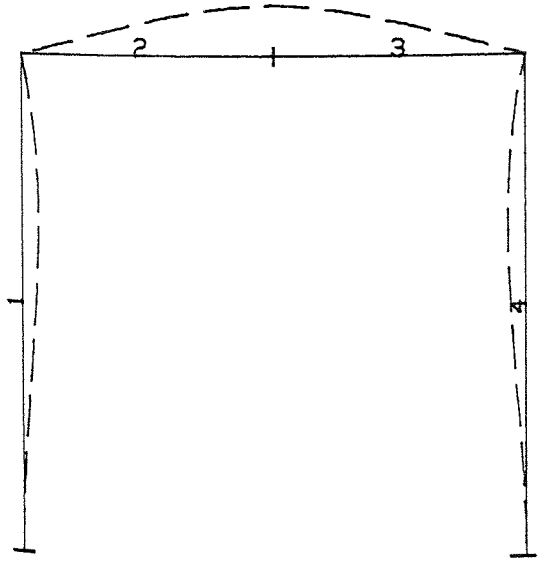

Theo. Mode Shape No. 2

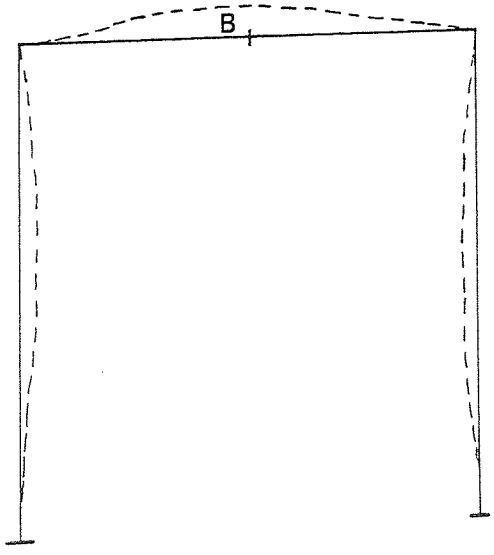

EXP. Static Deflection
Load at B

Fig. 8.6 COMPARISON BETWEEN DYNAMIC & STATIC DEFLECTION SHAPES FOR 40% DAMAGE MODEL

cases were similar to the experimental static deflections. These results are not shown.

To conclude, reasonable agreement was obtained between the computed and experimental vibration characteristics of the damaged model frame. Thus, this damage model proved to be reliable for use.

8.5 THEORETICAL AND EXPERIMENTAL MODAL SHAPES.

In the preceding study, the effect of the damage on the natural frequencies of the structure was investigated both theoretically and experimentally. This section is devoted to the study of the changes in the modal shapes due to the structural damage. Also, comparisons were made between the experimental and theoretical mode shapes.

8.5.1 Theoretical Modal Shapes.

I- The Symmetric Cross-Brace Portal Frame.

A comparison between the theoretical modal shapes of partially damaged structures and those of the undamaged structure is shown in Fig. 8.7, for damage located at the middle of the top member and equivalent to a 50% reduction in the stiffness and simulated by a spring model. It is seen that the first and second modal shapes are not significantly

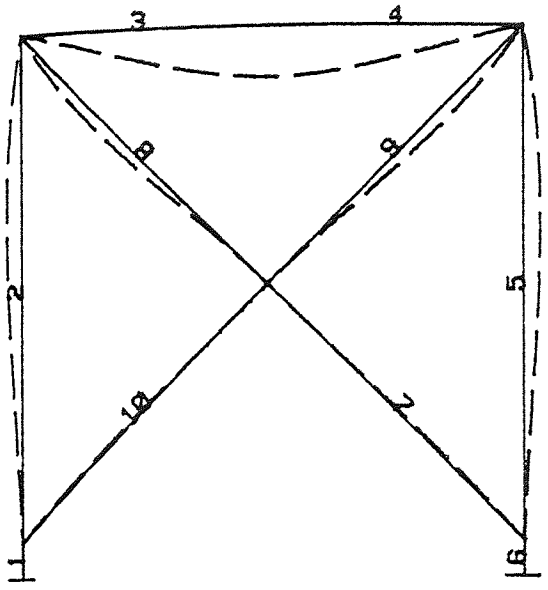

a– 1st Undamaged Modal Shape

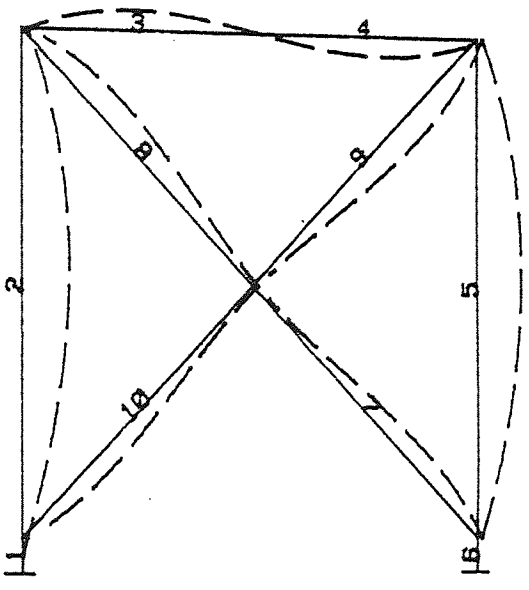

b– 2nd Undamaged Modal Shape

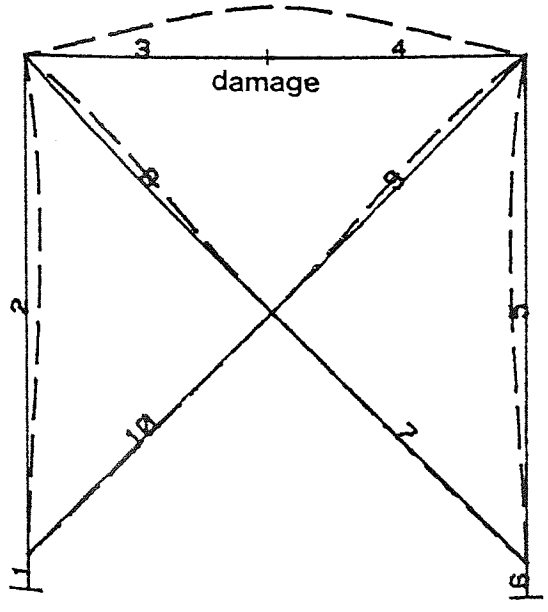

c– 1st Damaged Modal Shape

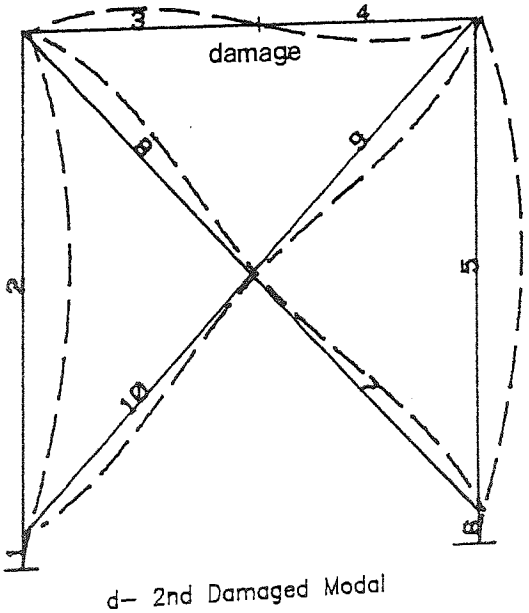

d– 2nd Damaged Modal Shape

Fig. 8.7 THEORETICAL MODAL SHAPES OF THE CROSS PORTAL FRAME

affected by partial damage.

II- The Asymmetric Cross-Brace Portal Frame.

A further comparison of the theoretical modal shapes between the partially damaged and undamaged structure is shown in Fig. 8.8. In this case damage to member 3 was simulated by a reduction in rigidity equivalent to 50%. It is seen that the first and second modal shapes were not significantly altered by partial damage, thus justifying the assumptions made in the sensitivity analysis described in section 4.4.

III- The Asymmetric Tower Frame.

Figure 8.9 shows the first four theoretical modal shapes of the structure with complete failure at a position between elements 17 and 18. It can be seen that the deflection at the point of failure has a greater value than at any of the other members as would be expected.

8.5.2 Comparison Between the Theoretical and Experimental Modal Shapes.

I- The symmetric Tower Frame.

Figs. 8.10 and 8.11 show a comparison between the theoretical and experimental modal shapes of the first four modes. In all four cases, the theoretical and experimental shapes are

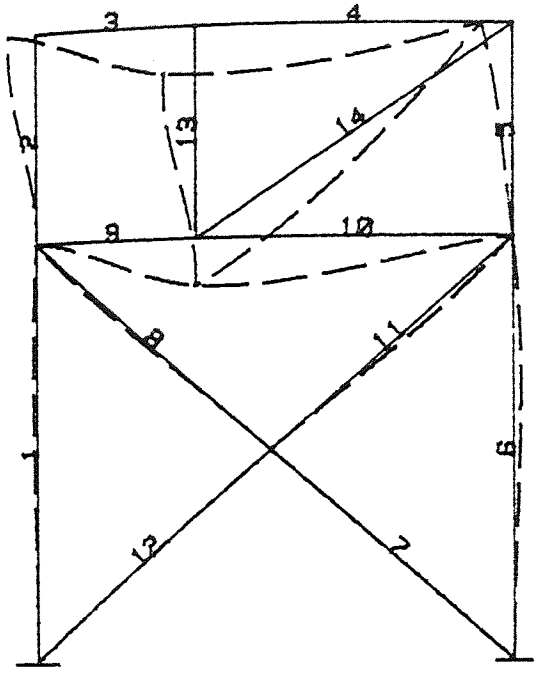

a– 1st Undamaged Modal Shape

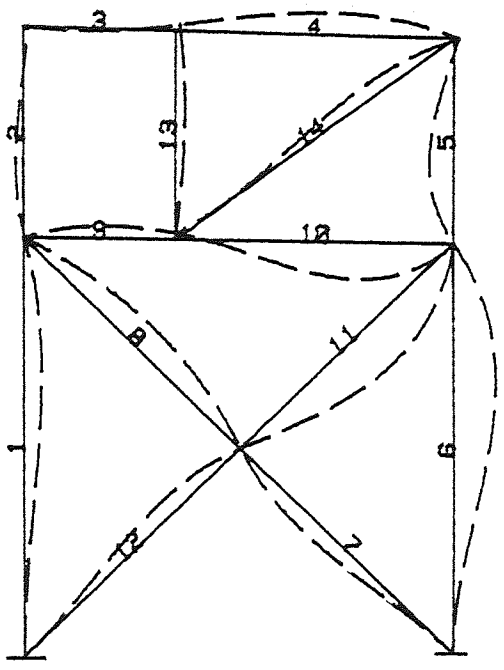

b– 2nd Undamaged Modal Shape

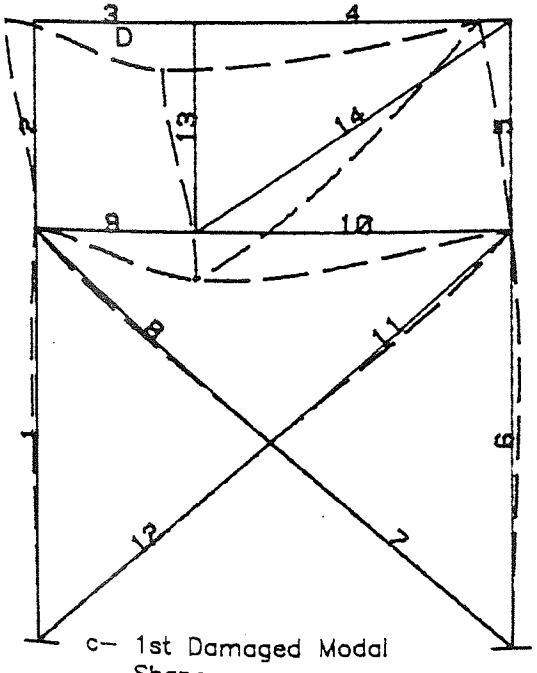

c– 1st Damaged Modal Shape

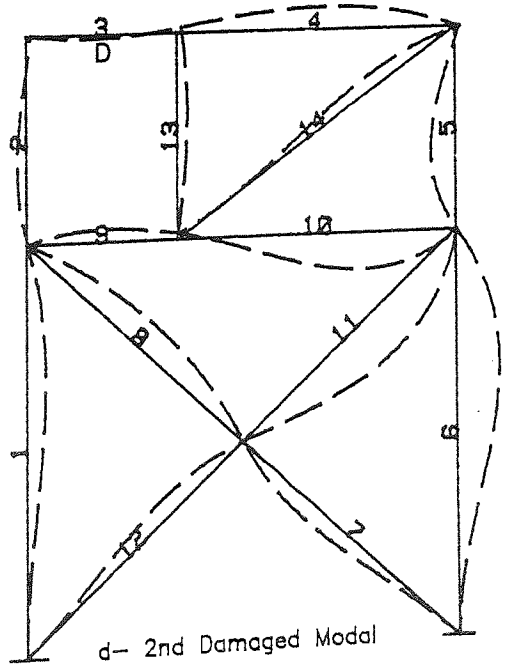

d– 2nd Damaged Modal Shape

Fig. 8.8 THEORETICAL MODAL SHAPES OF ASYMMETRIC PLANE FRAME

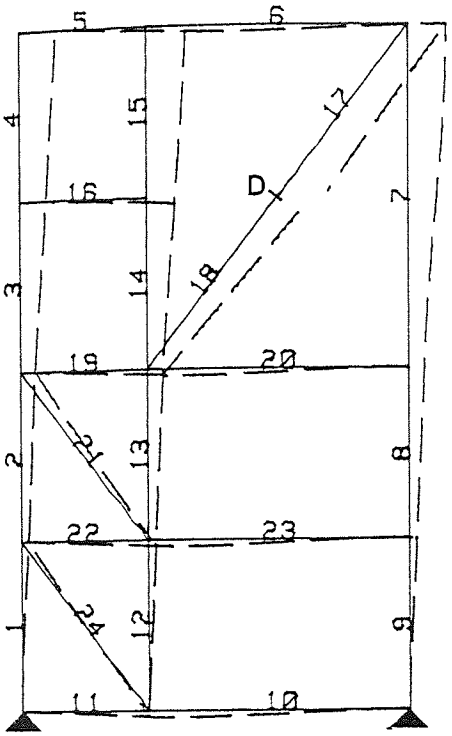

a— 1st Modal Shape

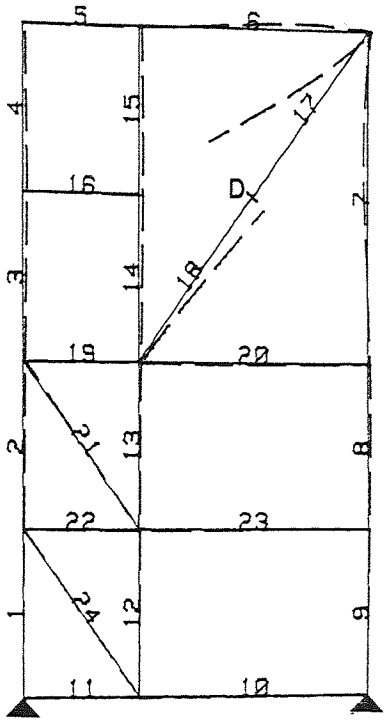

b— 2nd Modal Shape

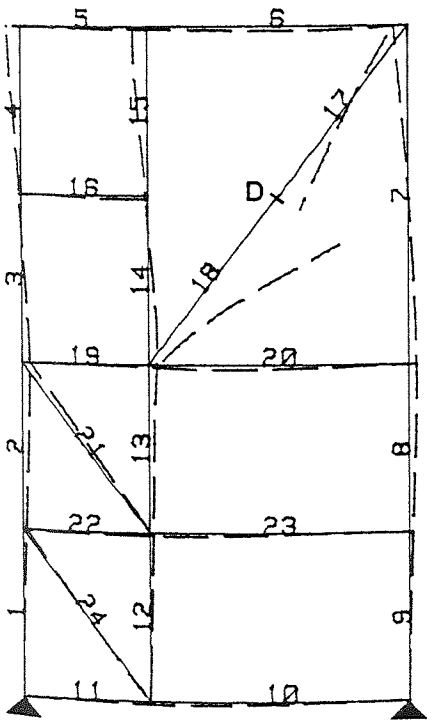

c— 3rd Modal Shape

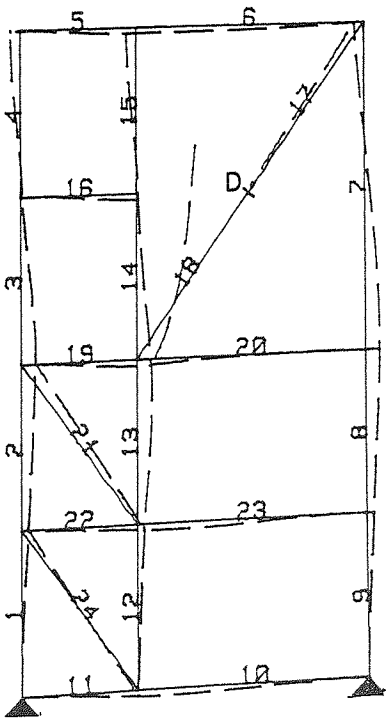

d— 4th Modal Shape

Fig. 8.9 THEORETICAL MODAL SHAPES OF COMPLETE FAILURE

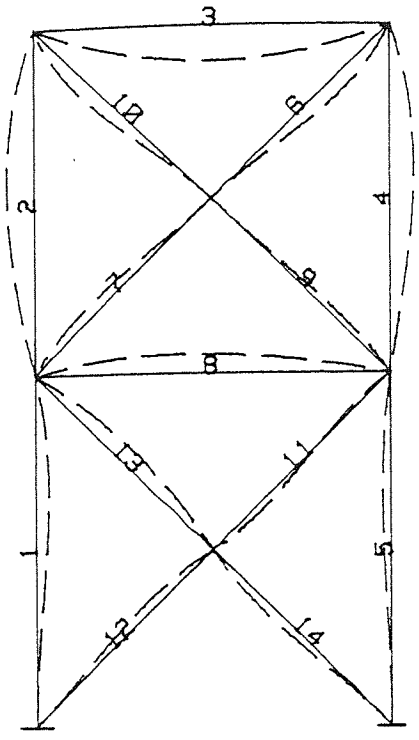

a– 1st Theo. Modal Shape

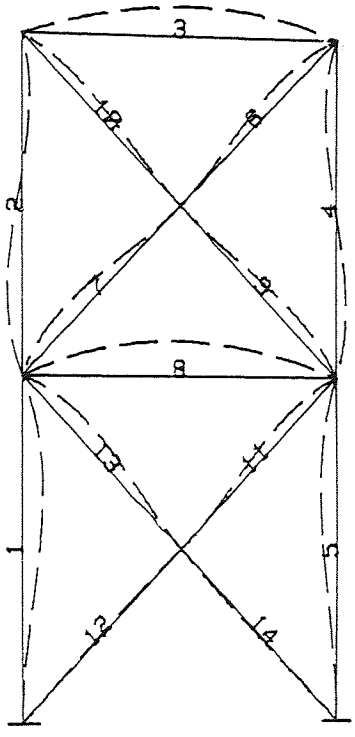

b– 2nd Theo. Modal Shape

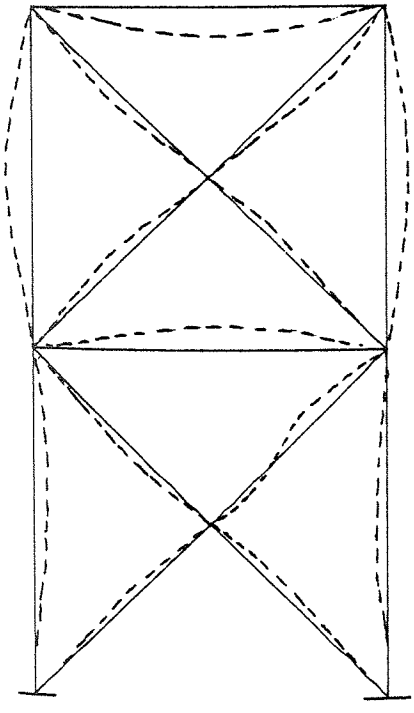

c– 1st Exp. Modal Shape

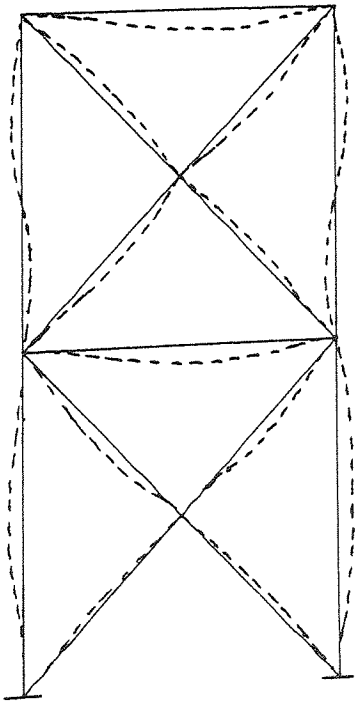

d– 2nd Exp. Modal Shape

Fig. 8.10 THEORETICAL & EXPERIMENTAL MODAL SHAPES
(1st AND 2nd MODES)

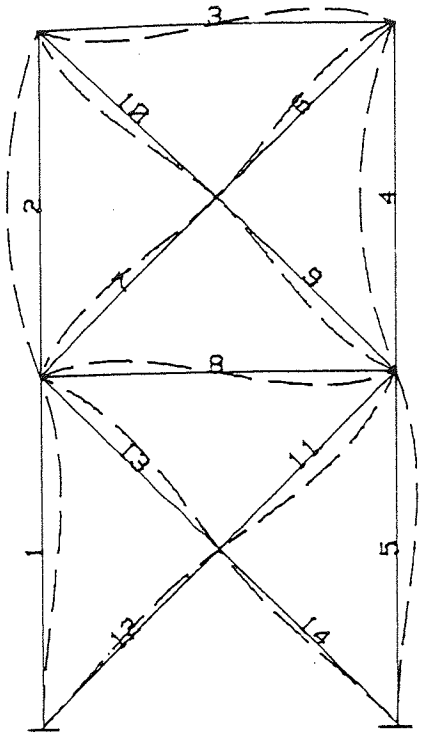

a– 3rd Theo. Modal Shape

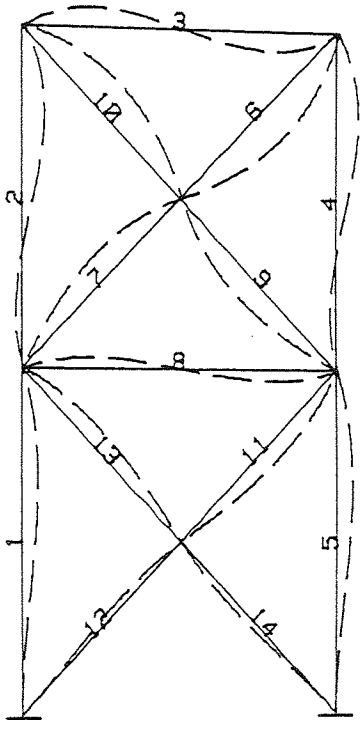

b– 4th Theo. Modal Shape

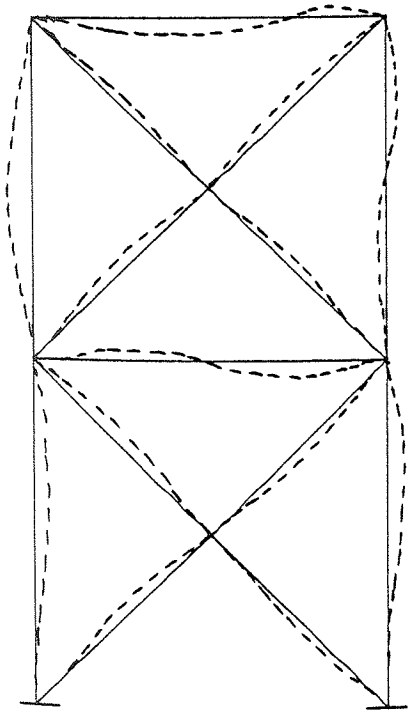

c– 3rd Exp. Modal Shape

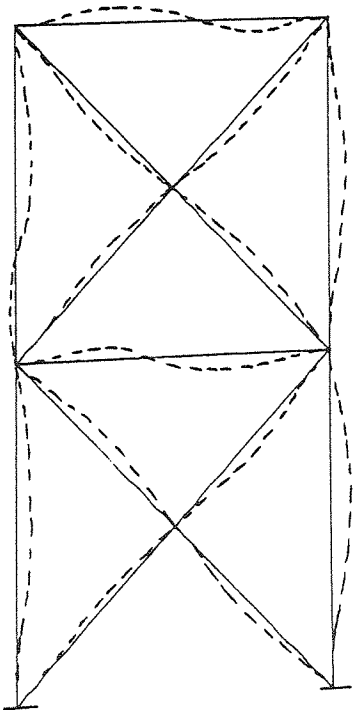

d– 4th Exp. Modal Shape

Fig. 8.11 THEORETICAL & EXPERIMENTAL MODAL SHAPES
(3rd AND 4th MODES)

similar, although for certain members there is a 180° phase shift between the predicted and measured mode shape.

II- The Symmetric Space Frame.

Before proceeding with the presentation of the predicted modal shape of the space frame model, it should be remembered that it is not an easy task to plot a three-dimensional modal shape of such a complex structure. It may be possible to draw the mode shapes corresponding to part of the structure. In order to gain a visual representation of the modal shape of a three-dimensional frame it is necessary to construct four plane plots. These plots are presented for the space frame shown in Fig. 8.12, by examining the X- and Z-direction components of the displacement vectors of the opposite sides A&C and B&D.

The results are displayed in Fig. 8.12 from which it is seen that the theoretical and experimental modal shapes are similar in all cases, although the phase angle error for some members is 180°.

Also, Fig. 8.13 shows the theoretical and experimental modal shapes of the space frame in an X- and Z-direction for sides B&D and A&C respectively, obtained for the case of complete failure in one of the top diagonal members at position F. It can be seen from the deflections of sides D and B in the X-direction, that the experimental modal shape is identical to the theoretical one, while for sides A and C in the

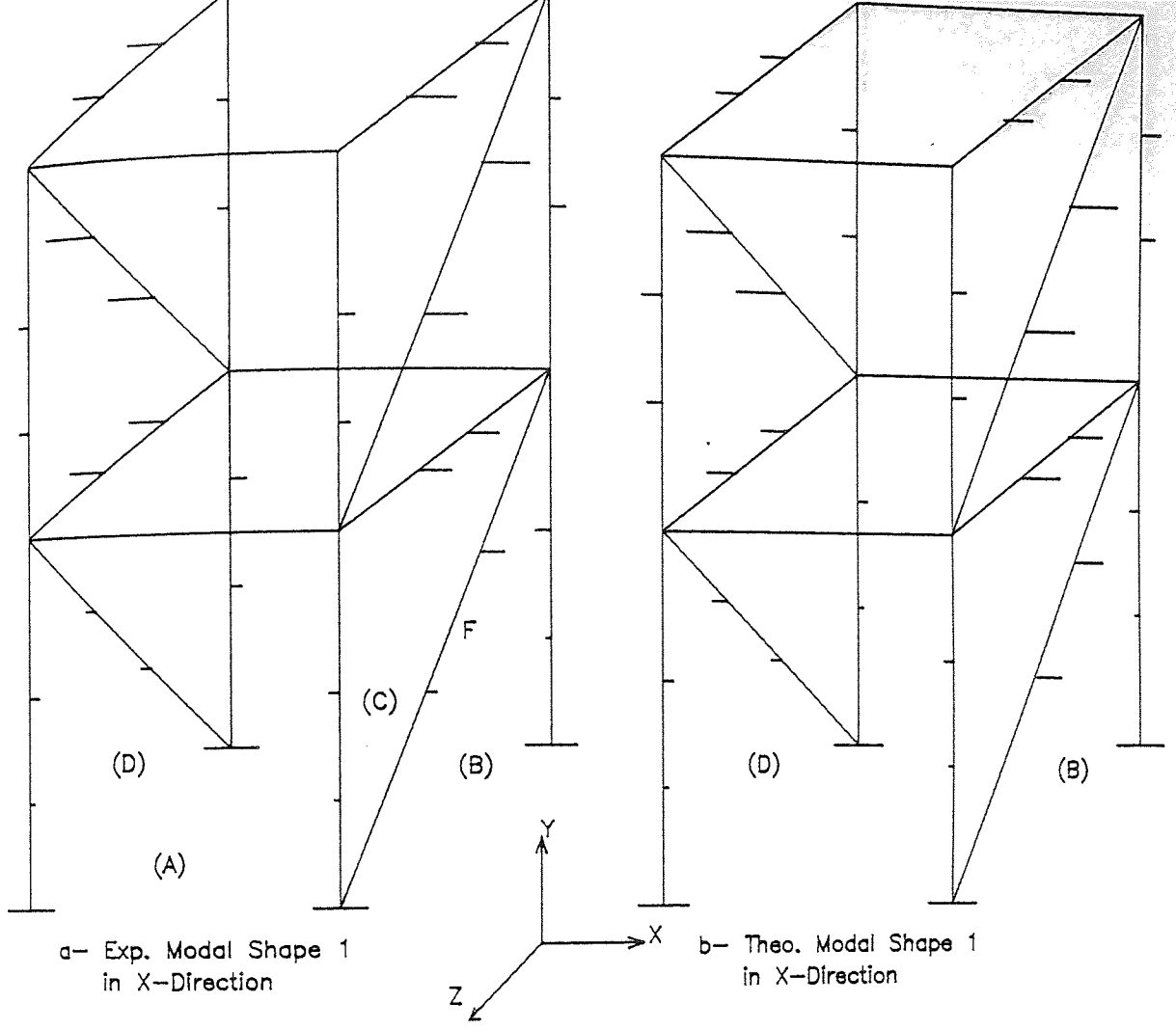

a– Exp. Modal Shape 1 in X–Direction

b– Theo. Modal Shape 1 in X–Direction

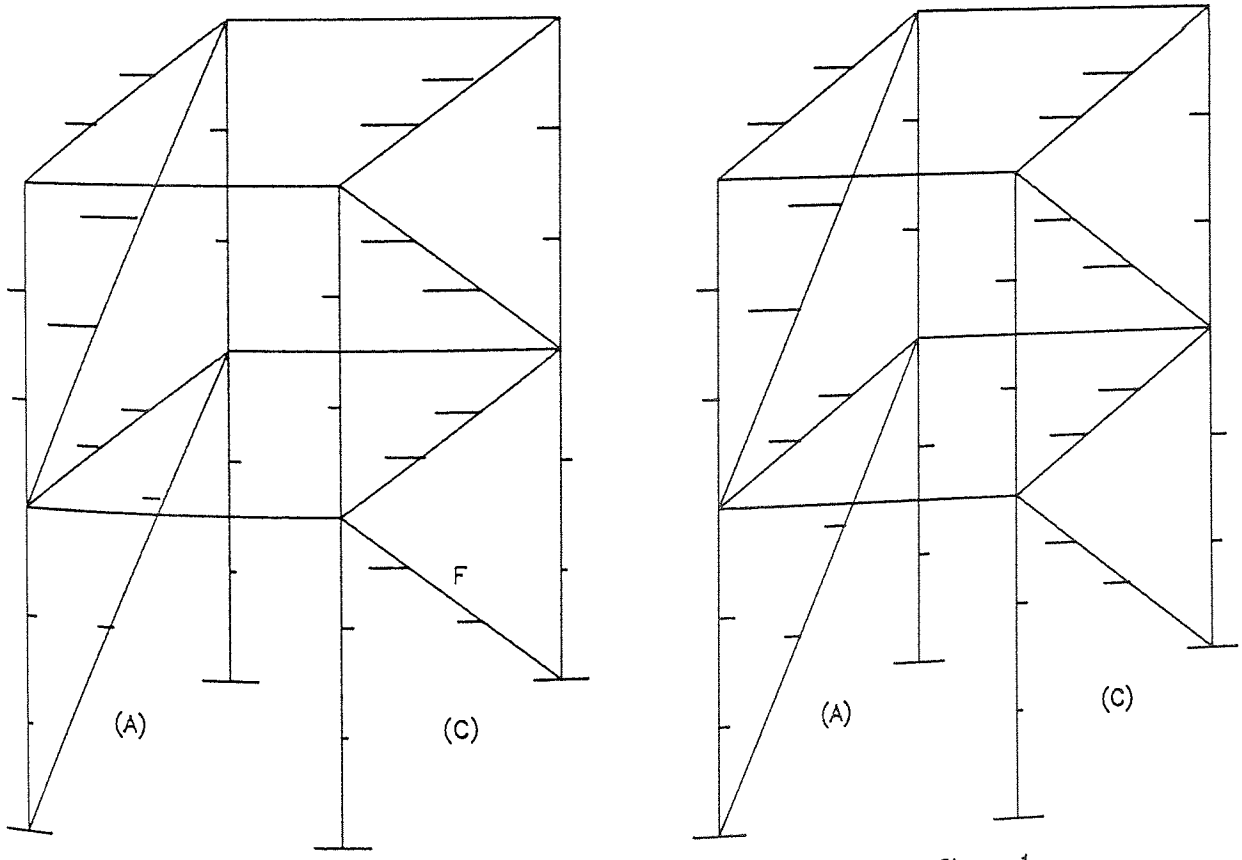

c– Exp. Modal Shape 1 in Z–Direction

d– Theo. Modal Shape 1 in Z–Direction

Fig. 8.12 EXPERIMENTAL & THEORETICAL MODAL SHAPES OF SPACE FRAME

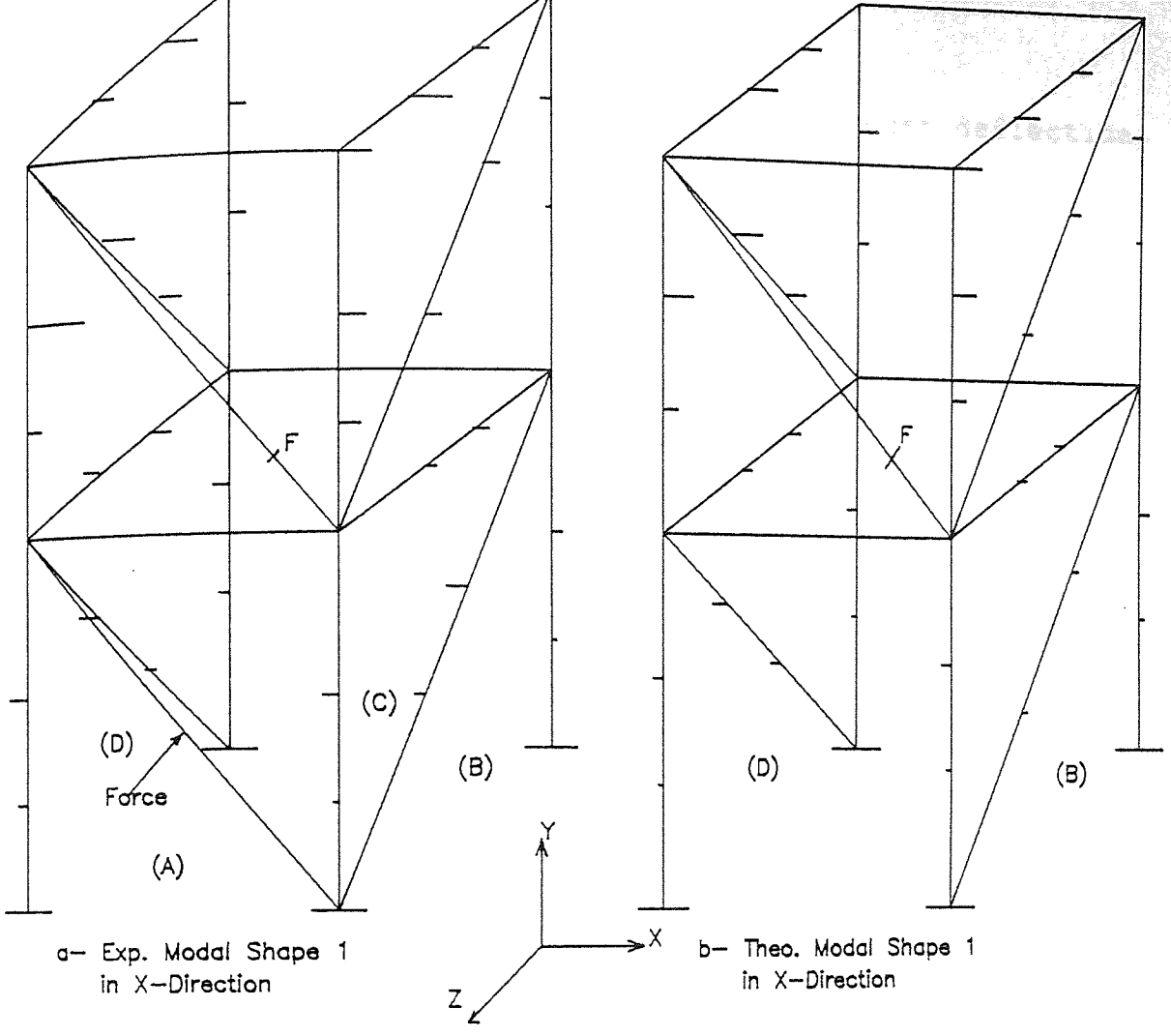

a– Exp. Modal Shape 1 in X–Direction

b– Theo. Modal Shape 1 in X–Direction

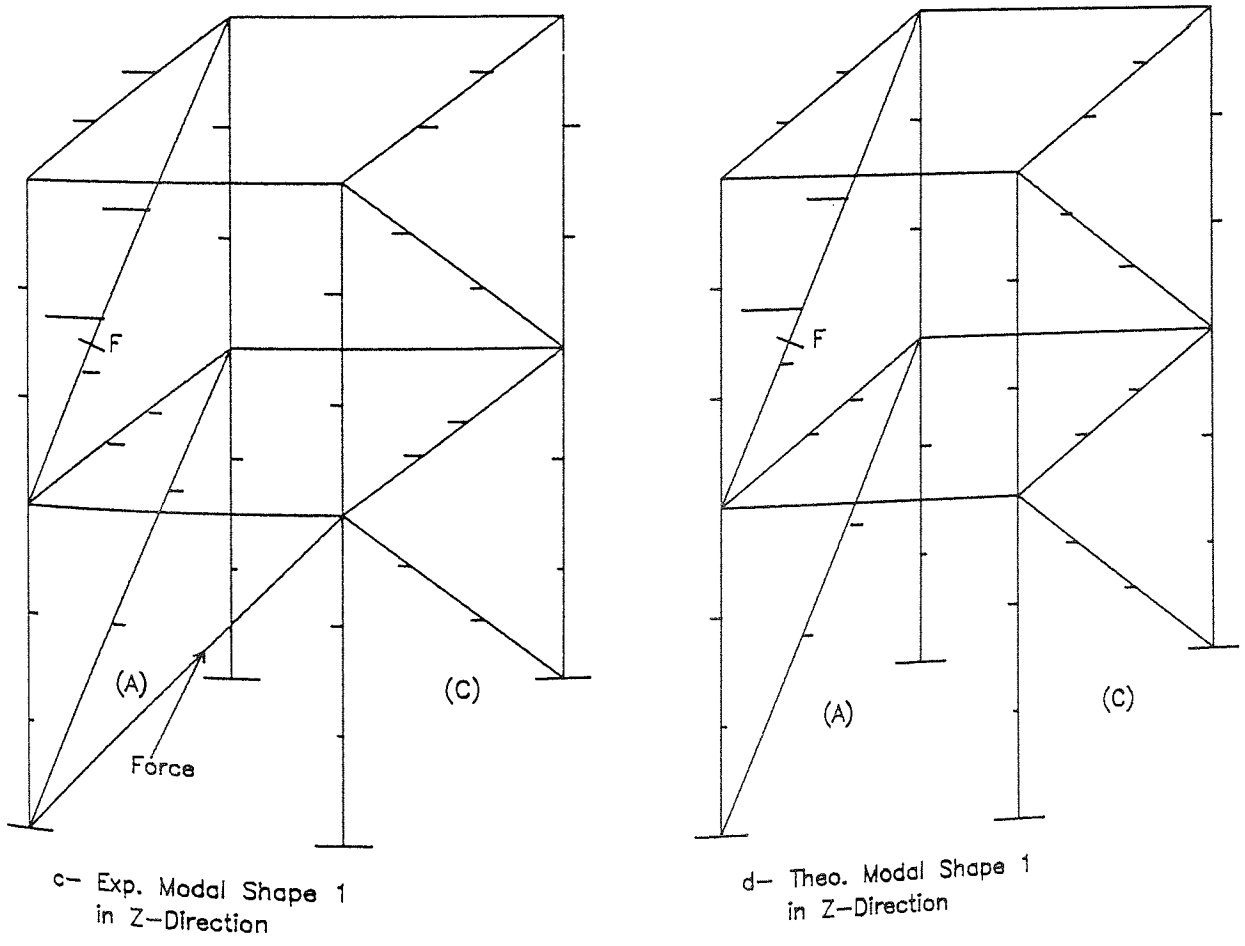

c– Exp. Modal Shape 1 in Z–Direction

d– Theo. Modal Shape 1 in Z–Direction

Fig. 8.13 EXPERIMENTAL & THEORETICAL MODAL SHAPES OF DAMAGED SPACE FRAME

Z-direction the broken member showed the largest deflection.

8.6 CLOSING REMARKS.

In this chapter the changes in the experimental and predicted natural frequencies have been examined to determine their sensitivity to the location and extent of structural damage. The frequency changes were obtained from the inertance measurements: it was found that the spring and the two-cantilever models were adequate representations of partial and complete failure respectively.

It was observed that failure of a structural member would produce appreciable frequency shifts in some modes and comparatively small shifts in others, depending upon the extent and position of the damage. Also, it was found that the frequencies of the undamaged structure had different values after the structures were repaired.

The effects of structural damping were negligible and an acceptable correlation has been obtained between experimental and theoretical behaviour of the undamaged and the damaged structures. The percentage errors in frequencies, for most of the tests, were within 10%, which is within normally accepted engineering design limits.

The results of this and the preceding chapters will be used in order to obtain the defect location charts which will be the subject for discussion in the next chapter.

CHAPTER NINE

DAMAGE LOCATION RESULTS

9.1 INTRODUCTION.

The theoretical predictions of change in natural frequency spectrum (chapter seven) due to damage in each member are now compared with the experimental values (chapter eight) to examine the possibility of determining damage location by monitoring changes in natural frequencies.

The defect location chart will consist of a plot of the structure, with elements labelled using either the Cawley-Adams Normalised Percentage Error (NPE) or the coefficient of determination, $100R^2$. The NPE or $100R^2$ values for several pairs of modes are displayed in the diagram: the predicted damage site being represented by either the NPE value 100 (see equation 3.9) or by the highest value of $100R^2$ for the two parameter model (β_0 and β_1), or by the reduced model (β_1 only), see section 3.6. Comparisons show that the new method works even if $\beta_0 \neq 0$ or $\beta_1 \neq 1$, which is the case for most of the results shown in this chapter: the Cawley-Adams method effectively assumes that $\beta_0 = 0$ and $\beta_1 = 1$.

Series of tests for defect location analysis were carried out on the plane and space frame structures using various damage models. Perturbation analysis was used to simulate damage by the reduced rigidity of the whole model. From these results it will be possible to establish the generality and validity of the methods used in order to deal with such structures.

9.2 PRELIMINARY TESTS ON CANTILEVER.

The tests reported here were of a preliminary nature and were carried out on simple cantilever beams. These beams have already been discussed in section 8.2 with reference to Tables 8.1 and 8.2. The aim of these tests was to determine the accuracy of the proposed techniques for locating the damage.

Damage was inflicted in the form of saw cuts and a fatigue crack. The first tests were carried out on the cantilever of dimension 700*50*12mm, with various saw cut depths at a position 100mm from the fixed end. Since the defect location methods lead to difficulties in predicting the damage at a position between the two elements, the finite element discretization of the cantilever shown in Fig. 9.1 was made by representing damage at a position between element 1 and 2. Then, the defect location charts produced from the frequency measurements set out in Table 8.1 and from the theoretical frequency changes produced from the reduction in rigidity of the whole element model are shown.

Figs. 9.1a,c,e,g show the defect location charts obtained by the Cawley-Adams method, see sections 3.3 and 3.5 (first method). It can be seen that the value of NPE (100) was either positioned at element 1 or 2. Figs. 9.1b,d,f,h show the defect location charts for the new method of statistical analysis, described in section 3.6 (second method) using $100R^2$ in place of the NPE. From these charts it can be seen

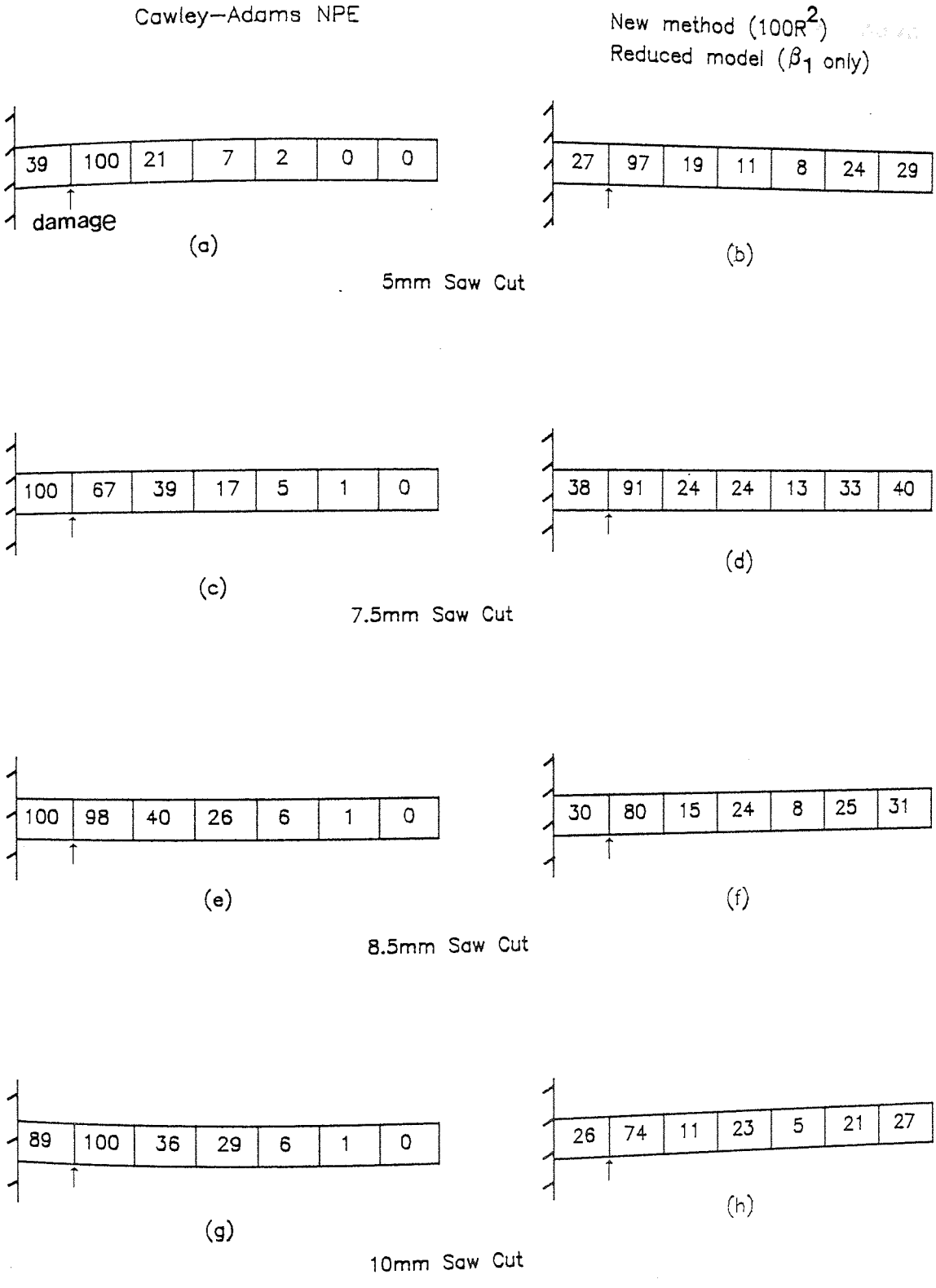

Damage between Elements 1&2
4 modes are considered
Reduction in Rigidity of Whole Element (Red. rig. whole elem.)

Fig. 9.1 DEFECT LOCATION CHARTS OF CANTILEVER BEAM WITH VARIOUS SAW CUT DEPTHS

that the highest number obtained is found at element 2, by considering the reduced model with values of β_1 are shown in Table 9.1. In this table the figures quoted in brackets with $\pm$ represent the standard error of the estimated values of β_1.

A comparison was also made between the first and second method using the cantilever with different damage models and considering a different number of modes. In each case the damage was detected and located successfully. These results are not shown here because only a representative sample of the results are presented.

Another defect location investigation was performed on the steel cantilever of dimension 480*40*6mm which was damaged by a crack produced by the fatigue machine at the position shown in Fig. 9.2 and penetrating through 64% of the cross-section. The figure shows the damage location charts which were produced from the frequency measurements displayed in Table 8.2.

Comparisons were made between the first and second method of the defect location analysis using three different damage models as shown in Fig. 9.2. In the first comparison the reduction in rigidity of the whole element model was used. In the second a torsional spring model was used. Finally, in the third comparison, a reduction of the cross-sectional area model was used. The results of these tests are shown in Figs. 9.2a,c,e and Figs. 9.2b,d,f, for the Cawley-Adams and new methods respectively.

It can be observed from these figures that damage was successfully located by both methods in all cases except in Fig. 9.2e, where the Cawley-Adams method gave the second highest NPE (=99) at the true site. This may be due to the fact that this damage model had no effect on the first mode when the damage was simulated at position 3 as shown in Fig. 7.3, and the frequency was increased when the damage was simulated at position 4. Another possible reason is that the Cawley-Adams assumption of β_1 =1 is not actually true for this particular case. Table 9.1 summarizes all the cantilever results.

The above results showed that a fatigue crack could be detected and located as accurately as a saw cut and so it was considered reasonable to use saw cuts for most of the remaining investigations. The practical advantage of this is that saw cuts are more easily to produce than fatigue cracks, especially in a complicated structure. The use of this type of damage on various structures will be discussed in the following sections. From the results of the cantilever beam it can be concluded that there is no definite choice between the Cawley-Adams and new methods of statistical analysis.

Cawley–Adams NPE

New method ($100R^2$)
Reduced model (β_1 only)

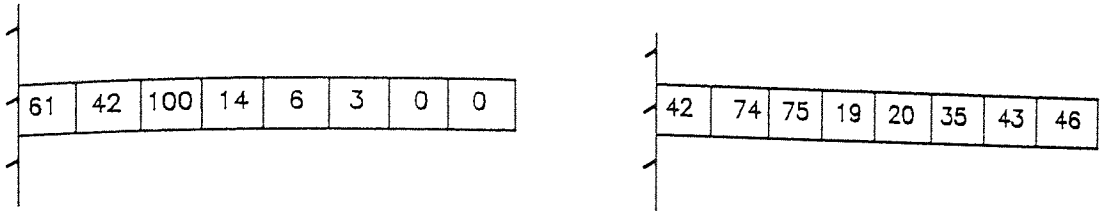

a– Damage at Element 3

b– Damage at Element 3

Red. rig. whole elem.

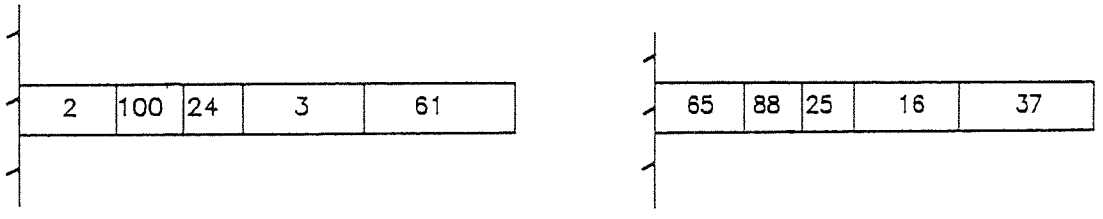

c– Damage at Element 2

d– Damage at Element 2

Spring model

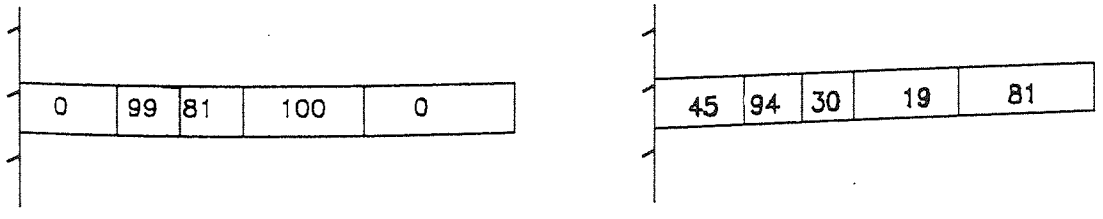

e– Damage at Element 2

f– Damage at Element 2

Reduction in cross–sectional area model

4 modes are considered

Fig. 9.2 DEFECT LOCATION CHARTS OF CANTILEVER BEAM WITH FATIGUE CRACK

No. of modes	Damage position	Severity of damage	Theo. damage model	New method						Cawley–Adams		
				Fig. No.	Damage located	$100R^2$	Two–parameter		Reduced β_1	NPE	Damage located	Fig. No.
4	Between elem. 1 & 2	5 mm (42%)	Red. rig. whole elem. (50%)	9.1b	Yes	27, 97			.7(±.1)	39, 100	Yes	9.1a
4	Between elem. 1 & 2	7.5 mm (63%)	Red. rig. whole elem. (50%)	9.1d	Yes	38, 91			.5(±.1)	100, 67	Yes	9.1c
4	Between elem. 1 & 2	8.5 mm (71%)	Red. rig. whole elem. (50%)	9.1f	Yes	30, 80			.6(±.2)	100, 98	Yes	9.1e
4	Between elem. 1 & 2	10 mm (83%)	Red. rig. whole elem. (50%)	9.1h	Yes	26, 74			.6(±.2)	89, 100	Yes	9.1g
4	Element 3	25.6mm (64%)	Red. rig. whole elem. (50%)	9.2b	Yes	75			.6(±.2)	100	Yes	9.2a
4	Element 2	25.6mm (64%)	Spring (25%)	9.2d	Yes	88			.6(±.2)	100	Yes	9.2c
4	Element 2	25.6mm (64%)	Red. in C–S area (25%)	9.2f	Yes	94			.5(±.1)	99	No	9.2e

Red. rig. whole elem. = Reduction in rigidity of whole element
Red. in C–S area = Reduction in cross–sectional area
Fig. No. = Figure number
elem. = element

TABLE 9.1 SUMMARY OF DEFECT LOCATION CHARTS FOR CANTILEVER BEAM

9.3 TESTS ON PLANE FRAME STRUCTURES.

9.3.1 Damage by a Saw Cut.

A series of tests for defect location analysis was carried out on plane frame structure damaged by saw cuts. The defect location charts for these tests were constructed using the $100R^2$ method will be discussed in this section. Tables 9.2 to 9.4 summarize the defect location results for the plane frame structures.

I- The symmetric cross-brace portal frame.

The first plane frame structure (shown in Fig. 6.5) was initially damaged by a saw cut of depth 10mm on both sides of the member at position A, this damage was equivalent to 50% of the cross-sectional area. Fig. 9.3a shows the defect location chart, produced from the frequency measurements of Table 8.3. The theoretical changes in natural frequencies were calculated by modelling the damage as a torsional spring. Using this model, it was necessary to re-solve the non-linear EVP for each element damaged in turn. This procedure required extensive calculation and for this reason each member was considered as a single element. A further advantage of this was that it became possible to determine whether the damage was adequately predicted by simulating each member as one element. Fig. 9.3a shows that the damage was successfully detected and located. As the structure is symmetrical, two damage locations are indicated on the

location chart.

The location charts produced from the frequency measurements set out in Table 8.3, for which the damage had been increased to produce complete failure at position A, are shown in Figs. 9.3b-d. In this case two damage models were used to produce the theoretical changes in frequencies. The first model used the reduction in rigidity of the whole element and the second was the two-cantilever model for both fixed and pinned end conditions of the structural foundations respectively. Referring to Fig. 9.3b, it is seen that most of the members are divided into elements. This was done because the rigidity reduction model reduces the stiffness of the whole element, hence it will be more efficient if the members are divided into many elements particularly since it is not necessary to re-solve the EVP for each position. In these tests the reduced model was used because the standard error for β_0 was so large.

It can be observed from Figs. 9.3b-d that the damage was correctly located. The value of the coefficient of determination ($100R^2$) in Fig. 9.3c is greater than in Fig. 9.3d, the significance of this is that the frequencies predicted for fixed boundary conditions are closer to the experimental values than those predicted for pinned ends.

The defect location charts using the Cawley-Adams method for these tests are shown in Appendix 3, see Figs. A3.1a-d. For the cases A3.1a and b, $\beta_0 \neq 0$ and $\beta_1 \neq 1$ and, as anticipated, the

New method ($100R^2$)

a– Spring model

Two parameter model (β_0 & β_1)
10mm Saw Cut at A

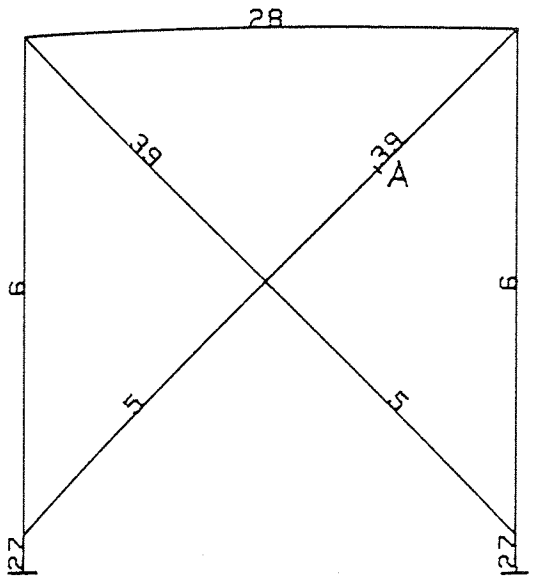

b– Red. rig. whole elem.

Reduced model (β_1 only)
Complete Cut at A

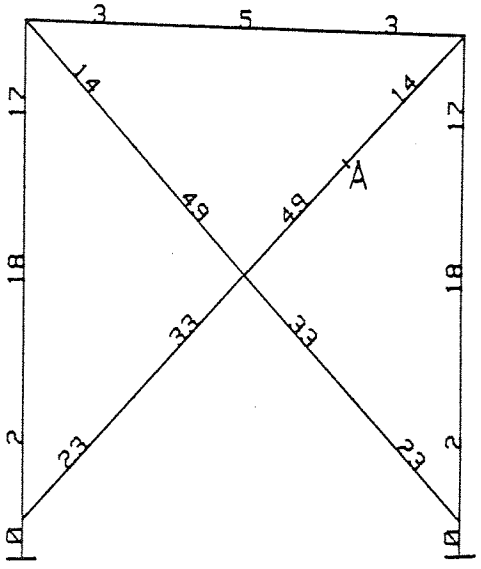

9 modes are considered

Two–cantilever model

c– Fixed ends
Reduced model
Complete Cut at A

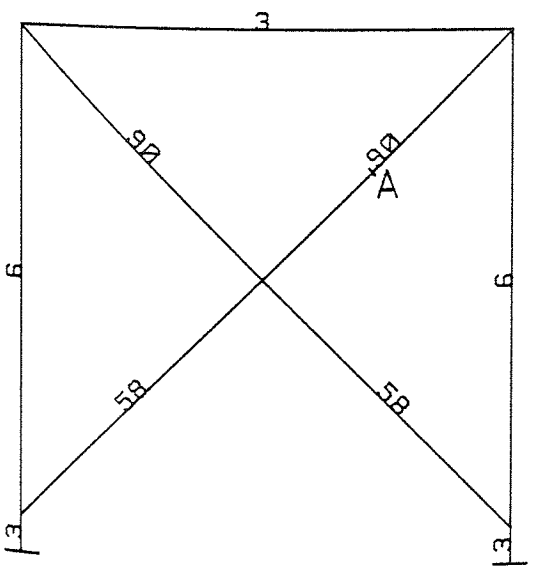

d– Pinned ends
Reduced model
Complete Cut at A

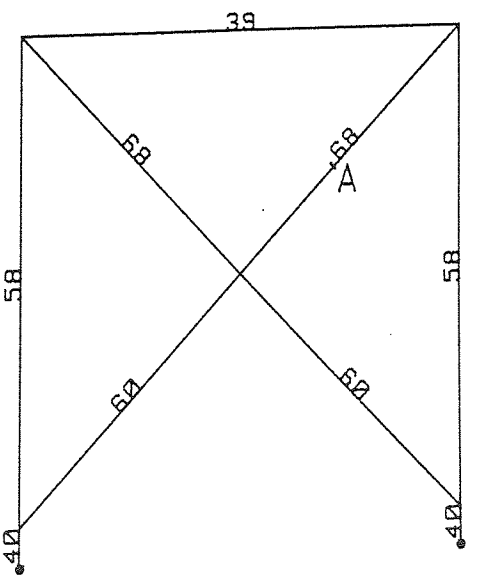

Fig. 9.3 DEFECT LOCATION CHARTS OF CROSS BRACE PORTAL FRAME FOR PARTIAL AND COMPLETE FAILURE

damage was not successfully located (see Table 9.2). However, Figs. A3.1c-d, show that the damage was successfully located.

Figs. 9.4a-b and 9.4c show the defect location analysis prediction for a structure damaged by various saw cuts made of 10mm and 15mm depth and also by complete failure at position B. The location charts were produced from the frequency measurements set out in Table 8.3. For Figs. 9.4a-b the theoretical changes in frequencies were predicted using the two models of damage discussed earlier. In the first model each member consisted of a number of elements. This enables more accurate location of the damage site, as the damage site is identified by the element rather than the member. For the case of complete failure the defect location charts shown in Fig. 9.4c was constructed using the two-cantilever model to determine frequency changes.

The charts show that the damage was detected and correctly located in each case, although the damage was predicted at the member rather than the element in Fig. 9.4a (hence "Yes/No" in column six of Table 9.2). In Fig. 9.4c the values of $100R^2$ is low, this may have been caused by the structure being repaired many times, so that the experimental undamaged frequencies were no longer similar to the theoretical. Having already chosen the fixed boundary conditions, the members were divided into many elements and therefore the structure was fully analysed as shown in Fig. 9.4c.

The corresponding location charts using the Cawley-Adams

New method ($100R^2$)

a– Red. rig. whole elem.
Two parameter model
10 mm cut at B
9 modes

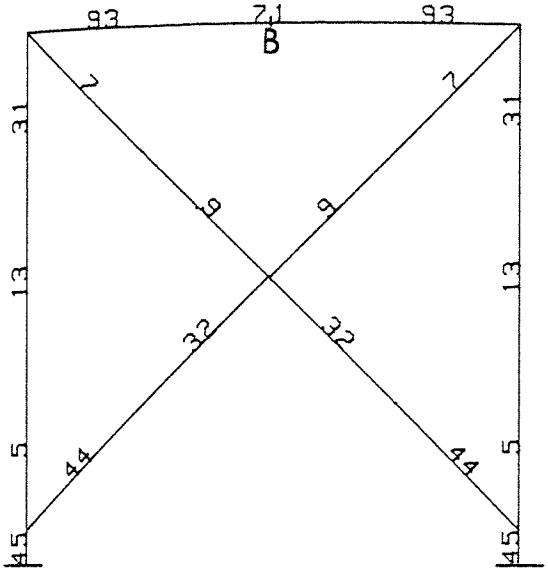

b– Spring model
Reduced model
15mm saw cut at B
4 modes

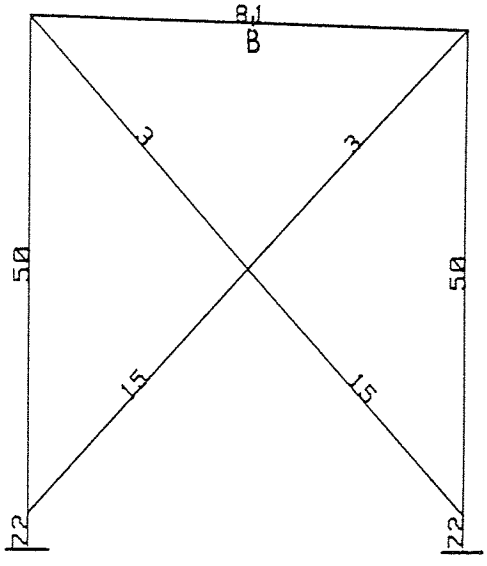

c– Two–cantilever model
Two parameter model
Complete cut at B
9 modes

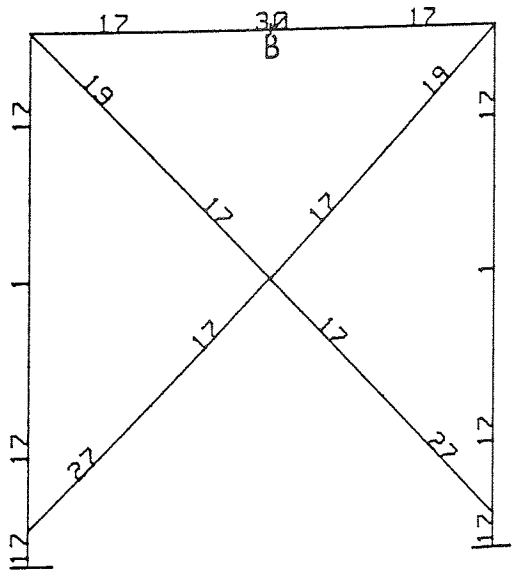

Fig. 9.4 DEFECT LOCATION CHARTS OF CROSS–BRACE PORTAL FRAME FOR VARIOUS SAW CUT DEPTHS

method are shown in Appendix 3 (see Figs. A3.2a-c). As expected damage was not correctly located for the reason mentioned above except in Fig. A3.2b, although the second highest NPE (=93) occurred at the true damage site in Fig. A3.2c.

II- The asymmetric cross-brace portal frame.

Figures 9.5a-d show the defect location charts produced from the frequency measurements set out in Table 8.4 for the asymmetric cross-brace portal frame and represent a 2mm saw cut and a complete failure at A. In Fig. 9.5a a spring model was used to produce the theoretical frequency changes. In Fig. 9.5b the reduction in rigidity of the whole element model was used to produce the frequency changes for complete failure. It is apparent that the damage is successfully located in each case. The value of $100R^2$ is very low in Fig. 9.5b. This may indicate that the reduced rigidity model is not suited to the representation of total failure because this model will reduce the stiffness of the whole element, hence it will be more efficient if the members are divided into many elements. Another possible reason may be due to that the first ten modes considered were not accurate using this configuration for the linear EVP. Hence, the two-cantilever model was used for Figs. 9.5c-d. Two configurations were simulated and the damage was successfully located with a higher value of $100R^2$ than before. Since this frame is asymmetrical, the damaged member is uniquely located on the chart.

New method ($100R^2$)
Reduced model

a– Spring model
2mm Saw Cut at A

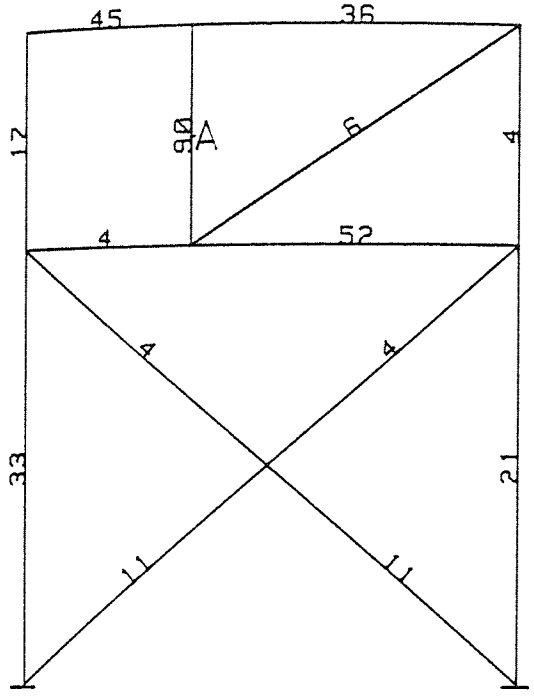

10 modes

b– Red. rig. whole elem.
Complete Cut at A

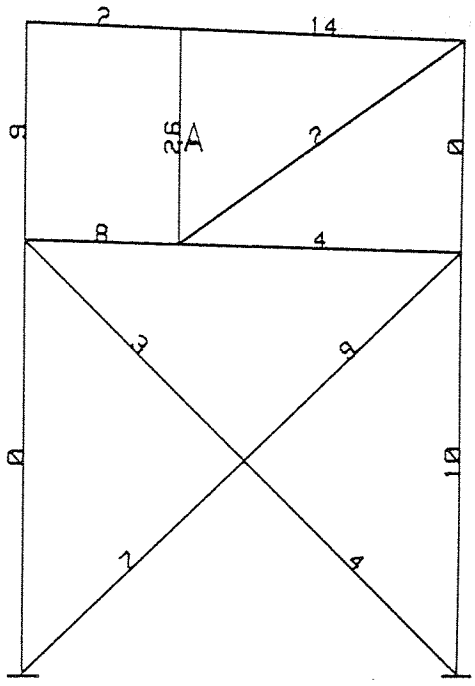

Two–cantilever model

c– 9 modes
Complete Cut at A

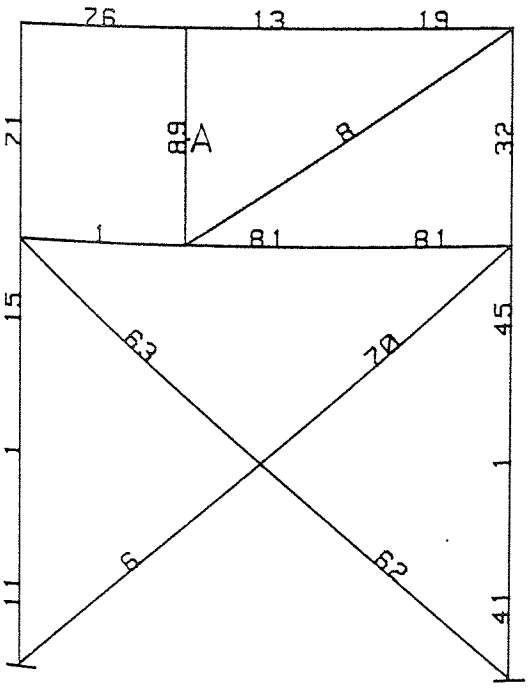

d– 8 modes
Complete Cut at A

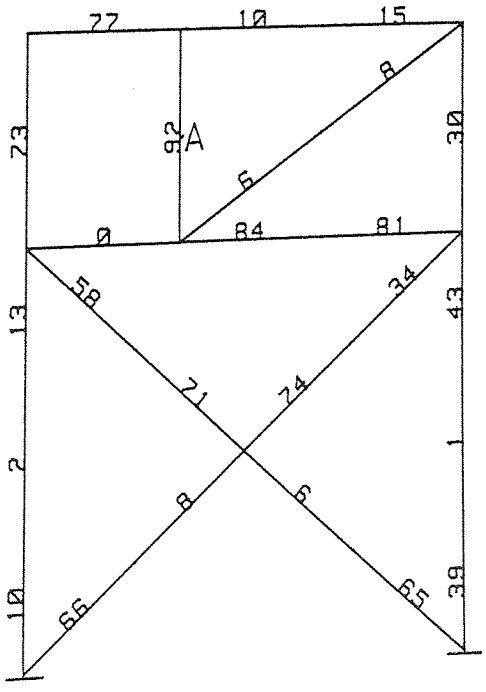

Fig. 9.5 DEFECT LOCATION CHARTS OF ASYMMETRIC FRAME FOR VARIOUS DAMAGE MODELS

The corresponding location charts using the Cawley-Adams method are shown in Appendix 3 (see Figs. A3.3a-d). In figures A3.3a and A3.3c-d, where β_1 equal 1, the damage was correctly located. In Fig. A3.3b for which β_1 was not significant the damage was not located successfully (see Table 9.2).

III- The symmetric tower frame.

The defect location charts shown in Figs. 9.6a-b have been produced from the frequency measurements set out in Table 8.5 and represent a 5mm deep saw cut at D. Again two damage models were used to predict the frequency changes, the reduction in rigidity of the whole element and the two-cantilever model. As can be seen the damage was successfully located by both models. It is evident that the new method can predict the location of the partial damage in a structure even if the damage was simulated as a complete failure (see Fig. 9.6b). Fig. 9.6c shows the defect location chart for a complete saw cut at position D. The two-cantilever model was used to compute the theoretical frequency changes. Again, the damage was correctly located.

The results for this structure show that there is a lack of symmetry, this may be due to variations in dimensions due to dimensional tolerance and distortion in the frame. In all the above tests β_o was rejected, hence the reduced model was chosen. The location charts for the Cawley-Adams method for

				New method						Cawley–Adams		
No. of modes	Damage position	Severity of damage	Theo. damage model	Fig. No.	Damage located	$100R^2$	Two–parameter model		Reduced	NPE	Damage located	Fig. No.
							β_o	β_1	β_1			
9	A	10 mm (50%)	Spring (62%)	9.3a	Yes	39	−2.1(±.7)	−.7(±.5)		12	No	A3.1a
9	A	Complete cut	Red. rig. whole elem. (100%)	9.3b	Yes	49			.5(±.2)	74	No	A3.1b
9	A	Complete cut	Two–cant.	9.3c	Yes	90			1.1(±.1)	100	Yes	A3.1c
9	A	Complete cut	Two–cant. (Pinned ends)	9.3d	Yes	68			.9(±.2)	100	Yes	A3.1d
9	B	10 mm (50%)	Red. rig. whole elem. (20%)	9.4a	Yes/No	71	2(±.3)	−.3(±.2)		20	No	A3.2a
4	B	15 mm (75%)	Spring (62%)	9.4b	Yes	81			.8(±.3)	100	Yes	A3.2b
9	B	Complete cut	Two–cant.	9.4c	Yes	30	2.3(±1.1)	2.1(±1.6)		93	No	A3.2c
10	A	2 mm (33%)	Spring (50%)	9.5a	Yes	90			.8(±.1)	100	Yes	A3.3a
10	A	Complete cut	Red. rig. whole elem. (100%)	9.5b	Yes	26			−.4(±.3)	21	No	A3.3b
9	A	Complete cut	Two–cant.	9.5c	Yes	89			1.1(±.1)	100	Yes	A3.3c
8	A	Complete cut	Two–cant.	9.5d	Yes	92			1.1(±.1)	100	Yes	A3.3d

TABLE 9.2 SUMMARY OF DEFECT LOCATION CHARTS FOR SYMMETRIC AND ASYMMETRIC CROSS–BRACE PORTAL FRAMES

New method ($100R^2$)
Reduced model
4 modes

a– Red. rig. whole elem.
5mm saw cut at D

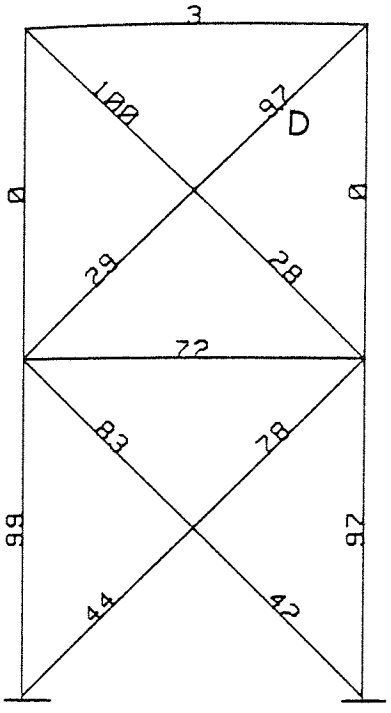

b– Two–cantilever model
5mm saw cut at D

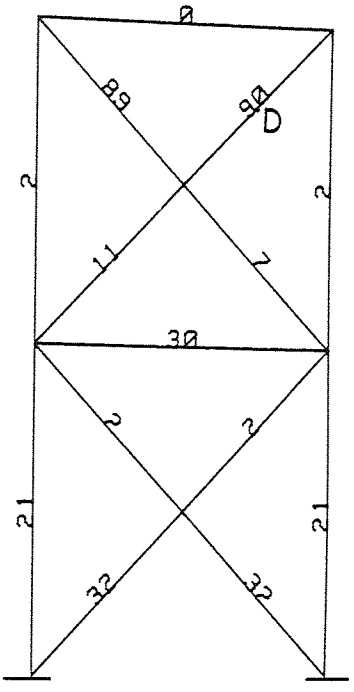

c– Two–cantilever model
Complete cut at D

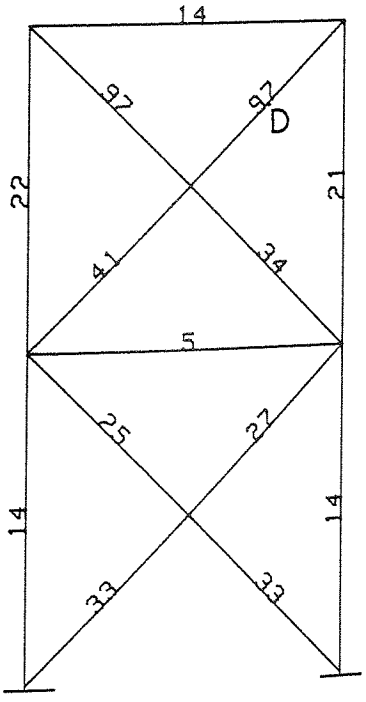

Fig. 9.6a–c DEFECT LOCATION CHARTS OF SYMMETRIC TOWER FRAME 1 FOR VARIOUS DAMAGE MODELS (CUT AT D)

these tests are shown in Appendix 3 (see Figs. A3.4a-c). It is observed that the damage was correctly located in each case.

The defect location charts shown in Figs. 9.7a-b and 9.7c-d were produced from the frequency measurements set out in Table 8.5 for complete failure at positions C and A, respectively, of the symmetric tower frame. The reduced rigidity and two-cantilever models were again used to produce the theoretical frequency changes. Referring to Fig. 9.7b, most of the members were divided to several elements, so that this discretization could predict not only the failure at the structural member but also at which element within the member. It can be seen that the damage was successfully located except in Fig. 9.7c. The reasons for this may be that the damage model was not accurate enough to calculate the frequency changes, hence the first natural frequency was slightly increased and the second frequency remained practically unchanged when the damage was simulated at position 8 (see Fig. 7.8b). Another possible reason may be that the structure was re-used, hence the experimental undamaged frequencies were changed due to the effect of welding. Also, as can be seen from Table 9.3, β_1 for the two parameter model has high standard error. For the above reasons and those mentioned for Fig. 9.5b, the highest value of $100R^2$ in Fig. 9.7d is very small.

The location charts obtained from the Cawley-Adams method are shown in Appendix 3 (see Figs. A3.5a-d). For this frame the

New method ($100R^2$)
Two parameter model
9 modes

a– Two–cantilever model
Complete Cut at C

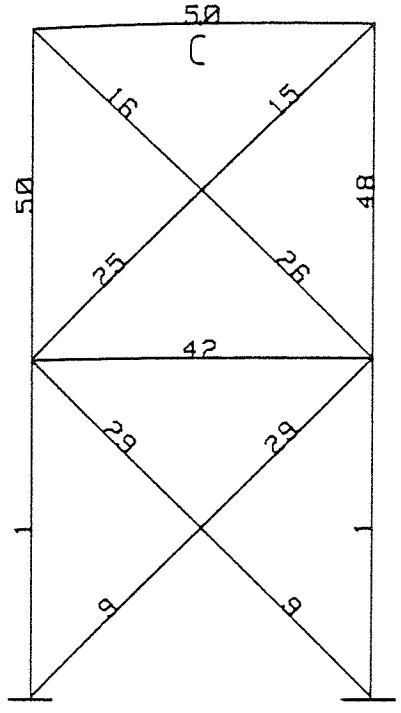

b– Red. rig. whole elem.
Complete Cut at C

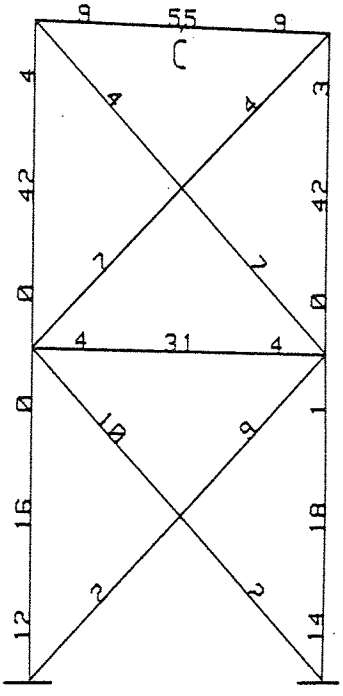

c– Two–cantilever model
Complete Cut at A

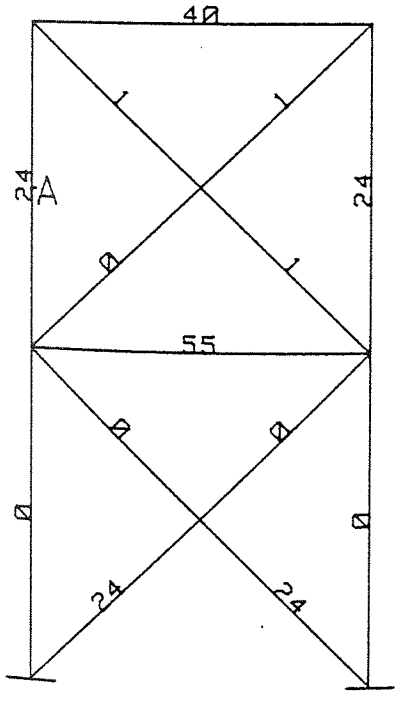

d– Red. rig. whole elem.
Complete Cut at A

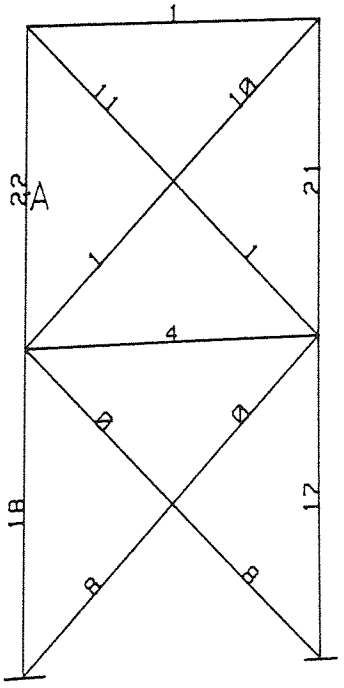

Fig. 9.7a–d DEFECT LOCATION CHARTS OF SYMMETRIC TOWER FRAME 1 FOR VARIOUS DAMAGE MODELS(CUT AT C&A)

damage was not correctly located except in the case of Fig. A3.5b which locates the damaged member instead of the specific element (hence "Yes/No" in column twelve of Table 9.3). These findings are to be expected because for some cases, as shown in Table 9.3, the two parameter model estimates values of β_0 and β_1 with a large standard error and in other cases a negative value. This indicates that the true value may be positive but near zero. If that is so it is purely fortuitous that the damage was correctly located in this case.

Another symmetrical tower frame having similar dimensions to the first structure was damaged with a series of saw cuts at position E. Tests were carried out in order to study the effect of welding damage on natural frequencies and the effect on the defect location analysis. Also, the effect of simulating the damage at the middle of each element in turn rather than at the actual damage site (100mm from the free end) was investigated to determine whether or not the actual site could be predicted. The defect location charts relating to these tests are shown in Figs. 9.8a-c and 9.9a-d which produced from the frequency measurements illustrated in Table 8.6. Figs. 9.8a-b represent the location charts for the first complete failure at position E, using the two-cantilever model and the reduction in rigidity of the whole element model to predict the theoretical frequency changes. The damaged member was correctly located in both cases. Using the first model, the damage was simulated at the middle of each element so that only the damaged member could be predicted,

but when using the second model the damage can be predicted at the correct element within the member.

Fig. 9.8c represents the location chart for the second complete failure at the same position E after welding the first cut. Damage is modelled in the same way as for Fig. 9.8b. It is seen that the second highest $100R^2$ occurs at the actual damage location. The discrepancy may have been caused by material property changes arising from the welding and re-use of the structure.

The defect location charts obtained by the Cawley-Adams method for this frame are shown in Appendix 3 (see Figs. A3.6a-c). These charts show that the damage was not located successfully, except in Fig. A3.6c. This may be because the reduced model in Fig. 9.8b gave the estimate $\beta_1 = -7.2(\pm 4)$; a large standard error indicating that the true value of β_1 may be positive but near zero, and the accurate prediction is only fortuitous, see Table 9.3.

Figures 9.9a-d represent the defect location charts for the third saw cut made at position E following rewelding. The section was damaged to depths of 6mm, 10mm and 15mm and then to complete failure (see Table 8.6). Two damage models were used, the reduction in rigidity of the whole element for Figs. 9.9a,b&d and the two-cantilever model for Fig. 9.9c. The location charts show that the damage was detected and located in each case even when a 30% reduction in rigidity of the whole element was used to represent the three different

New method ($100R^2$)
Reduced model
4 modes

a– Two–cantilever model
1st complete cut at E

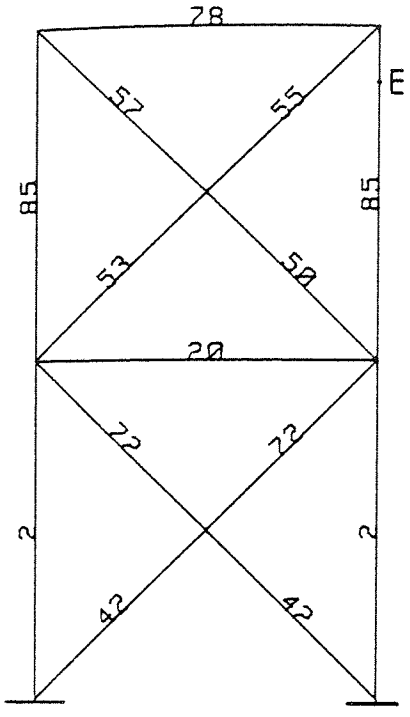

b– Red. rig. whole elem.
1st complete cut at E

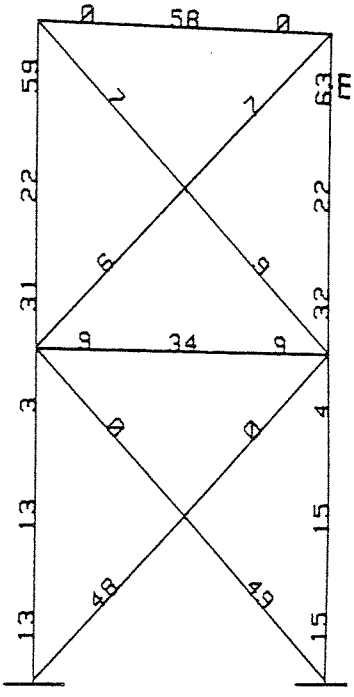

c– Red. rig. whole elem.
2nd complete cut at E

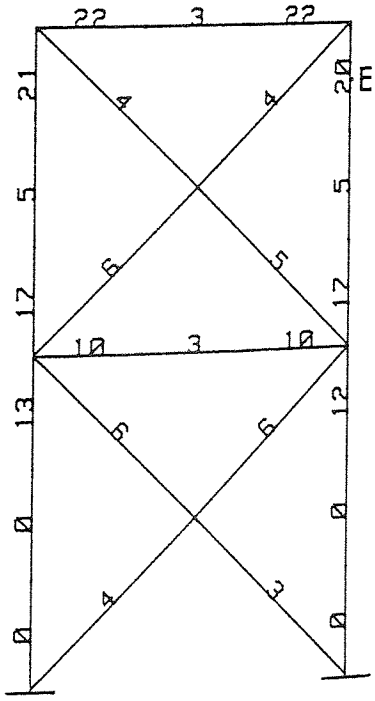

Fig. 9.8a–c DEFECT LOCATION CHARTS OF SYMMETRIC TOWER FRAME 2 FOR VARIOUS DAMAGE MODELS

No. of modes	Damage position	Severity of damage	Theo. damage model	New method						Cawley–Adams		
				Fig. No.	Damage located	$100R^2$	Two parameter model		Reduced	NPE	Damage located	Fig. No.
							β_0	β_1	β_1			
4	D	5 mm (50%)	Red. rig. whole elem. (50%)	9.6a	Yes	97			2.1(±.3)	96	Yes	A3.4a
4	D	5 mm (50%)	Two–cant.	9.6b	Yes	90			.8(±.2)	100	Yes	A3.4b
4	D	Complete cut	Two–cant.	9.6c	Yes	97			4.5(±.5)	92	Yes	A3.4c
9	C	Complete cut	Two–cant.	9.7a	Yes	50	−1(±.4)	.8(±.4)		85	No	A3.5a
9	C	Complete cut	Red. rig. whole elem. (30%)	9.7b	Yes	55	−1.5(±.5)	.5(±.2)		41	Yes/No	A3.5b
9	A	Complete cut	Two–cant.	9.7c	No	24	−2.3(±.4)	.5(±.8)		60	No	A3.5c
9	A	Complete cut	Red. rig. whole elem. (50%)	9.7d	Yes	22	−2.1(±.4)	.2(±.4)		17	No	A3.5d
4	E	Complete cut (1st)	Two–cant.	9.8a	Yes	85			5.7(±1.7)	59	No	A3.6a
4	E	Complete cut (1st)	Red. rig. whole elem. (30%)	9.8b	Yes	63			−7.2(±4)	10	No	A3.6b
10	E	Complete cut (2nd)	Red. rig. whole elem. (30%)	9.8c	No	20			.2(±.1)	98	Yes	A3.6c

TABLE 9.3 SUMMARY OF DEFECT LOCATION CHARTS FOR SYMMETRIC TOWER FRAME

a– Red. rig. whole elem.
6mm Saw Cut at E

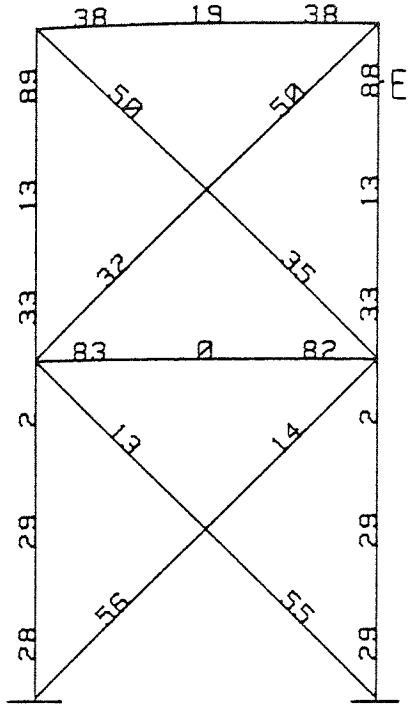

4 modes
Reduced model

b– Red. rig. whole elem.
10mm Saw Cut at E

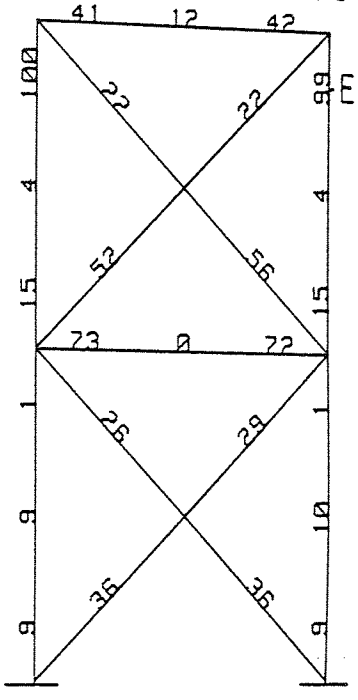

c– Two–cantilever,
Two parameter model
15mm Saw Cut at E
8 modes

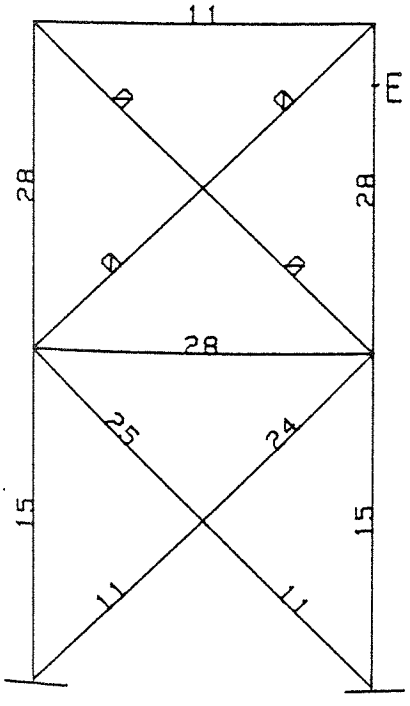

d– Red. rig. whole elem.
Reduced model
3rd Complete Cut at E
9 modes

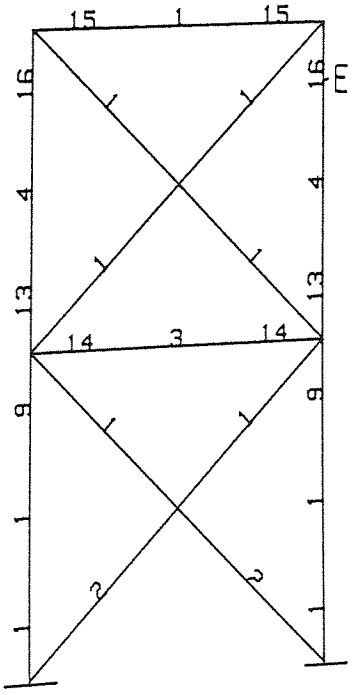

Fig. 9.9a–d DEFECT LOCATION CHARTS OF SYMMETRIC TOWER FRAME 2 FOR VARIOUS SAW CUT DEPTHS

extents of damage including complete failure. It can now be concluded that the values of $100R^2$ are reduced for a structure which has been repaired by welding.

The location charts using the Cawley-Adams method are shown in Appendix 3 in Figs. A3.7a-d. The charts indicate that the damage was correctly located in the case of the 10mm and complete failure (see Figs. A3.7b&d). The second highest NPE occurred at the actual damage site as shown in Fig. A3.7a but the damage was incorrectly located in Fig. A3.7c.

IV- The asymmetric tower frame.

Defect location charts were constructed for the asymmetrical tower frame using the frequency measurements given in Table 8.8. Damage was located at positions A and B and the results are shown in Figs. 9.10c-d. These figures are the defect location charts for complete failure at position A and for a cut 10mm in depth at position B respectively. The two-cantilever model and the reduction in rigidity of the whole element model were again used to predict changes in natural frequency. In Fig. 9.10d, for damage at position B 200mm away from one end of the diagonal member, the member was divided into two elements, to facilitate the prediction of the exact damage site. In both cases damage was successfully located.

The saw cut at position B was then extended to give complete failure. The corresponding damage location charts are shown

in Figs. 9.10a-b, using the previous damage models. Both models located the damage correctly.

The defect location charts using the Cawley-Adams method for this frame are shown in Appendix 3 (see Figs. A3.8a-d). These charts show that the damage was correctly located only in Figs. A3.8a&c in which the two-cantilever model was used. This was expected: in both cases the reduced model was used and $\beta_1 \simeq 1$, which agrees with the assumptions. In Figs. A3.8b&d the damage was not located.

9.3.2 Tests with Various Crack Depths.

The frequency measurements shown in Table 8.7 for test on a symmetrical tower frame and cracks produced by spark erosion were used to produce defect location charts shown in Fig. 9.11a. The first crack was 1.5mm depth at position B. The reduction in rigidity of the whole element model was used to produce the theoretical frequency changes. It can be seen from Fig. 9.11a that the actual damage was located at the position with second highest $100R^2$ (=87 as opposed to the highest value of 88). The first crack was extended until a complete failure occurred. In order to predict the theoretical frequency changes due to damage at the middle of each member the two-cantilever model was used. The defect location chart in Fig. 9.11b shows that the crack was correctly located, even though each member was represented as one element and the damage was simulated at the middle of

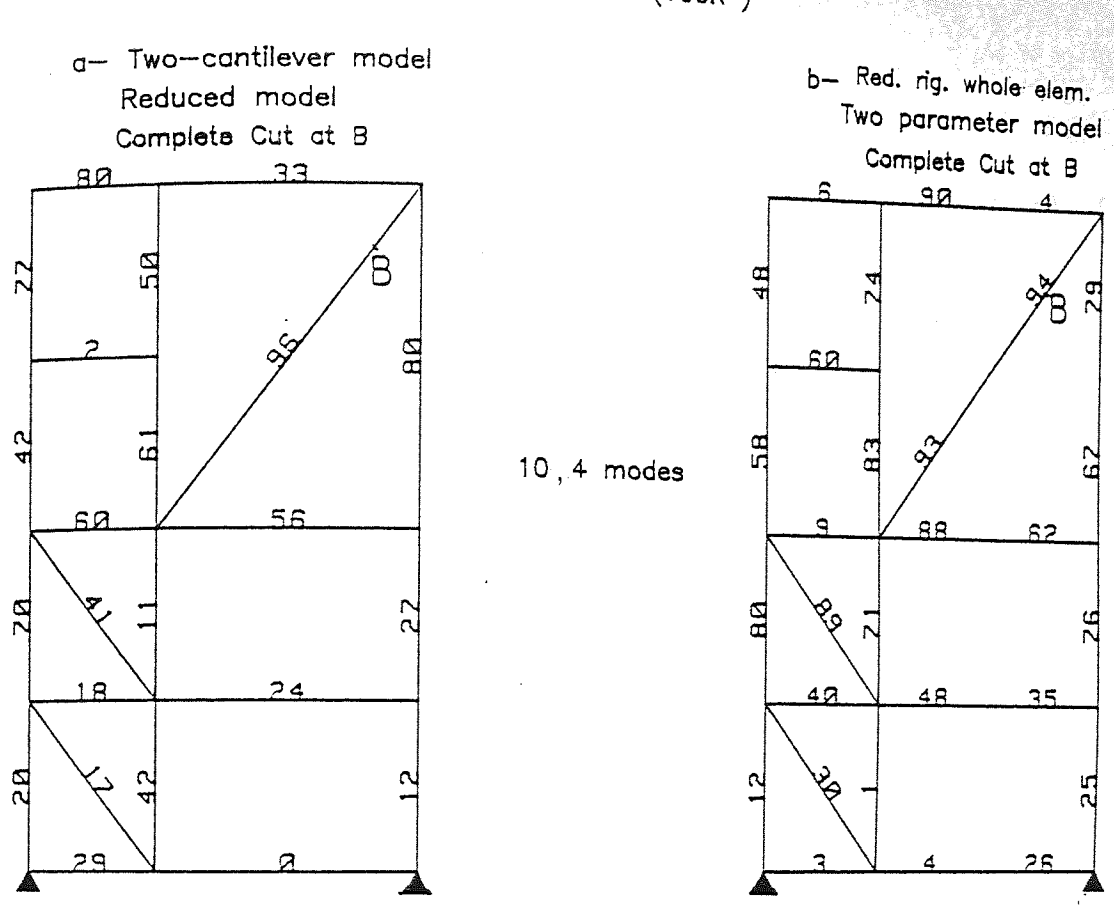

Fig. 9.10a–b DEFECT LOCATION CHARTS OF ASYMMETRIC TOWER FRAME FOR VARIOUS DAMAGE MODELS

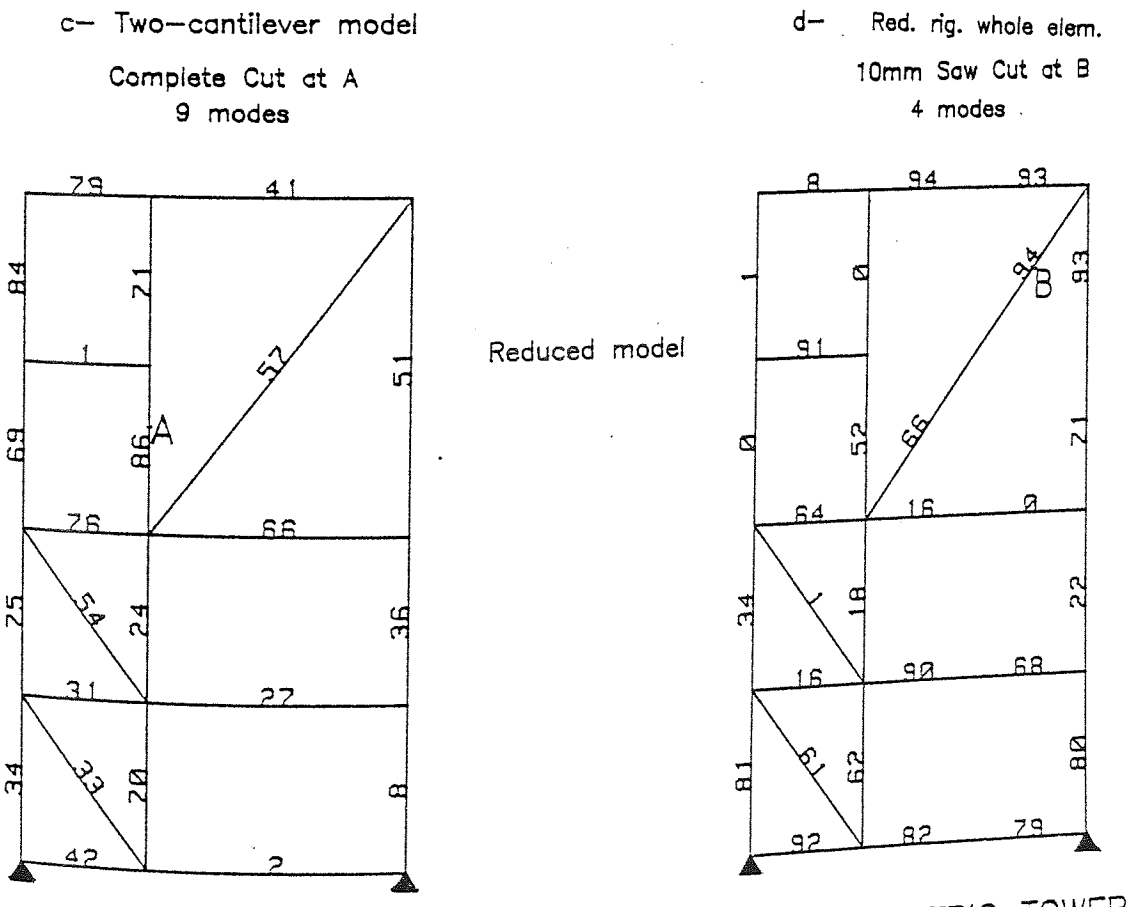

Fig. 9.10c–d DEFECT LOCATION CHARTS OF ASYMMETRIC TOWER FRAME FOR VARIOUS DAMAGE SITES

each member.

The defect location charts for this frame using the Cawley-Adams method are shown in Appendix 3 (See Figs. A3.9a-b). These charts show that the damage is correctly located only in Fig. A3.9b, for which the reduced model gave the estimate $\beta_1 \simeq 1$, see Table 9.4.

9.3.3 Tests with More Than One Damage Site.

In all the foregoing investigations the methods were applied when the damage was located at one site only. It would be difficult to amend the technique to enable the location of simultaneously occurring damage at two or more sites, a case which might arise infrequently. The methods were tested with damage at two sites B and C by using the measured frequency changes for Case I and Case II (see Table 8.8). The defect location charts for these cases are shown in Figs. 9.11c-d. For case I the reduction in rigidity of the whole element model was used and for case II the two-cantilever model. As might be expected the method can predict only one damage location. Thus, the chart in Fig. 9.11c predicted damage at position C by using case I and in Fig. 9.11d predicted damage at position B by using case II (hence "Yes/No" in columns six and twelve of Table 9.4). It might be said that the damage sites were located successfully by considering both cases, but the highest $100R^2$ values were only 54 and 64 respectively, indicating the difficulty of discriminating

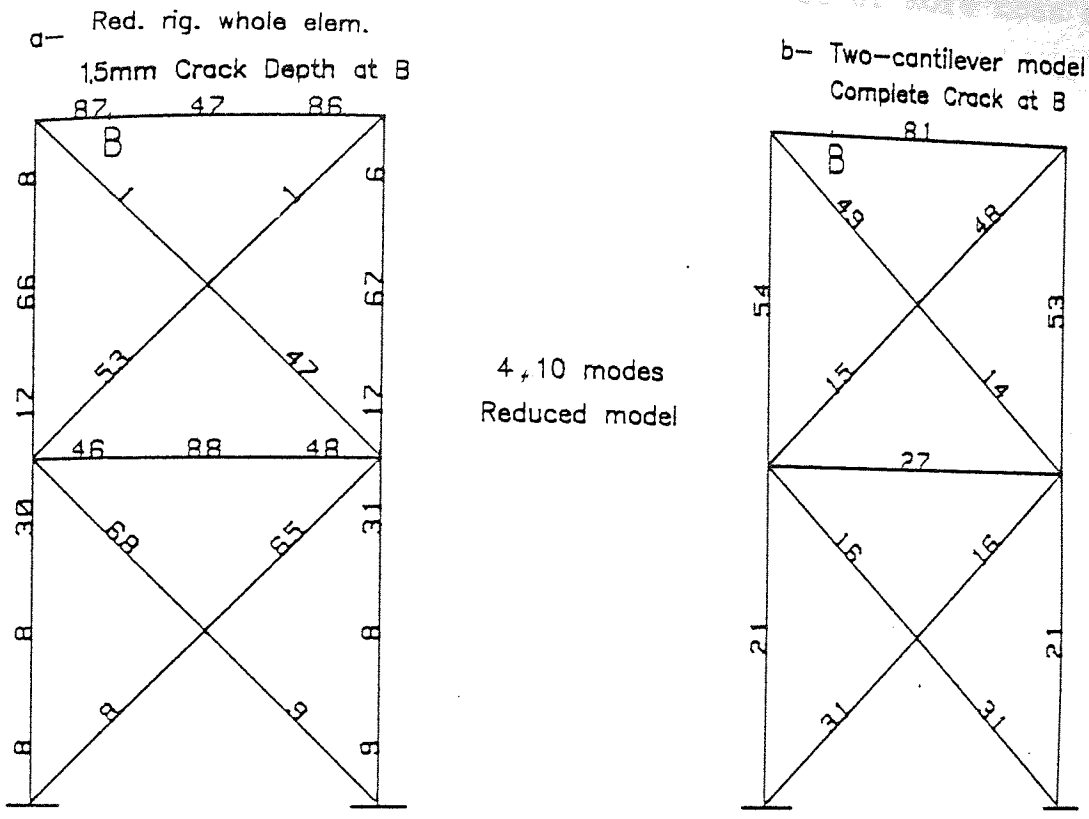

Fig. 9.11 a–b DEFECT LOCATION CHARTS OF SYMMETRIC TOWER FRAME 3 FOR VARIOUS CRACK DEPTHS

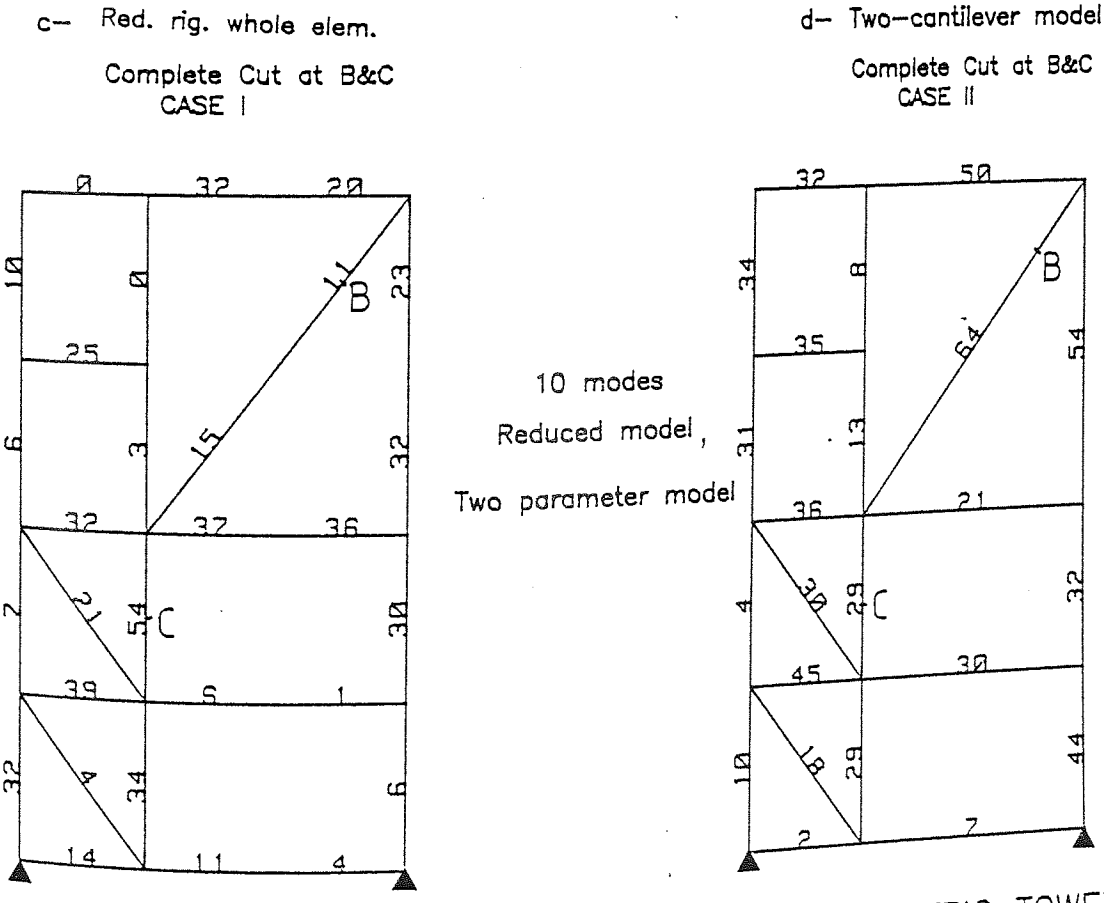

Fig. 9.11c–d DEFECT LOCATION CHARTS OF ASYMMETRIC TOWER FRAME WITH TWO DAMAGE SITES

between possible damage location in case of more than one damage in the structure.

The defect location charts using the Cawley-Adams method for these tests are shown in Appendix 3 (see Figs. A3.9c-d). In case I, the Cawley-Adams method gave the second highest NPE (=97) at C, but in case II it gave the highest NPE at B, superficially agreeing with the new method in both cases.

The normalised percentage error of the Cawley-Adams criterion (NPE) conceals the difficulty of discrimination highlighted by the new method. Also, the Cawley-Adams method has proved to be less generally reliable in locating the damaged member and the site of the damage within that member.

No. of modes	Damage position	Severity of damage	Theo. damage model	New method						Cawley–Adams		
				Fig. No.	Damage located	$100R^2$	Two–parameter model		Reduced	NPE	Damage located	Fig. No.
							β_0	β_1	β_1			
4	E	6 mm (30%)	Red. rig. whole elem. (30%)	9.9a	Yes	88			3(±.8)	57	No	A3.7a
4	E	10 mm (50%)	Red. rig. whole elem. (30%)	9.9b	Yes	99			1.6(±.1)	100	Yes	A3.7b
8	E	15 mm (75%)	Two–cant.	9.9c	Yes	28	−2.1(±.8)	.6(±.4)		31	No	A3.7c
9	E	3rd Compl. cut	Red. rig. whole elem. (30%)	9.9d	Yes	16			.2(±.15)	99	Yes	A3.7d
10	B	Complete cut	Two–cant.	9.10a	Yes	96			.99(±.1)	100	Yes	A3.8a
4	B	Complete cut	Red. rig. whole elem. (20%)	9.10b	Yes	94	−1.5(±.1)	−.2(±.1)		20	No	A3.8b
9	A	Complete cut	Two–cant.	9.10c	Yes	86			.9(±.1)	100	Yes	A3.8c
4	B	10 mm (50%)	Red. rig. whole elem. (20%)	9.10d	Yes	94			1.5(±.3)	59	No	A3.8d
4	B	1.5 mm (50%)	Red. rig. whole elem. (30%)	9.11a	No	87			−3.4(±.9)	34	No	A3.9a
10	B	Complete crack	Two–cant.	9.11b	Yes	81			1.5(±.3)	100	Yes	A3.9b
10	B&C	Complete cut	Red. rig. whole elem. (20%)	9.11c	Yes/No	54,11			.96(±.3) .3(±.3)	97,1	No	A3.9c
10	B&C	Complete cut	Two–cant.	9.11d	Yes/No	64,29	−.6(±.2) −1.1(±.2)	.6(±.2) .3(±.4)		100,33	Yes/No	A3.9d

TABLE 9.4 SUMMARY OF DEFECT LOCATION CHARTS FOR SYMMETRIC AND ASYMMETRIC TOWER FRAMES

9.4 TESTS ON SPACE FRAME STRUCTURES.

9.4.1 Space Frame Symmetric about Both Diagonals.

The defect location charts shown in Figs. 9.12a-b have been constructed from the data of Table 8.9 and predictions of frequency change based on the reduced rigidity of the whole element and the two-cantilever models respectively. The symmetrical space frame structure was damaged by complete failure at position A (at a quarter point on the upper diagonal member, as shown). Failure was correctly located for both damage models but four possible sites were indicated because of symmetry. Because the damage was located at one quarter of the diagonal member, it was necessary to divide most of the structural members into two elements, to locate the position of the damage not only in the right structural member but also in the correct element of that member, using either the reduced rigidity or the two-cantilever model. It can be seen that the values of $100R^2$ of Fig. 9.12b were similar for the most of the damage sites. This may on account of the theoretical frequency changes being of the same order for most of the damage sites, as shown in Figs. 7.12a-f.

Defect location charts using the Cawley-Adams method for these tests are shown in Appendix 3 (see Figs. A3.10a-b). These charts show that the damage was not correctly located using the reduced rigidity model whereas it was successful for the two-cantilever model. This may be explained by the values of β_1 shown in Table 9.5: the reduced model gave a

New method ($100R^2$)

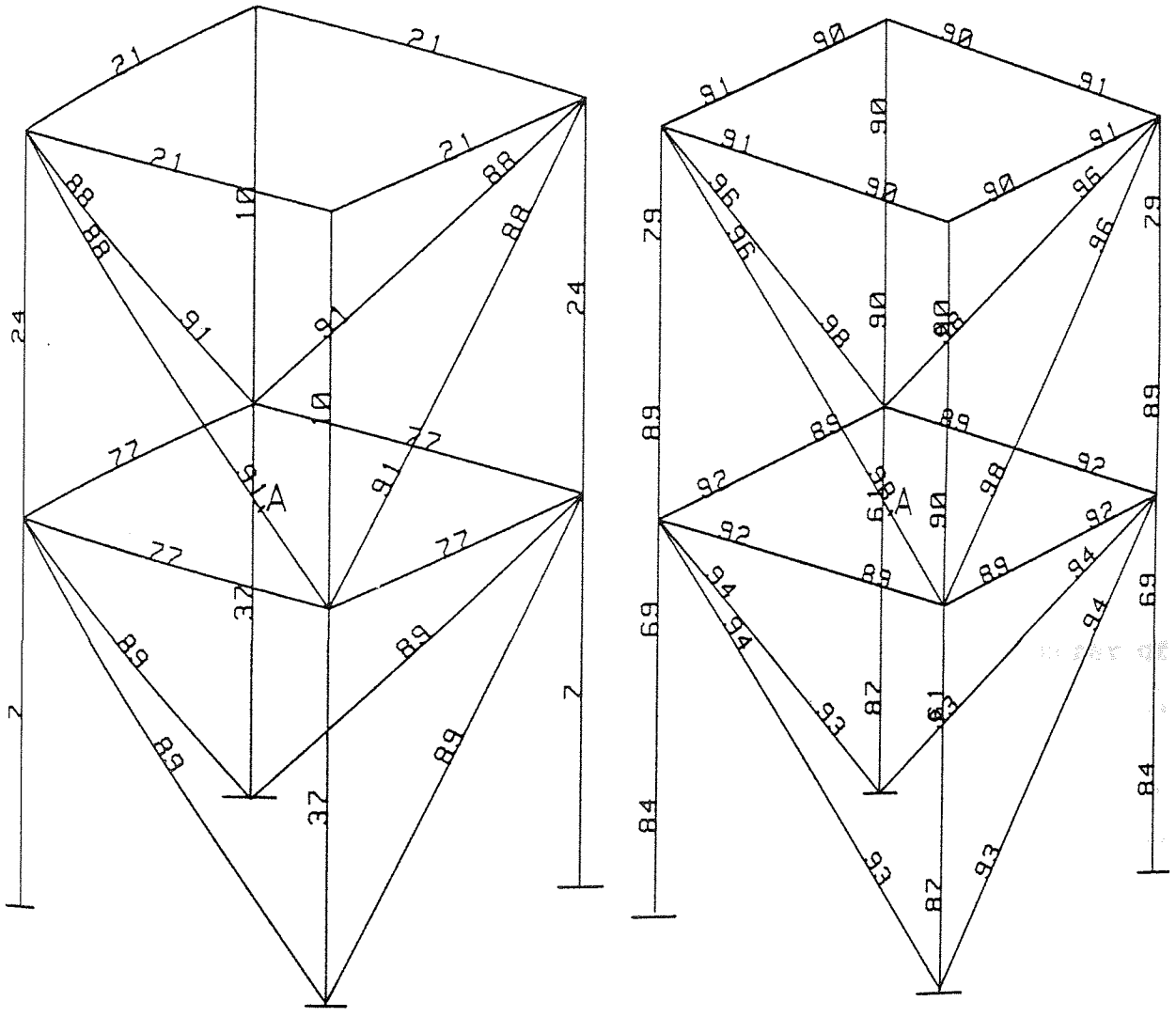

a– Complete Saw Cut at A
Red. rig. whole elem.
Reduced model
4 modes

b– Complete Saw Cut at A
Two–cantilever model
Reduced model
8 modes

Fig. 9.12a–b DEFECT LOCATION OF SYMMETRICAL SPACE FRAME FOR VARIOUS DAMAGE MODELS(CUT AT A)

negative value for β_1 using the reduced rigidity model but a value of 1 for the two-cantilever model.

The number of modes are varied to study the effect of the defect location analysis using the Cawley-Adams method. Measurements from modes 1 to 10 were considered and each mode neglected in turn. This procedure was repeated by considering modes 2 to 10 and so on up to modes 9 to 10. Over forty tests were carried out on the same symmetrical space frame. Defect location charts were produced from the frequency measurements set out in Table 8.9 and from the theoretical frequency changes predicted for the removal of a structural member. Results of these tests are shown in Appendix 3 (see Table A3.1). As can be seen the damage was successfully located for most cases. From this it can be concluded that the number of modes recommended for use depends on the damage model and also on the accuracy of the measurement of the frequency changes. If these were chosen any number of modes could be selected. This is an advantage of the method which permits the selection of the number of modes.

A further test was carried out on this structure with complete failure at position B (Figs. 9.13a-b) after the damage at A had been repaired by welding. The defect location charts produced from the frequency measurements set out in Table 8.9 are shown in Figs. 9.13a-b. Two damage models were used in order to produce the theoretical frequency changes the first by member removal, and the second the two-cantilever model. In both cases damage was successfully

located. Again, two possible sites were indicated because of symmetry.

Defect location charts using the Cawley-Adams method for these tests are shown in Appendix 3 (see Figs. A3.11a-b). These charts show that the damage was not correctly located when damage was modelled by removal of the member whereas it was successful when the two-cantilever model was used. As shown in Table 9.5 the two parameter model was used in Fig. 9.13a, whereas the reduced model was used in Fig. 9.13b. This may account for the above findings.

Also, by employing the two-cantilever model for calculating the theoretical frequency changes, the Cawley-Adams method was applied by considering all the modes 1 to 10, then with each mode neglected in turn. This procedure was repeated by considering modes 2 to 10 and so on up to modes 9 to 10. On each occasion the defect location charts were obtained. The results of these tests are shown in Appendix 3 (see Table A3.2). It was discovered that the damage was located successfully for most of the modes considered. Table A3.2 also shows that when only the higher modes are considered the probability of the damage location is less than when the lower modes are included. This may be because in the higher modes the theoretical frequency changes are insensitive to the damage (see Figs. 7.12a-f). It may be concluded that the two-cantilever model should be used for most of the remaining evaluations.

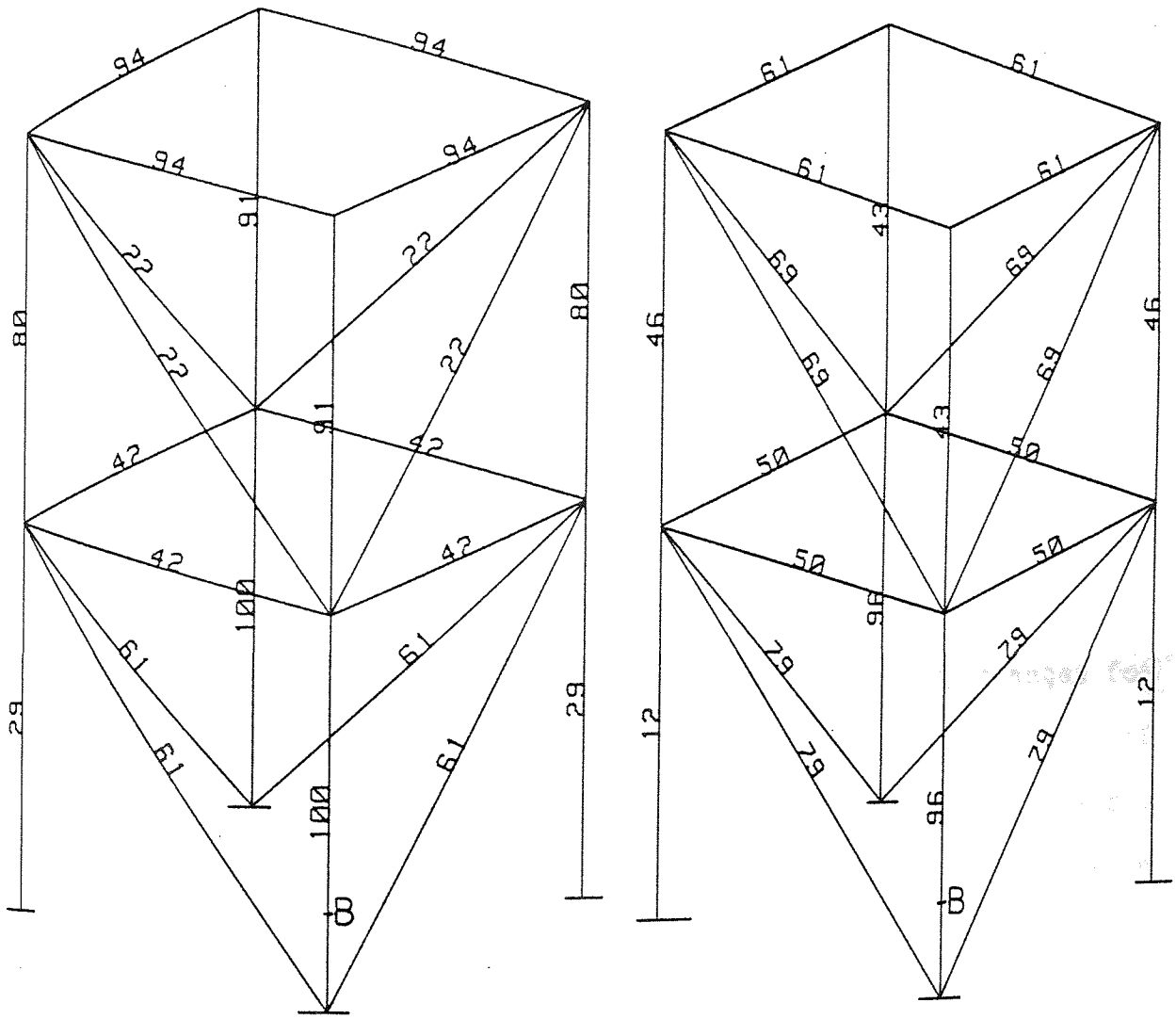

a– Complete Saw Cut at B
Member removal
Two parameter model
4 modes

b– Complete Saw Cut at B
Two–cantilever model
Reduced model
10 modes

Fig. 9.13a–b DEFECT LOCATION OF SYMMETRICAL SPACE FRAME FOR VARIOUS DAMAGE MODELS(CUT AT B)

9.4.2 Space Frame Symmetric about One Diagonal.

Figures 9.14a-b and 9.15a show the defect location charts for this structure damaged by removal of 60% and 70% of cross-sectional area and by complete failure at position A respectively. The charts use the frequency measurements of Table 8.10 and theoretical frequency changes predicted from the two-cantilever model. It is seen that the damage is correctly located for each case. Also, referring to these figures, the values of $100R^2(34,35,53)$ are increased as the damage increases. The small values may be due to the use of the two-cantilever model, which represents the damage as a complete failure, even for the partial damage. Another possible reason is that the theoretical frequency changes for most modes were insensitive to the damage at the middle of each member, as explained in section 7.4 (see Figs. 7.14a-c). As the method was successful in these conditions, this is an indication that it can be used in practice.

Defect location charts using the Cawley-Adams method for these tests are shown in Appendix 3 (see Figs. A3.12a-b and Fig. A3.13a). Damage was incorrectly located as shown in Fig. A3.12a. The second highest NPE occurred at the actual damage site as shown in Fig. A3.12b and in the case of complete failure damage was correctly located (Fig. A3.13a). The reasons for these findings may be discovered from Table 9.5, where it is seen that β_0 and β_1 are not significant.

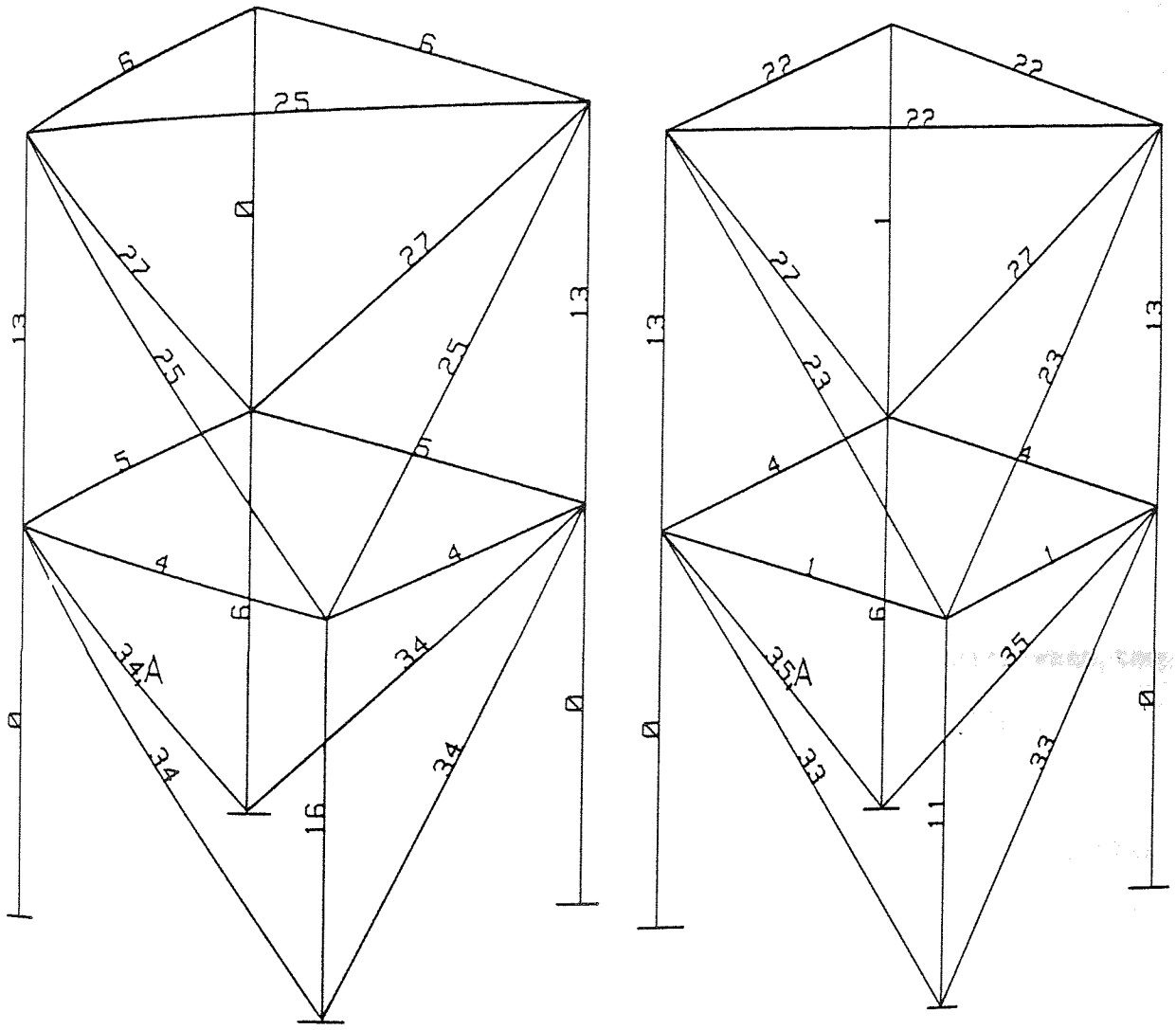

a– 60% Saw Cut of Cross Sectional Area at Position A

Two–cantilever modal
Reduced model
10modes

b– 70% Saw Cut of Cross Sectional Area at Position A

Two–cantilever model
Two parameter model
10 modes

Fig. 9.14a–b DEFECT LOCATION OF SYMMETRICAL SPACE FRAME ALONG ONE DIAGONAL WITH VARIOUS SAW CUT DEPTHS

9.4.3 Non-Symmetrical Space Frame.

Figure 9.15b shows the defect location chart for this structure damaged by complete failure at position A. The chart uses the frequency measurement of Table 8.11 and the theoretical frequency changes predicted from the two-cantilever model. It is seen that the actual damage is located at the position with second highest $100R^2$ (=78 as opposed to the highest value of 89). This may be due to the fact that this structure had been repaired. Another possible reason was mentioned in section 7.4: the percentage frequency changes were approximately 7% when damage was simulated at the middle of the members. For the same reasons the second highest NPE occurred at the actual damage site when the Cawley-Adams method was used (Appendix 3, Fig. A3.13b).

Figures 9.16a-b shows the defect location charts for this structure with a 40% crack of the cross-sectional area and complete failure at position B respectively, following repair by welding of the damage at A. The charts use the frequency measurements of Table 8.11 and the predicted frequency changes were obtained either by the reduction in rigidity of the whole element or the two-cantilever model. Figs. 9.16a-b show that the damage was correctly located in both cases.

Defect location charts using the Cawley-Adams method for these tests are shown in Appendix 3 (see Figs. A3.14a-b). In both cases the damage was correctly located. This was

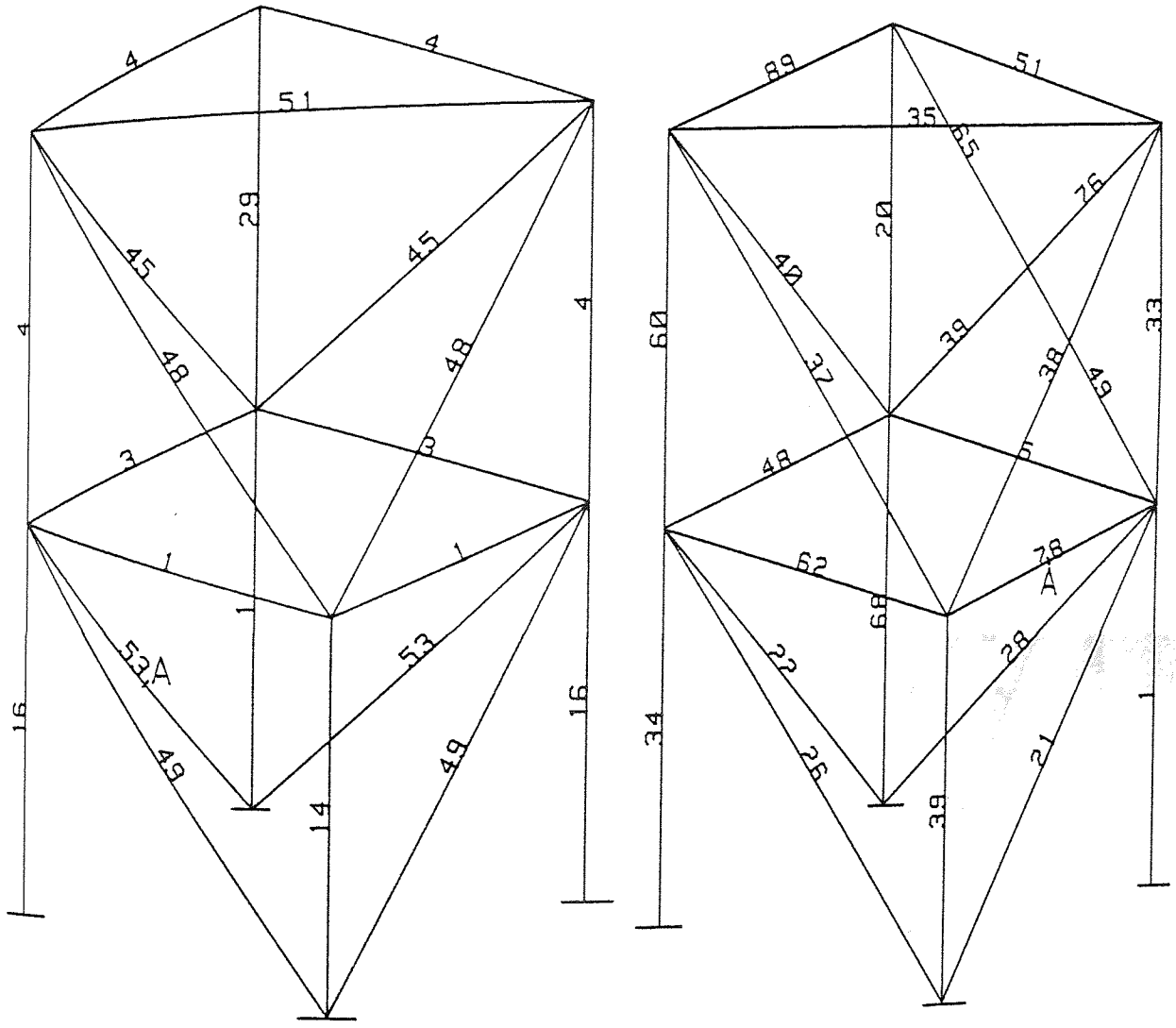

a– Complete Saw Cut at A
Two–cantilever model
Two parameter model
9 modes

b– Complete Saw Cut at A
Two–cantilever model
Reduced model
10 modes

Fig. 9.15a–b DEFECT LOCATION OF SYMMETRICAL AND ASYMMETRICAL SPACE FRAME MODELS

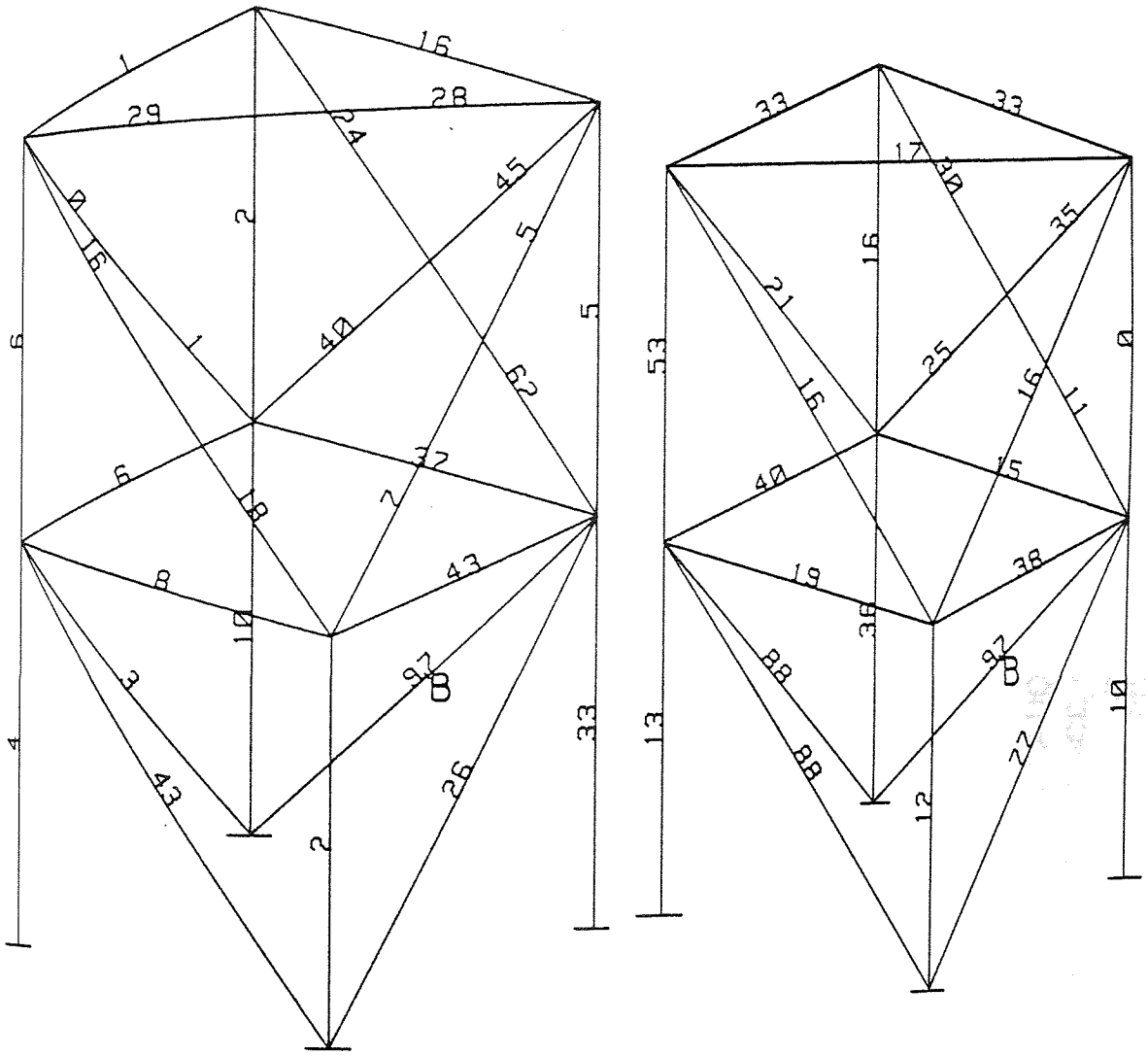

a– 40% Crack Depth at B
Red. rig. whole elem.
8 modes

b– Complete Crack at B
Two–cantilever model
10 modes

Fig. 9.16a–b DEFECT LOCATION OF ASYMMETRICAL SPACE FRAME MODEL WITH VARIOUS CRACK DEPTHS

No. of modes	Damage position	Severity of damage	Theo. damage model	New method						Cawley–Adams		
				Fig. No.	Damage located	$100R^2$	Two parameter model		Reduced	NPE	Damage located	Fig. No.
							β_0	β_1	β_1			
4	A	Complete cut	Red. rig. whole elem. (100%)	9.12a	Yes	91			−3.5(±.8)	18	No	A3.10a
8	A	Complete cut	Two–cant.	9.12b	Yes	98			1.1(±.1)	100	Yes	A3.10b
4	B	Complete cut	Member removal	9.13a	Yes	100	3(±.1)	−.9(±.2)		82	No	A3.11a
10	B	Complete cut	Two–cant.	9.13b	Yes	96			.9(±.1)	100	Yes	A3.11b
10	A	6 mm (60%)	Two–cant.	9.14a	Yes	34			−5.3(±2.6)	57	No	A3.12a
10	A	7 mm (70%)	Two–cant.	9.14b	Yes	35	−1.6(±.6)	−2(±1.4)		65	No	A3.1 b
9	A	Complete cut	Two–cant.	9.15a	Yes	53	.11(±.16)	.8(±.3)		100	Yes	A3.13a
10	A	Complete cut	Two–cant.	9.15b	No	78			.9(±.2)	83	No	A3.13b
8	B	4 mm (40%)	Red. rig. whole elem. (50%)	9.16a	Yes	97			1.1(±.1)	100	Yes	A3.14a
10	B	Complete crack	Two–cant.	9.16b	Yes	97			1.1(±.1)	100	Yes	A3.14b

TABLE 9.5 SUMMARY OF DEFECT LOCATION CHARTS FOR SYMMETRIC AND ASYMMETRIC SPACE FRAMES

expected because the new method indicated the reduced model with $\beta_1 = 1$, so that the Cawley-Adams assumptions would more or less apply, see Table 9.5.

9.4.4 Simulate the Effect of Experimental and Other Errors.

In most of the previous tests it was found that $\beta_0 \neq 0$ and $\beta_1 \neq 1$ hence, another test using the Cawley-Adams method was performed to show that these parameters should be considered. When measuring frequency changes experimentally there may be an element of error attributable to an experimental factor. Thus, experimental frequency changes may be generated from either the theoretical or experimental changes in frequency after multiplying these values by random error. In an attempt to examine the effect of this on damage location a theoretical study was undertaken as follows;

$$Dltaw(I) = Dltaw(I) * \{1 - P*(1 - 2*RND)\} \qquad (9.1)$$

or

$$Dltaw(I) = Sen(J,I) * \{1 - P*(1 - 2*RND)\} \qquad (9.2)$$

Where

I = Identifies the modes considered (I= 1-N),

Sen(J,I) = Sensitivity matrix (Theoretical changes in natural frequencies I due to reduction in stiffness of element J),

Dltaw(I) = Experimental changes in natural frequency I

RND = Random variable in the range of 0 to 1,

{1 - P*(1 - 2*RND)} = Random Error (RE),

P = Variable which will define the multiplication factor, e.g. if P=0.1, random error of ±10%.

By using equation 9.1, for P equal 0.2 (i.e. RE = ±20%) and by generating a random number 100 times, the defect location probability in each element, 1 to 48, was calculated for the damage at position A of the same space frame mentioned in section 9.4.1. The theoretical frequency changes were calculated using the two-cantilever model. The results of the defect location analysis are presented as a bar chart, shown in Appendix 3 (see Fig. A3.15a). Also, Fig. A3.15b represents the results of defect location for P equal 0.3 (i.e. RE = ±30%). Again, the damage was accurately located not only in the correct member but also in the exact element.

The above procedure was repeated using equation 9.2 for the same tests and the results are shown in Appendix 3 (see Figs. A3.16a-b). The damage is correctly located for any modes which were considered and the percentage location of exact element is higher as the number of modes increased.

Further tests were carried out on the same structure mentioned in section 9.4.3 for the case of a complete crack at position B and using the Cawley-Adams method. Setting P=0.3 in equation 9.1 (i.e. the experimental frequency changes are varied in the range ±30%) and by generating a random number 100 times (see equation 9.1), the probability of defect location was calculated. The true damage site was

correctly located by 80% of the predictions while the damage site corresponded to the position with second highest NPE for 20% of predictions using the first ten modes. The results of this test are not shown.

9.5 CLOSING REMARKS.

The damage location techniques described earlier in this thesis and the results shown in this chapter, rely for their success on the measurements of small changes in natural frequencies and on the theoretical prediction of these frequency changes. The results of this chapter show that these methods can be used to detect and locate damage not only in the structural member, but also in the correct element within the member. The Cawley-Adams method depends on the parameters β_o =0 and β_1 =1. Investigation has shown that these values are frequently quite different. The new method overcomes this problem.

Tests have shown that damage equivalent to a crack through 20% of the cross-sectional area of the plane frame structure can be located. Also, with space frame structures, damage equivalent to a crack through 40% of the cross-sectional area can be located.

The method has the advantage that only one dynamic finite element analysis needs to be performed on a given type of structure. Also, it can be applied to large structures in the

field much more easily than any other method. It is possible to use the method to monitor the growth of damage without the need to have measured the frequencies of the virgin structure by using a damaged state as the baseline for future measurements.

In spite of the crude model used in some of the tests, damage was still accurately located. Thus, it is hoped that this technique will prove a useful method of in-service condition monitoring for plane and space frame structures obviating the need to use the expensive and inconvenient conventional tests.

In the following chapter, a general discussion and conclusions of the whole research, as well as recommendations for further work are presented.

CHAPTER TEN

DISCUSSION, CONCLUSION AND RECOMMENDATIONS FOR FURTHER WORK

10.1 Discussion.

10.1.1 General Theoretical Discussion.

10.1.2 General Experimental Discussion.

10.1.3 General Defect Location Discussion.

10.2 Conclusion.

10.3 Recommendations for Further Work.

10.1 DISCUSSION.

The location of damage by frequency monitoring has been shown to require the accurate prediction of frequency spectra both for the undamaged and damaged structure and a statistical comparison of these predictions with measured values. It is convenient to discuss the principle areas of the investigation under three headings.

I- The theoretical analysis developed for calculating the changes in mode shapes and natural frequency spectrum.

II- The experimental technique developed for measuring inertance to the required accuracy.

III- The statistical techniques developed for defect location analysis.

10.1.1 General Theoretical Discussion.

The natural frequencies and associated mode shapes for the structure, based on both the exact displacement function and the polynomial displacement function methods, have been compared using the finite element analysis. The prediction of frequency spectra using the polynomial displacement function leads to the formulation of frequency independent mass and stiffness matrices and thus to the solution of a linear eigenvalue problem. Using this method, the accuracy of the results depends on the number of elements into which the

structure is divided: the greater the number of elements the more accurate the result. However, a very high accuracy requires a large computer facility and hence the method is limited by the computing system available. For a reasonable number of elements, the calculated lower natural modes are a good approximation to the exact solution. A great advantage of this method is that perturbation analysis can be used to determine the changes in frequency caused by small changes in stiffness. This is simpler and quicker than resolve the EVP.

The exact displacement function leads to the frequency dependent dynamic stiffness matrix and thus to the resulting non-linear EVP. The determinant method of solution, together with an algorithm providing the sign count and asymptotic pole count, proved to be an infallible means of finding the eigenvalues. It was found to be sufficient to treat each complete member of a complex structure as an element: no further sub-division was necessary.

For the exact displacement method the frequency changes need the EVP to be re-calculated for each damage position, whereas for the polynomial displacement function a single dynamic analysis is needed. The first method saves computing capacity at the expense of time; the second saves time at the expense of capacity. The exact method was preferred on account of its accuracy and the limited computing capacity available.

Five different models of damage have been tested in this study. The adequacy of damage modelling was tested by the

comparison of theoretical predictions with experimental measurements from simple structures. The portal frame, in particular, showed that if the nodal reduction in stiffness is represented by a torsional spring, a good agreement is obtained with the experimental measurements. This spring model is a good representation of a local reduction in stiffness, especially for partial damage. The spring and the other models are expensive in computing time and capacity (when applied to a complex structure) unless the overall mode shapes are already known. In this case it is possible to use perturbation analysis to avoid any need to re-solve the EVP. It is evident from the results shown in chapter nine, that the complete failure represented by the two-cantilever model proved to be more accurate in predicting the frequency changes.

In the vibrational analysis of a cantilever, it is observed that the more heavily loaded is the member, the bigger will be the effect of its failure on the vibrational characteristics of the structure.It is clear from the results obtained for different damage models and differing extents of the damage at various positions that the resonant frequencies are sensitive to damage. Generally, as may be expected it can be seen that as the depth of the cut increases (or as the stiffness decreases), so the natural frequencies decrease.

10.1.2 General Experimental Discussion.

The most important part in the experimental investigation was to perfect a measuring technique for obtaining the inertance data. To obtain such extremely high quality measurements was not only demanding in terms of the quality of instrumentation, but also required a great degree of care in the experimental technique.

In the test configuration which was adopted the structure was connected to a vibrator via a decoupler assembly and force transducer. For convenience and to ensure maximum force measuring accuracy, the force transducer was connected directly to the structure. The transducers and the adapter are within the measuring system boundary and the resulting inertance includes these extra elements. For a light structure these elements may be considered as concentrated masses; an additional dummy mass is required within this measuring system boundary in order to maintain consistency when measuring the cross-inertance. A useful way of checking the accuracy of the measurements was to compare cross-inertance, since the reciprocity relationships should be maintained for a linear system. However, it is changes in frequencies which are ultimately required and not the magnitude of inertance, hence the effects of these additions were cancelled out. In order to obtain meaningful results from a structure, before and after damage, it was necessary to maintain consistency in all the boundary conditions between both tests.

If the inertance measurement is made at a point for which the modal shape vector has zero magnitude at a certain frequency, then no peak will occur at that natural frequency. So, the measurement of resonance depends on the positions at which the input force is applied and the accelerometer located. High dynamic ranges are associated with low damped structures and a change of 80 dB´s from an anti-resonant to a resonant peak in the inertance levels was found to be typical. Fortunately, the frequency response analyser and the spectrum analyser used in the investigation were able to measure in a dynamic range in excess of 80 dB.

It was noted that for a point inertance resonances and anti-resonances alternate along the frequency axis. There is not always a true anti-resonance between adjacent resonances in the transfer inertance.

The tests carried out show that the presence of a crack in a structural member will produce a change in the vibration characteristics of the structure, in the form of reduced natural frequencies. Thus, one of the first major decisions to be made in the experimental work was that of crack representation. As already discussed, it was found that a fatigue crack could be detected as easily as a saw cut. However, since saw cuts are much easier to produce and to control than fatigue cracks, the hacksaw cut was used as a means of crack representation. As can be seen from the tests with saw cuts the damage equivalent to cutting through less than 20% of the cross-sectional area was detected.

10.1.3 General Defect Location Discussion.

Two statistical approaches have been used to locate structural damage. The first one, based on the method of Cawley and Adams, was applied to plane and space frame structures. The results discussed in chapter nine and shown in Appendix 3 indicate that this method can be used to locate damage in such structures, although some inaccuracies exist in part of the results due to the assumption that the parameters β_0 and β_1 defined in Cawley-Adams are assumed to be 0 and 1 respectively.

The second approach was based on a generalised least squares regression model. From the results surveyed in chapter nine, it is clear that this method could be used to locate damage in a structural member that is not easily accessible for inspection. It has the advantage of being easily applicable to steel frames. The results from a wide range of the structures indicate that the method does not require great accuracy in the analysis of the structure, depending only on the relative frequency changes in the different modes caused by damage at a given site. Consequently, this technique would be well suited in the practical situation.

The results of the defect location analysis in the previous chapter are summarised in Figs. 10.1 and 10.2, to show how the new method (GLS) compares with Cawley-Adams method to

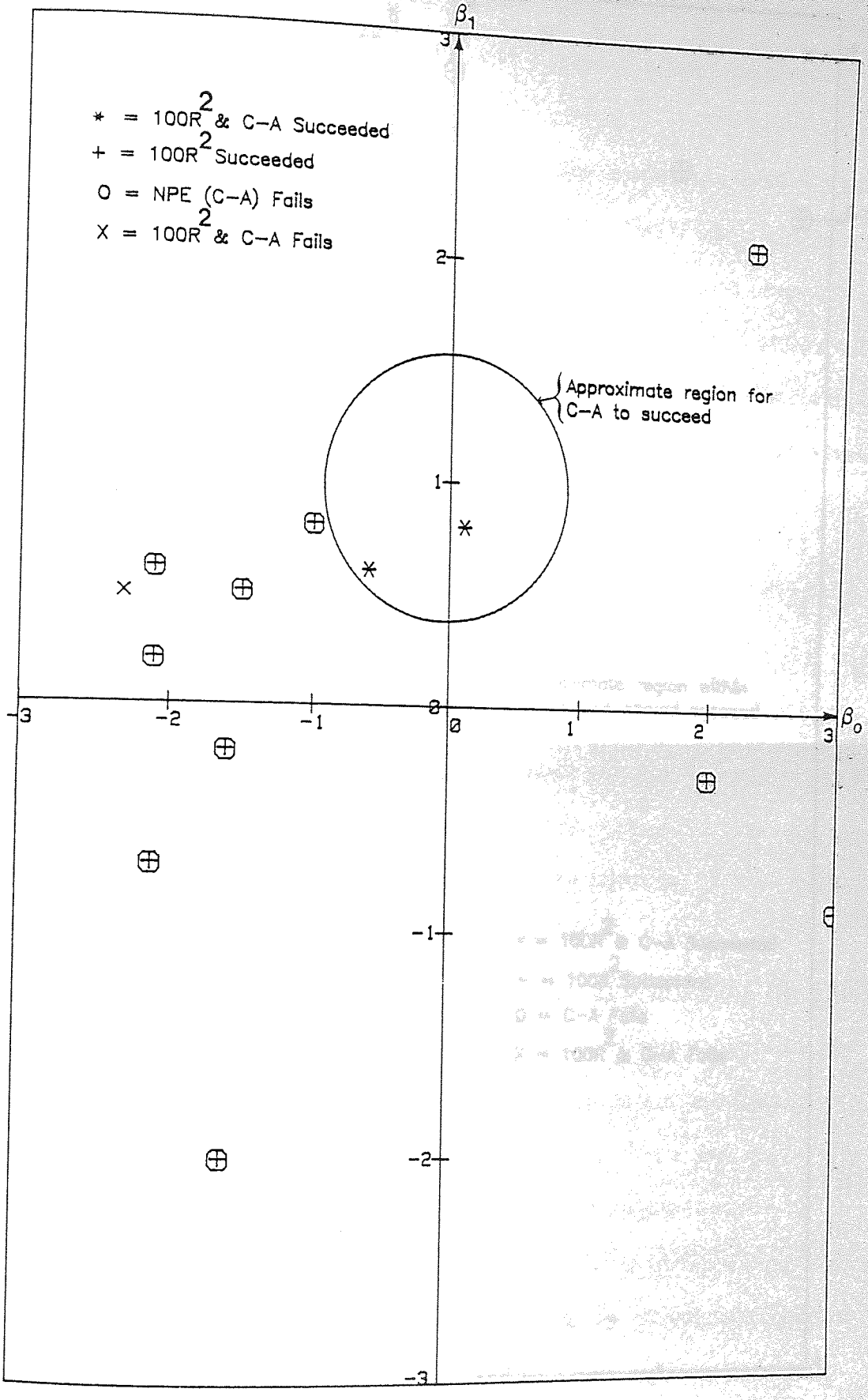

Fig. 10.1 SYNOPSIS OF DEFECT LOCATION RESULTS WHEN 2-PARAMETER MODEL IS OPTIMAL (Based on Tables 9.2 TO 9.5)

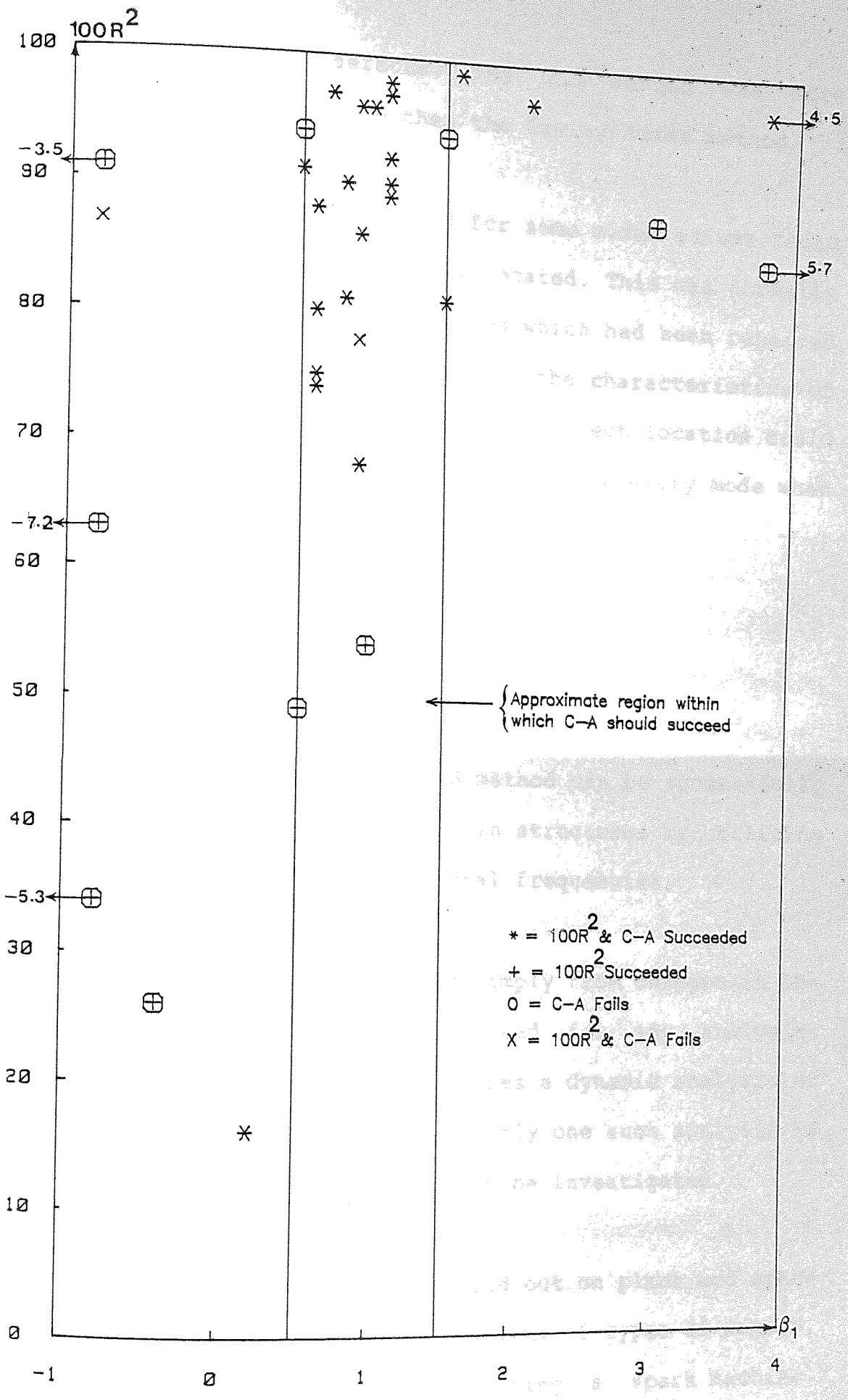

Fig. 10.2 SYNOPSIS OF DEFECT LOCATION RESULTS WHEN 1–PARAMETER MODEL IS OPTIMAL (Based on Tables 9.1 TO 9.5)

detect the structural defects. The GLS method was more successful in locating damage than the Cawley-Adams method.

In a small number of cases and for some modes it was found that the damage was incorrectly located. This was normally associated with tests on structures which had been repaired by welding, with consequent changes in the characteristics of the material. On other occasions the incorrect location could be attributed to the difficulty of measuring every mode when resonant frequencies lay close together.

10.2 CONCLUSION.

The test results show that the GLS method can be successfully used to detect and locate damage in structures by utilizing measurements of the structures natural frequencies.

The presence of damage is detected simply from changes in the natural frequencies without the need for any analysis. Locating the damage, however, requires a dynamic analysis of the structure to be carried out. Only one such analysis is required for each type of structure to be investigated.

Tests have been successfully carried out on plane and space frame steel structures, with a variety of types of damage, including saw cut, crack and by using a spark machine. Throughout the investigation, instrumentation techniques have been developed which are capable of measuring the structural

frequencies with sufficient accuracy and reliability for monitoring purposes. Also, changes in natural frequencies due to minor structural failure, are clearly observed and confirm the validity of this technique as a means of inspection for the onset of structural damage.

The major observations and conclusions which can be drawn from this study may be listed as follows:

1- The damage of a structural member will produce appreciable changes in some natural frequencies and comparatively small changes in others. The effects will depend on the location of the damage and will increase as the extent of the damage increases. Therefore, damage of the structural member can be detected by these changes.

2- It was established that except for a few of the most insignificant members, the determination of changes in natural frequency was accurate enough to indicate the particular structural member which had suffered damage. However, symmetrically disposed members would produce identical changes.

3- In laboratory conditions excellent agreement has been found between the predicted and actual location of damage sites.

4- Maximum amplitudes in the mode shapes are generally reached at points near the site of damage, although in some

modes maximum amplitudes arise at other locations.

5- Good agreement was obtained between the experimental and theoretical results both for the integral structures and the damaged structures. The effect of the structural damping was not considered in the dynamic analysis.

This complicated engineering problem was conveniently handled by a desk-top computer with a suitable memory size, which was also used as a control element for the experimental programme, allowing the work to be performed quickly and accurately. It would be possible to introduce the computer programs within a CAD package to provide a useful design tool for both plane and space frames, and for this reason the programs have been designed to be used easily by engineers with limited computer experience.

10.3 RECOMMENDATIONS FOR FURTHER WORK.

The following recommendations for further study are made to improve the present work and to carry this research forward:

1- The coverance matrix used in the GLS method is only based on what seems a reasonable assumption, namely that observations of frequency changes become more inaccurate (as measured by their variance) in direct proportion to the mode number. There is no direct proof that this is justified and further work might indicate a different relationship between

variance and mode number.

2- The computer programs were implemented in general terms which makes it feasible to investigate the effect of mass on natural frequencies and mode shapes of a structure under different boundary conditions. This may be useful for other engineering applications.

3- Other types of space frame models should be investigated, e.g. K-braced, with the geometric proportions of an oil rig structure.

4- A further study of a more realistic situation, would be to investigate the effect of hydrodynamic forces on the dynamic characteristics of the structure. One method would be to surround the structure with water, e.g. a large tank of water with appropriate dimensions, surrounding the rig.

5- As the structures tested in the experimental programme were constructed with welded joints, it might be worthwhile to investigate one using bolted joints.

APPENDIX 1

THEORY OF LEAST SQUARES METHODS

A1.1 Ordinary Least Squares (OLS).

A1.2 Generalised Least Squares (GLS).

A1.3 The Transformation Matrix.

A1.4 Adequacy of a Regression Model.

A1.5 Reduced Regression Models.

A1.6 Confidence Limits for Regression Coefficients.

A1.1 Ordinary Least Squares (OLS).

Further details of the standard theory summarised below are given in a convenient form by Johnston, chapters 5 and 7 (65).

Suppose there are n pairs of observations, (x_i, y_i) for i=1 to n, in which it is assumed each x_i and y_i are related by a model

$$y_i = \beta_0 + \beta_1 x_i + \varepsilon_i \quad , \qquad (A1.1)$$

where β_0 and β_1 are unknown constants and ε_i is a random error, whose properties are considered in more detail below.

If β_0 and β_1 are estimated by b_0 and b_1 respectively, the model may also be written

$$y_i = b_0 + b_1 x_i + e_i \quad , \qquad (A1.2)$$

Where $e_i = y_i - (b_0 + b_1 x_i)$ can be considered as an estimate of the random error, ε_i, and is called a residual.

In the ordinary least squares (OLS) method, b_0 and b_1 are chosen, so as to minimise the sum of squared residuals,

$$\Sigma e_i^2 = \sum (y_i - b_0 - b_1 x_i)^2 \qquad (A1.3)$$

Where Σ denotes summation over all values of i from 1 to n.

This may be restated in matrix terms as follows.

Let

$$y = \begin{Bmatrix} y_1 \\ y_2 \\ . \\ . \\ y_n \end{Bmatrix}, \quad x = \begin{Bmatrix} x_1 \\ x_2 \\ . \\ . \\ x_n \end{Bmatrix}, \quad \varepsilon = \begin{Bmatrix} \varepsilon_1 \\ \varepsilon_2 \\ . \\ . \\ \varepsilon_n \end{Bmatrix}, \quad e = \begin{Bmatrix} e_1 \\ e_2 \\ . \\ . \\ e_n \end{Bmatrix}, \quad \beta = \begin{Bmatrix} \beta_0 \\ \\ \beta_1 \end{Bmatrix} \text{ and } b = \begin{Bmatrix} b_0 \\ \\ b_1 \end{Bmatrix}$$

Also let $X = (u,x)$, where u denotes an n*1 vector in which each element is unity. This model may then be written

$$y = X\beta + \varepsilon = Xb + e \qquad \text{(A1.4)}$$

and, using the (t) to denote a transpose, the sum of squared residuals is

$$e^t e = (y - Xb)^t (y - Xb) . \qquad \text{(A1.5)}$$

It is convenient to define

$$A = X^t X = \begin{bmatrix} a_{00} & a_{01} \\ \\ a_{10} & a_{11} \end{bmatrix} \quad \text{and} \quad g = X^t y = \begin{Bmatrix} g_0 \\ \\ g_1 \end{Bmatrix} . \qquad \text{(A1.6)}$$

Then the b which minimises $e^t e$ can be shown to satisfy what are called the normal equations, which may be written simply in matrix form as $Ab = g$. Hence it follows that $b = A^{-1}g$.

This solution for b provides the best linear unbiased estimate of β, provided that the random error terms are

independent and identically distributed, each with zero mean and a constant variance, say σ^2 . Using matrices and the expectation operator, E, these conditions may be stated compactly by saying that it is required that $E(\varepsilon)$ be 0, a null n*1 vector, and $V = E(\varepsilon\varepsilon^t)$, known as the covariance matrix of ε , be of the form $\sigma^2 I$, where I is an n*n identity matrix.

A1.2 Generalised Least Squares (GLS).

If the random errors in the regression model have a covariance matrix $V = \sigma^2\Omega$, where Ω is some symmetric positive definite matrix which is not an identity matrix, then the $b = A^{-1}g$ given by the OLS method, while still an unbiased estimate of β , is no longer the best linear unbiased estimate. However, such an estimate can be found when $V = \sigma^2\Omega$ by using the generalised least squares (GLS) method proposed by Aitken (**66**), which involves a transformation of the original variables.

Suppose that $y = X\beta + \varpi$, where ϖ denotes a vector of random errors with $E(\varpi) = 0$ and $E(\varpi\varpi^t) = \sigma^2\Omega$. Provided that Ω is positive definite, there exists a matrix P such that $P\Omega P^t = I$ and this may be used to transform ϖ to $\varepsilon = P\varpi$, so that the transformed random errors, ε , will have a covariance matrix $E(\varepsilon\varepsilon^t) = \sigma^2 E(P\Omega P^t) = \sigma^2 I$.

With this in mind, each term of $y = X\beta + \varpi$ is premultiplied

by P, which will be called the transformation matrix, to obtain expressions similar to those considered in the OLS method:

$$\eta = \Xi\beta + \varepsilon = \Xi b + e \,, \qquad \text{(A1.7)}$$

Where $\eta = Py$ and $\Xi = PX$. Since $X = (u,x)$, the corresponding transformed matrix is $\Xi = (c, \xi)$, where $c = Pu$ and $\xi = Px$.

By comparison with the OLS theory, it can be seen that the b which will minimise

$$e^te = (\eta - \Xi b)^t(\eta - \Xi b) \qquad \text{(A1.8)}$$

is given by $b = A^{-1} g$, where

$$A = \Xi^t\Xi = \begin{bmatrix} c^tc & c^t\xi \\ \xi^tc & \xi^t\xi \end{bmatrix} \text{ and } g = \Xi^t\eta = \begin{Bmatrix} c^t\eta \\ \xi^t\eta \end{Bmatrix}$$

It follows that the optimal b is

$$b = \frac{1}{(c^tc)(\xi^t\xi) - (c^t\xi)^2} \begin{Bmatrix} (\xi^t\xi)(c^t\eta) - (c^t\xi)(\xi^t\eta) \\ -(c^t\xi)(c^t\eta) + (c^tc)(\xi^t\eta) \end{Bmatrix} \qquad \text{(A1.9)}$$

Reverting to Σ notation, the two elements of the optimal b may be expressed as

$$b_0 = (\Sigma \xi_i^2 \Sigma c_i\eta_i - \Sigma c_i\xi_i \Sigma \xi_i\eta_i)/D \qquad \text{, (A1.10)}$$

$$b_1 = (\Sigma c_i^2 \Sigma \xi_i \eta_i - \Sigma c_i \xi_i \Sigma c_i \eta_i)/D \qquad (A1.11)$$

where $D = \Sigma c_i^2 \Sigma \xi_i^2 - (\Sigma c_i \xi_i)^2$

If $\Omega = I$, the transformation matrix P is simply an identity matrix, so that $\eta_i = y_i$, $\xi_i = x_i$ and $c_i = 1$ in these expressions for b_0 and b_1, which are then simply the OLS estimates of β_0 and β_1.

The GLS b may be shown to be the best linear unbiased estimate of β and, if the random errors are normally distributed, the GLS b has the stronger property of being the best of all unbiased estimates of β.

A1.3 The Transformation Matrix.

To find the P needed for applying the GLS theory, let us first find the eigenvalues and the associated eigenvectors of Ω.

Suppose the eigenvalues are $\lambda_1, \lambda_2, \ldots, \lambda_n$ and let $z_i = (z_{i_1}, z_{i_2}, \ldots, z_{in})$ denote the normalised eigenvector corresponding to eigenvalue λ_i, where the normalisation is such as to make

$$z_{i_1}^2 + z_{i_2}^2 + \ldots + z_{in}^2 = 1 . \qquad (A1.12)$$

The required matrix is then

$$P = \begin{bmatrix} P_{11} & P_{12} & \cdot\cdot & P_{1n} \\ P_{21} & P_{22} & \cdot\cdot & P_{2n} \\ \cdot & \cdot & & \cdot \\ \cdot & \cdot & & \cdot \\ P_{n1} & P_{n2} & \cdot\cdot & P_{nn} \end{bmatrix} = \begin{bmatrix} z_{11}/\sqrt{\lambda}_1 & z_{12}/\sqrt{\lambda}_1 & \cdot\cdot & z_{1n}/\sqrt{\lambda}_1 \\ z_{21}/\sqrt{\lambda}_2 & z_{22}/\sqrt{\lambda}_2 & \cdot\cdot & z_{2n}/\sqrt{\lambda}_2 \\ \cdot & \cdot & & \cdot \\ \cdot & \cdot & & \cdot \\ z_{n1}/\sqrt{\lambda}_n & z_{n2}/\sqrt{\lambda}_n & \cdot\cdot & z_{nn}/\sqrt{\lambda}_n \end{bmatrix} \qquad \text{(A1.13)}$$

The elements of c, ξ and η may then be evaluated using

$$c_i = \sum_{j=1}^{n} P_{ij} \;,\quad \xi_i = \sum_{j=1}^{n} P_{ij} x_j \quad \text{and} \quad \eta_i = \sum_{j=1}^{n} P_{ij} y_j$$

for i = 1 to n.

A1.4 Adequacy of a Regression Model.

Let us now consider how to assess the value of x in explaining y in the GLS model. This may be approached by assessing how well $\xi = Px$ explains $\eta = Py$ in terms of reducing the total sum of squares, $\eta^t\eta = \Sigma\eta_i^2$.

The reduction due to our model with β_0 and β_1,

$$\eta = \beta_0 c + \beta_1 \xi + \varepsilon \;, \qquad \text{(A1.14)}$$

is conventionally denoted by $R(\beta_0 , \beta_1)$ and is given by

$$R(\beta_0, \beta_1) = b^t g = b_0 \Sigma\, c_i \eta_i + b_1 \Sigma\, \xi_i \eta_i \quad . \qquad (A1.15)$$

The reduction due to a model with β_0 but no β_1,

$$\eta = \beta_0 c + \varepsilon \quad , \qquad (A1.16)$$

is $R(\beta_0) = (g_0 / a_{00}) g_0 = (\Sigma\, c_i \eta_i)^2 / (\Sigma\, c_i^2)$ (A1.17)

The proportion of the total sum of squares which is explained by assuming dependence of η upon ξ in the model with β_0 and β_1 is then given by

$$R^2 = \frac{R(\beta_0, \beta_1) - R(\beta_0)}{\eta^t \eta - R(\beta_0)} \qquad (A1.18)$$

which is called the coefficient of determination. This R^2 is formally equivalent to the square of a coefficient of correlation between η and ξ.

Assuming that the random errors are (at least approximately) normally distributed allows the use of the standard sampling theory to assess the statistical significance of various values of R^2. Broadly speaking, values of R^2 near 1 indicate that ξ explains most of the variation in η (hence x explains most of the variation in y), whereas values of R^2 near zero indicate that ξ (hence x) has little explanatory value. However, high values of R^2 can arise by chance even

when ξ really contributes nothing to explaining the variation in η. The probability of such high values depends upon n, the number of observed pairs (x_i, y_i) being considered.

In practice it is convenient to multiply both R^2 and the probabilities by 100. The following table shows values of $100R^2$ that would be exceeded by chance with probability α (the 100α % points of the distribution of $100R^2$) when x (or ξ) has no true explanatory value. The table may be extended for other values of α and n by noting that R^2_α, the 100α% point of the distribution of R^2 is related to the $100\,\alpha/2$ % point of the distribution of Student's t with n-2 degrees of freedom by $R^2_\alpha = t^2_{\alpha/2} / (t^2_{\alpha/2} + n - 2)$. If the observed $100R^2$ is greater than the tabulated value for a certain α, it is said that it is significant at the 100α % level.

n	α =0.10	α =0.05	α =0.02	α =0.01	α =.005	α =.001
3	97.6	99.4	99.9	99.9+	99.9+	99.9+
4	81.0	90.3	96.0	98.0	99.0	99.8
5	64.9	77.1	87.3	91.9	94.9	98.2
6	53.2	65.8	77.8	84.1	88.7	94.9
7	44.8	56.9	69.4	76.5	82.0	90.4
8	38.6	49.9	62.2	69.6	75.7	85.5
9	33.9	44.4	56.2	63.6	69.9	80.7

Table A1.1 Critical Values of $100R^2$

This table is based on Fisher & Yates (67) and Pearson &

Hartley (68). For example, if n=9 and $100R^2$ is found to be 65, this is significant at the 1% level since it is greater than 63.6, the tabulated value at α =0.01. In other words, there is a probability of less than 0.01 that a value of $100R^2$ as high as 65 would occur by chance, so it may be concluded that the observed x-values do play a considerable part in explaining the observed y-values when our regression model is used.

Note that when n is small the probability of $100R^2$ being over 90 (implying that over 90% of the variation in y is explained by x) is quite large even when x really has no explanatory value, so to draw sensible inferences from observed values of $100R^2$ it is important to take account of sample size.

A1.5 Reduced Regression Models.

Having found b_0 , b_1 and R^2 for the model with β_0 and β_1 , it is often advisable to check whether a reduced model with no β_0 would increase the value of R^2 . To do this, the standard error of b_0 is first calculated. This is

$$SE(b_0) = (\Sigma \xi_i^2 / D)^{\frac{1}{2}} s \quad , \qquad (A1.19)$$

where s is the unbiased estimate of σ , the standard deviation of the random errors, and is given by

$$s = \left[\frac{\Sigma \eta_i^2 - R((\beta_0, \beta_1)}{n-2} \right]^{\frac{1}{2}}, \qquad (A1.20)$$

where n is number of values of η_i, e.g. if considering 10 modes, the value of n is 9.

The ratio

$$t = b_0 / SE(b_0) \qquad (A1.21)$$

is then calculated.

Assuming normally distributed randon errors, this ratio is distributed as Student's t with n-2 degrees of freedom when β_0 is zero. For practical purposes, one may use the rule that if the t-ratio is much less than 2, there is a strong indication that β_0 is zero, so that b_1 and R^2 should be recalculated for the model.

$$Y_i = \beta_1 x_i + \varpi_i \quad (\text{or } \eta_i = \beta_1 \xi_i + \varepsilon_i) . \qquad (A1.22)$$

It is then found that

$$b_1 = \Sigma \xi_i \eta_i / \Sigma \xi_i^2 . \qquad (A1.23)$$

The reduction in $\Sigma \eta_i^2$ due to β_1 alone is

$$R(\beta_1) = b_1 g_1 = (\Sigma \xi_i \eta_i)^2 / \Sigma \xi_i^2 \qquad (A1.24)$$

and the proportion of the total sum of squares explained by

the x-terms is

$$R^2 = R(\beta_1) / \Sigma \eta_i^2 = (\Sigma \xi_i \eta_i)^2 / (\Sigma \xi_i^2 \Sigma \eta_i^2) \quad \text{(A1.25)}$$

If the t-test had indicated that β_0 was zero, it should normally be found that R^2 for the reduced model is greater than that previously calculated for the model with β_0. Critical values for $100R^2$ may be found by noting that R^2 for the reduced model is related to Student's t with n-1 degrees of freedom by $R^2_\alpha = t^2_{\alpha/2} / (t^2_{\alpha/2} + n-1)$.

A1.6 Confidence Limits for Regression Coefficients.

Approximate confidence limits for β_0 and β_1 can be obtained from b_0 and b_1 and their respective standard errors. For the model with β_0 and β_1, an expression for $SE(b_0)$ has already quoted above in equation A1.19. The corresponding result for b_1 is

$$SE(b_1) = (\Sigma c_i^2 / D)^{\frac{1}{2}} s . \quad \text{(A1.26)}$$

For the reduced model,

$$SE(b_1) = (s^2 / \Sigma \xi_i^2) , \quad \text{(A1.27)}$$

where $s^2 = \Sigma \eta_i^2 (1-R^2) / (n-1)$.

The confidence limits may then be calculated from

$$b_j \pm t\ SE(b_j)\ ,\quad j = 0,1,$$

where t is 1 for approximately 65% confidence or 2 for approximately 90% confidence, more exact values being obtainable from tables of Student's t for n-2 degrees of freedom (model with β_0 and β_1) or n-1 degrees of freedom (model with β_1 only).

APPENDIX 2

LISTINGS OF THE DEFECT LOCATION PROGRAMS

1- Program: START2

2- Program: PFDELO

3- Program: SFDELO

4- Program: SPGLS

```
10    ! RE-SAVE"START2:F8"
20    ! ************************************************************
30    ! *
40    ! *This control program identifies and loads the appropriate *
50    ! *program for the class of problem identified.               *
60    ! *
70    ! *Two types of method are selectable:                        *
80    ! *1- Cawley-Adams Method                                     *
90    ! *   Program "PFDEL0" - Plane Frame Defect Location         *
100   ! *           "SFDEL0" - Space Frame Defect Location         *
110   ! *2- New Method                                             *
120   ! *   Program "SPGLS"  - Space & Plane frame Gen. Least Squa.*
130   ! *
140   ! *Author : Adnan Al-Tamimi Dept. Mech. Eng.                 *
150   ! *
160   ! ************************************************************
170   PRINTER IS 16
180   GRAPHICS
190   LIMIT 0,184,0,149
200   FRAME
210   CSIZE 13
220   MOVE 35,85
230   LABEL "PROGRAM"
240   MOVE 35,66
250   LABEL "START 2 "
260   CSIZE 10
270   MOVE 54,48
280   LABEL "FOR"
290   CSIZE 13
300   MOVE 41,30
310   LABEL "DEFECT"
320   MOVE 35,10
330   LABEL "LOCATION"
340   WAIT 2000
350   GCLEAR
360   EXIT GRAPHICS
370   PRINT PAGE;TAB(30);"  SELECT SOLUTION TYPE  "
380   PRINT LIN(3),"Enter : 1 For Method 1 "   ! Cawley-Adams
390   PRINT LIN(1),"        2 For Method 2 "   ! New Proposed Met
hod
400   WAIT 1000
410   INPUT Ans1
420   IF (Ans1=1) OR (Ans1=2) THEN 460
430   BEEP
440   PRINT LIN(1),"Enter 1 or 2 only"
450   GOTO 400
460   IF Ans1=1 THEN GOTO 480
470   LOAD "SPGLS:F8"
480   PRINT PAGE;TAB(30);"  SELECT STRUCTURE TYPE  "
490   PRINT LIN(3),"Enter : P For Plane Frame"
500   PRINT LIN(1),"        S For Space Frame"
510   WAIT 1000
520   INPUT Ans2
530   IF (Ans2=P) OR (Ans2=S) THEN 570
540   BEEP
550   PRINT LIN(1),"Enter P or S only"
560   GOTO 510
570   IF Ans2=P THEN GOTO 590
580   LOAD "SFDEL0:F8"
590   LOAD "PFDEL0:F8"
```

```
10    ! RE-SAVE"PFDELO:F8"
20    ! ************************************************************
30    ! *                  Plane Frame DEfect LOcation             *
40    ! *                                                          *
50    ! * The Program Has Facility To Read From The Disc           *
60    ! * The Sensitivity Matrix Has Already Been Calculated       *
70    ! * This program calculated the probability of the damage    *
80    ! * Site in order to create the necessary data for the       *
90    ! * drawing of a defect location chart for plane frame       *
100   ! * structure. From the fact that the ratio of the frequency*
110   ! * changes in two modes was only a function of the damage   *
120   ! * location. The position where the theoretically           *
130   ! * determined ratio equaled the experimentally measured     *
140   ! * values were therefore possible damage sites. This was    *
150   ! * done by computing an error function at each element      *
160   ! * which was a calculation of the error in assuming the     *
170   ! * the damage to be at that element. Consequently, the most *
180   ! * probable damage site was taken to be the one at which    *
190   ! * the value of total error was at a minimum.               *
200   ! *                                                          *
210   ! * ORIGIN A.AL-TAMIMI : Mech. Eng. Dept.; Aston University  *
220   ! *                                                          *
230   ! ************************************************************
240   PRINTER IS 16
241   PLOTTER IS 13,"GRAPHICS"
250   GRAPHICS
260   LIMIT 0,184,0,149
270   FRAME
280   CSIZE 12
290   MOVE 35,85
300   LABEL "PROGRAM"
310   MOVE 40,66
320   LABEL "PFDELO"
330   CSIZE 10
340   MOVE 54,48
350   LABEL "FOR"
360   CSIZE 12
370   MOVE 41,30
380   LABEL "DEFECT"
390   MOVE 35,10
400   LABEL "LOCATION"
410   WAIT 2000
420   GCLEAR
430   EXIT GRAPHICS
440   OPTION BASE 1
450   COM Sen(60,60),K(60,60),Err(60,60),Freq(60),Ans2,B,M2,W(60)
460   COM Error(60),Noco(2,60),Nmode,Elco(2,60),Xkk(3,60),Xr(2,60)
470   COM Sn(60),Title$,Dtaw(60),T$[40],M$[40],M2$[80],No$[5]
480   PRINTER IS 16
490   PRINT PAGE;"INPUT THE TITLE OF THE PROBLEM FOR WHICH THE "
500   PRINT "SENSITIVITY MATRIX HAS ALREADY BEEN CAL. AND STORED."
510   WAIT 1000
520   INPUT Title$
530   MASS STORAGE IS ":F8"
540   ASSIGN #1 TO Title$
550   READ #1;N,Nelem,Nmode,U1,U2
560   REDIM Sen(Nelem,N),Sn(Nelem),Noco(2,Nmode),Elco(2,Nelem)
570   REDIM Error(Nelem),Freq(N)
580   MAT READ #1;Sen,Sn,Noco,Elco,Freq
590   ASSIGN * TO #1
```

```
600       FOR I=1 TO N
610       IF Freq(I)<>0 THEN 640
620       NEXT I
630    GOTO 680
640    IF U2=0 THEN U2$="Hz"
650    IF U2=1 THEN U2$="RAD/S"
660    PRINT "THE ORIGINAL MEASURED FREQUENCIES IN ";U2$;" WERE:"
670    PRINT Freq(*)
680    PRINT PAGE;"AT LEAST 2 AND NOT MORE THAN ";N;"MEASURED "
690    PRINT "CHANGES IN FREQUENCIES MUST BE AVAILABLE FOR DEFECT "
700    PRINT "LOCATION ANALYSIS."
710    PRINT
720    PRINT PAGE;"INPUT THE NUMBER OF MEASURED FREQUENCIES WHICH "
730    PRINT "YOU WANT TO DO THE DEFECT LOCATION ANALYSIS."
740    INPUT N1
750    REDIM W(N1),Dltaw(N1)
760    IF U1=0 THEN U1$="Hz"
770    IF U1=1 THEN U1$="RAD/S"
780    PRINT PAGE;"INPUT MEASURED REDUCTION IN Freqs. 1,...,";N1;
790    PRINT " IN ";U1$
800    MAT INPUT W
810    PRINT PAGE;"Zero or Negative Changes in Freqs. is Required?"
820    INPUT "1 For Yes; 0 For No ",Ans
830    FOR I=1 TO N1
840    Dltaw(I)=W(I)
850    NEXT I
860    PRINT PAGE;
870    INPUT "Input Number of Modes You Want to Consider ",N
880    REDIM Err(N,N),Dltaw(N)
890    PRINTER IS 0
900    PRINT "Number Of Modes Considered IS =1 TO ";N
910    PRINT "**********************************"
920    PRINT
930    PRINTER IS 16
940    IF Ans=0 THEN GOTO 1170
950    REM FIND SMALLEST REDUCTION #0
960    Wmin=0
970       FOR I=1 TO N
980       IF (Dltaw(I)>0) AND (Wmin=0) THEN Wmin=Dltaw(I)
990       IF (Dltaw(I)>0) AND (Dltaw(I)<Wmin) THEN Wmin=Dltaw(I)
1000      NEXT I
1010   REM MAKE Dltaw:s=0 TO 1/1000 OF Wmin
1020      FOR I=1 TO N
1030      IF Dltaw(I)<=0 THEN Dltaw(I)=Wmin/1000
1040      NEXT I
1050      Senmin=0
1060      FOR I=1 TO Nelem
1070      FOR J=1 TO N
1080      IF (Sen(I,J)>0) AND (Senmin=0) THEN Senmin=Sen(I,J)
1090      IF (Sen(I,J)>0) AND (Sen(I,J)<Senmin) THEN Senmin=Sen(I,J)
1100      NEXT J
1110      NEXT I
1120      FOR I=1 TO Nelem
1130      FOR J=1 TO N
1140      IF Sen(I,J)<=0 THEN Sen(I,J)=Senmin/1000
1150      NEXT J
1160      NEXT I
1170   ! CALCULATE ERROR IN ASSUMING THE DAMAGE TO BE AT POSITION H
1180   MAT Errtot=ZER
1190   MAT Err=ZER
```

```
1200      FOR H=1 TO Nelem
1210         FOR I=1 TO N
1220            FOR J=1 TO N
1230            IF Ans=1 THEN GOTO 1250
1240            IF (Sen(H,J)=0) OR (Sen(H,I)=0) THEN GOTO 1310
1250            IF (Ditaw(I)=0) OR (Ditaw(J)=0) THEN GOTO 1310
1260            IF Sen(H,I)/Sen(H,J)<Ditaw(I)/Ditaw(J) THEN 1290
1270            Err(I,J)=Sen(H,I)/Sen(H,J)/(Ditaw(I)/Ditaw(J))^2
1280            GOTO 1300
1290            Err(I,J)=Ditaw(I)/Ditaw(J)*(Sen(H,I)/Sen(H,J))^2
1300            Errtot(H)=Errtot(H)+Err(I,J)
1310            NEXT J
1320         NEXT I
1330      IF H=1 THEN Errmin=Errtot(1)
1340      IF Errtot(H)<Errmin THEN Errmin=Errtot(H)
1350      NEXT H
1360   IF Errmin>0 THEN 1490
1370   REM FIND SMALLEST ERRTOT#0
1380   Errmin=0
1390      FOR I=1 TO Nelem
1400   IF (Errtot(I)<>0) AND (Errmin=0) THEN Errmin=Errtot(I)
1410   IF (Errtot(I)<>0) AND (Errtot(I)<Errmin) THEN Errmin=Errtot(I)
1420      NEXT I
1430   REM MAKE ERRTOT:S=0 TO 1 1000 OF ERRMIN
1440      FOR I=1 TO Nelem
1450      IF Errtot(I)=0 THEN Errtot(I)=Errmin*1000
1460      NEXT I
1470   REM REDUCE ALSO ERRMIN
1480    Errmin=Errmin/1000
1490   REM CALCULATE THE DEFECT PROBABILITY
1500      FOR H=1 TO Nelem
1510      IF Errtot(H)=0 THEN GOTO 1530
1520      Errtot(H)=INT(100*Errmin/Errtot(H))
1530      NEXT H
1540      ! ********** PLOTTING DEFECT LOCATION CHART **********
1550   Ans2=4
1560   IF Ans2=4 THEN REDIM Noco(2,Nnode),Elco(2,Nelem)
1570   REM FIND THE DIMENSIONS OF THE STRUCTURE
1580      FOR I=1 TO Nnode
1590      IF Noco(1,I)>Xmax THEN Xmax=Noco(1,I)
1600      IF Noco(1,I)<Xmin THEN Xmin=Noco(1,I)
1610      IF Noco(2,I)>Ymax THEN Ymax=Noco(2,I)
1620      IF Noco(2,I)<Ymin THEN Ymin=Noco(2,I)
1630      NEXT I
1640   IF Xmax-Xmin>0 THEN 1670
1650   Xmin=Ymin
1660   Xmax=Ymax
1670   IF Ymax-Ymin>0 THEN 1700
1680   Ymin=Xmin
1690   Ymax=Xmax
1700   Min=MIN(Xmax-Xmin,Ymax-Ymin)
1710   INPUT "Figure number?(If no Title is required input 0",No$
1720   IF No$="0" THEN GOTO 1760
1730   LINPUT "Main Title Of PLOT No.1",M$
1740   LINPUT "Main Title Of PLOT No.2",M2$
1750   LINPUT "Title Of Plot",T$
1760   INPUT "Select Corner Plot? 0,1,2,3,4 ;Default Value=0",Corn
1770   PRINTER IS 16
1780   PRINT PAGE,"Select The Plotter Device With Following Codes"
1790   PRINT SPA(20)," 1: For Screen (CRT)"
```

```
1800  PRINT SPA(20)," 2  For Benson Plotter"
1810  PRINT SPA(20)," 3  For 9872A  Plotter"
1820  INPUT Plottercode
1830  IF (Plottercode>0) AND (Plottercode<4) THEN GOTO 1860
1840  BEEP
1850  GOTO 1820
1860  Sety=Dump=Benson=0
1870  IF Plottercode=1 THEN Plotter=13
1880  IF Plottercode=2 THEN Plotter=5
1890  IF Plottercode=3 THEN Plotter=7
1900  IF Plotter=13 THEN GOTO 2520
1910  IF Plotter=5 THEN GOTO 2450
1920  IF Plotter=7 THEN GOTO 1950
1930  BEEP
1940  GOTO 1790
1950  PLOTTER IS 7,5,"9872A"
1960  PRINTER IS 7,5
1970  PRINT "V32"
1980  PRINTER IS 16
1990  Scay=1
2000  Scax=285/260
2010  Sety=0
2020  PEN 1
2030  SETUU
2040  INPUT "If You Want Vertical 1 ;Otherwie 0 ",Ver
2050  IF (Ver=0) OR (Ver=1) THEN GOTO 2080
2060  BEEP
2070  GOTO 2040
2080  IF Ver<>1 THEN GOTO 2270
2090  LIMIT 20,190,0,280
2100  MOVE 50*Scax,Sety+155*Scay
2110  LORG 6
2120  CSIZE 3.3*Scay
2130  LABEL M$
2140  MOVE 50*Scax,Sety+150*Scay
2150  CSIZE 3.1*Scay
2160  LABEL M2$
2170  IF Corn=0 THEN LIMIT 0,200,0,280
2180  IF Corn=1 THEN LIMIT 10,110,10,140
2190  IF Corn=2 THEN LIMIT 10,110,140,280
2200  IF Corn=3 THEN LIMIT 100,200,10,140
2210  IF Corn=4 THEN LIMIT 100,200,140,280
2220  MOVE 50*Scax,Sety+15*Scay
2230  LORG 6
2240  CSIZE 3.8*Scay
2250   LABEL ""&No$&" "&T$
2260  GOTO 2590
2270  LIMIT 30,280,0,200
2280  MOVE 50*Scax,Sety+8*Scay
2290  LORG 6
2300  CSIZE 2.7*Scay
2310  LABEL M$
2320  MOVE 50*Scax,Sety+4*Scay
2330  CSIZE 2.7*Scay
2340  LABEL M2$
2350  IF Corn=0 THEN LIMIT 0,285,0,200
2360  IF Corn=1 THEN LIMIT 0,142,5,100
2370  IF Corn=2 THEN LIMIT 0,142,90,185
2380  IF Corn=3 THEN LIMIT 142,285,5,100
2390  IF Corn=4 THEN LIMIT 142,285,90,185
```

```
2400  MOVE 65*Scax,Sety+12*Scay
2410  LORG 6
2420  CSIZE 3.8*Scay
2430  LABEL ""&No$&" "&T$
2440  GOTO 2590
2450  Benson=1
2460  PLOTTER IS 5,"INCREMENTAL",.05
2470  PRINT "VS2"
2480  LIMIT 0,1000,0,930
2490  Scay=210/930
2500  Scax=29700/930/130
2510  GOTO 2590
2520  IF Again THEN GOTO 2530
2530  INPUT "To Dump Graphics INPUT 1,Otherwise INPUT 0",Dump
2540  PLOTTER IS 13,"GRAPHICS"
2550  Pcount=0
2560  Scax=Scay=1
2570  GRAPHICS
2580  REM PLOT *****
2590  IF Ver=1 THEN LOCATE 0,90*Scax,Sety,Sety+120*Scay
2600  LOCATE 0,130*Scax,Sety,Sety+100*Scay
2610  IF Plotter=13 THEN GOTO 2650
2620  IF Plotter=7 THEN GOTO 2690
2630  CALL Frame(Sety,Scax,Scay)
2640  GOTO 2690
2650  MOVE 65,94
2660  CSIZE 3.3*Scay
2670  LORG 4
2680  LABEL ""&No$&" "&T$
2690  IF Ver=1 THEN GOTO 2720
2700  LOCATE 20*Scax,110*Scax,Sety+(Benson*5+20)*Scay,85*Scay+Sety
2710  GOTO 2780
2720  LOCATE 20*Scax,80*Scax,Sety+(Benson*5+20)*Scay,100*Scay+Sety
2730  GOTO 2780
2740   FRAME
2750   PRINTER IS 0
2760  SHOW Xmin-.25*Min,Xmax+.25*Min,Ymin-.25*Min,Ymax+.25*Min
2770  GOTO 2800
2780  SHOW Xmin,Xmax,Ymin,Ymax
2790  REM PLOT UNDEFLECTED STRUCTURE
2800  LINE TYPE 1
2810     FOR I=1 TO Nelem
2820     MOVE Noco(1,Elco(1,I)),Noco(2,Elco(1,I))
2830     DRAW Noco(1,Elco(2,I)),Noco(2,Elco(2,I))
2840     NEXT I
2850  REM LABEL THE ELEMENTS
2860  CSIZE 3.8
2870     FOR I=1 TO Nelem
2880     Ax=(Noco(1,Elco(1,I))+Noco(1,Elco(2,I)))/2
2890     Ay=(Noco(2,Elco(1,I))+Noco(2,Elco(2,I)))/2
2900     REM MOVE TO MIDDLE OF ELEMENT
2910     LORG 4
2920     MOVE Ax,Ay
2930     ! MAKE LABEL PERP TO ELEM AND/OR LEGIBLE FROM RIGHT SIDE
2940     Dx=Noco(1,Elco(2,I))-Noco(1,Elco(1,I))
2950     IF Dx>0 THEN 2990
2960     IF Dx<0 THEN 3010
2970     Ang=PI/2
2980     GOTO 3020
2990     Ang=ASN(Sn(I))
```

```
3000      GOTO 3020
3010      Ang=-ASN(Sn(I))
3020      LDIR Ang
3030      IF Ans2=4 THEN 3070
3040      REM LABEL ELEMENT NUMBER
3050      LABEL I
3060      GOTO 3090
3070      REM LABEL DEFECTPROBABILITY
3080      LABEL Errtot(I)
3090      NEXT I
3100   IF Ans2=4 THEN 3110
3110   PAUSE
3120   IF Plotter<>13 THEN GOTO 3210
3130   IF NOT Dump THEN GOTO 3210
3140   PRINT LIN(6)
3150   DUMP GRAPHICS
3160   PRINT ""&No$&" "&T$
3170   EXIT GRAPHICS
3180   PRINT RPT$("-",80),LIN(2)
3190   PRINTER IS 16
3200   GOTO 3260
3210   MOVE 65*Scax,Sety+10*Scay
3220   CSIZE 3*Scay
3230   MOVE 65*Scax,Sety+7*Scay
3240   CSIZE 2*Scay
3250   CSIZE 3.3*Scay
3260   IF Plotter=13 THEN 3290
3270   IF INT(No/4)*4-No=0 THEN GOTO 3310
3280   MOVE 0,Benson*110*Scay
3290   IF Again THEN GOTO 3420
3300   GOTO 3410
3310   IF Plotter=7 THEN GOTO 3390
3320   LOCATE 0,140*Scax,0,110*Scay  !PLOTTER IS 5
3330   SETGU
3340   MOVE 140*Scax,0
3350   PLOTTER IS 5,"INCREMENTAL",.05
3360   LIMIT 0,1000,0,-930
3370   MOVE 0,330*Scay
3380   GOTO 3400
3390   GCLEAR 330
3400   Sety=0
3410   Again=1
3420   PEN 0
3430   IF Ans2<>3 THEN 3440
3440   EXIT GRAPHICS
3450   PRINTER IS 16
3460   PRINT PAGE;
3470   INPUT "Another Modes Required ?, 1-Yes, 0-No",Res
3480   IF (Res<>1) AND (Res<>0) THEN GOTO 3460
3490   IF Res=0 THEN GOTO 3520
3500   INPUT "Input Number of Modes You Want to Consider",N
3510   GOTO 880
3520   PRINT PAGE;
3530   GCLEAR
3540   EXIT GRAPHICS
3550   DISP "Compution is Finished"
3560   END
```

```
10    !  RE-SAVE"SFDELO:F8"
20    ! ************************************************************
30    ! *              Space Frame DEfect LOcation Program         *
40    ! *                                                          *
50    ! * This program calculated the probability of the damage    *
60    ! * site in order to create the necessary data for the       *
70    ! * drawing of a defect location chart for space frame. From *
80    ! * the fact that the ratio of the frequency changes in two  *
90    ! * modes was only function of the damage location. The      *
100   ! * position where the theoretical determined ratio equaled  *
110   ! * the experimental measred values were therefore possible  *
120   ! * damage sites. This was done by computing an error        *
130   ! * function at each element which was a calculation of the  *
140   ! * error in assuming the damage to be at that element.      *
150   ! * Consequently, the most probable damage site was taken    *
160   ! * to be the one at which the value of total error was at   *
170   ! * minimum.                                                 *
180   ! *                                                          *
190   ! * ORIGIN A.AL-TAMIMI; Mech. Eng. Dept.;Aston University    *
200   ! *                                                          *
210   ! ************************************************************
220   PRINTER IS 16
230   GRAPHICS
240   LIMIT 0,184,0,149
250   FRAME
260   CSIZE 12
270   MOVE 35,85
280   LABEL "PROGRAM"
290   MOVE 40,66
300   LABEL "SFDELO"
310   CSIZE 10
320   MOVE 54,48
330   LABEL "FOR"
340   CSIZE 12
350   MOVE 41,30
360   LABEL "DEFECT"
370   MOVE 35,10
380   LABEL "LOCATION"
390   WAIT 2000
400   GCLEAR
410   EXIT GRAPHICS
420   OPTION BASE 1
430   COM N,Nelem,Nmode,K(72,72),Sen(72,72),Err(72,72),Freq(72),Ans2
440   COM B,M2,Units,W(72),Errtot(72),Offd2(72),D1(72),Coup(12,72)
450   COM Tc(2,72),Elco(2,72),L(72),Lx(72),Ly(72),Lz(72),Lb,Ub
460   COM Lxz(72),Sn(72),Cs(72),E(72),G(72),Prgr(72),Xt(2,72)
470   DIM Xtk$(3,72),Noco(3,72),Dlbaw(72),T$[40],M$[40],M2$[80]
480   PRINT PAGE;"INPUT THE TITLE OF THE PROBLEM FOR WHICH THE "
490   PRINT "SENSITIVITY MATRIX HAS ALREADY BEEN CAL. AND STORED."
500   INPUT Title$
510   MASS STORAGE IS ":F8"
520   ASSIGN #1 TO Title$
530   READ #1;N,Nelem,Nmode,U1,U2
540   REDIM Sen(Nelem,N),Sn(Nelem),Noco(3,Nmode),Elco(2,Nelem)
550   REDIM Freq(N),Errtot(Nelem)
560   MAT READ #1;Sen,Sn,Noco,Elco,Freq
570   ASSIGN * TO #1
580      FOR I=1 TO N
590      IF Freq(I)<>0 THEN 620
600      NEXT I
```

```
610     GOTO 660
620     IF U2=0 THEN U2$="Hz"
630     IF U2=1 THEN U2$="RAD/S"
640     PRINT "THE ORIGINAL MEASURED FREQUENCIES IN ";U2$;" WERE:"
650     PRINT Freq(*)
660     PRINT PAGE;"AT LEAST 2 AND NOT MORE THAN ";N;"MEASURED "
670     PRINT "CHANGES IN  Freqs. MUST BE AVAILABLE FOR THE DEFECT"
680     PRINT "LOCATION ANALYSIS."
690     PRINT PAGE;"INPUT THE NUMBER OF MEASURED FREQUENCIES WHICH "
700     PRINT "YOU WANT TO DO THE DEFECT LOCATION ANALYSIS."
710     INPUT N1
720     REDIM W(N1),Dltaw(N1)
730     IF U1=0 THEN U1$="Hz"
740     IF U1=1 THEN U1$="RAD/S"
750     PRINT PAGE;"INPUT MEASURED REDUCTION IN FREQUENCY 1,...,";N1;
760     PRINT " IN ";U1$
770     MAT INPUT W
780     PRINT PAGE;"Zero or Negative Changes in Freqs. is Required?"
790     INPUT "1 For Yes ; 0 For No",Ans
800     FOR I=1 TO N1
810     Dltaw(I)=W(I)
820     NEXT I
830     PRINT PAGE;
840     INPUT "Input Number of Modes You Want to Consider",N
850     REDIM Err(N,N),Dltaw(N)
860     PRINTER IS 0
870     PRINT "NUMBER OF MODES CONSIDERED IS =1 TO ";N
880     PRINT "*****************************"
890     PRINT
900     IF Ans=0 THEN GOTO 1130
910     REM FIND SMALLEST REDUCTION #0
920     Wmin=0
930        FOR I=1 TO N
940        IF (Dltaw(I)<>0) AND (Wmin=0) THEN Wmin=Dltaw(I)
950        IF (Dltaw(I)<>0) AND (Dltaw(I)<Wmin) THEN Wmin=Dltaw(I)
960        NEXT I
970     REM MAKE Dltaw;s=0 TO 1/1000 OF Wmin
980        FOR I=1 TO N
990        IF Dltaw(I)=0 THEN Dltaw(I)=Wmin/1000
1000       NEXT I
1010       Senmin=0
1020       FOR I=1 TO Nelem
1030       FOR J=1 TO N
1040       IF (Sen(I,J)<>0) AND (Senmin=0) THEN Senmin=Sen(I,J)
1050       IF (Sen(I,J)<>0) AND (Sen(I,J)<Senmin) THEN Senmin=Sen(I,J)
1060       NEXT J
1070       NEXT I
1080       FOR I=1 TO Nelem
1090       FOR J=1 TO N
1100       IF Sen(I,J)<=0 THEN Sen(I,J)=Senmin/1000
1110       NEXT J
1120       NEXT I
1130    ! CALCULATE ERROR IN ASSUMING THE DAMAGE TO BE AT POSITION H
1140    MAT Errtot=ZER
1150    MAT Err=ZER
1160       FOR H=1 TO Nelem
1170          FOR I=1 TO N
1180             FOR J=1 TO N
1190             IF Ans=1 THEN GOTO 1220
1200             IF (Sen(H,J)=0) OR (Sen(H,I)=0) THEN GOTO 1270
```

```
1210            IF (Dltaw(I)=0) OR (Dltaw(J)=0) THEN GOTO 1270
1220            IF Sen(H,I)/Sen(H,J)<Dltaw(I)/Dltaw(J) THEN 1250
1230            Err(I,J)=Sen(H,I)/Sen(H,J)/(Dltaw(I)/Dltaw(J))^2
1240            GOTO 1260
1250            Err(I,J)=Dltaw(I)/Dltaw(J)/Sen(H,I)/Sen(H,J)^2
1260            Errtot(H)=Errtot(H)+Err(I,J)
1270            NEXT J
1280         NEXT I
1290      IF H=1 THEN Errmin=Errtot(1)
1300      IF Errtot(H)<Errmin THEN Errmin=Errtot(H)
1310      NEXT H
1320   IF Errmin>0 THEN 1440
1330   REM FIND SMALLEST ERRTOT#0
1340      FOR I=1 TO Nelem
1350   IF (Errtot(I)<>0) AND (Errmin=0) THEN Errmin=Errtot(I)
1360   IF (Errtot(I)<>0) AND (Errtot(I)<Errmin) THEN Errmin=Errtot(I)
1370      NEXT I
1380   REM MAKE ERRTOT:S=0 TO 1/1000 OF ERRMIN
1390       FOR I=1 TO Nelem
1400       IF Errtot(I)=0 THEN Errtot(I)=Errmin*1000
1410       NEXT I
1420   REM REDUCE ALSO ERRMIN
1430    Errmin=Errmin/1000
1440   REM CALCULATE THE DEFECT'PROBABILITY'
1450      FOR H=1 TO Nelem
1460      IF Errtot(H)=0 THEN GOTO 1480
1470      Errtot(H)=INT(100*Errmin/Errtot(H))
1480      NEXT H
1490   ! ************* PLOTTING DEFECT LOCATION CHART ********
1500   Ans2=4
1510   DIM Sin(72)
1520   REDIM Tc(2,Nnode),Sin(Nelem)
1530   DEG                          ! [Tc]= Transformed coord matix
1540   ! INPUT "Angle about X, Y, Z",Anglex,Angley,Anglez
1550   Anglex=-25
1560   Angley=35
1570   Anglez=15
1580   C1=COS(Anglex)
1590   S1=SIN(Anglex)
1600   C2=COS(Angley)
1610   S2=SIN(Angley)
1620   C3=COS(Anglez)
1630   S3=SIN(Anglez)
1640       FOR I=1 TO Nnode
1650   Tc(1,I)=C3*C2*Noco(1,I)+(S3*C1+S1*C3*S2)*Noco(2,I)+(S1*S3-C1*C
3*S2)*Noco(3,I)
1660   Tc(2,I)=-S3*C2*Noco(1,I)+(C1*C3-S1*S2*S3)*Noco(2,I)+(S1*C3+C1*
S2*S3)*Noco(3,I)
1670       NEXT I
1680   REM FIND THE DIMENSIONS OF THE STRUCTURE
1690      FOR I=1 TO Nnode
1700      IF Tc(1,I)>Xmax THEN Xmax=Tc(1,I)
1710      IF Tc(1,I)<Xmin THEN Xmin=Tc(1,I)
1720      IF Tc(2,I)>Ymax THEN Ymax=Tc(2,I)
1730      IF Tc(2,I)<Ymin THEN Ymin=Tc(2,I)
1740      NEXT I
1750   IF Xmax-Xmin>0 THEN 1780
1760   Xmin=Ymin
1770   Xmax=Ymax
1780   IF Ymax-Ymin>0 THEN 1810
```

```
1790  Ymin=Xmin
1800  Ymax=Xmax
1810  Min=MIN(Xmax-Xmin,Ymax-Ymin)
1820  INPUT "Figure Number?(If no Title is required input 0",No$
1830  IF No$="0" THEN GOTO 1870
1840  LINPUT "Main Title Of PLOT No.1",M$
1850  LINPUT "Main Title Of PLOT No.2",M2$
1860  INPUT "Select Corner ? 0,1,2 ;-Default Value=0",Corn
1870  PRINTER IS 16
1880  PRINT PAGE,"Select The Plotter Device With Following Codes"
1890  PRINT SPA(20)," 1  For Screen (CRT)"
1900  PRINT SPA(20)," 2  For Benson Plotter"
1910  PRINT SPA(20)," 3  For 9872A  Plotter"
1920  INPUT Plottercode
1930  IF (Plottercode>0) AND (Plottercode<4) THEN GOTO 1970
1940  BEEP
1950  GOTO 1930
1960  Sety=Dump=Benson=0
1970  IF Plottercode=1 THEN Plotter=13
1980  IF Plottercode=2 THEN Plotter=5
1990  IF Plottercode=3 THEN Plotter=7
2000  IF Plotter=13 THEN GOTO 2580
2010  IF Plotter=5 THEN GOTO 2520
2020  IF Plotter=7 THEN GOTO 2060
2030  BEEP
2040  GOTO 1900
2050  PLOTTER IS 7,5,"9872A"
2060  PRINTER IS 7,5
2070  PRINT "VS2"
2080  PRINTER IS 16
2090  Scay=1
2100  Scax=285/260
2110  Sety=0
2120  PEN 1
2130  SETUU
2140  INPUT "If You Want Vertical 1 ;Otherwie 0 ",Ver
2150  IF (Ver=0) OR (Ver=1) THEN GOTO 2190
2160  BEEP
2170  GOTO 2150
2180  IF Ver<>1 THEN GOTO 2360
2190  LIMIT 20,190,0,280
2200  MOVE 50*Scax,Sety+155*Scay
2210  LORG 6
2220  CSIZE 3.3*Scay
2230  LABEL M$
2240  MOVE 50*Scax,Sety+150*Scay
2250  CSIZE 3.1*Scay
2260  LABEL M2$
2270  IF Corn=0 THEN LIMIT 0,200,0,280
2280  IF Corn=1 THEN LIMIT 0,110,10,270
2290  IF Corn=2 THEN LIMIT 90,200,10,270
2300  MOVE 50*Scax,Sety+15*Scay
2310  LORG 6
2320  CSIZE 3.8*Scay
2330  LABEL ""&No$&" "&T$
2340  GOTO 2650
2350  LIMIT 30,280,0,200
2360  MOVE 50*Scax,Sety+8*Scay
2370  LORG 6
```

```
2390  CSIZE 2.7*Scav
2400  LABEL M$
2410  MOVE 50*Scax,Sety+4*Scav
2420  CSIZE 2.7*Scav
2430  LABEL M2$
2440  IF Corn=0 THEN LIMIT 0,285,0,200
2450  IF Corn=1 THEN LIMIT 0,145,5,175
2460  IF Corn=2 THEN LIMIT 120,265,5,175
2470  MOVE 65*Scax,Sety+15*Scav
2480  LORG 6
2490  CSIZE 3.3*Scav
2500  LABEL ""&No$&" "&T$
2510  GOTO 2650
2520  Benson=1
2530  PLOTTER IS 5,"INCREMENTAL",.05
2540  LIMIT 0,1000,0,930
2550  Scav=210/930
2560  Scax=29700/930/130
2570  GOTO 2650
2580  IF Again THEN GOTO 2590
2590  INPUT "To Dump Graphics INPUT 1,Otherwise INPUT 0",Dump
2600  PLOTTER IS 13,"GRAPHICS"
2610  Pcount=0
2620  Scax=Scav=1
2630  GRAPHICS
2640  REM PLOT *****
2650  IF Ver=1 THEN 2680
2660  LOCATE 0,130*Scax,Sety,Sety+130*Scav
2670  GOTO 2690
2680  LOCATE 0,90*Scax,Sety,Sety+120*Scav
2690  IF Plotter=13 THEN GOTO 2730
2700  IF Plotter=7 THEN GOTO 2770
2710  CALL Frame(Sety,Scax,Scay)
2720  GOTO 2770
2730  MOVE 65,94
2740  CSIZE 3.3*Scav
2750  LORG 4
2760  LABEL ""&No$&" "&T$
2770  IF Ver=1 THEN GOTO 2810
2780  IF Plottercode=1 THEN GOTO 2830
2790  LOCATE 5*Scax,120*Scax,Sety+(Benson*5+20)*Scav,110*Scav+Sety
2800  GOTO 2870
2810  LOCATE 5*Scax,100*Scax,Sety+(Benson*5+50)*Scav,180*Scav+Sety
2820  GOTO 2870
2830  LOCATE 5*Scax,120*Scax,Sety+(Benson*5+10)*Scav,90*Scav+Sety
2840  GOTO 2870
2850   FRAME
2860   PRINTER IS 0
2870  SHOW Xmin,Xmax,Ymin,Ymax
2880  REM PLOT UNDEFLECTED STRUCTURE
2890  LINE TYPE 1
2900      FOR I=1 TO Nelem
2910      MOVE Tc(1,Elco(1,I)),Tc(2,Elco(1,I))
2920      DRAW Tc(1,Elco(2,I)),Tc(2,Elco(2,I))
2930      NEXT I
2940  REM LABEL THE ELEMENTS
2950  CSIZE 3.8
2960      FOR I=1 TO Nelem
2970      Ax=(Tc(1,Elco(1,I))+Tc(1,Elco(2,I)))/2
2980      Ay=(Tc(2,Elco(1,I))+Tc(2,Elco(2,I)))/2
```

```
2990        L1=Tc(1,Elco(1,I))-Tc(1,Elco(2,I))
3000        L2=Tc(2,Elco(1,I))-Tc(2,Elco(2,I))
3010        S=SQR(L1^2+L2^2)
3020        Sin(I)=(Tc(2,Elco(2,I))-Tc(2,Elco(1,I)))/S
3030        REM MOVE TO MIDDLE OF ELEMENT
3040        LORG 4
3050        MOVE Ax,Ay
3060        ! MAKE LABEL PERP TO ELEM AND/OR LEGIBLE FROM RIGHT SIDE
3070        IF L1>0 THEN Ang=-ASN(Sin(I))
3080        IF L1<0 THEN Ang=ASN(Sin(I))
3090        IF L1=0 THEN Ang=PI/2
3100        LDIR Ang
3110        REM ** LABEL Deffect Probability **
3120        LABEL Errtot(I)
3130        NEXT I
3140        PAUSE
3150        IF Plotter<>13 THEN GOTO 3240
3160        IF NOT Dump THEN GOTO 3240
3170        PRINT LIN(6)
3180        DUMP GRAPHICS
3190        PRINT ""&No$&" "&T$
3200        EXIT GRAPHICS
3210        PRINT RPT$("-",80),LIN(2)
3220        PRINTER IS 16
3230        GOTO 3290
3240        MOVE 65*Scax,Sety+10*Scay
3250        CSIZE 3*Scay
3260        MOVE 65*Scax,Sety+7*Scay
3270        CSIZE 2*Scay
3280        CSIZE 3.3*Scay
3290        IF Plotter=13 THEN 3320
3300        IF INT(No/4)*4-No=0 THEN GOTO 3340
3310        MOVE 0,Benson*110*Scay
3320        IF Again THEN GOTO 3450
3330        GOTO 3440
3340        IF Plotter=7 THEN GOTO 3420
3350        LOCATE 0,140*Scax,0,110*Scay  !PLOTTER IS 5
3360        SETGU
3370        MOVE 140*Scax,0
3380        PLOTTER IS 5,"INCREMRNTAL",.05
3390        LIMIT 0,1000,0,-930
3400        MOVE 0,330*Scay
3410        GOTO 3430
3420        GCLEAR 330
3430        Sety=0
3440        Again=1
3450        PEN 0
3460        IF Ans2<>3 THEN 3470
3470        EXIT GRAPHICS
3480        PRINT LIN(6)
3490        PRINTER IS 16
3500        PRINT PAGE;
3510        INPUT "Another Modes Required ?, 1-Yes, 0-No",Res
3520        IF (Res<>1) AND (Res<>0) THEN GOTO 3500
3530        IF Res=0 THEN GOTO 3560
3540        INPUT "Input Number of Modes You Want to Consider",N
3550        GOTO 850
3560        PRINT PAGE
3570        PRINT LIN(10);"** Compution Is Finished **"
3580        END
```

```
10    ! RE-SAVE"SPGLS:F8"
20    ! ************************************************************
30    ! **       GENERALISED LEAST SQUARES - 12-12-1983           **
40    ! **       MODIFY  THE PROGRAM ON 23-4-1984                 **
50    ! ** Application of Generalised Least Squares to the        **
60    ! ** Damage location problem. Program has facility to       **
70    ! ** read the sensitivity matrix which has already been     **
80    ! ** calculated. This program applies the Generalised      **
90    ! ** Least Squares method, which allows for unequal        **
100   ! ** variances and covariances. The covariance matrix      **
110   ! ** must be positive definite.                            **
120   ! ** Based on the Log ratios of freq. change in first      **
130   ! ** mode to change at each other mode up to N mode.       **
140   ! ** It is assumed that the variance of the Log freq.      **
150   ! ** changes increases linearly with the order of freq.    **
160   ! ** considered. From this assumption the Eigenvalue and   **
170   ! ** Eigenvector can be calculated from the covariance     **
180   ! ** matrix, in order to find transformation matrix.       **
190   ! ** Then uses  AITKEN'S Generalised Least Squares         **
200   ! ** Method, which involves transforming the variables    **
210   ! ** of the original problem to a new set which obeys      **
220   ! ** the assumptions of the simple Least Squares model     **
230   ! **                                                       **
240   ! ** ORIGIN A.N.J. AL-TAMIMI ** Mech. Eng., ASTON Univ.   **
250   ! **                                                       **
260   ! ************************************************************
270   PRINTER IS 16
280   PLOTTER IS 13,"GRAPHICS"
290   GRAPHICS
300   LIMIT 0,184,0,149
310   FRAME
320   CSIZE 12
330   MOVE 35,85
340   LABEL "PROGRAM"
350   MOVE 40,66
360   LABEL "SPGLS"
370   CSIZE 10
380   MOVE 54,48
390   LABEL "FOR"
400   CSIZE 12
410   MOVE 41,30
420   LABEL "DEFECT"
430   MOVE 35,10
440   LABEL "LOCATION"
450   WAIT 2000
460   GCLEAR
470   EXIT GRAPHICS
480   OPTION BASE 1
490   DIM A(20),T(20),X(80),Y(80),Sen(50,72),Sn(50),Nocc(3,50)
500   DIM Elco(2,50),Freq(72),D(10),Z(10,10),Q(10,10),Dd(10,10)
510   DIM P(10,10),Eta(10),Ci(10),Zeta(10),Zi(10,10),Errtot(50)
520   DIM T$[40],M$[40],M2$[40],Tc(2,50),Sin(50),B11(50),Rss(50)
530   DIM Sa1(50),Errtot1(50),Rs(50),B0(50),B1(50),Sa0(50)
540   PRINT PAGE
550   INPUT "Input Title Of The Problem ",Title$
560   MASS STORAGE IS ":F8"
570   ASSIGN #1 TO Title$
580   READ #1;N,Nelem,Nmode,U1,U2
590   IF U1=0 THEN GOTO 610
600 ! REDIM Sen(Nelem,N)
```

```
610    REDIM Sen(Nelem,N),Sn(Nelem),Elco(2,Nelem),Freq(N)
620    REDIM Se1(Nelem),B11(Nelem),Rss(Nelem),Rs(Nelem),B0(Nelem)
630    REDIM B1(Nelem),Se0(Nelem)
640    INPUT "IF THE STRUCTURE  PLANE-Input 1, SPACE-Input 0",St
650    IF (St<>1) AND (St<>0) THEN GOTO 640
660    IF St=1 THEN REDIM Noco(2,Nnode)
670    IF St=0 THEN REDIM Noco(3,Nnode)
680    REDIM Errtot(Nelem)
690    MAT READ #1;Sen,Sn,Noco,Elco,Freq
700    ASSIGN * TO #1
710    PRINT PAGE;"Input number of measured frequencies which"
720    PRINT "you want to do the defect location analysis."
730    INPUT N
740    REDIM A(N),T(N),X(N-1),Y(N-1)
750    IF Mo=1 THEN GOTO 780
760    PRINT PAGE;"INPUT Exp. Changes in Nat. Freq's. 1,-------";N
770    MAT INPUT A
780    ! ********** FIND SMALLEST NON-ZERO SENSITIVITY *********
790    STANDARD
800    Count=1
810 Start:FOR Q=1 TO Nelem
820    FOR P=1 TO N
830    IF Mo<>0 THEN GOTO 960
840    Senmin=0
850    FOR I=1 TO Nelem
860    FOR J=1 TO N
870    IF (Sen(I,J)>0) AND (Senmin=0) THEN Senmin=Sen(I,J)
880    IF (Sen(I,J)>0) AND (Sen(I,J)<Senmin) THEN Senmin=Sen(I,J)
890    NEXT J
900    NEXT I
910    Amin=0
920    FOR I=1 TO N
930    IF (A(I)>0) AND (Amin=0) THEN Amin=A(I)
940    IF (A(I)>0) AND (A(I)<Amin) THEN Amin=A(I)
950    NEXT I
960    T(P)=Sen(Q,P)
970    IF T(P)<=0 THEN T(P)=Senmin/100*P
980    IF A(P)<=0 THEN A(P)=Amin/100
990    NEXT P
1000   FOR M=1 TO N-1
1010   X(M)=LOG(T(1))-LOG(T(M+1))
1020   Y(M)=LOG(A(1))-LOG(A(M+1))
1030   NEXT M
1040   REM *** READ EIGENVALUE & EIGENVECTOR *******
1050   N=N-1
1060   IF Count<>1 THEN GOTO 1240
1070   REDIM D(N),Z(N,N),Q(N,N),Dd(N,N),P(N,N),Eta(N),Ci(N)
1080   REDIM Zeta(N),Z1(N,N)
1090   IF N=9 THEN CALL Dof9(N,D(*),Z(*))  !If Considered 10 dof
1100   IF N=8 THEN CALL Dof8(N,D(*),Z(*))  !If Considered 9  dof
1110   IF N=7 THEN CALL Dof7(N,D(*),Z(*))  !If Considered 8  dof
1120   IF N=6 THEN CALL Dof6(N,D(*),Z(*))  !If Considered 7  dof
1130   IF N=5 THEN CALL Dof5(N,D(*),Z(*))  !If Considered 6  dof
1140   IF N=4 THEN CALL Dof4(N,D(*),Z(*))  !If Considered 5  dof
1150   IF N=3 THEN CALL Dof3(N,D(*),Z(*))  !If Considered 4  dof
1160   MAT Dd=ZER
1170   FOR I=1 TO N
1180   Dd(I,I)=1/D(I)     !To Find Matrix of 1/W
1190   NEXT I
1200   MAT Z1=TRN(Z)
```

```
1210  MAT Q=Z1*Dd
1220  MAT P=TRN(Q)
1230  ! !***************  TO FIND R^2  ******************
1240  ! ! *** To Calculate Matrix Ci  ****
1250  FOR I=1 TO N
1260  Ci(I)=0
1270  FOR J=1 TO N
1280  Ci(I)=Ci(I)+P(I,J)   !To Find Ci=Sigma Qij
1290  NEXT J
1300  NEXT I
1310  ! !**** To Calculate Matrix Of Sigma Square Ci  *****
1320  Ci2=0
1330  FOR J=1 TO N
1340  Ci2=Ci2+Ci(J)*Ci(J)
1350  NEXT J
1360  ! ! **** To Find Zeta  *****
1370  FOR I=1 TO N
1380  Zeta(I)=0
1390  FOR J=1 TO N
1400  Zeta(I)=Zeta(I)+P(I,J)*X(J)
1410  NEXT J
1420  NEXT I
1430  ! ! **** To Find Eta  ****
1440  FOR I=1 TO N
1450  Eta(I)=0
1460  FOR J=1 TO N
1470  Eta(I)=Eta(I)+P(I,J)*Y(J)
1480  NEXT J
1490  NEXT I
1500  ! ! **** To Find Sum Of Ci*Zeta  *****
1510  Cizeta=0
1520  FOR I=1 TO N
1530  Cizeta=Cizeta+Ci(I)*Zeta(I)
1540  NEXT I
1550  ! !**** To Find Sum Of Ci*Eta  *****
1560  Cieta=0
1570  FOR I=1 TO N
1580  Cieta=Cieta+Ci(I)*Eta(I)
1590  NEXT I
1600  ! !**** To Find Sum Of Squar Zeta  ****
1610  Zeta2=0
1620  FOR I=1 TO N
1630  Zeta2=Zeta2+Zeta(I)*Zeta(I)
1640  NEXT I
1650  ! !**** To Find Sum Of Zeta Eta  ****
1660  Zetaeta=0
1670  FOR I=1 TO N
1680  Zetaeta=Zetaeta+Zeta(I)*Eta(I)
1690  NEXT I
1700  ! ! **** To Find Sum Of Eta *****
1710  Sumeta=0
1720  FOR I=1 TO N
1730  Sumeta=Sumeta+Eta(I)
1740  NEXT I
1750  ! ! ****** To Find Sum Of Squar Eta  ****
1760  Sumeta2=0
1770  FOR I=1 TO N
1780  Sumeta2=Sumeta2+Eta(I)*Eta(I)
1790  NEXT I
1800  Bzn=0
```

```
1810   Bzn=Ci2*Zetaeta-Cizeta*Cieta
1820   Bzn=Bzn*Bzn/(Ci2*Zeta2-Cizeta*Cizeta)
1830   Bzn=Bzn+Cieta*Cieta
1840   Bzn=Bzn/Ci2
1850   Rs(Q)=0
1860   Rs(Q)=Bzn-Cieta*Cieta/Ci2
1870   Rs(Q)=Rs(Q)/(Sumeta2-Cieta*Cieta/Ci2)  !To Find R^2
1880   Errtot(Q)=Rs(Q)*100
1890   IF Count=1 THEN GOSUB Print
1900   Bd=Ci2*Zeta2-Cizeta*Cizeta
1910   B0(Q)=(Zeta2*Cieta-Cizeta*Zetaeta)
1920   B1(Q)=(Ci2*Zetaeta-Cizeta*Zetaeta)/Bd
1930   S2=(Sumeta2-Bzn)/(N-2)
1940   Se0(Q)=SQR(Zeta2*S2/Bd)
1950   Se1(Q)=SQR(Ci2*S2/Bd)
1960   B11(Q)=Zetaeta/Zeta2
1970   Rss(Q)=B11(Q)*Zetaeta/Sumeta2
1980   Se1(Q)=SQR(Sumeta2*(1-Rss(Q))/(Zeta2*(N-1)))
1990.  Errtot1(Q)=Rss(Q)*100
2000   Count=Count+1
2010   N=N+1
2020   IF Count>Nelem THEN GOTO 2130
2030   IF Q=1 THEN Errmin=Errtot(1) AND (Errmin1=Errtot1(1))
2040   IF Errtot(Q)<Errmin THEN Errmin=Errtot(H)
2050   IF Errtot1(Q)<Errmin1 THEN Errmin1=Errtot1(H)
2060   NEXT Q
2070   IF (Errmin>0) AND (Errmin1>0) THEN GOTO 2130
2080   ! Find Smallest Errtot & Errtot1 #0
2090   FOR I=1 TO Nelem
2100   IF Errtot(I)=0 THEN Errtot(I)=Errmin/1000
2110   IF Errtot1(I)=0 THEN Errtot1(I)=Errmin1/1000
2120   NEXT I
2130   PRINT PAGE;
2140   INPUT "Do You Want Print the Results, 1-Yes, 0-no",Res
2150   IF (Res<>1) AND (Res<>0) THEN GOTO 2130
2160   IF Res=1 THEN GOSUB Result
2170   PRINT PAGE;
2180   INPUT "Do You Want Plot, 1-Yes, 0-No",Pl
2190   IF (Pl<>1) AND (Pl<>0) THEN GOTO 2180
2200   IF Pl=1 THEN GOSUB Plot1
2210   PRINT PAGE;
2220   INPUT "Another Modes Required ?, 1 -Yes, 0 -NO",Mo
2230   IF Mo=0 THEN GOTO 2260
2240   INPUT " Input Number Of Modes You Want to Consider",N
2250   GOTO 740
2260   GCLEAR
2270   EXIT GRAPHICS
2280   PRINT PAGE;"COMPUTATION IS FINISHED"
2290   STOP
2300 Print: IF Mo<>0 THEN GOTO 2410
2310   PRINTER IS 0
2320   PRINT LIN(2);"Title of the problem is ";Title$
2330   PRINT LIN(1);"Experimental changes in Nat. Freq. is = "
2340   MAT PRINT A;
2350   PRINT "We seek largest Coeff. of Determination  (Rs or Rss)"
2360   PRINT "to match experimental changes in natural frequencies"
2370   PRINT "with set of theoretical,  by using Generalised Least"
2380   PRINT "Squares method to locate the most likly damage sites "
2390   PRINT LIN(1)
2400   PRINTER IS 16
```

```
2410  RETURN
2420 Result:PRINTER IS 0
2430  FIXED 3
2440  PRINT "Two Parameter Model (B0+B1x)"
2450  PRINT "Modes Considered is = 1 to ";N
2460  PRINT LIN(1)
2470  IMAGE 5A,3X,2A,3X,4X,2A,3X,4X,3A,3X,3X,2A,3X,4X,3A
2480  IMAGE DD,X,MDD.DDD,2X,MDD.DDD,2X,MDD.DDD,2X,MDD.DDD,2X,MDD.DDD
2490  PRINT USING 2470;"Nelem","Rs","B1","SE1","B0","SE0"
2500  PRINT USING 2470;"*****","**","**","***","**","***"
2510  PRINT LIN(1)
2520  FOR I=1 TO Nelem
2530  PRINT USING 2480;I,Rs(I),B1(I),Se1(I),B0(I),Se0(I)
2540  NEXT I
2550  PRINT LIN(2)
2560  INPUT "Reduced Model Required", 1-Yes, 0-No",Rm
2570  IF Rm<>1 THEN GOTO 2680
2580  PRINT "Reduced Model (B1 Only)"
2590  IMAGE X,5A,4X,5A,4X,5A,4X,5A
2600  IMAGE 2X,DD,2X,MDD.DDD,2X,MDD.DDD,2X,MDD.DDD
2610  PRINT USING 2590;"Nelem","Rss","B1:","SE1"
2620  PRINT USING 2590;"*****","***","***","***"
2630  PRINT LIN(1)
2640  FOR I=1 TO Nelem
2650  PRINT USING 2600;I,Rss(I),B11(I),Se1(I)
2660  NEXT I
2670  PRINTER IS 16
2680  RETURN
2690   ! ************************************************************
2700 Plot1: !
2710  FOR X=1 TO 2
2720  Ans2=4
2730  FIXED 0
2740  IF St=1 THEN GOTO 3030
2750  REDIM Tc(2,Nnode),Sin(Nelem) !Tc]=Transform Coord. Matrix
2760  DEG
2770  ! INPUT "Angle about X,Y,Z",Anglex,Angley,Anglez
2780  Anglex=-25
2790  Angley=35
2800  Anglez=15
2810  C1=COS(Anglex)
2820  S1=SIN(Anglex)
2830  C2=COS(Angley)
2840  S2=SIN(Angley)
2850  C3=COS(Anglez)
2860  S3=SIN(Anglez)
2870  FOR I=1 TO Nnode
2880  Z1=C3*C2*Nodo(1,I)+(S3*C1+S1*C3*S2)*Nodo(2,I)
2890  Z2=(S1*S3-C1*C3*S2)*Nodo(3,I)
2900  Tc(1,I)=Z1+Z2
2910  Z3=-S3*C2*Nodo(1,I)+(C1*C3-S1*S2*S3)*Nodo(2,I)
2920  Z4=(S1*C3+C1*S2*S3)*Nodo(3,I)
2930  Tc(2,I)=Z3+Z4
2940  NEXT I
2950  ! !TO FIND THE DIMENSIONS OF THE STRUCTURE
2960  FOR I=1 TO Nnode
2970  IF Tc(1,I)>Xmax THEN Xmax=Tc(1,I)
2980  IF Tc(1,I)<Xmin THEN Xmin=Tc(1,I)
2990  IF Tc(2,I)>Ymax THEN Ymax=Tc(2,I)
3000  IF Tc(2,I)<Ymin THEN Ymin=Tc(2,I)
```

```
3010  NEXT I
3020  GOTO 3100
3030  REM FIND THE DIMENSIONS OF THE STRUCTURE
3040     FOR I=1 TO Nnode
3050     IF Noco(1,I)>Xmax THEN Xmax=Noco(1,I)
3060     IF Noco(1,I)<Xmin THEN Xmin=Noco(1,I)
3070     IF Noco(2,I)>Ymax THEN Ymax=Noco(2,I)
3080     IF Noco(2,I)<Ymin THEN Ymin=Noco(2,I)
3090     NEXT I
3100  IF Xmax-Xmin>0 THEN 3130
3110  Xmin=Ymin
3120  Xmax=Ymax
3130  IF Ymax-Ymin>0 THEN 3160
3140  Ymin=Xmin
3150  Ymax=Xmax
3160  Min=MIN(Xmax-Xmin,Ymax-Ymin)
3170  IF X=1 THEN GOTO 3200
3180  INPUT "Figure Number of Reduced Model?",No$
3190  GOTO 3210
3200  INPUT "Figure Number?(If no Title is required input 0",No$
3210  IF No$="0" THEN GOTO 3250
3220  LINPUT "Main Title Of PLOT No.1",M$
3230  LINPUT "Main Title Of PLOT No.2",M2$
3240  LINPUT "Title Of Plot",T$
3250  INPUT "Select Corner ?; 0-4 FOR PLANE, 0-2 FOR SPACE",Corn
3260  PRINTER IS 16
3270  PRINT PAGE,"Select Plotter Device With The Following Codes"
3280  PRINT SPA(20)," 1  For Screen (CRT)"
3290  PRINT SPA(20)," 2  For Benson Plotter"
3300  PRINT SPA(20)," 3  For 9872A  Plotter"
3310  INPUT Plottercode
3320  IF (Plottercode>0) AND (Plottercode<4) THEN GOTO 3350
3330  BEEP
3340  GOTO 3310
3350  Sety=Dump=Benson=0
3360  IF Plottercode=1 THEN Plotter=13
3370  IF Plottercode=2 THEN Plotter=5
3380  IF Plottercode=3 THEN Plotter=7
3390  IF Plotter=13 THEN GOTO 4110
3400  IF Plotter=5 THEN GOTO 4050
3410  IF Plotter=7 THEN GOTO 3440
3420  BEEP
3430  GOTO 3280
3440  PLOTTER IS 7,5,"9872A"
3450  PRINTER IS 7,5
3460  PRINT "VS2"
3470  PRINTER IS 16
3480  Scay=1
3490  Scax=285/260
3500  Sety=0
3510  PEN 1
3520  SETUU
3530  INPUT "If You Want Vertical 1 ;Otherwie 0 ",Ver
3540  IF (Ver=0) OR (Ver=1) THEN GOTO 3570
3550  BEEP
3560  GOTO 3530
3570  IF Ver<>1 THEN GOTO 3820
3580  LIMIT 20,190,0,280
3590  MOVE 50*Scax,Sety+155*Scay
3600  LORG 6
```

```
3610  CSIZE 3.3*Scax
3620  LABEL M$
3630  MOVE 50*Scax,Sety+150*Scay
3640  CSIZE 3.1*Scax
3650  LABEL M2$
3660  IF St=1 THEN GOTO 3710
3670  IF Corn=0 THEN LIMIT 0,200,0,280
3680  IF Corn=1 THEN LIMIT 5,115,10,270
3690  IF Corn=2 THEN LIMIT 90,200,10,270
3700  GOTO 3760
3710  IF Corn=0 THEN LIMIT 0,200,0,280
3720  IF Corn=1 THEN LIMIT 10,110,10,140
3730  IF Corn=2 THEN LIMIT 10,110,140,280
3740  IF Corn=3 THEN LIMIT 100,200,10,140
3750  IF Corn=4 THEN LIMIT 100,200,140,280
3760  MOVE 50*Scax,Sety+15*Scay
3770  LORG 6
3780  CSIZE 3.8*Scay
3790  LABEL ""&No$&" "&T$
3800 ! GOTO 4040
3810  GOTO 4190
3820  LIMIT 30,280,0,200
3830  MOVE 50*Scax,Sety+8*Scay
3840  LORG 6
3850  CSIZE 2.7*Scay
3860  LABEL M$
3870  MOVE 50*Scax,Sety+4*Scay
3880  CSIZE 2.7*Scay
3890  LABEL M2$
3900  IF St=1 THEN GOTO 3950
3910  IF Corn=0 THEN LIMIT 0,285,0,200
3920  IF Corn=1 THEN LIMIT 0,145,5,175
3930  IF Corn=2 THEN LIMIT 120,265,5,175
3940  GOTO 4000
3950  IF Corn=0 THEN LIMIT 0,285,0,200
3960  IF Corn=1 THEN LIMIT 0,142,5,100
3970  IF Corn=2 THEN LIMIT 0,142,90,185
3980  IF Corn=3 THEN LIMIT 142,285,5,100
3990  IF Corn=4 THEN LIMIT 142,285,90,185
4000  MOVE 65*Scax,Sety+12*Scay
4010  LORG 6
4020  CSIZE 3.8*Scay
4030  LABEL ""&No$&" "&T$
4040  GOTO 4190
4050  Benson=1
4060  PLOTTER IS 5,"INCREMENTAL",.05
4070  LIMIT 0,1000,0,930
4080  Scay=210/930
4090  Scax=29700/930/130
4100  GOTO 4190
4110  IF Again THEN GOTO 4130
4120  PRINTER IS 16
4130  INPUT "To Dump Graphics INPUT 1,Otherwise INPUT 0",Dump
4140  PLOTTER IS 13,"GRAPHICS"
4150  Pcount=0
4160  Scax=Scay=1
4170  LOCATE 5*Scax,120*Scax,Sety+(Benson*5+100)*Scax,90*Scay+Sety
4180  GRAPHICS
4190  REM PLOT *****
4200  IF Plotter=13 THEN GOTO 4210
```

```
4210  IF Plotter=7 THEN GOTO 4280
4220  CALL Frame(Sety,Scax,Scay)
4230  GOTO 4280
4240  MOVE 65,94
4250  CSIZE 3.3*Scay
4260  LORG 4
4270  LABEL ""&No$&" "&T$
4280  IF (Ver=1) AND (St=0) THEN GOTO 4340
4290  IF (Ver=1) AND (St=1) THEN GOTO 4370
4300  IF Plottercode=1 THEN GOTO 4390
4310  LOCATE 5*Scax,120*Scax,Sety+(Benson*5+20)*Scay,110*Scay+Sety
4320  GOTO 4450
4330  ! FOR SPACE FRAME
4340  LOCATE 15*Scax,77*Scax,Sety+(Benson*5+10)*Scay,260*Scay+Sety
4350  GOTO 4450
4360  ! FOR PLANE FRAME
4370  LOCATE 20*Scax,75*Scax,Sety+(Benson*5+20)*Scay,100*Scay+Sety
4380  GOTO 4450
4390  LOCATE 5*Scax,120*Scax,Sety+(Benson*5+10)*Scay,90*Scay+Sety
4400  GOTO 4450
4410   FRAME
4420   PRINTER IS 0
4430  SHOW Xmin-.25*Min,Xmax+.25*Min,Ymin-.25*Min,Ymax+.25*Min
4440  GOTO 4470
4450  SHOW Xmin,Xmax,Ymin,Ymax
4460  REM PLOT UNDEFLECTED STRUCTURE
4470  LINE TYPE 1
4480  IF St=1 THEN GOTO 4780
4490  FOR I=1 TO Nelem
4500  MOVE Tc(1,Elco(1,I)),Tc(2,Elco(1,I))
4510  DRAW Tc(1,Elco(2,I)),Tc(2,Elco(2,I))
4520  NEXT I
4530  ! ! LABEL DEFECT PROBABILITY
4540  CSIZE 3.8
4550  FOR I=1 TO Nelem
4560  Ax=(Tc(1,Elco(1,I))+Tc(1,Elco(2,I)))/2
4570  Ay=(Tc(2,Elco(1,I))+Tc(2,Elco(2,I)))/2
4580  L1=Tc(1,Elco(1,I))-Tc(1,Elco(2,I))
4590  L2=Tc(2,Elco(1,I))-Tc(2,Elco(2,I))
4600  S=SQR(L1^2+L2^2)
4610  Sin(I)=(Tc(2,Elco(2,I))-Tc(2,Elco(1,I)))/S
4620  ! ** MOVE TO THE MIDDLE OF ELEMENT
4630  LORG 4
4640  MOVE Ax,Ay
4650  ! ! ** LABEL PERP. TO ELEM. **
4660  IF L1>0 THEN Ang=-ASN(Sin(I))
4670  IF L1<0 THEN Ang=ASN(Sin(I))
4680  IF L1=0 THEN Ang=PI/2
4690  LDIR Ang
4700  IF X=1 THEN GOTO 4730
4710  LABEL Errtot1(I)
4720  GOTO 4740
4730  LABEL Errtot(I)
4740  NEXT I
4750  PAUSE
4760  GOTO 5130
4770  ! !!FOR PLANE FRAME
4780     FOR I=1 TO Nelem
4790     MOVE Noco(1,Elco(1,I)),Noco(2,Elco(1,I))
4800     DRAW Noco(1,Elco(2,I)),Noco(2,Elco(2,I))
```

```
4810      NEXT I
4820   REM LABEL THE ELEMENTS
4830   CSIZE 3.8
4840      FOR I=1 TO Nelem
4850      Ax=(Noco(1,Elco(1,I))+Noco(1,Elco(2,I)))/2
4860      Ay=(Noco(2,Elco(1,I))+Noco(2,Elco(2,I)))/2
4870      REM MOVE TO MIDDLE OF ELEMENT
4880      LORG 4
4890      MOVE Ax,Ay
4900      ! MAKE LABEL PERP TO ELEM AND OR LEGIBLE FROM RIGHT SIDE
4910      Dx=Noco(1,Elco(2,I))-Noco(1,Elco(1,I))
4920      IF Dx>0 THEN 4960
4930      IF Dx<0 THEN 4980
4940      Ang=PI/2
4950      GOTO 4990
4960      Ang=ASN(Sn(I))
4970      GOTO 4990
4980      Ang=-ASN(Sn(I))
4990      LDIR Ang
5000      IF Ans2=4 THEN 5040
5010      REM LABEL ELEMENT NUMBER
5020      LABEL I
5030      GOTO 5100
5040      REM LABEL DEFECTPROBABILITY
5050      FIXED 0
5060      IF X=1 THEN GOTO 5090
5070      LABEL Errtot1(I)
5080      GOTO 5100
5090      LABEL Errtot(I)
5100      NEXT I
5110   IF Ans2=4 THEN 5120
5120   PAUSE
5130   IF Plotter<>13 THEN GOTO 5220
5140   IF NOT Dump THEN GOTO 5220
5150   PRINT LIN(6)
5160   DUMP GRAPHICS
5170   PRINT ""&No$&" "&T$
5180   EXIT GRAPHICS
5190   PRINT RPT$("-",80),LIN(2)
5200   PRINTER IS 16
5210   GOTO 5270
5220   MOVE 65*Scax,Saty+10*Scay
5230   CSIZE 3*Scay
5240   MOVE 65*Scax,Saty+7*Scay
5250   CSIZE 2*Scay
5260   CSIZE 3.3*Scay
5270   IF Plotter=13 THEN 5300
5280   IF INT(No/4)*4-No=0 THEN GOTO 5320
5290   MOVE 0,Benson+110*Scay
5300   IF Again THEN GOTO 5430
5310   GOTO 5420
5320   IF Plotter=7 THEN GOTO 5400
5330   LOCATE 0,140*Scax,0,110*Scay  !PLOTTER IS 5
5340   SETGU
5350   MOVE 140*Scax,0
5360   PLOTTER IS 5,"INCREMENTAL",.05
5370   LIMIT 0,1000,0,-900
5380   MOVE 0,330*Scay
5390   GOTO 5410
```

```
5410  Sety=0
5420  Again=1
5430  PEN 0
5440  IF Ans2<>3 THEN 5450
5450  EXIT GRAPHICS
5460  GCLEAR
5470  ! DSIP"COMPUTION IS FINISHED"
5480  NEXT X
5490  PRINTER IS 16
5500  RETURN
5510  SUB Frame(Sety,Scax,Scay)
5520  MOVE 0,Sety
5530  DRAW 0,Sety+100*Scay
5540  DRAW 130*Scax,Sety+100*Scay
5550  DRAW 130*Scax,Sety
5560  DRAW 0,Sety
5570  SUBEND
5580  ! ++++++++++++++++++++++++++++++++++++++++++++++++++++++++++++++++++++
5590  SUB Dof9(N,D(*),Z(*))
5600  MAT READ D    !Eigevalues
5610  MAT READ Z    !Eigenvectors
5620  ! ! INPUT Eigenvalues, Start From Largest One, Which was Cal.
5630  ! ! From Covariance Matrix to Fit The Best Regression Line
5640  DATA 3.966,3.101,2.92,2.733,2.534,2.319,2.0824,1.815,1.497
5650  ! ! INPUT Eienvectors, Start From Largest One, Which Was Cal.
5660  ! ! From Covarance Matrix to Fit the Best Regression Line
5670  DATA .21,.2264,.2457,.269,.2962,.3301,.373,.4283,.5031
5680  DATA -.0414,-.04764,-.056,-.0683,-.0872,-.121,-.1953,-.514,.81
5
5690  DATA -.0503,-.0593,-.073,-.093,-.13,-.215,-.6231,.6923,.2225
5700  DATA -.0594,-.073,-.094,-.1316,-.2214,-.6954,.6093,.212,.1282
5710  DATA .0713,.0921,.1302,.222,.751,-.5423,-.1992,-.122,-.088
5720  DATA .0891,.1266,.2185,.7978,-.483,-.1354,-.1147,-.083,-.0651
5730  DATA -.1211,-.2116,-.841,.4263,.17,.1062,.0772,.061,.04994
5740  DATA .201,.884,-.3674,-.1521,-.0959,-.07,-.0551,-.0455,-.0387
5750  DATA .9382,-.2958,-.1278,-.082,-.0598,-.0472,-.039,-.0333,-.02
9
5760  SUBEND
5770  SUB Dof8(N,D(*),Z(*))
5780  MAT READ D    !Eigevalues
5790  MAT READ Z    !Eigenvectors
5800  ! ! INPUT Eienvalues, Start From Largest One, Which Was Cal.
5810  ! ! From Covarance Matrix to Fit the Best Regression Line
5820  DATA 3.761,2.933,2.7404,2.54,2.323,2.09,1.818,1.499
5830  ! ! INPUT Eienvectors, Start From Largest One, Which Was Cal.
5840  ! ! From Covarance Matrix to Fit the Best Regression Line
5850  DATA .224,.244,.268,.297,.334,.3803,.4422,.5282
5860  DATA -.049,-.0572,-.07,-.089,-.1232,-.2,-.534,.801
5870  DATA .06,.073,.094,.1312,.2181,.6461,-.672,-.221
5880  DATA .073,.094,.132,.223,.72,-.5841,-.208,-.1264
5890  DATA .091,.129,.221,.778,-.513,-.193,-.119,-.086
5900  DATA -.124,-.215,-.828,.448,.1762,.11,.08,.063
5910  DATA -.2042,-.876,.383,.157,.099,.072,.057,.047
5920  DATA -.935,.306,.131,.084,.0613,.0484,.04,.0341
5930  SUBEND
5940  SUB Dof7(N,D(*),Z(*))
5950  MAT READ D    !Eigevalues
5960  MAT READ Z    !Eigenvectors
5970  ! ! INPUT Eigenvalues For 7 d.o.f
5980  DATA 3.544,2.754,2.548,2.33,2.0904,1.8212,1.5015
```

```
5990  ! ! INPUT Eigenvectors For 7 d.o.f
6000  DATA .241,.266,.297,.3363,.38753,.45723,.5575
6010  DATA -.05834,-.07107,-.0909,-.1261,-.20563,-.55754,.784
6020  DATA .0735,.09451,.1325,.2214,.6732,-.54671,-.21843
6030  DATA .093,.1313,.22345,.75,-.5533,-.2021,-.12361
6040  DATA .12644,.21875,.81024,-.4755,-.1338,-.11393,-.08254
6050  DATA .2083,.8657,-.4015,-.163,-.10222,-.07447,-.05857
6060  DATA -.9302,.31745,.1356,.0862,.0632,.0499,.0412
6070  SUBEND
6080  SUB Dof3(N,D(*),Z(*))
6090  MAT READ D    !Eigevalues
6100  MAT READ Z    !Eigenvectors
6110  ! ! INPUT Eigenvalues For 3 d.o.f
6120  DATA 2.493,1.86,1.525
6130  ! ! INPUT Eigenvectors For 3 d.o.f
6140  DATA .3971,.5207,.7558,-.2332,-.739,.632,.8877,-.427,-.172
6150  SUBEND
6160  SUB Dof5(N,D(*),Z(*))
6170  MAT READ D    !Eigevalues
6180  MAT READ Z    !Eigenvectors
6190  ! ! INPUT Eigenvalues For 5 d.o.f
6200  DATA 3.064,2.354,2.106,1.832,1.509
6210  ! ! INPUT Eigenvectors For 5 d.o.f
6220  DATA .2911,.3366,.3991,.48998,.6345,-.09514,-.1326,-.2187
6230  DATA -.6233,.733,.1334,.2263,.7469,-.5745,-.2075,.2139,.8023
6240  DATA -.4617,-.1807,-.1124,-.9168,.3525,.14782,.09352,.0634
6250  SUBEND
6260  SUB Dof6(N,D(*),Z(*))
6270  MAT READ D    !Eigevalues
6280  MAT READ Z    !Eigenvectors
6290  ! ! INPUT Eigenvalues For 6 d.o.f
6300  DATA 3.313,2.562,2.338,2.0966,1.8258,1.5048
6310  ! ! INPUT Eigenvectors For 6 d.o.f
6320  DATA .2623,.2952,.3376,.3941,.4733,.5923,-.0726,-.093,-.1292
6330  DATA -.2118,-.5867,.7618,-.0486,-.1333,-.2243,-.7059,.6154
6340  DATA 2143,-.1297,-.2227,-.7857,.5143,.1937,.1193,-.21314,-.852
6350  DATA .4265,.1706,.1066,.078,-.9245,.3325,.141,.0894,.0655,.052
6360  SUBEND
6370  SUB Dof4(N,D(*),Z(*))
6380  MAT READ D    !Eigevalues
6390  MAT READ Z    !Eigenvectors
6400  ! ! INPUT Eigenvalues For 5 d.o.f
6410  DATA 3.0644,2.3538,2.1059,1.83211,1.5092
6420  ! ! INPUT Eigenvectors For 5 d.o.f
6430  DATA .2911,.33664,.3991,.48998,.6345,-.09514,-.1326,-.21866
6440  DATA -.62329,.73285,.1334,.22633,.74685,-.5745,-.20746
6450  DATA .21894,.33285,-.46167,-.18074,-.112365
6460  DATA -.916785,.35247,.14782,.09352,.068395
6470  SUBEND
```

APPENDIX 3

RESULTS OF DEFECT LOCATION BASED ON CAWLEY-ADAMS METHOD

Cawley–Adams (NPE)

a– Spring model
10mm Saw Cut at A

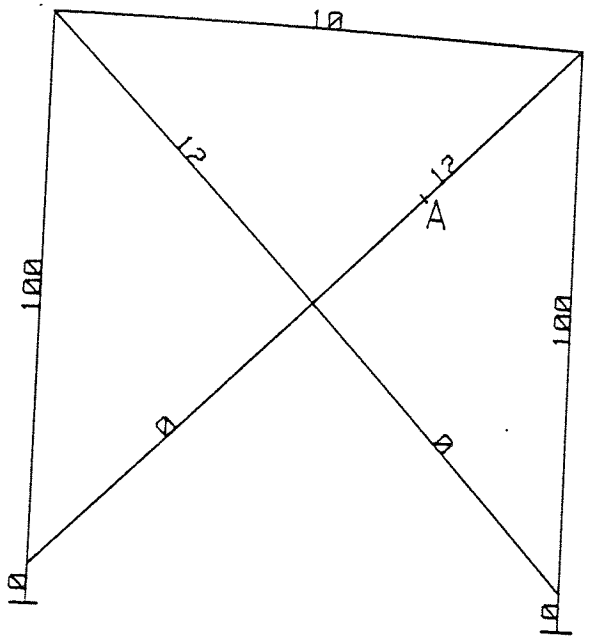

b– Red. rig. whole elem.
Complete Cut at A

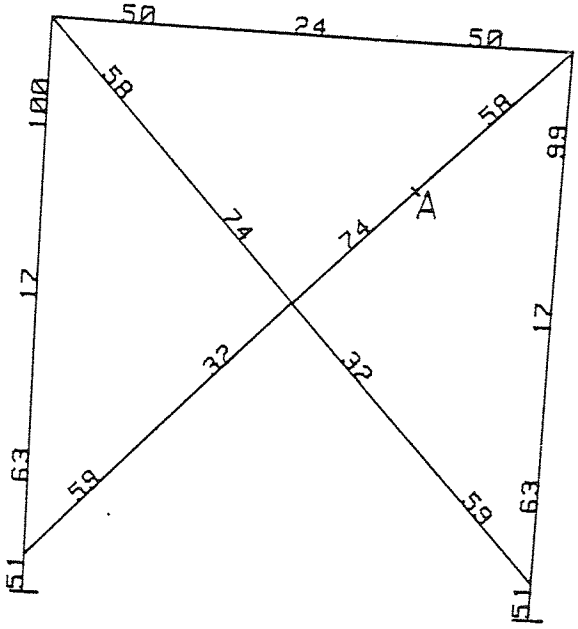

9 modes are considered

Two–cantilever model

c– Fixed ends
Complete Cut at A

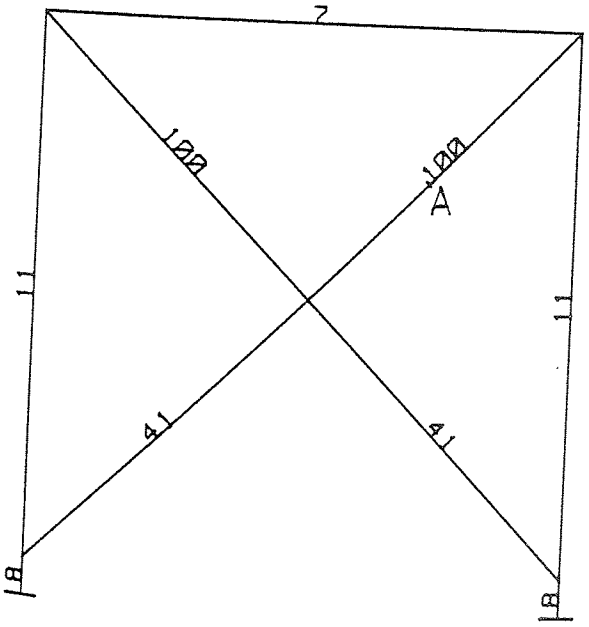

d– Pinned ends
Complete Cut at A

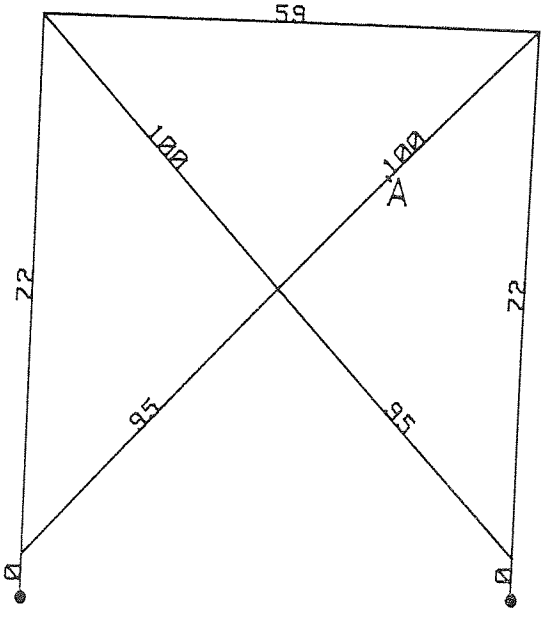

Fig. A3.1 a–d DEFECT LOCATION CHARTS OF CROSS BRACE PORTAL

a– Red. rig. whole elem.
10 mm cut at B
9 modes

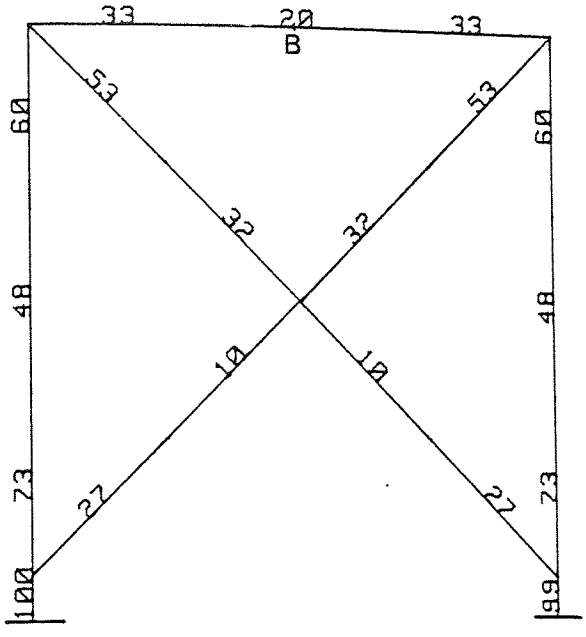

b– Spring model
15mm saw cut at B
4 modes

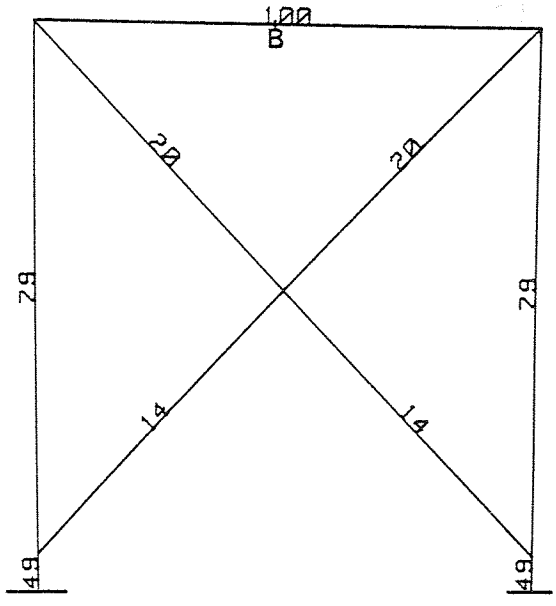

c– Two–cantilever model
Complete cut at B
9 modes

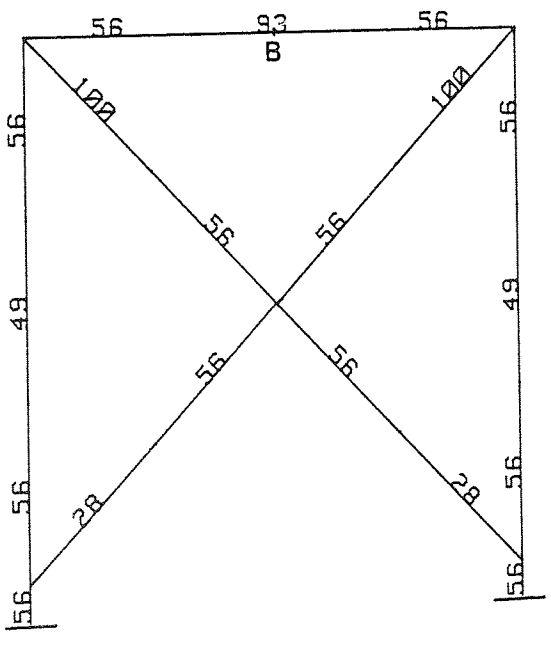

Fig. A3.2 DEFECT LOCATION CHARTS OF CROSS–BRACE PORTAL FRAME FOR VARIOUS SAW CUT DEPTHS

Cawely–Adams (NPE)

a– Spring model
2mm Saw Cut at A

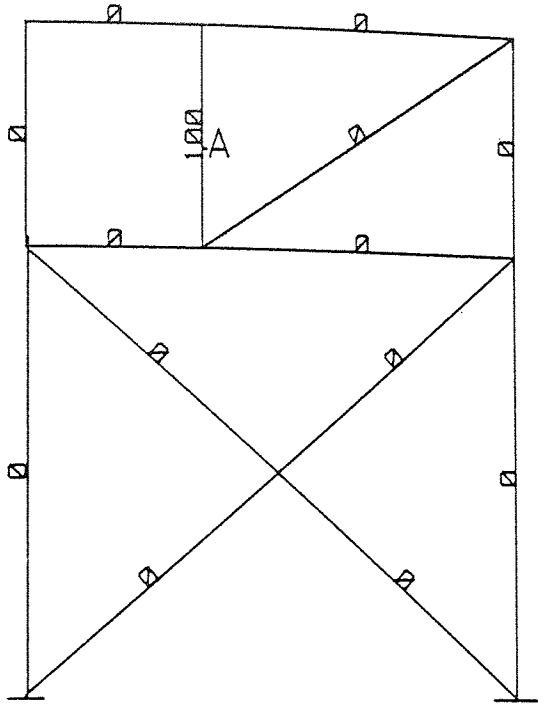

10 modes

b– Red. rig. whole elem.
Complete Cut at A

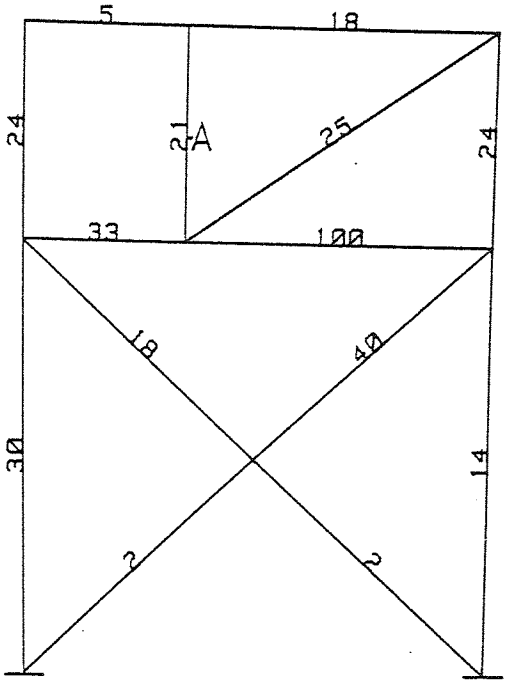

Two–cantilever model

c– 9 modes
Complete Cut at A

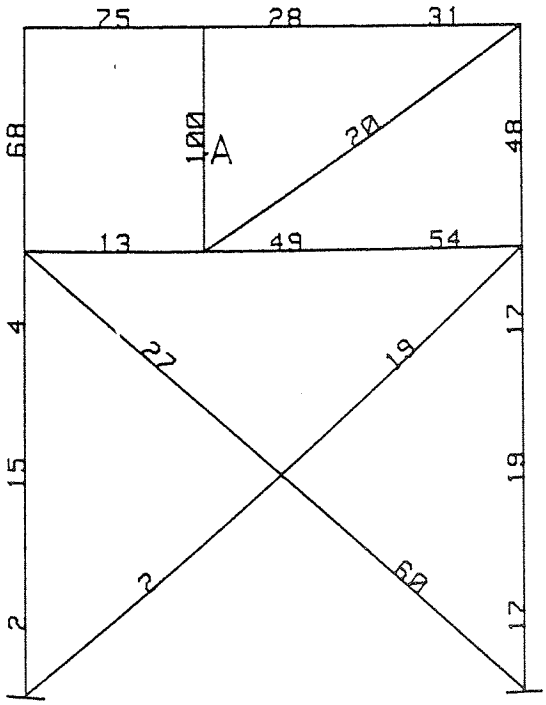

d– 8 modes
Complete Cut at A

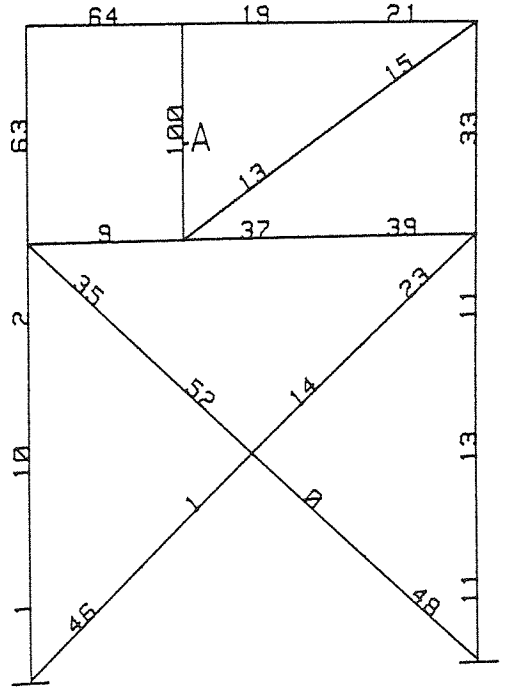

Fig. A3.3 a–d DEFECT LOCATION CHARTS OF ASYMMETRIC FRAME

Cawley–Adams (NPE)
4 modes

a– Red. rig. whole elem.
5mm saw cut at D

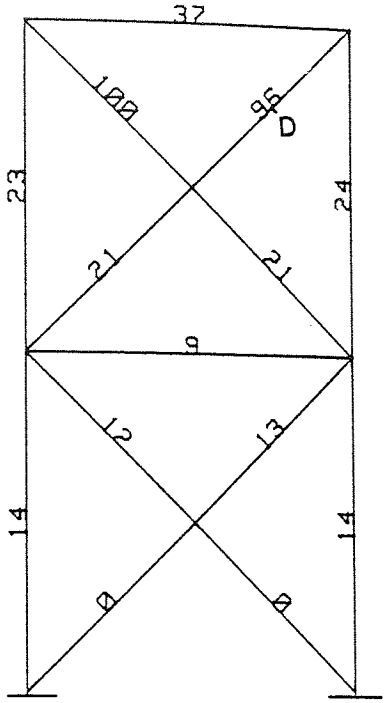

b– Two–cantilever model
5mm saw cut at D

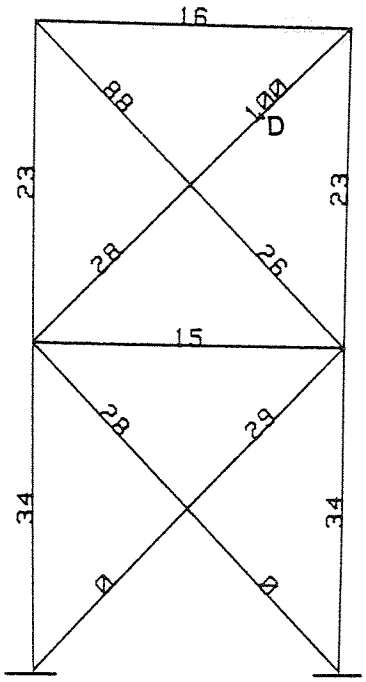

c– Two–cantilever model
Complete cut at D

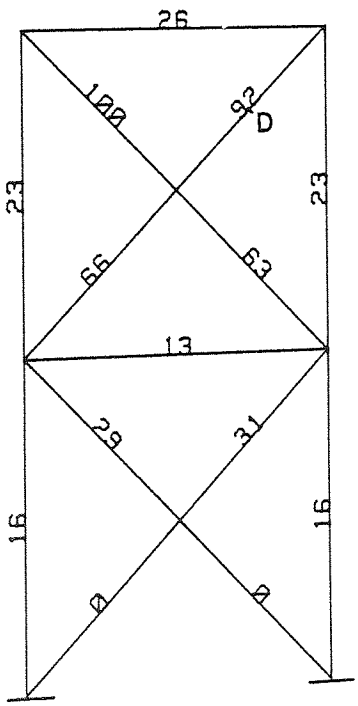

Fig. A3.4a–c DEFECT LOCATION CHARTS OF SYMMETRIC TOWER
FOR VARIOUS DAMAGE MODELS (CUT AT D)

Cawley–Adams(NPE)
9 modes

a– Two–cantilever model
Complete Cut at C

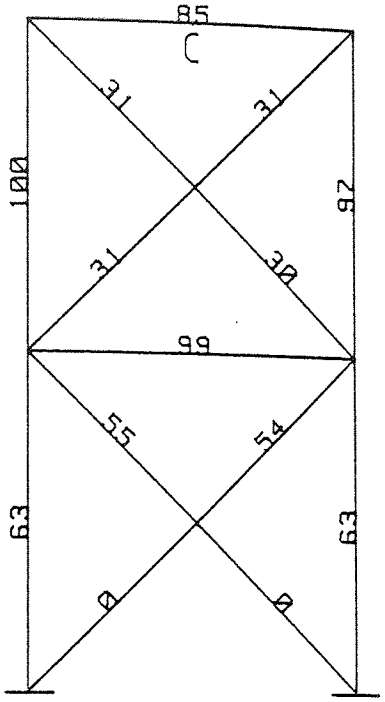

b– Red. rig. whole elem.
Complete Cut at C

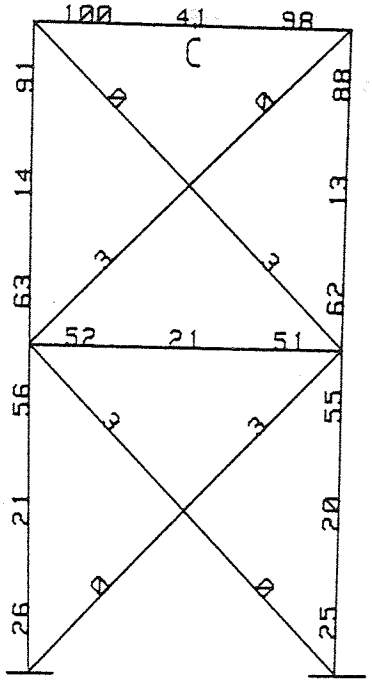

c– Two–cantilever model
Complete Cut at A

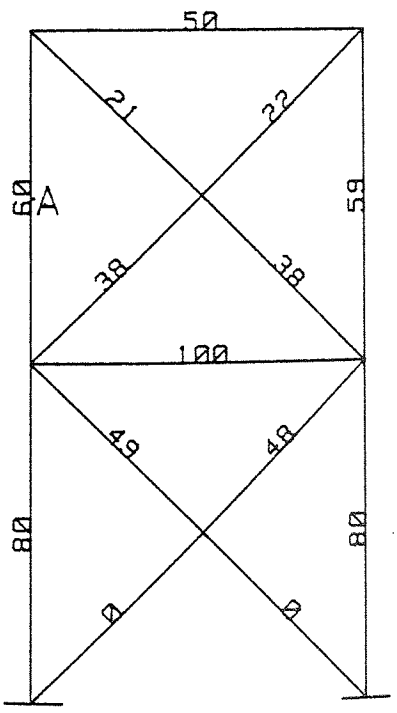

d– Red. rig. whole elem.
Complete Cut at A

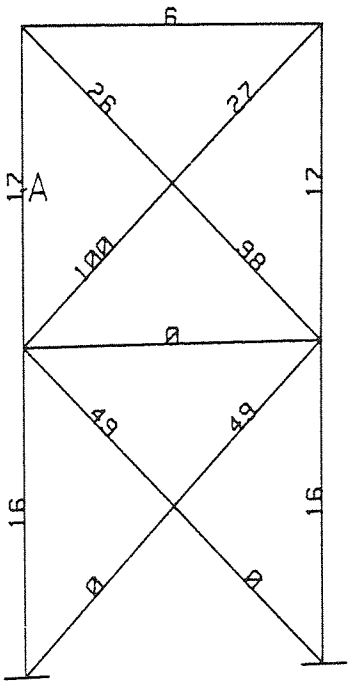

Fig. A 3.5a–d DEFECT LOCATION CHARTS OF SYMMETRIC TOWER FRAME 1 FOR VARIOUS DAMAGE MODELS(CUT AT C&A)

Cawley–Adams (NPE)
4 modes

a– Two–cantilever model
1st complete cut at E

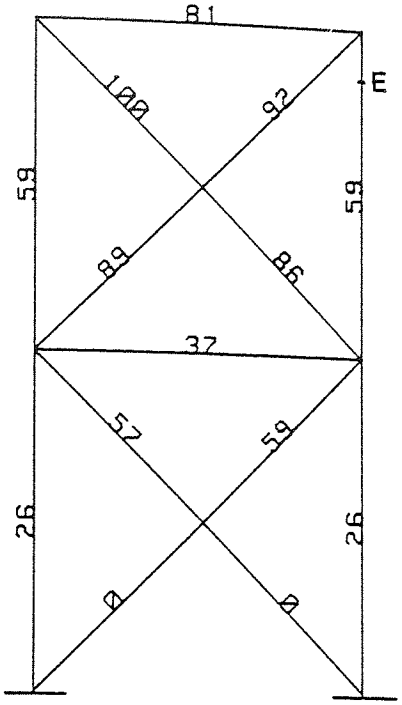

b– Red. rig. whole elem.
1st complete cut at E

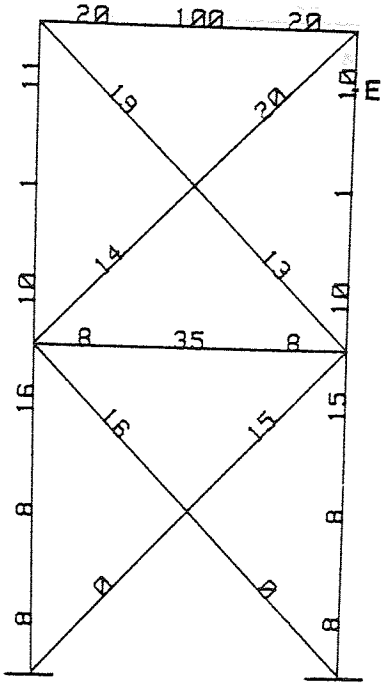

c– Red. rig. whole elem.
2nd complete cut at E

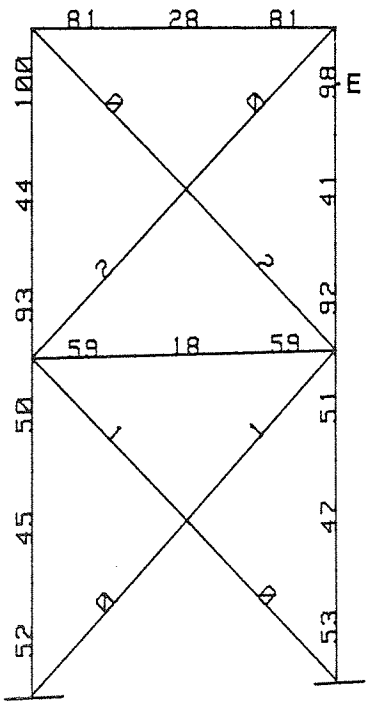

Fig. A3.6a–c DEFECT LOCATION CHARTS OF SYMMETRIC TOWER FRAME 2 FOR VARIOUS DAMAGE MODELS

a– Red. rig. whole elem.
6mm Saw Cut at E

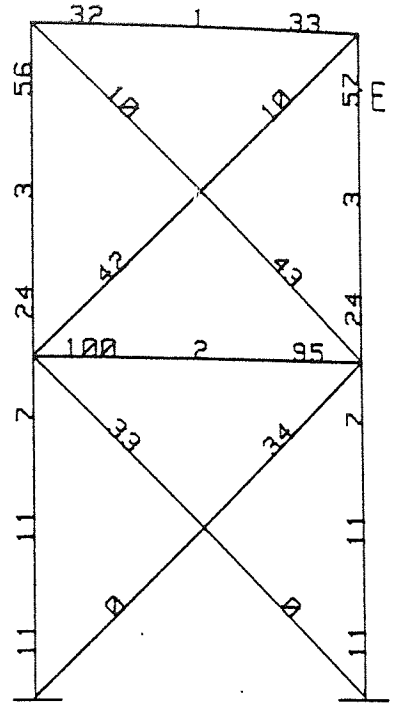

4 modes

b– Red. rig. whole elem.
10mm Saw Cut at E

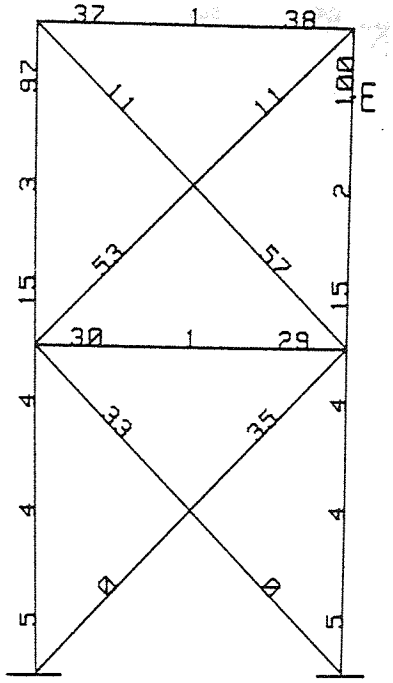

c– Two–cantilever,
15mm Saw Cut at E
8 modes

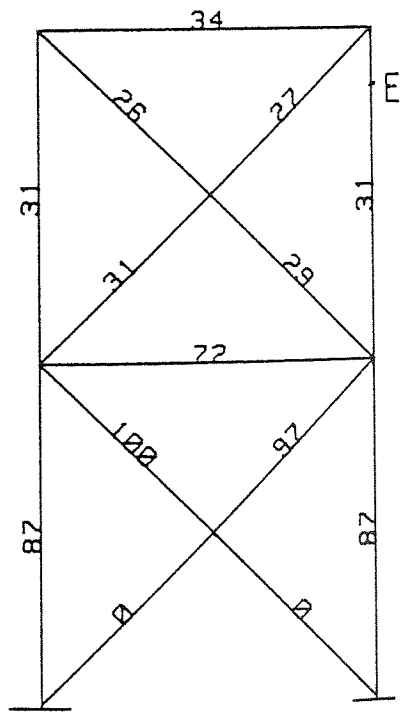

d– Red. rig. whole elem.
3rd Complete Cut at E
9 modes

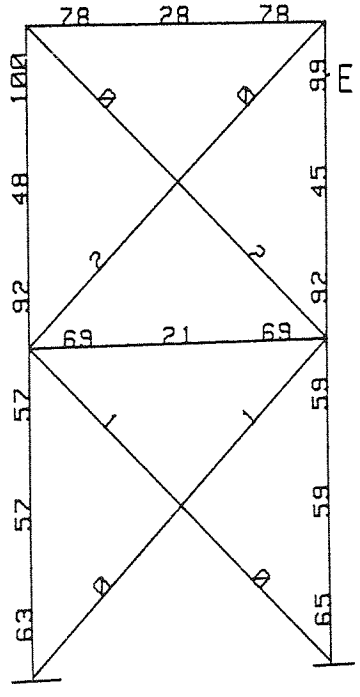

Fig. A3·7a–d DEFECT LOCATION CHARTS OF SYMMETRIC TOWER FRAME 2 FOR VARIOUS SAW CUT DEPTHS

a– Two–cantilever model
Complete Cut at B

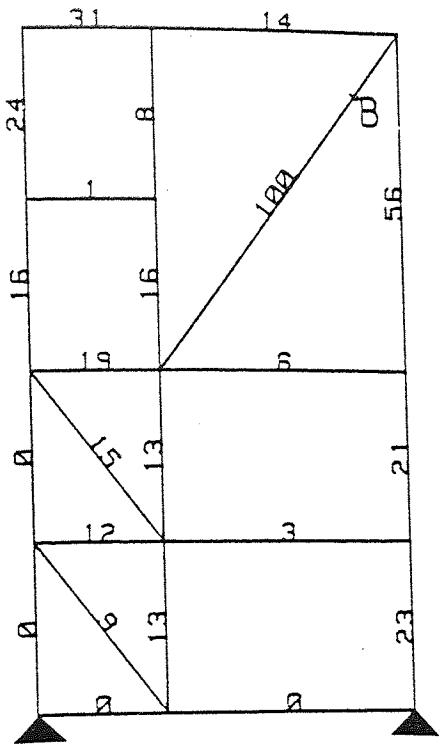

10, 4 modes

b– Red. rig. whole elem.
Complete Cut at B

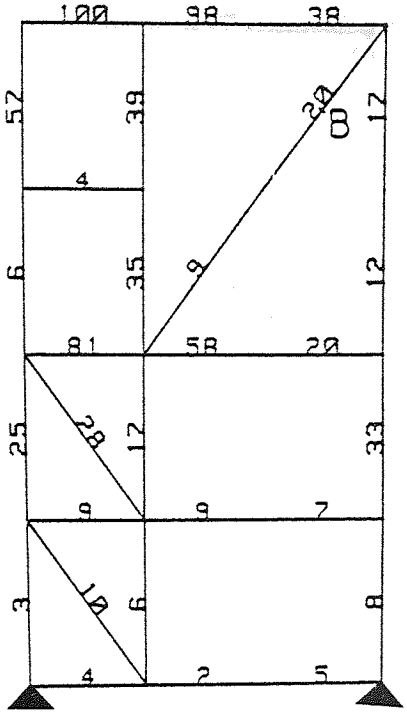

Fig.A3.8a–b DEFECT LOCATION CHARTS OF ASYMMETRIC TOWER FRAME FOR VARIOUS DAMAGE MODELS

c– Two–cantilever model
Complete Cut at A
9 modes

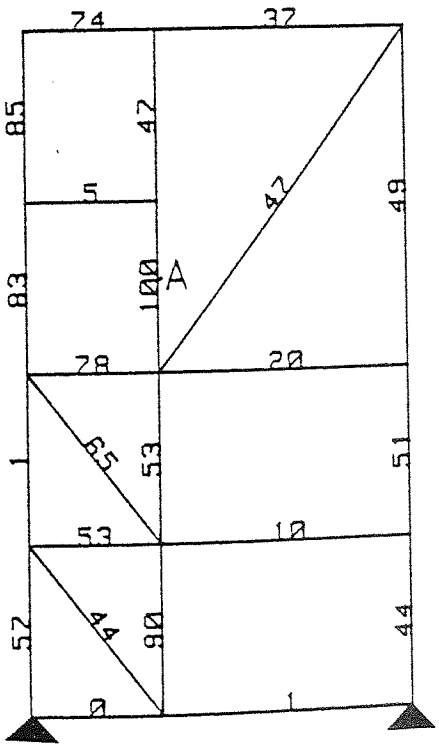

d– Red. rig. whole elem.
10mm Saw Cut at B
4 modes

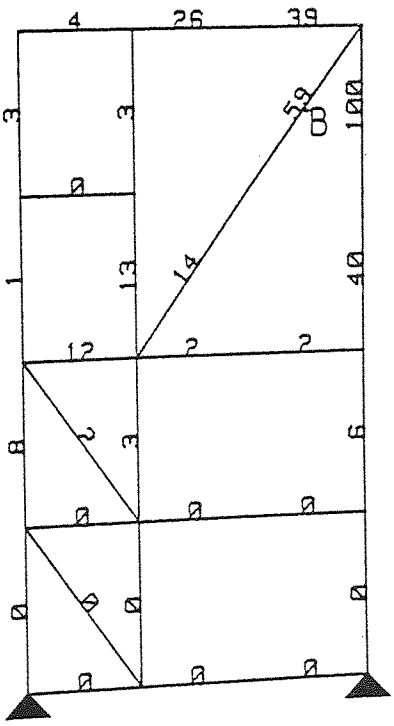

Fig.A3.8c–d DEFECT LOCATION CHARTS OF ASYMMETRIC TOWER FRAME FOR VARIOUS DAMAGE SITES

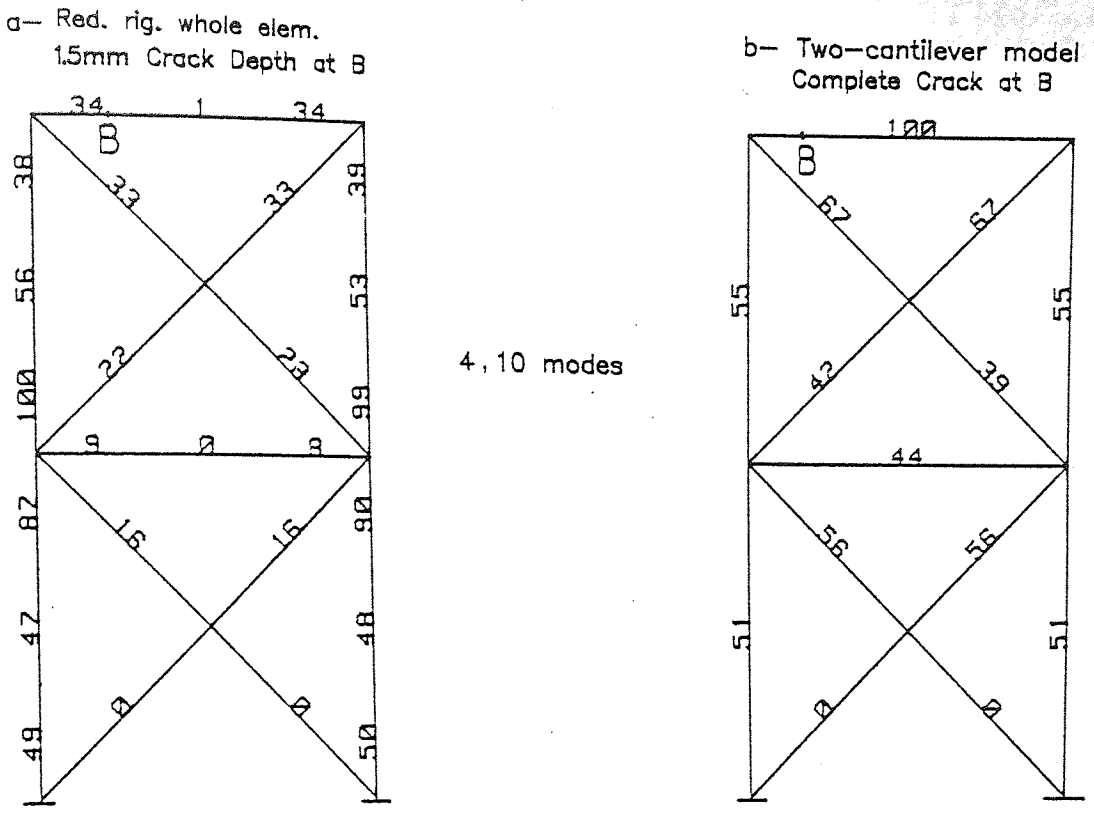

Fig.A3.9 a–b DEFECT LOCATION CHARTS OF SYMMETRIC TOWER FRAME 3 FOR VARIOUS CRACK DEPTHS

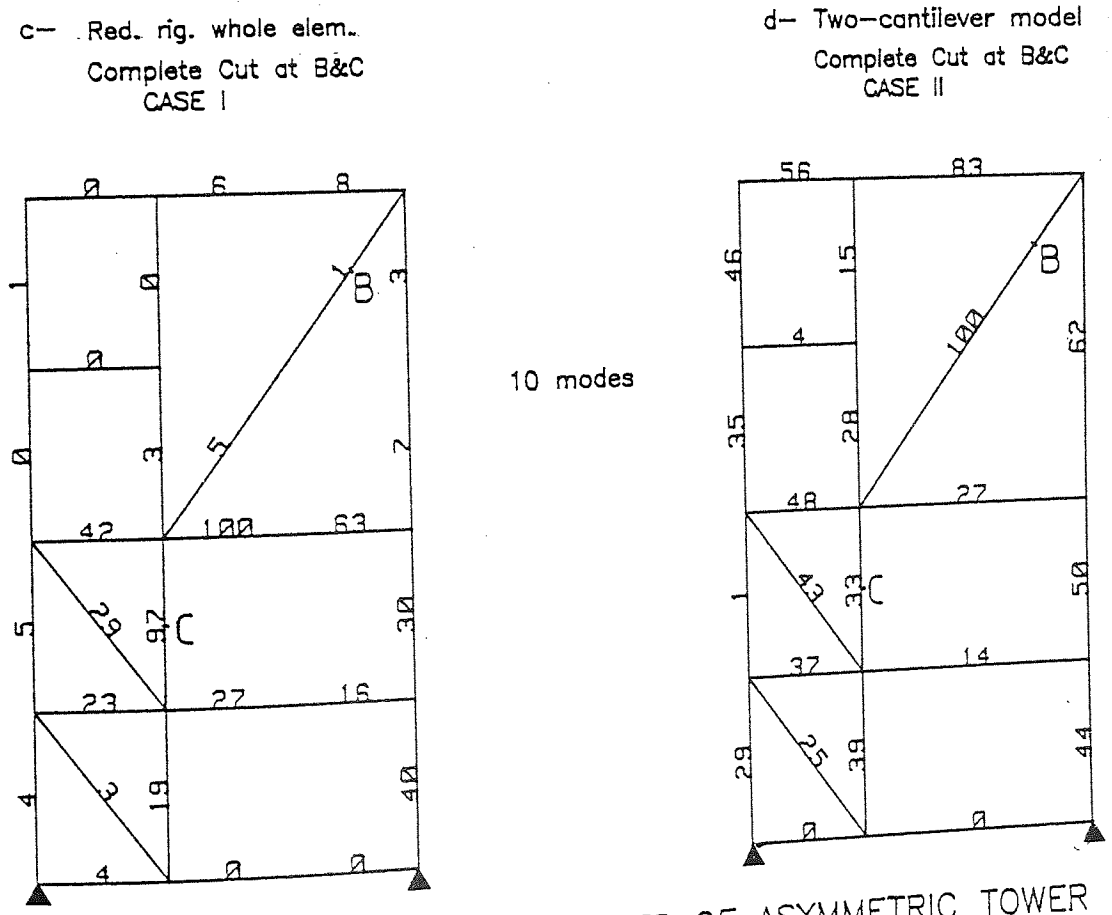

Fig.A3.9c–d DEFECT LOCATION CHARTS OF ASYMMETRIC TOWER FRAME WITH TWO DAMAGE SITES

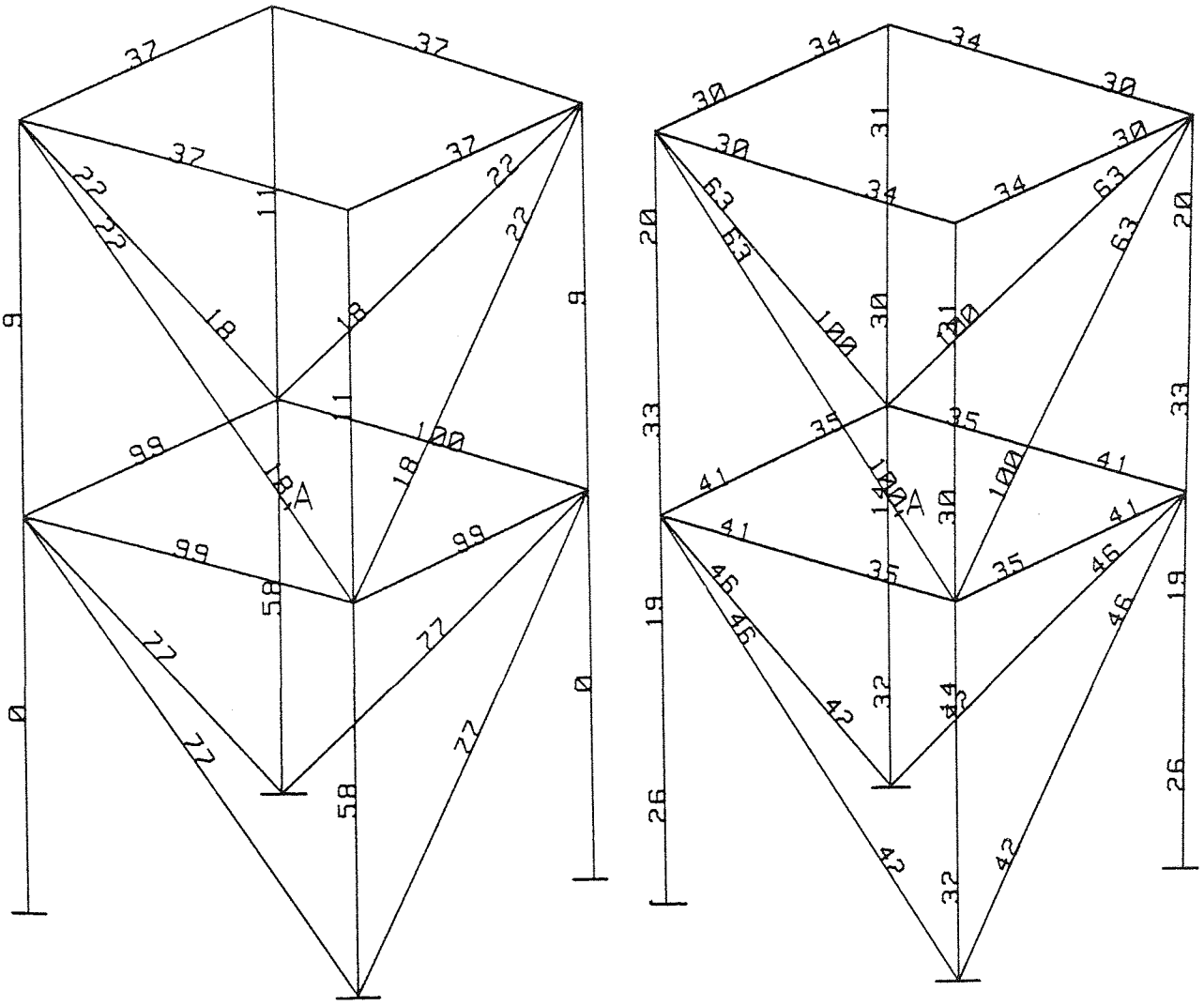

a– Complete Saw Cut at A
Red. rig. whole elem.
4 modes

b– Complete Saw Cut at A
Two–cantilever model
8 modes

Fig.A3.10a–b DEFECT LOCATION OF SYMMETRICAL SPACE FRAME FOR VARIOUS DAMAGE MODELS(CUT AT A)

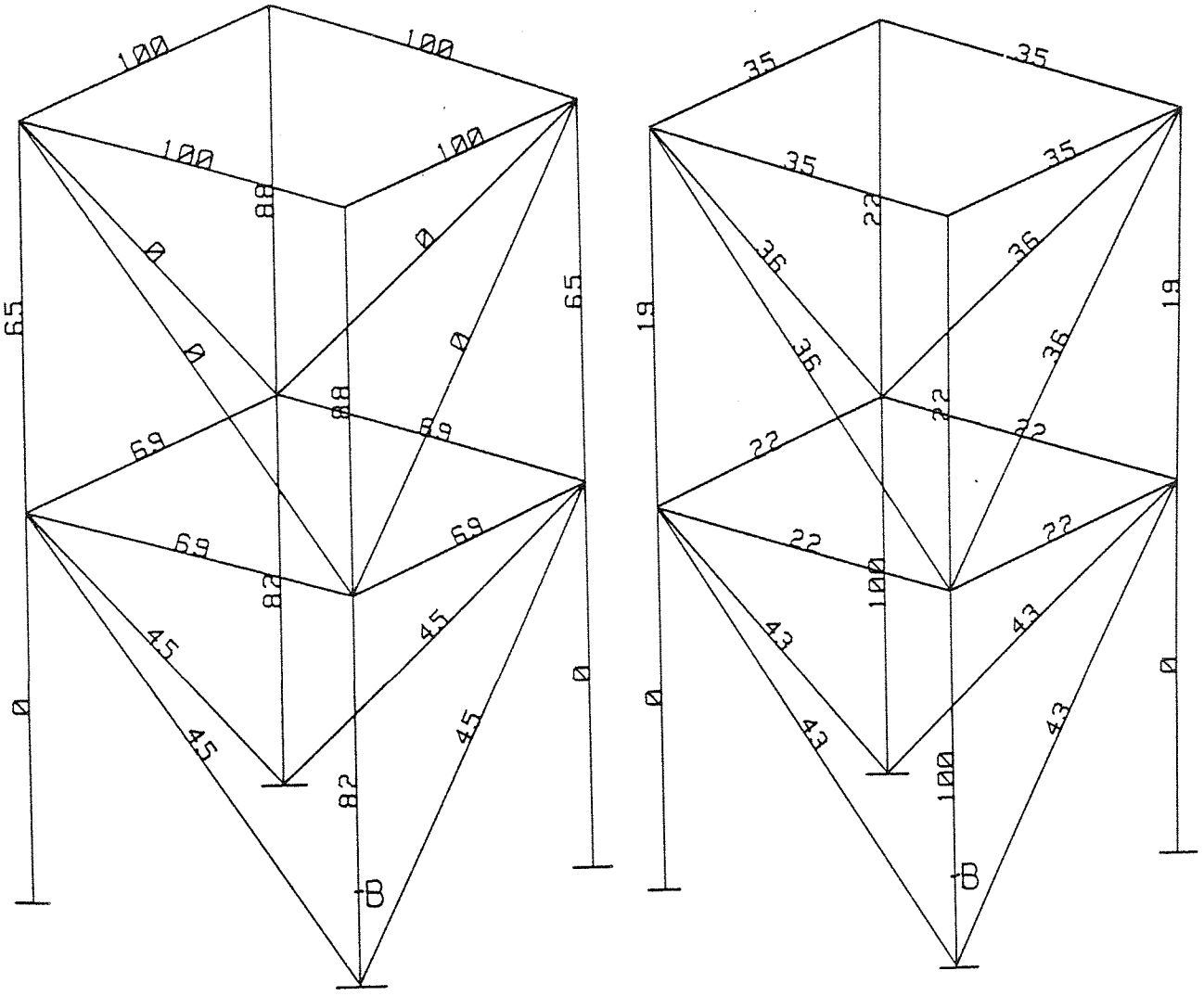

a– Complete Saw Cut at B
Member removal
4 modes

b– Complete Saw Cut at B
Two–cantilever model
10 modes

Fig.A3.11a–b DEFECT LOCATION OF SYMMETRICAL SPACE FRAME FOR VARIOUS DAMAGE MODELS(CUT AT B)

Mode Considered →

End / Start	1	2	3	4	5	6	7	8	9	10
1		N	Y	Y	Y	Y	Y	Y	Y	Y
2			Y	Y	Y	Y	Y	Y	N	S
3				Y	Y	Y	Y	Y	N	N
4					Y	N	Y	Y	N	N
5						N	Y	Y	N	N
6							Y	Y	Y	Y
7								N	Y	Y
8									Y	Y
9										N

Damage at Position A
(See Fig. 6.9)

Where:

Y = Damage was Correctly Located

N = Damage was Incorrectly Located

S = Damage was Located at Second Probability

TABLE A3.1 PROBABILITY OF DEFECT LOCATION OF STRUCTURAL MEMBER FOR SYMMETRICAL SPACE FRAME (CUT AT A)

Mode Considered →

End / Start	1	2	3	4	5	6	7	8	9	10
1		Y	Y	Y	Y	Y	Y	Y	Y	Y
2			S	Y	Y	Y	Y	Y	Y	Y
3				Y	Y	Y	Y	Y	Y	Y
4					S	S	N	N	Y	Y
5						N	N	N	Y	Y
6							N	N	Y	Y
7								S	Y	Y
8									S	S
9										N

Damage at Position B
(See Fig. 6.9)

Where:

Y = Damage was Correctly Located

N = Damage was Incorrectly Located

S = Damage was Located at Second Probability

TABLE A3.2 PROBABILITY OF DEFECT LOCATION OF STRUCTURAL MEMBER FOR SYMMETRICAL SPACE FRAME (CUT AT B)

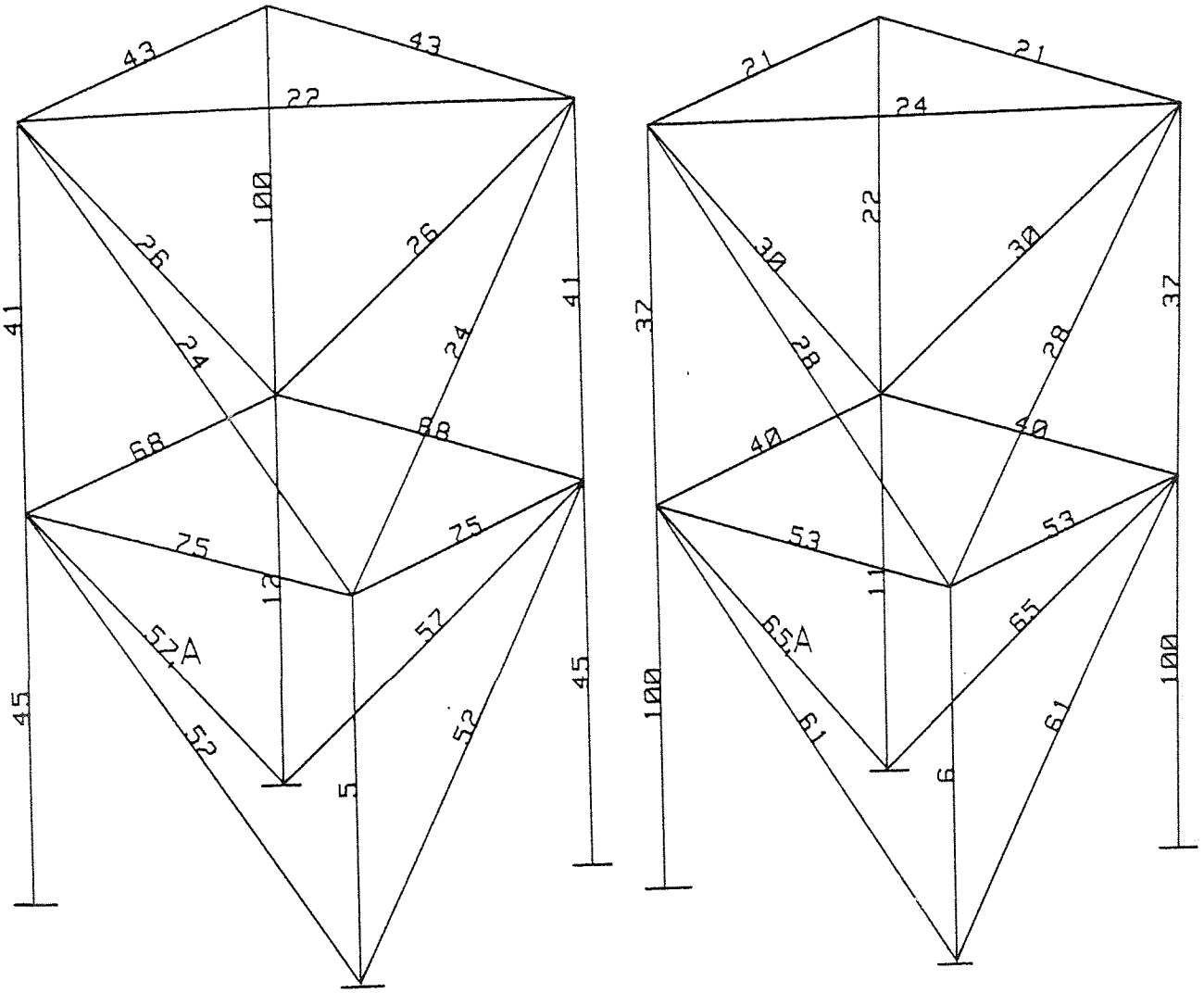

a– 60% Saw Cut of Cross Sectional Area at Position A

Two–cantilever model
10 modes

b– 70% Saw Cut of Cross Sectional Area at Position A

Two–cantilever model
10 modes

Fig.A3.12a–b DEFECT LOCATION OF SYMMETRICAL SPACE FRAME ALONG ONE DIAGONAL WITH VARIOUS SAW CUT DEPTHS

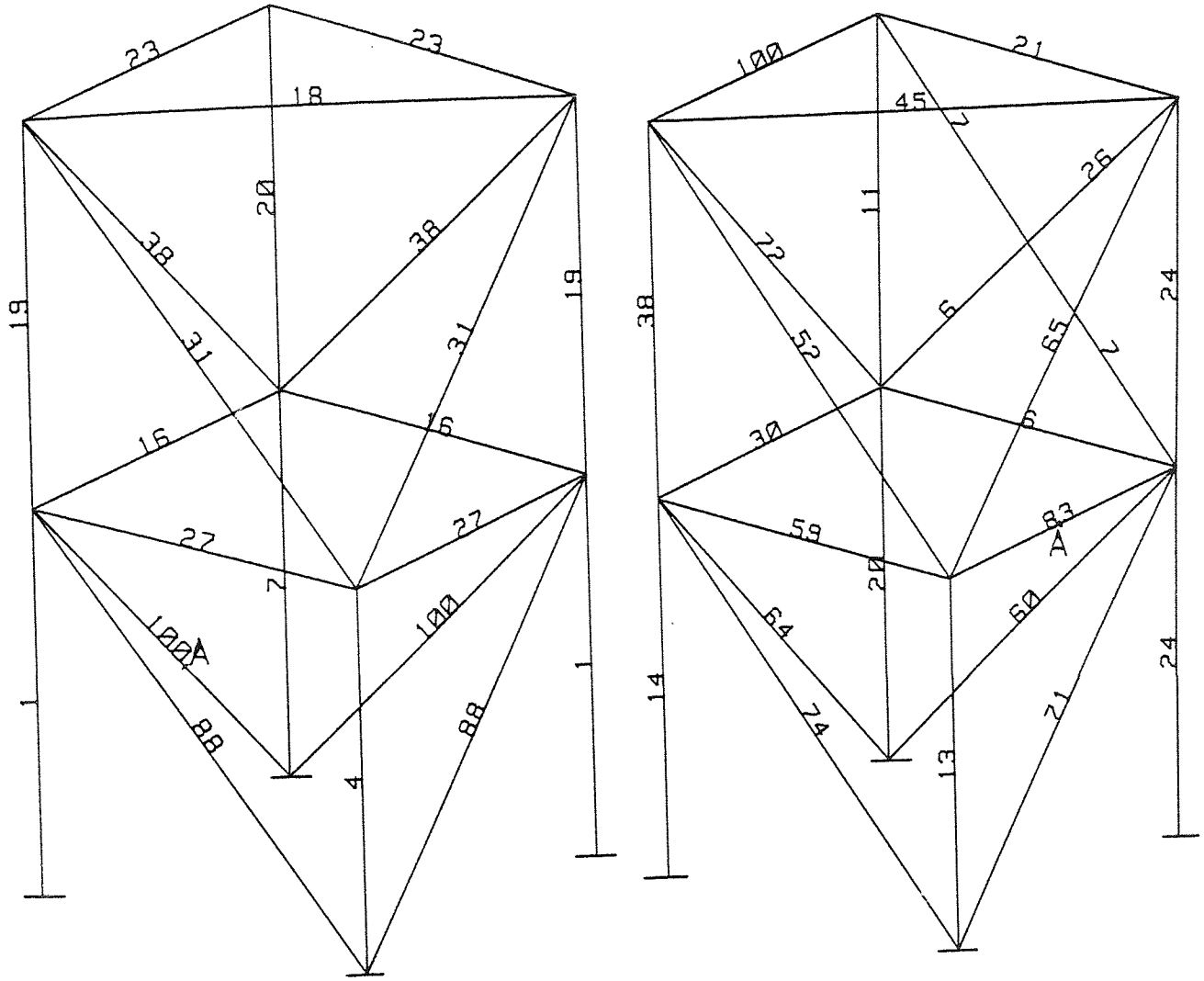

a– Complete Saw Cut at A
Two–cantilever model
9 modes

b– Complete Saw Cut at A
Two–cantilever model
10 modes

Fig.A3.13a–b DEFECT LOCATION OF SYMMETRICAL AND ASYMMETRICAL SPACE FRAME MODELS

752

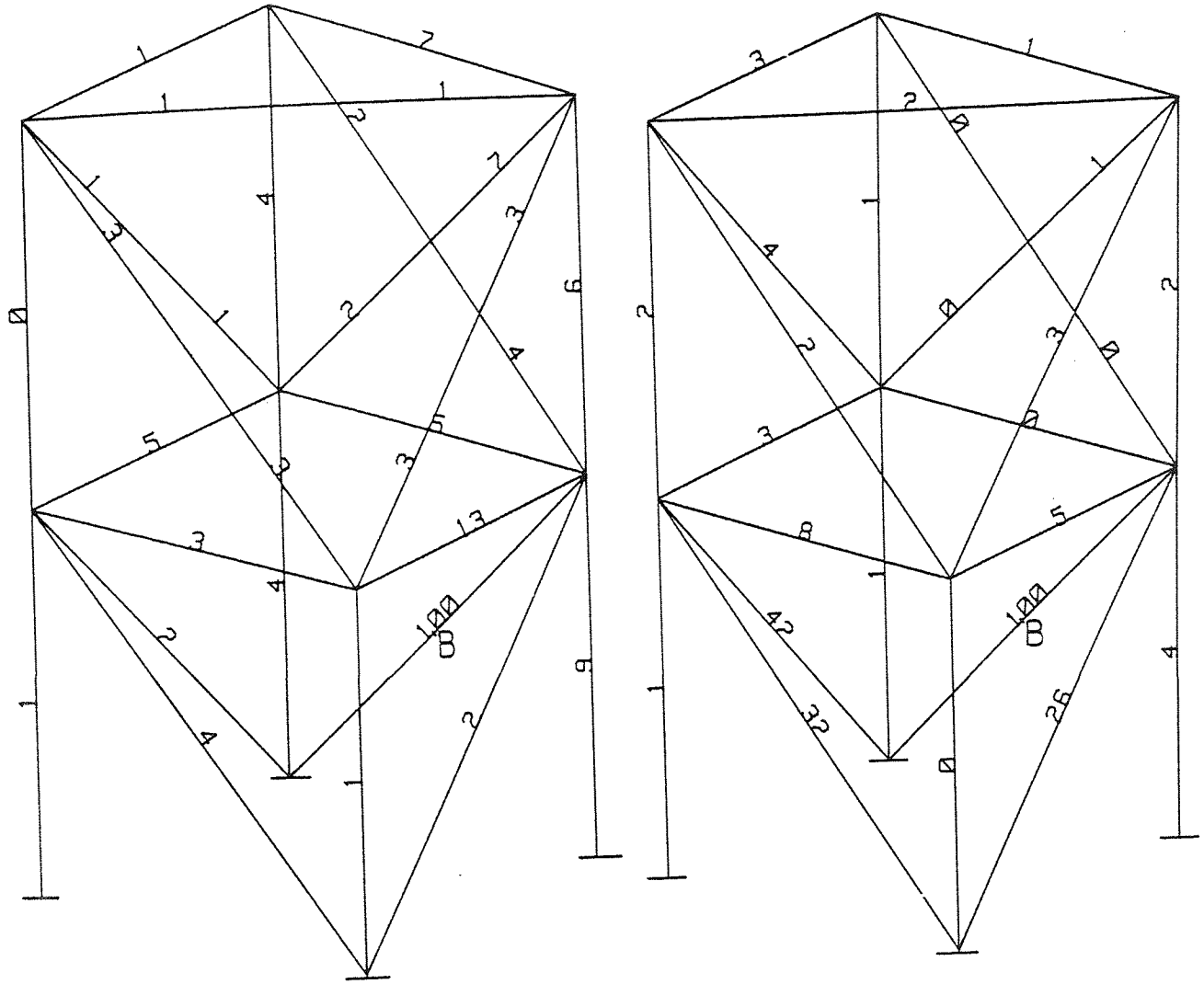

a– 40% Crack Depth at B
Red. rig. whole elem.
8 modes

b– Complete Crack at B
Two–cantilever model
10 modes

Fig.A3.14a–b DEFECT LOCATION OF ASYMMETRICAL SPACE FRAME MODEL WITH VARIOUS CRACK DEPTHS

a- P=0.2 (See Equation 9.1)

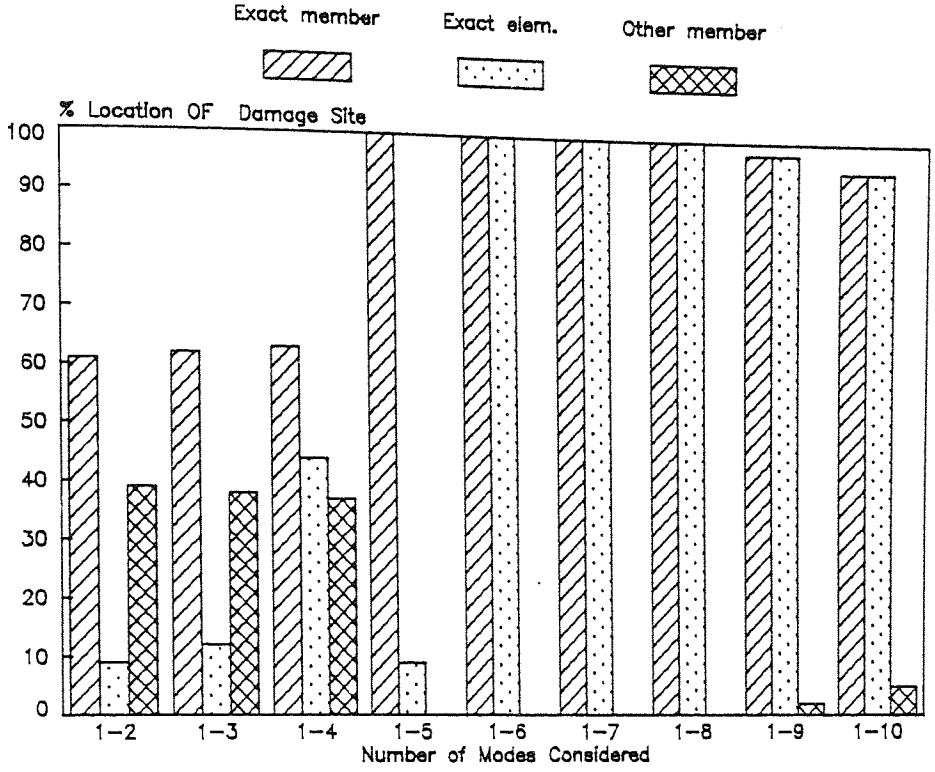

b- P=0.3 (See Equation 9.1)

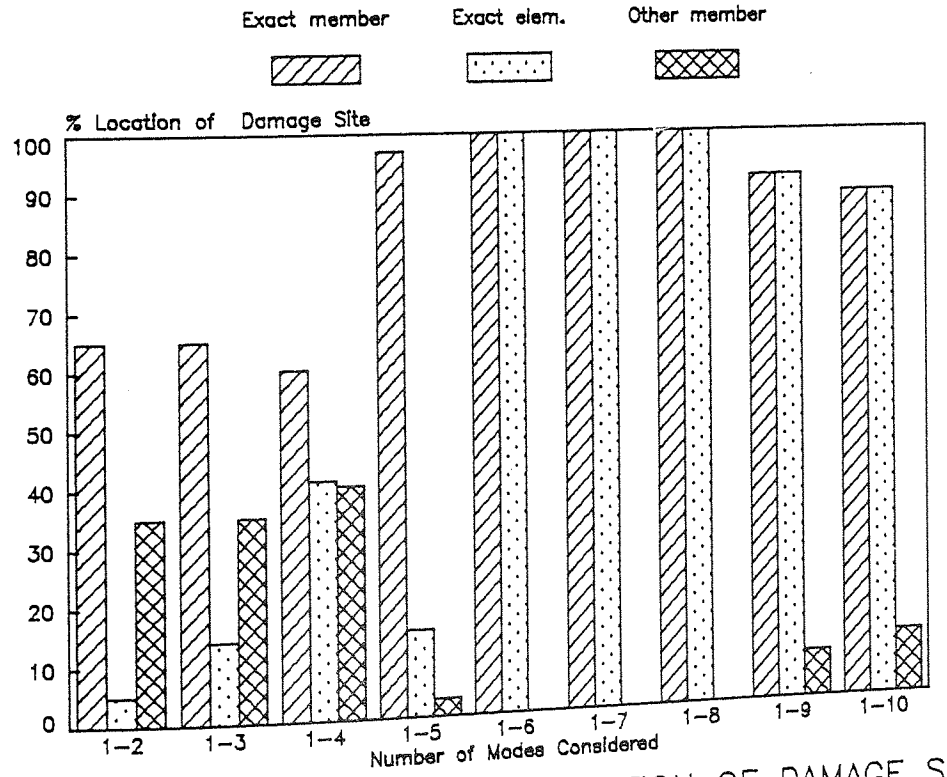

Fig.A3.15a-b PERCENTAGE LOCATION OF DAMAGE SITE OF SYMMETRICAL SPACE FRAME

a- P=0.2 (See Equation 9.2)

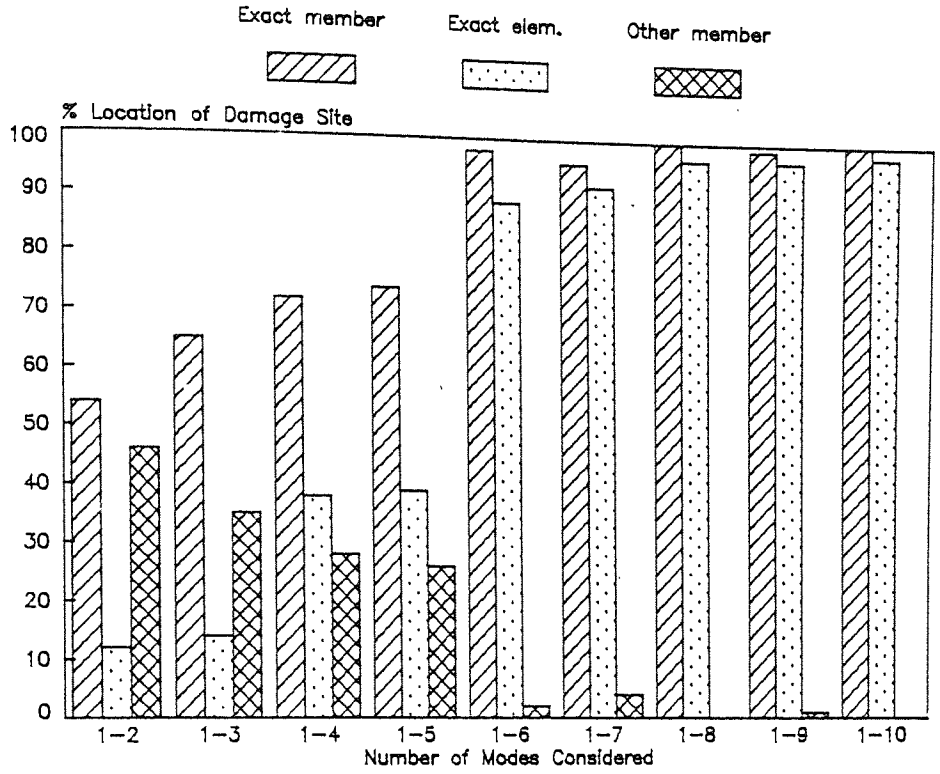

b- P=0.3 (See Equation 9.2)

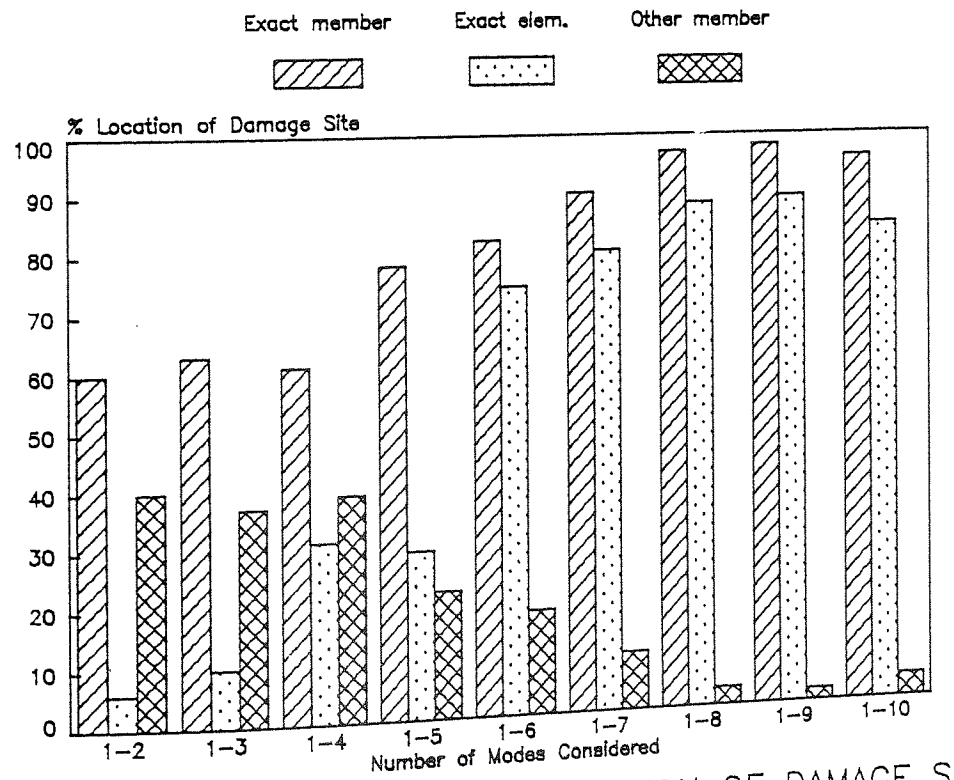

Fig.A3.16a-b PERCENTAGE LOCATION OF DAMAGE SITE OF SYMMETRICAL SPACE FRAME

APPENDIX 4

DETAILS OF THE ELEMENTS STIFFNESS AND MASS MATRICES

The elements of stiffness matrix $[K_f]$ for equation (5.14) are given below:

$$K_{11} = \frac{\lambda^2 (C - Ch)^2 \lambda L}{4 (1 - C Ch)^2} + \frac{\lambda^2 (S Ch + C Sh)}{4 (1 - C Ch)}$$

$$K_{12} = \frac{\lambda (S - Sh)(C - Ch) \lambda L}{4 (1 - C Ch)^2} + \frac{\lambda S Sh}{2(1 - C Ch)}$$

$$K_{13} = \frac{\lambda^2 (C - Ch) S Sh \lambda L}{4 (1 - C Ch)^2} - \frac{\lambda^2 (S + Sh)}{4 (1 - C Ch)}$$

$$K_{14} = \frac{- \lambda (S - Sh) S Sh \lambda L}{4 (1 - C Ch)^2} - \frac{(C - Ch)}{2 (1 - C Ch)}$$

$$K_{22} = \frac{(S - Sh)^2 \lambda L}{4 (1 - C Ch)^2} + \frac{3(S Ch - C Sh)}{4 (1 - C Ch)}$$

$$K_{23} = \frac{\lambda (S - Sh) S Sh \lambda L}{4 (1 - C Ch)^2} + \frac{\lambda (C - Ch)}{2 (1 - C Ch)}$$

$$K_{24} = \frac{\{ 2(C - Ch) + S Sh (C + Ch) \} \lambda L}{4 (1 - C Ch)^2} - \frac{3 (S - Sh)}{4 (1 - C Ch)}$$

$$K_{33} = \frac{\lambda^2 (C - C\,Ch)^2 \lambda L}{4\,(1 - C\,Ch)^2} + \frac{\lambda^2 (S\,Ch + C\,Sh)}{4\,(1 - C\,Ch)}$$

$$K_{34} = \frac{\lambda (S - Sh)\,(C - Ch)\,\lambda L}{4\,(1 - C\,Ch)^2} \cdot \frac{\lambda\,S\,Sh}{2\,(1 - C\,Ch)}$$

$$K_{44} = \frac{(S - Sh)\,\lambda L}{4\,(1 - C\,Ch)^2} + \frac{3\,(S\,Ch - C\,Sh)}{4\,(1 - C\,Ch)}$$

The elements of mass matrix $[m_f]$ for equation (5.15) are given below:

$$m_{11} = \frac{\lambda^2 (C - Ch)^2 \lambda L}{4\,(1 - C\,Ch)^2} - \frac{3\lambda^2 (S\,Ch + C\,Sh)}{4\,(1 - C\,Ch)}$$

$$m_{12} = \frac{\lambda (S - Sh)(C - Ch)\,\lambda L}{4\,(1 - C\,Ch)^2} - \frac{\lambda\,S\,Sh}{2\,(1 - C\,Ch)}$$

$$m_{13} = \frac{\lambda^2 (C - Ch)\,S\,Sh\,\lambda L}{4\,(1 - C\,Ch)^2} + \frac{3\lambda^2 (S + Sh)}{4\,(1 - C\,Ch)}$$

$$m_{14} = \frac{-\lambda (S - Sh)\, S\, Sh\, \lambda L}{4\,(1 - C\,Ch)^2} + \frac{\lambda (C - Ch)}{2\,(1 - C\,Ch)}$$

$$m_{22} = \frac{(S - Sh)^2 \lambda L}{4(1 - C\,Ch)^2} - \frac{S\;Ch - C\;Sh}{4(1 - C\,Ch)}$$

$$m_{23} = \frac{\lambda (S - Sh)\, S\, Sh\, \lambda L}{4\,(1 - C\,Ch)^2} - \frac{\lambda (C - Ch)}{2\,(1 - C\,Ch)}$$

$$m_{24} = \frac{\{\, 2(C - Ch) + S\,Sh\,(C + Ch)\,\}\,\lambda L}{4\,(1 - C\,Ch)^2} + \frac{S - Sh}{4\,(1 - C\,Ch)}$$

$$m_{33} = \frac{(C - Ch)^2 \lambda L}{4(1 - C\,Ch)^2} - \frac{3\lambda^2 (S\,Ch + C\,Sh)}{4\,(1 - C\,Ch)}$$

$$m_{34} = \frac{\lambda (S - Sh)(C - Ch)\, \lambda L}{4\,(1 - C\,Ch)^2} + \frac{\lambda\, S\, Sh}{2\,(1 - C\,Ch)}$$

$$m_{44} = \frac{(S - Sh)\, \lambda L}{4(1 - C\,Ch)^2} - \frac{S\;Ch - C\;Sh}{4\,(1 - C\,Ch)}$$

REFERENCES

1. Adams, R.D., Flitcroft, J.E, Reynolds, W.N. and Hancox, N.L — "Effects of shear damage on the torsional behaviour of carbon fibre reinforced plastics", J. composite mat., Vol. 7, Jan 1973, P. 68-75.

2. Adams, R.D., Walton, D., Flitcroft, J.E. and Short, D. — "Vibration testing as a non-destructive test tool for composite materials", Composite Reliability, ASTM STP 580, American society for testing and materials, 1975, P.159.

3. DiBenedetto,A.T Gauchel, J.V., Thomas, R.L. and Barlow,J.W — "Non-destructive determination of fatigue crack damage in composites using vibration tests", J. of materials, JMLSA, Vol. 7, No. 2, June 1972, P. 211-215.

4. Clarkson, V.W. — "The requirement for the non-destructive testing of airframe", British J. of NDT, July 1975, P.118

5. Tiedemann, H.M. — "Shortcomings of offshore subsurface engineering inspections", Marine technology, Jan. 1974, Vol. ii, No 1 P. 19-30.

6. Loland, O. and Dodds, C.J. — "Experiences in developing and operating integrity monitoring system in the north sea" Offshore Technology Conference (OTC) 2551, 1976, P. 313.

7. Silk, M.G., Williams, N.R. and Bainton, K.F — "The potential role of NDT techniques in the monitoring of fixed offshore structures", British J. of NDT, May 1975, P. 83-87.

8. Silk, M.G and Lidington, B.H. — "Defect sizing using an ultrasonic time dealy approach", British J. of NDT, March 1975, P. 33-36

9. Halmshaw, R. and Hunt, C.A. — "Can cracks be found by radiography" British J. of NDT, May 1975, P. 71.

10. Begg, R.D., Mackenzie, A.C Dodds, C.J.and — "Structural integrity monitoring using digital processing of vibration signals", 8th annual OTC 2549, Vol.2 1976.

11. Duggan, D.M. Wallace, E.R and Galdwell,S — "Measured vibrational behaviour of a Gulf of Maxico platform", 13th annual OTC 4137, May 4-7, 1981.

12. Forbes,P.D and Mathew,C.N — "Vibration technique of integrity monitoring of offshore rig structure" NEL Symposium, Dynamic analysis of structures, Paper No. 2, 8 Oct. 1975.

13. Nezu, K. and Kidognchi, H. — "A new damage detecting method by mechanical impedance measurements", Bullentin of the JSME ,Vol. 23 No. 186, Dec. 1980, P. 2125-2131.

14. Cawley, P. — "Defect location in structures by a vibration technique", Ph.D. Thesis, 1978, university of bristol.

15. Cawley, P.and Adams,'R.D. — "The location of defects in structure from measurements of natural frequencies", J. of strain analysis Vol. 14, No. 2, 1979.

16. Cawley, P.and Adams, R.D. — "A vibration technique for non-destructive testing of fibre composite structures", J. composite mat., Vol. 13, April 1979, P. 161.

17. Adams, R.D, Cawley, P., Pye, C.J.and Stone, B.J. — "A vibration technique for non-destructively assessing the integrity of structures", J. Mech. Eng. Sci. 1978, Vol. 20, No. 2, P. 93-100.

18. Loland, O.and Mackenzie, A.C — "On the natural frequencies of damaged offshore oil platforms", Mech. Res. Comm., Vol. 1, 1974,P.353.

19. Loland, O., Begg, R.D.and Mackenzie, A.C — "The dynamic response of a fixed, steel offshore oil platform", BSSM/ RINA Conf. Edinburgh, Sept. 1975.

20. Loland, O. Mackenzie, A.C and Begg, R.D — "Integrity monitoring of fixed steel offshore oil platforms", BSSM/INA Conf. Edinburgh, Sept 1975.

21. Matias, E.and Reddy, N.E. — "Structural integrity evaluation of a fixed platform using vibration criteria", 9th annual OTC 2909, May 2-5, 1977.

22. Vandiver, J.K — "Detection of structural failure on fixed platforms by measurement of dynamic response", 7th annual OTC 2267, May 5-8, 1975.

23. Turner, J.D. and Pretlove, A.J. — "Location of damage to bridges by measurements of traffic-induced vibration", Presented at Euromech 168 Conference, June 1983 Manchester.

24. Cawley, P.and Adams, R.D. "Defect location in structures by a vibration technique", 9th world Conference on non-destructive testing, Nov. 19-23 1979.

25. Zienkiewicz,O.C "The finite element method in Engineering Science", McGraw-Hill Book company, New York, 1971.

26. Zienkiewicz,O.C "The finite element method", 3rd edition, McGraw-Hill, 1977.

27. Wilkinson,J.H "Calculation of the eigenvalues of a symmetric tridiagonal matrix by the method of bisection", Numer. math. 4, 1962, P. 362-367.

28. Martin,R.S.and Wilkinson, J.H "Reduction of the symmetric eigen-problem $Ax= \lambda Bx$ and related problems to standard form", Numer. math. 11, 1968, P. 110.

29. Wilkinson,J.H. "Convergence of the LR, QR, and related algorithms", Computer J. Vol. 8, 1965, P. 77-84.

30. Francis,J.G.F "The QR transformation, parts, i and ii", Computer J., Vol. 4, 1961 P. 265 and 332.

31. Bowdler, H., Martin, R.S., Reinsch, C.and Wilkinson,J.H. "The QR and QL algorithms for symmetric matrices", Numer. math. 11 1968, P. 293-306.

32. Richards, T.H. "Energy method in stress analysis" Ellis-Horwood series in Eng. Sci. London, 1977.

33. Timoshenko,S. "Elements of strength of materials" D.van Nostrand company, New Jersey 1962.

34. Przemieniecki, J.S. "Theory of matrix structural analysis", McGraw-Hill, 1968.

35. Hurty,W.C and Rubinstein,M.F. "Dynamics of structures",1964 Prentice-Hall, Inc.

36. Meirovitch, L. "Elements of vibration analysis",1975 McGraw-Hill.

37. Courant,R. and Hilbert, D. "Methods of mathematical physics" Vol. 1, Interscience, 1953.

38. Stevens, L.K. "Design of frames with deformation the prime criterion", J. of the structural division proceedings of the ASCE, Feb. 1962, Vol. 103, P. 55-73.

39. Burgreen, D. "Effect of end-fixity of the vibration of rods", J. of the Eng. Mech. Division, Proceedings of the ASCE, Oct. 1958, EM4, P. 1791-1.

40. Nyholm, G.E. "Computer solution of the Eigenvalue problem in vibration analysis", M.Sc. project report, The University of Aston in Birmingham, Nov. 1979.

41. Xaidaras, A. "Computing frame vibrations", M.Sc. report, The University of Aston in Birmingham, Oct. 1981.

42. Wilkinson, J.H "Householder´s method for symmetric matrices", Numer. math. 11, 1968, P. 354.

43. Wittrick, W.H and Williams, F.W. "A general algorithm for computing natural frequencies of elastic structures", Quart. J. Mech. and applied Math., Vol. XXIV, pt. 3, 1971 P. 263.

44. Williams, F.W and Wittrick, W.H. "An automatic computational procedure for calculating natural frequencies of skeletal structures", Int. J. Mech. Sci., Vol. 12, 1970, P. 781-791.

45. Williams, F.W. and Howson,W.P "Compact computation of natural frequencies and buckling loads for for plane frames", Int. J. for numerical methods in Eng., Vol. 11, 1977, P.1067.

46. Richards, T.H. and Leung, Y.T "An accurate method in structural vibration analysis", J. of sound and vibration, 55(3), 1977, P. 363-376.

47. Basci, M.I, Toridis,T.G.and Khozeimeh, K. "Improved method of free vibration analysis of frame structures", Comp. & structures, Vol. 10, 1979, P. 255.

48. Leung, Y.T. "Dynamics of structural vibrations by frequency dependent matrices and modal analysis", Ph.D Thesis, April 1976, Mech. Eng. Dept., Aston University.

49. Howson,W.P. "The computer programs CEEGAS and CEEMAS", Private Communcation.

50. Lam, P.K.S. "Vibrational behaviour of plane frame structures composed of prismatic and tapered sections", Ph.D. Thesis, Dept. of Civil Eng., Sept. 1979, Aston Univ.

51. Kennedy, C.C. and Pancu,C.D "Use of vectors in vibration measurement and analysis", J. Aeronautical Sci. Vol. 14, 1947, P. 603-625.

52. Ewins, D.J. "Measurement and application of mechanical impedance data", parts 1, 2 & 3, J. of the Society of Environmental Eng Dec. 1975, March 1976 & June 1976.

53. Bishop,R.E and Johnson,D.C "The mechanics of vibration", cambridge University press, 1960.

54. Ewins,D.J and Gleeson,P.T. "Experimental determination of multi-directional mobility data for beam", Shock and vibration Bulletin, 45(5) page 158-173.

55. White, R.G. "Evaluation of the dynamic characteristics of structures by transient testing", J. sound & vibration, 1971 15(2), Page 147-161.

56. Holmes,P.J and White, R.G. "Data analysis criteria and instrumentation requirements for the transient measurement of mechanical impedance", J. sound & vib., 1972, 25(2), P.217.

57. Cawley,P. and Adams, R.D. "Improved frequency resolution from transient tests with short record lengths", J. sound & vibration, 1979 64(1), P. 123-132.

58. Pessu, A. M. "Vibration charateristic of fabricated space frame", Ph.D Thesis, Mech. Eng. Dept., Aston University.

59. Salter, J.P "Steady state vibration", Mason, 1969.

60. Clark, A.R "An investigation into the effect of interface dynamics of the response of coupled systems", Ph.D. Thesis, Mech. Eng. Dept., Aston University.

61. Felgar, R.P,Jr "Formulas for integrals containing characteristic functions of a vibrating beam" The University of Texas circular No. 14, 1950.

62. Young, D and Felgar,R.P,Jr "Tables of characteristic functions representing normal modes of vibration of a beam" The University of Texas publication No. 4913, July 1949.

63. White,R.G and Pinnington,R.J "Practical application of the rapid frequency sweep technique for structural frequency response measurement" Aeronantical J., May 1982

64. Penny,J.E.T and Clark, A.R. "Measuring the frequency response of mechanical structures", Transducer/ Tempcon Conference, July 1982, London.

65. Johnston, J "Econometric methods", 2nd edition, International student edn. Tok yo 1972. McGraw - Hill.

66. Aitken, A.C. "On least squares and linear combination of observations"Proc. Roc. Soc. Edinburgh, 55, P. 42-48, 1934.

67. Fisher, R.A and Yates, F. "Statistical tables for biological agricultural and medical research", 5th edition, Edinburgh: Oliver & Boyd 1957.

68. Pearson,E.S and Hartley, H.O "Biometrika tables for statisticians, Vlume 1, Cambridge: Cambridge Univers-ity Press. 1956.